SYNTHESIS AND CHARACTERIZATION OF THE

ZEOLITES ZSM-5 AND FERRIERITE

by

PHOKOANE BETTY RAMATSETSE

Submitted in fulfillment of the requirements for the degree of Doctor of Philosophy

in the School of Physical and Mineral Sciences

in the Faculty of Sciences, Health and Agriculture

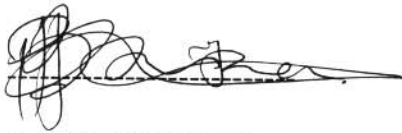University of the North

Turfloop

South Africa

January 2003

Supervisor :   Prof. J.J. Prinsloo

Co-Supervisor : Dr. C.P. Nicolaides

THIS THESIS IS DEDICATED TO THE MEMORY OF MY

BROTHER

DECLARATION

I declare that the thesis hereby submitted to the University of the North for the degree of Doctor of Philosophy has not been previously submitted by me for a degree at any other University, that it is my own work in design and execution, and that all material contained therein has been duly acknowledged.

RAMATSETSE P.B

ACKNOWLEDGEMENTS

I wish to express my sincere gratitude to the following people and institutions whose interest and financial support made it easier for me to prepare and complete this thesis.

To my supervisor, Prof. J.J. Prinsloo (UNIN), for what he did.

To my supervisor, Dr. C.P. Nicolaides (Wits) for always being prepared to drop his own work at a moment's notice to assist me throughout the course of this project and for his advise in writing this thesis.

To P.S. Sincadu (Wits), whose willingness to lend a hand and solve technical problems I encountered during the catalytic studies and the characterization by XRD made it easier for me to complete my research.

To Prof. M.E. Lee (UNIN), who allowed me to the instruments in the Centre of Microscopy and Microanalysis for the characterization of the samples by SEM.

I wish to thank NRF and Standard Bank for financial support.

To my family, your perseverance and the emotional support you gave me during the time of my studies are highly acknowledged.

I finally wish to thank God for granting me the serenity to change things I can, courage to accept

things I cannot change and the wisdom to know the difference.

ABBREVIATIONS

AAS	Atomic absorption spectroscopy
BET	Brunauer, Emmett and Teller isotherm
BJH	Barret, Joyner and Halenda method for pore size distribution determination
BTX	Benzene, toluene and xylene
C_6DN	1,6-Hexanediamine
CP	Cross polarization
CFC	Chlorofluorocarbon
CTR	Catalytic test reaction
d	Diameter
1-D	One dimensional
2-D	Two dimensional
3-D	Three dimensional
EDS	Energy dispersive electron X-ray spectroscopy
FCC	Fluidized catalytic cracking
FER	Ferrierite
FM	Flow meter
FTIR	Fourier transform infrared spectroscopy
GC	Gas chromatograph
HREM	High-resolution electron microscopy
IR	Infrared spectroscopy
MAS	Magic angle spinning

MgAPO-5	Magnesiumaluminophosphate-5
MnPO-11	Manganesephosphate-11
MOGD	Mobil olefin to gasoline and distillate
MTBE	Methyl *tert*-butyl ether
MTG	Methanol to gasoline
NMR	Nuclear magnetic resonance
py	Pyridine
p/p_0	Relative pressure of the nitrogen adsorbed per saturated vapour pressure
REY	Rare-earth zeolite Y
rpm	Revolutions per minute
SAPO	Silicoaluminophosphate
SBU	Secondary building unit
SEM	Scanning electron microscopy
STEM	Scanning transmission electron microscopy
TAA	Tetraalkylammonium
TBA	Tetrabutylammonium
temp.	Temperature
TCC	Thermofor catalytic cracking
TEM	Transmission electron microscopy
TMA	Tetramethylammonium
TOS	Time-on-stream
TPA	Tetrapropylammonium
TPA-Br	Tetrapropylammonium bromide
TPA-OH	Tetrapropylammonium hydroxide

TPD	Temperature programmed desorption
WS	Without stirring
wt%	Weight percentage
XRD	X-ray diffraction
XPS	X-ray photoelectron spectroscopy
ZSM	Zeolite Secony Mobil

TABLE OF CONTENTS

3 **CHARACTERIZATION OF ZEOLITES**

4 **EXPERIMENTAL**

6 RESULTS AND DISCUSSION ON THE SYNTHESIS OF THE FERRIERITE-BASED ZEOLITIC MATERIALS

SUMMARY

Both the zeolite ZSM-5 and ferrierite have found application as catalysts for a variety of industrial processes. Apart from the various shape-selective applications of ZSM-5 as industrial catalysts, ferrierite has also been shown to be an active, selective and stable catalyst for the skeletal isomerization of 1-butene to isobutene. It was also reported recently that ZSM-5 zeolites of lower levels of percentage crystallinity can successfully be utilised as catalysts for this isomerization reaction. One of the products that can be synthesized from isobutene is methyl *tert*-butyl ether (MTBE), which is currently still being used as an octane enhancer in gasoline. MTBE is produced from the reaction of methanol and isobutene over the acid resin catalyst Ambelyst 15. As a consequence of the industrial significance of these zeolites, further knowledge on the reproducible synthesis of these zeolites is of crucial importance. A detailed study was therefore undertaken of different synthetic procedures in terms of achieving reproducibly the synthesis of zeolitic materials that spanned the whole range of crystallinities, ranging from the substantially amorphous to the highly crystalline. Parameters that were varied in the different recipes used were temperature, stirring mode, seeding, source of silica, particle size of silica source, etc.

An evaluation of the literature was carried out on zeolite syntheses and characterization as well as on the problems that may be encountered during these processes. ZSM-5 and ferrierite zeolite-based materials were prepared using seven different recipes. The zeolite crystallinities were determined by X-ray powder diffraction (XRD) and the morphology by scanning electron microscopy (SEM). Catalytic test reactions, such as *n*-hexane and propane cracking, were carried out on some of the ZSM-5-based materials in order to evaluate their catalytic pro-

perties as a function of XRD crystallinity and particle size.

For the ZSM-5-based materials synthesized using the different methods, the percentage XRD crystallinities increased with increasing synthesis temperature up to a certain synthesis temperature according to a sigmoidal relationship. Above that temperature, the percentage XRD crystallinity decreased with an increase in synthesis temperature due to amorphotization and/or due to the formation of α-quartz. One of these methods, the silicic acid method under the unstirred mode of synthesis, deviated from this trend. It showed a direct proportionality between the percentage XRD crystallinity and the synthesis temperature up to the highest temperature investigated, i.e. 210°C. This method therefore appears to have some outstanding features. It also gave the highest percentage XRD crystallinity sample (as compared to all other samples prepared with different recipes and/or methodologies). Furthermore, it was the most controllable method for the synthesis of partially crystalline material.

Although different methods of synthesizing the zeolite ZSM-5 gave samples with the same percentage XRD crystallinities, their morphologies were different, ranging from the spheroidal to octagonal structures. With some methods, stirring delayed the formation of crystallites of definite shapes and facilitated the formation of small spheroids. It also influenced the formation of α-quartz in the required phase.

The cracking of the alkanes tested, viz. propane and *n*-hexane, showed an exponential increase in conversion with an increase in percentage XRD crystallinty of the ZSM-5-based materials tested as catalysts. Furthermore, the zeolite samples of almost the same percentage XRD crystallinities synthesized in different ways do not necessarily have the same catalytic properties. It also

indicated that the stirred samples, containing spheroids, are more active for alkane cracking than the highly crystalline samples obtained without stirring. This effect was more explicit for the higher alkane, i.e. n-hexane, than for propane. For n-hexane cracking and with samples prepared without stirring a lower percentage conversion was even obtained for the 80% crystalline sample than for the 63% sample. This could be ascribed to the lower diffusional limitation with propane due to its smaller chain length. This suggests, therefore, that n-hexane cracking is a more discriminating catalytic test reaction in detecting differences in ZSM-5 samples such as crystallite size and form. The products obtained indicated that for the cracking of propane solely monomolecular cracking occurred for conversions up to 2% after which the contribution of the classical bimolecular mechanism played a significant role. Similarly for n-hexane, cracking followed exclusively the Haag-Dessau mechanism of protolytic cracking up to 9% conversion.

For ferrierite-based materials, it was observed that there is an increase in percentage XRD crystallinity with increasing synthesis temperature up to a certain temperature. Above that temperature, a decline in percentage XRD crystallinity of the ferrierite phase was found with concomitant formation of α-quartz and/or analcime in the required phases. It was shown that the morphologies, obtained with the three different recipes used for ferrierite synthesis, also differed, ranging from "snow-flakes" to rectangular structures. The top and bottom stirred modes of synthesis both resulted in the breaking up of the crystals of the ferrierite-based zeolites. The studies showed that different silica sources produce different crystallinities of zeolite ferrierite-based material under the same conditions. For the silica gel method, the reproducibility was not good at 130°C which is the temperature at which crystallinity commence, and the highest percentage XRD crystallinity (79%) was obtained at 150°C. It was also observed that the larger the particle sizes of silica gel used, the lower the percentage XRD crystallinities. With the

Ludox HS-30 method substantially amorphous to partially crystalline ferrierite-based materials could be synthesized, and the highest percentage XRD crystallinity (37%) was obtained at 185°C. Although this is the most controllable method for preparing samples at lower level of percentage XRD crystallinity α-quartz and analcime were detected as impurities with most of the samples prepared.

When different autoclaves were used for the hydrothermal synthesis of the zeolites ZSM-5 and ferrierite, and using the same method, the resultant percentage XRD crystallinities differed in most cases. The different rates at which the reaction mixtures were stirred in the two autoclaves and seeding were found to be responsible for these differences.

CHAPTER ONE

RATIONALE AND AIMS OF THE THESIS

1.1 INTRODUCTION TO ZEOLITES

The discovery of the first natural zeolite, stilbite, took place in the middle of the eighteenth century (Turkevich, 1968). According to Feijen *et al.* (1994) the most significant progress in the field of zeolites, however, was only made during the twentieth century as a result of the pioneering work by Barrer and Milton and the development of new and fast characterization techniques. Even nowadays, this area of science is fast expanding, resulting in the discovery of synthetic zeolites with new topologies and new catalytic, sorption and separation properties. It is, therefore, not surprising that much effort is currently being made to unravel the mechanisms responsible for the formation of zeolites from their precursors. From this knowledge it is hoped to derive concepts for "tailor-made zeolite synthesis" and to make the "art" of zeolite synthesis a real scientific issue.

Zeolites are crystalline microporous aluminosilicates of the general formula $M_{x/n}[(AlO_2)_x(SiO_2)_y].mH_2O$ and may be considered as open structures of silica in which aluminium has been substituted in a fraction $x/(x+y)$ of the tetrahedral sites. The net negative charge of the aluminosilicate framework is neutralized by extra-framework exchangeable cations, M, of valence n. The exchangeable counter ions are generally from Group I or Group II, although metal cations from other groups, non-metal and organic cations, may also be used to balance the framework charge. These cations are present during synthesis or can be changed

through post-synthesis ion exchange. The void space, which can be greater than 50% of the volume, is occupied by m molecules of water in the unit cell.

The porosity can consist of one, two or three-dimensional networks of interconnected channels and cavities of molecular dimensions, that is, the pore diameters or channel openings can range from 3Å to 8Å, depending on the structure of the zeolite. Specially noteworthy is the class of highly siliceous medium-pore zeolites, such as ZSM-5 (Zeolite Socony Mobil "number-5") and ferrierite, with largest pore diameters of 5.3Å X 5.6Å and 4.2Å X 5.4Å, respectively, both of which have seen application as industrial catalysts (Mooiweer et al., 1994; Venuto, 1994; Maxwell, 1997).

1.2 IMPORTANCE OF ZEOLITES

Zeolites are used as molecular sieves to separate molecules of different sizes. Uses range from the removal of toxic materials from blood, to the production of non-alcoholic beverages by the selective removal of alcohol, and to the decaffeination of coffee (Olson et al., 1980; Smart and Moore, 1995). They have also seen application as ion exchangers (e.g. in water softening) (Moscou, 1991), as animal feed supplements (e.g. pigs taking in clinoptilolite show beneficial weight gain and are less subject to disease than pigs fed by normal diet) (Dyer, 1988) and in the pharmaceutical industry (e.g. can be used as a drug releasing agent) (Davis and Higgins, 1992).

Zeolites are also used by the nuclear industry to decontaminate water from fission products, especially from the radioisotopes such as ^{137}Cs and ^{90}Sr/^{90}Y that occur in the pond water where the spent nuclear fuel reactors are stored. These ponds are major sources of medium-level radioactive waste and are decontaminated by zeolites such as clinoptilolite (Dyer, 1988).

Cheaper zeolites such as clinoptilolite, mordenite, chabasite, etc., are also used for the removal of protein breakdown products such as ammonia and ammonium ions from aqueous effluents. Zeolites can be used to control soil pH, moisture content and manure malodour, and around 600 tons per annum of clinoptilolite and mordenite are reported to have been used for this latter purpose in Japan in the 1980's (Dyer, 1988). Zeolite composite materials also find application as medical antibacteria materials, deodorisers, absorbent pads, sanitary napkins, gas separators, etc. (Mintova and Valtchev, 1996).

Moreover, zeolites are used extensively in the field of catalysis. Catalysis is a multidisciplinary science and is a very important tool for most industries, with heterogeneous catalysis being the most important one. At present, the main usages of catalysts are in oil refineries (25%), chemical and petrochemical industries (42%) and environmental control (33%) (Martino, 2000). Most of the technologically important catalytic reactions are being performed with microporous materials as catalyst or catalyst supports, of which zeolites are the most important (Occelli *et al.*, 1999). Due to this very important role that zeolites play in the field of catalysis, their use as catalysts will be further discussed in the next section.

1.3 Zeolites as catalysts

As indicated in the previous section, zeolites hold a dominant position in the field of catalysis. Since the 1970's zeolite catalysts have progressively replaced other families of catalysts in industrial applications (Martino, 2000). Zeolites are very useful catalysts displaying several important properties that are not found in conventional amorphous catalysts. Amorphous catalysts have always been prepared in a highly divided state in order to give a high surface area and thus a large number of catalytic sites. However, the presence of the cavities in the zeolites

provides a very large internal surface area that can accommodate as many as 100 times more molecules than the equivalent amount of amorphous catalyst (Smart and Moore, 1995). Zeolites are crystalline materials and can be prepared with high reproducibility: they tend not to show varying catalytic activity which is sometimes typical of amorphous catalysts. Furthermore, their molecular sieve action can be exploited to control which molecules have access to, or which molecules can depart from, the active sites. This is generally known as shape selective catalysis or "selectoforming".

The advantages of zeolites as catalysts, compared to amorphous materials, are numerous, with the most important ones being:

Solvent-like nature of the zeolite pores

Guest molecules in zeolites are enveloped by the small pores. The zeolite pores are like solvents; the microenvironments of the zeolites are in this case comparable to those of the clefts in enzymes and to the spaces between the chains of swellable synthetic polymers. The structure and composition of the zeolite pore, therefore, strongly influence the reactivity of a guest molecule (Gates, 1992).

High density of catalytic sites

For a catalyst to promote a reaction at a useful rate (e.g. with an activation energy of 125 kJ/mol at 500°C), it has been calculated that at least 10^{18} active centres per cm^3 of catalyst volume are required (Whan, 1981). Traditionally the high specific surface area which this implies has been provided by highly divided amorphous materials, and it was not until the late 1950's that it was shown that the high intracrystalline surface area of some zeolites provided such catalytic activity due to the high density of active sites.

Gates (1992) also indicated that this advantage of high density of the catalytic sites in zeolites can be combined with the additional important characteristic of structure stability at high temperatures; the latter is an advantage characterizing many inorganic solid acids and accounts for their wide application as industrial catalysts.

Well-defined active sites

Since amorphous materials inevitably display surface heterogeneity, they may offer a range of catalytic sites of different environment and of varying activity. Zeolites, on the other hand, are crystalline with regular structures (that can be characterized by e.g. X-ray powder diffraction (XRD)), and thus, the zeolitic catalytic sites are well defined and even the locations of the balancing cations in some zeolites have been identified (Whan, 1981).

Molecular sieving properties

Three varieties of shape selective catalysis are possible: (i) reactant selective catalysis, in which only reactants having dimensions less than a certain critical size can enter the pores of the zeolite and have access to the active centre, (ii) product selective catalysis, in which only products below a certain size have the ability to exit from the zeolite structure and (iii) transition state selective catalysis, in which the reaction products may be governed by the inability of the transition state of a particular reaction pathway to be accommodated in the available space (Dwyer, 1984).

Controllable electrostatic fields

If multivalent cations (e.g. Ce^{3+}) are used to replace the original singly charged cations (e.g. Na^+) in a zeolite, these cations are assumed to position themselves where each one is best able to relate to three separate $[AlO_4]^-$ tetrahedra (Whan, 1981). These tetrahedra may well not be close

together, particularly in the case of high silica zeolites, and the resultant separation of charges causes high electric field gradients. Such fields will be sufficiently large to ionize, or at least activate, adsorbed molecules and may well contribute to the catalytic activity of zeolites. Rabo *et al.* (1978) proposed that zeolites should be regarded as solid ionizing solvents, and it may thus be reasonable to liken some of the differences in catalytic performance between different zeolites to the use of different solvents in homogeneous chemistry. The possibility cannot be excluded, however, that the multivalent ions, e.g. M^{2+}, are actually present as $M(OH)^+$ (Biscardi *et al.*, 1998).

Sites for occluded and grafted species

One of the most attractive properties of zeolites is that when small particles of metals are deposited within a zeolite, the resultant material displays the properties associated with a supported metal catalyst, but only for molecules small enough to pass through the zeolite sieve (Whan, 1981). Similarly, zeolites may be used as well-defined backbones onto which organometallic or other entities with highly specific catalytic properties may be grafted, thus "heterogenizing" homogeneous catalysts. In some cases zeolites have been shown to be capable of stabilizing occluded complexes which have no homogeneous equivalents and are highly active for reactions of commercial importance (Verdonck *et al.*, 1979).

In addition to the above, other advantages offered by zeolites as catalysts include ease of separation, recovery and stability, safer handling than H_2SO_4, H_3PO_4, HF or solid Lewis acids, their capability of catalyzing multi-step reactions in a single catalyst bed and minimization, or even elimination, of large amounts of waste, due to the catalytic nature of the reaction as opposed to stoichiometric reactions (Venuto, 1994).

An even more impressive application of zeolite catalysts is in fluidized catalytic cracking (FCC) units which has led to enormous savings in crude oil usage in order to reach the desired gasoline outputs (Moscou, 1991). Thus, more economic use of our crude oil resources was made possible by zeolite catalysts. In recent years, not only gasoline yield, but additionally gasoline quality (octane number) has become important and the present tailoring of zeolitic acid site properties is directed to the optimum combination of gasoline yield with high octane quality.

Zeolites also play an important role as catalysts for environmental control (Iwamoto, 1994). For this purpose they need to operate under severe conditions, such as over a very wide temperature range, high space velocities, low concentrations of target materials and high concentrations of co-exiting gases and poisons. Thus the environmental catalysts must have extremely high activity, selectivity and durability. Zeolites with their characteristic regular and relatively stable crystalline structures, acidic and ion exchange properties fit these requirements and may have the potential to be used extensively in this field of catalysis.

Considerable research has therefore been undertaken on the use of zeolite-supported metal catalysts for gas purification. In this regard, zeolites have been evaluated as catalyst supports for the metal function in the reduction of NO_x and SO_x (Smirniotis *et al.*, 1999), which cause acid rain and are dangerous to both the terrestrial and aquatic ecosystems. Effective catalysts for these reactions are metal exchanged H-ZSM-5 zeolites, examples of which are CoH-ZSM-5, MnH-ZSM-5, CuH-ZSM-5, NiH-ZSM-5, etc. (Li and Armor, 1993; Iwamoto, 1994). CoH-ZSM-5 was found to be the best of these followed by MnH-ZSM-5, because their reactivity increases even in the presence of oxygen and higher temperature. CuH-ZSM-5 is less useful since it deactivates in the presence of water (Li and Armor, 1993).

Some other examples where zeolites are used as environmental catalysts are the following: zeolites can adsorb or decompose chlorofluorocarbon's (CFC's) which destroy the ozone layer. Examples of these processes are the adsorption of CFC-12 by alkali or alkali earth metal ion-exchanged faujasite zeolites and the decomposition of CFC-11 to CFC-12 by zeolites H-Y and Cr-Y (Karmakar and Greene, 1992). Zeolites are used to remove compounds with a bad smell, such as the oxidative decomposition of trimethylamine (Kuwabara *et al.*, 1992). The zeolite 13X has also been used to remove SO_x and NO_x (Karmakar and Greene, 1992) and 5A for the removal of methylmercaptans (Dyer, 1988).

An application of the H-ZSM-5 zeolite is as a component of FCC catalysts, designed to give a product of high octane number (Dyer, 1988; Gates, 1992). H-ZSM-5 is also an excellent catalyst for conversion of methanol to gasoline (Venuto, 1994; Stöcker, 1999). In the 1980's, the New Zealand government joined up with Mobil to develop a full-scale MTG (methanol-to-gasoline) plant at Motanui in north Taranaki. This could produce 1665 tons of petrol per day which could then satisfy 30% of New Zealand's gasoline demand at that stage (Sie, 1994).

In the conversion of methanol to hydrocarbons, the reaction sequence involves the dehydration of methanol to dimethyl ether, and the equilibrium mixture formed is then converted to alkenes and these then react to form alkanes, naphthenes and higher alkenes, with the reactions proceeding via the classical carbenium ion intermediates. Durene (1,2,4,5-tetramethylbenzene) is the highest boiling compound found in gasoline (Venuto, 1994). There is still, however, much speculation in the literature (see Stöcker, 1999) as to the mechanism for the formation of the first C-C bond. In the MOGD process, H-ZSM-5 has been used for the oligomerization of light olefins into gasoline and diesel (Venuto, 1994).

To enhance, for example, the catalytic activity of ZSM-5 for processes such as dehydrogenation and aromatization of alkanes, H-ZSM-5 may be ion-exchanged with a metal cation such as Ag^+, Ga^{3+} or Zn^{2+} to form AgH-ZSM-5, GaH-ZSM-5 or ZnH-HZSM-5 respectively (Ono et al., 1994; Mériaudeau and Naccache, 1995). The metal ion-exchanged, or even impregnated H-ZSM-5 zeolites, then act as bifunctional catalysts for the dehydrogenation of alkanes to alkenes (e.g. butane to butene) over the metal function, and the acid sites than catalyze reactions such as cracking, oligomerization and cyclization to produce aromatics. With ZnH-ZSM-5 and GaH-ZSM-5, dehydrogenation activity is enhanced as compared to H-ZSM-5 (Ono and Kanae, 1991; Kwak et al., 1994) and this is due to the fact that zinc and gallium cations are good dehydrogenation catalysts (Kwak and Sachtler, 1994).

The zeolite H-ZSM-5 has also found application in the thermocatalytic conversion of polyalkene waste (Pellet et al., 1995). The polymer is thermally or catalytically cracked at the external surface of the zeolite, then the subsequent cracking reactions taking place inside the zeolite pores are directed towards the desired products by appropriate choice of the reaction conditions.

The zeolite ferrierite is also one of the important shape selective catalysts which has seen industrial application (Mooiweer et al., 1994). It has been found to be a highly suitable catalyst for the skeletal isomerization of n-butene to isobutene (Grandvallet et al., 1992), which is the olefin procursor for the production of methyl tert-butyl ether (MTBE). This is the oxygenate which is currently still being used as an octane booster for gasoline.

The superior catalytic performance of ferrierite has been ascribed to the high acid strength of the zeolitic acid sites which allows the reactions to proceed at relatively lower reaction temperatures. The skeletal isomerization reaction has been proposed to proceed via the dimerization of the

butenes, skeletal isomerization and subsequent mild and selective cracking to *n*-butene and isobutene (Mooiweer *et al.*, 1994). The skeletal isomerization of *n*-butene to isobutene is a difficult reaction to control because the dimerization and aromatization reactions may interfere in terms of both selectivity and catalyst stability. Ferrierite, however, has been shown to be an excellent catalyst for this reaction and the selectivity to isobutene may be as high as 90% at *n*-butene conversion levels of 40% and higher (Naber *et al.*, 1994).

The isobutene so formed can then be reacted with methanol over Amberlyst 15 as catalyst to form MTBE (Hutchings *et al.*, 1992). It should be noted, however, that MTBE is currently under scrutiny and is been phased out as an octane booster in the USA due to its solubility in water, leading to the contamination of water supplies and other bodies of water. The usage of MTBE as an octane enhancer in Europe, however, might still be continued (Corma, 2001). Furthermore, isobutene could also be dimerized, to produce a high octane product (Sanfilippo, 2000).

When different catalyst options were considered for the skeletal isomerization reaction of linear butenes to isobutene, it was found that some zeolites and related molecular sieves show higher selectivity to isobutene than amorphous catalysts, such as the halogenated aluminas, which were previously extensively studied as catalysts for this reaction (see review by Butler and Nicolaides, 1993). The main reason for the superior catalytic behaviour of some zeolites comes from their unique pore architecture, which can limit the extent of the undesired oligomerization reactions occurring inside the microporous structure. It is then obvious that the zeolite structure plays a very important role in selectively catalyzing the isomerization of *n*-butene to isobutene.

Thus, apart from ferrierite, it has been shown that other medium-pore zeolites (ten-membered ring windows) were significantly more selective than large-pore ones (twelve-membered rings).

However, even with ten-membered ring zeolites, the presence of large cavities or channel intersections in the structure leads to a decrease in the isobutene selectivity. Therefore, the pore system is one of the primary factors governing isobutene selectivity in zeolite catalysts, and in this sense, zeolites such as ZSM-23, Theta-1 and its isostructural ZSM-22, as well as the aluminophosphates SAPO-11 and MnPO-11 with a monodirectional system of channels, show a high selectivity to isobutene (Asensi *et al.*, 1998).

As indicated above, the zeolite ZSM-35/ferrierite (FER structure), possessing a two dimensional system of intersecting ten-membered ring (4.2Å X 5.4Å) and eight-membered ring (3.5Å X 4.8Å) channels, has proven to be a highly selective butene isomerization catalyst, and unlike other catalysts, this zeolite also exhibits stable catalytic activity with time-on-stream (TOS) for this reaction (Grandvallet *et al.*, 1992). The narrow micropore diameter of ferrierite limits the formation of coke inside the channels (Pellet *et al.*, 1995; Xu *et al.*, 1995b).

It was also recently reported by Nicolaides (1999) that ZSM-5 zeolites-based materials with extremely low levels of percentage XRD crystallinity (e.g. of only 2% XRD crystallinity) can successfully be utilised as catalysts for the isomerization of 1-butene to isobutene. This work, therefore, illustrated the importance of the percentage crystallinity as a parameter in zeolite synthesis and catalysis.

1.4 AIM AND OBJECTIVES

Since zeolites are such an important family of catalysts for hydrocarbon conversion reactions, as well as for other applications, further understanding of the different methods of synthesizing and characterizing zeolites, and of the effect of the different parameters on the percentage

crystallinity and morphology of the zeolitic materials obtained, is of crucial importance. This is further accentuated by the fact that the level of crystallinity of a zeolite is an important parameter in terms of their catalytic properties, as was recently demonstrated by Nicolaides (1999).

In a previous study (Ramatsetse, 1998), the zeolites ZSM-5 and ferrierite were synthesized with and without stirring at different temperatures using one synthesis method for each zeolite and an in-house built autoclave. Of particular interest in this project, therefore, was to investigate the effect of different synthesis methods on the type of zeolitic products obtained in terms of percentage crystallinity and morphology. A detailed study was therefore undertaken of each synthetic procedure in terms of achieving reproducibly the synthesis of zeolitic materials that span the whole range of crystallinities, ranging from the substantially amorphous to the highly crystalline. Parameters that were varied in the different recipes used were temperature, stirring mode, seeding, source of silica, particle size of silica source, etc.

Catalytic test reactions (CTR's) were carried out on some of the zeolitic materials in order to determine differences in catalytic activity of the zeolitic materials which have approximately the same percentage XRD crystallinity, but were synthesized using different autoclaves and/or different hydrothermal synthesis procedures.

To attain the above-mentioned aims, a review of the literature was carried out on the methods of synthesis of the zeolites ZSM-5 and ferrierite, which are the two zeolite types that we will be focussing on in this thesis, and the factors affecting the zeolitization process (Chapter Two) as well as the characterization of zeolites (Chapter Three).

In this project the above-mentioned two types of zeolites were synthesized using both a Parr

autoclave and the in-house built autoclave. Seven different methods in total were used for synthesizing these two zeolites (four for ZSM-5 and three for ferrierite) and the zeolite or zeolite-based products obtained were then characterized by XRD, scanning electron microscopy (SEM) and CTR's.

CHAPTER TWO

SYNTHESIS OF ZEOLITES

2.1 INTRODUCTION

The formation of natural zeolites with volcanic glass and saline water as reactants occurred in the temperature range of 27°C to 55°C and required crystallization times of as long as 50 000 years. Barrer's gel method was proposed as early as 1940 as a means of simulating these natural conditions. The primary variables of this method are synthesis temperature, reactivity of the silica source, silica to alumina ratio and nature of the alkali (Jianquan *et al.*, 1994). Presently, a lot of work is being done on the mechanism of zeolitization and the development of novel zeolites.

2.2 ZEOLITIZATION IN GENERAL

The hydrothermal synthesis of zeolites involves a few elementary steps by which a mixture of silicon and aluminium species, metal cations, organic molecules and water is converted via an alkaline supersaturated solution into a microporous crystalline aluminosilicate. The complex chemical processes involved in this transformation can be denoted as zeolitization (Feijen *et al.*, 1994). Common precursors of the silicon species are colloidal silica, water glass, fumed silica or silicon alkoxides such as tetramethyl and tetraethyl orthosilicate. It is essential to realize that the silicon sources might be different in terms of the degree of polymerization of the silicon species. Aluminium species can be derived from sources such as gibbsite, pseudo-boehmite, aluminate

and metallic aluminium powder. Cationic or neutral organic molecules can act as solvent or as structure-directing agents (pore fillers) (Feijen *et al.*, 1994).

Examples of the above-mentioned structure-directing agents are tetraethylammonium ions, ethylenediamine, 1,6-hexanediamine, tetrabutylammonium ions, tetrabutylphosphonium ions, tetrapropylammonium bromide, pyridine, piperidine, pyrrolidine, etc. (Ernst *et al.*, 1989; Jansen and Wilson, 1991; Grandvallet *et al.*, 1992; Xu *et al.*, 1995a). From these templates, the linear ones (e.g. 1,6-hexanediamine) are used to synthesize the zeolites which have one dimensional (1-D) and two dimensional (2-D) channel systems, such as zeolites ZSM-22 and ZSM-48, while the branched templates (e.g. tetrapropylammonium bromide) are used for the synthesis of zeolites with three dimensional (3-D) channel systems, such as zeolites ZSM-5, ZSM-11, etc. (Gunawardane *et al.*, 1988).

The process of zeolitization is thermally activated and usually takes place at elevated temperatures in an autoclave (hydrothermal synthesis conditions) in order to achieve a high yield of crystals in an acceptable period of time. On the basis of the chemical phenomena occurring during zeolite genesis, the process can be divided into three basic steps: achievement of supersaturation, nucleation and crystal growth. The ageing or ripening of the gel describes the time period and the phenomena occurring after the preparation of the gel, when the gel is left below crystallization temperature. It should be noted that the addition of an aluminate solution to a silica sol increases the ionic strength of the solution, resulting in the immediate appearance of a gel, that is, the stabilized sol forms colloidal particles (Feijen *et al.*, 1994). After ageing, the hydrogel is heated (usually in an autoclave) up to the appropriate crystallization temperature, which is very often below 350°C.

When the desired crystalline products are obtained, the mother liquor is decanted. The crystals are then washed several times with distilled water to remove unwanted ions or unreacted reagents. If there is still a gel phase present, this may either precipitated out as a separate phase or be adsorbed onto the crystals. In both cases, the gel may be carefully dissolved in a dilute basic hydroxide solution at a slightly elevated temperature before the isolation of the zeolite (Jansen and Wilson, 1991).

After hydrothermal synthesis, the zeolite crystals must not be left in contact with its mother liquor for a long period of time since the crystals may re-crystallize with time to form another zeolitic phase. For example, when zeolite A is left in contact with its mother liquor for a long time, it re-crystallizes to zeolite P, and this latter phase will then transform into hydroxy sodalite (Szostak, 1989). According to Jacobs and Martens (1987), after prolonged ageing of ZSM-5 zeolite in its mother liquor, the metastable but open ZSM-5 structure is transformed into dense silica-rich and aluminium-rich structures, such as cristobalite and analcime respectively.

Furthermore, in the case of ZSM-5, at the early stages of the crystallization process, a silica framework with the MFI zeolite structure is formed where most of the aluminium atoms are excluded (Jacobs and Martens, 1987; Yi and Ihm, 1993). This structure gradually dissolves and the aluminium is incorporated in the lattice as re-crystallization occurs.

After purification, the zeolite is dried and calcined to burn off the template after which its void volume is free for different modifications and/or applications (Jansen and Wilson, 1991). Care must be taken not to deviate from the required temperature since too high a temperature may destroy the zeolite structure (Szostak, 1989).

2.3 FACTORS AFFECTING THE SYNTHESIS OF ZEOLITES

There are several factors that affect the crystallization kinetics and product formation during the synthesis of zeolites. Examples of such factors are: types of reagents used, alkalinity of the reaction mixture, the way the reaction mixture is made and the reaction conditions employed during the hydrothermal synthesis. Some of these factors are discussed below. Under types of reagents, the influence of the kind of template, silica source and the SiO_2/Al_2O_3 ratio will be described as well as the effect of the hydroxide concentration. In addition, the following hydrothermal reaction conditions will be dealt with: temperature, reaction time, stirring rate and seeding.

2.3.1 Template

Templates, or structure-directing species, are agents which in general kinetic and thermodynamic terms contribute to the formation of the zeolite lattice during the zeolitization process by (i) influencing the gelation and/or nucleation processes where the TO_4 (T = Si or Al) units are organized into a particular geometry around the template species and, as a result, provide precursor species for further nucleation or crystal growth; (ii) lowering the chemical potential of the lattice formed upon inclusion of the templates during zeolite synthesis. This template inclusion contributes to the stability by new interactions (hydrogen bonds, electrostatic and London dispersion interactions) and further controls the formation of a particular topology through its geometry (form and size). Changes in the cation density provoked by the geometrical or physical properties of the template will be reflected in the chemical composition (SiO_2/Al_2O_3 ratio) of a given topology (Szostak, 1989; Feijen *et al.*, 1994).

Cations as well as neutral molecules are able to fulfill this structure-directing and composition-directing function. Each of these types can be organic or inorganic in nature (Feijen *et al.*, 1994). Besides acting as counterions to balance the zeolite framework charge, the inorganic cations present in the reaction mixture often appear as the dominant factor determining which structure is obtained (Szostak, 1989).

In the literature, it is commonly found that authors refer to the addition of organic structure-directing reagents to the reaction mixture as templated synthesis, while if the synthesis is templated by inorganic (primary) cations present in the hydrogel, it is referred to as a template-free synthesis. This terminology will also be adopted in this work. Besides its structure-directing role, the organic template can:

(i)   act as a gel modifier, which would result in the formation of structures with higher SiO_2/Al_2O_3 ratio than could have been obtained in the absence of the organic additive;

(ii)   interact chemically with other components of the gel, altering the character of the gel (e.g. increasing the pH of the solution by the presence of amines and quaternary ammonium hydroxides);

(iii)   interact physically with other components of the gel so as to alter the gelling process, solubility of the various species, ageing characteristics, transport and thermal properties, and time of crystallization (Szostak, 1989).

Even though the presence of the organic species in solution exerts a strong influence on the structure that is crystallized, water (a neutral molecule) too can "tip the balance" to which structure crystallizes (Szostak, 1989). In an examination of the system containing pyrrolidine, Suzuki *et al.* (1986) found that in the crystallization of ZSM-39, ZSM-48 and KZ-1 (ZSM-23), by only changing the H_2O/SiO_2 ratio from 20 to 80 shifted the type of zeolite structure that could

be obtained from the synthesis mixture. Their results showed that the crystalline products obtained from the reaction mixture with SiO_2/Al_2O_3 molar ratio of ~280, were ZSM-39 in a lower H_2O/Al_2O_3 field (~24) and ZSM-48 in a higher H_2O/Al_2O_3 field (~75). Moreover, when the H_2O/Al_2O_3 molar ratio was increased from 24 to 79, the solid product that crystallized from the reaction mixture with SiO_2/Al_2O_3 molar ratio of 205 was changed from KZ-1 to ZSM-48. Other templating neutral molecules that have been used are amines, ethers, alcohols, di- and triols, etc. (Jansen and Wilson, 1991).

The size and shape of the zeolite obtained could also depend on the type of template used in its synthesis. For example, if pyrrolidine is used as template in the synthesis of the ZSM-5 zeolite, cubic and elliptical crystallite structures (see Figure 2.1(a)) are obtained and their sizes range from 0.7 μm to 3 μm. When all the other reagents are kept the same, and pyrrolidine is substituted by tetrapropylammonium bromide, only twinned cubical crystal structures (see Figure 2.1(b)) with diameters of 3 μm to 10 μm are obtained (Suzuki et al., 1986).
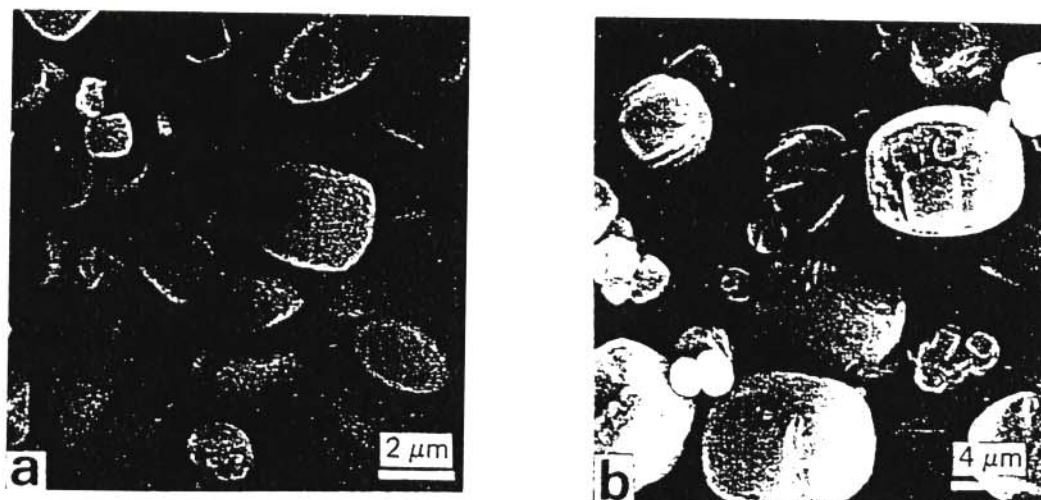
Figure 2.1 Scanning electron micrographs of (a) ZSM-5 (pyrrolidine) showing the cubed and elliptical morphology and (b) ZSM-5 (tetrapropylammonium bromide) showing the twinned cubic morphology (taken from Suzuki et al., 1986).

So far, it has not been possible to predict which template is required for a given structure and composition. The same zeolite can be synthesized by using different templates. An example of this is the use of tetrapropylammonium bromide (Van Grieken *et al.*, 2000) or 1,6-hexane-diamine (Jianquan *et al.*, 1994) as templates for the synthesis of the zeolite ZSM-5. Similarly, the same template can be used to synthesize *different* zeolites, and an example of this situation is that 1,6-hexanediamine can also be used as template for the synthesis of the zeolite ZSM-22 (Simon *et al.*, 1994; Byggningsbacka *et al.*, 1998). In selecting possible templates, however, one has to bear in mind some general criteria regarding templating potential in zeolitization, such as solubility in the solution, stability under synthesis conditions, steric compatibility and possible framework stabilization. The removal of the template without destroying the framework of the zeolites can also be an important practical issue (Feijen *et al.*, 1994).

Zeolites can also be synthesized without an organic structure-directing template. For instance, although the zeolite ZSM-5 can be synthesized with different organic templates as mentioned above, it can also be synthesized without using any structure-directing organic template (Dyer, 1988; Otero Areán *et al.*, 2000). The main thrust for template-free synthesis is its lower cost and reduced use of toxic reagents. However, successful template-free preparations of the MFI structure are limited to a narrow range of aluminium concentrations (SiO_2/Al_2O_3 ratios between 50 and 100) (Szostak, 1989; Otero Areán *et al.*, 2000). At higher ratios, non-zeolitic phases precipitate, including kenyaite and magandiite. Another disadvantage is that the template-free ZSM-5 is not stable in its mother liquor.

The zeolite ferrierite can also be synthesized without using any structure-directing organic template, but the template-free ferrierite has a higher mesopores/micropores ratio than the templated ferrierite (Xu *et al.*, 1995a) prepared using pyrrolidine as template. Another dis-

advantage of the template-free ferrierite is that it is of lower crystallinity than the template-synthesized ferrierite samples. Different morphologies for the templated and untemplated materials were also reported (see Figure 2.2). Dutta *et al.* (1992) also synthesized ferrierite with and without an organic template and it was found that the template-free samples took a longer time (648 hours) and higher temperatures (220°C) to crystallize than the templated samples, which required only 80 hours at 165°C.

(a)   (b)
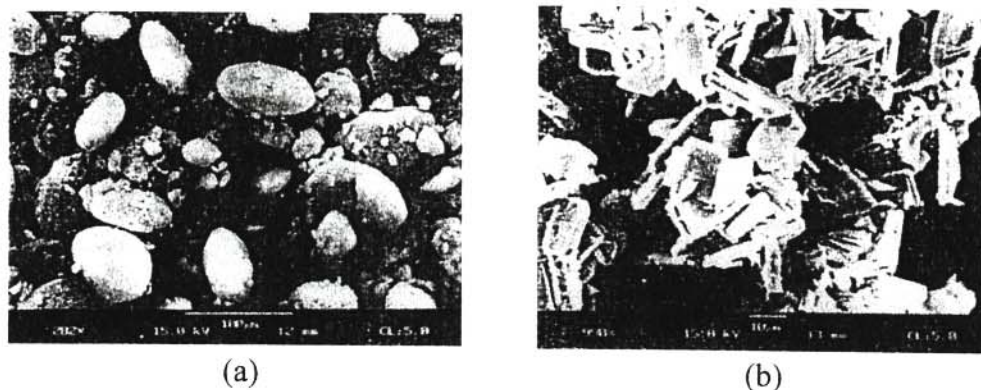
Figure 2.2 SEM micrographs of different ferrierite samples obtained from: (a) untemplated and (b) templated synthesis (taken from Xu *et al.*, 1995a).

2.3.2 **Silica source**

A review of the literature (Jansen and Wilson, 1991) has revealed that for the laboratory scale synthesis of zeolites, certain silica sources are commonly preferred. Depending on the particular synthesis used, a certain quality of silica source might favour the rate of product formation. For instance, Aerosil 200 can be more readily dissolved compared to the Optipur and Gold Label materials because of the difference in particle size. As the rate of dissolution can influence the rate of nucleation and crystallization, the rate of product formation is also affected. Jacobs and Martens (1987) also reported on the effect of different silica sources on the morphology of the zeolite ZSM-5 formed. Aerosil 200, with different gel concentrations, and water glass were used

to synthesize the zeolite. The Aerosil 200 method with relatively diluted gel concentrations gave crystals in the shape of elongated hexagons (Figure 2.3(a)) while with the more concentrated solution smaller twinned cubes were obtained (Figure 2.3(b)). On the other hand, with the water glass method, ZSM-5 with a different morphology, consisting of smaller elementary crystallites agglomerated together within a spheroidal formation, was obtained (Figure 2.3(c)).
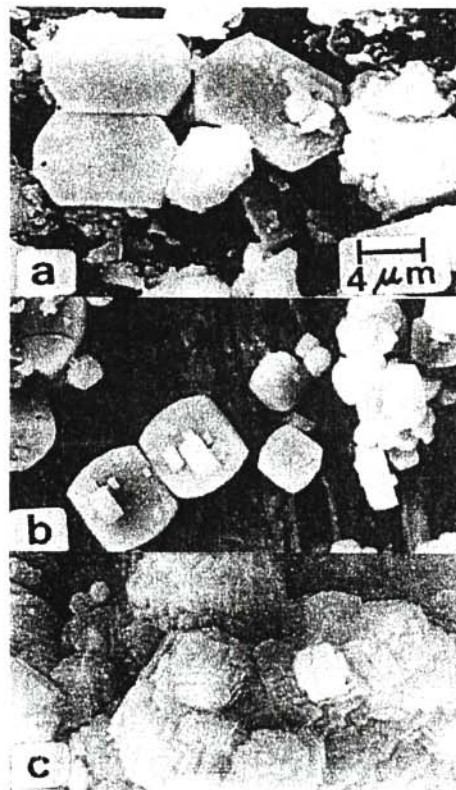
Figure 2.3 SEM micrographs of ZSM-5 prepared using different silica sources: (a) and (b) with Aerosil 200 and (c) with water glass (taken from Jacobs and Martens, 1987).

Impurities can also influence the crystal form and its chemical properties (Jansen and Wilson, 1991). Therefore a careful choice of reactants is needed. The high grade silicon alkoxides, of which even double alkoxides like -Si-O-Al- are available, do not have the above discussed disadvantages, except for the rate of hydrolysis of the alkoxide group.

2.3.3 **Molar composition of the hydrogel**

The chemical composition of a synthesis hydrogel is expressed generally in terms of an oxide formula of the following form:

$$aSiO_2:Al_2O_3:bM_xO:cN_yO:dR:eH_2O$$

in which M and N stand for (alkali) metal ions (if more than one is used in the synthesis) and R for the organic template. The relative amounts of Si, Al, M, N and R are one of the key factors determining the outcome of the crystallization. Apart from the nature of the templates used (organic or inorganic cations), the ratios SiO_2/Al_2O_3, $(M_xO + N_yO)/SiO_2$, R/SiO_2 and H_2O/SiO_2 can also influence the zeolitization process. This influence is exerted at the level of nucleation and crystallization kinetics, the nature of the crystalline material, the lattice aluminium content and distribution, and the crystal size and morphology. For example, the organic-free synthesis of ZSM-5 and mordenite was shown to be dependent on the Na_2O/SiO_2 ratio as well as on the SiO_2/Al_2O_3 ratio. ZSM-5 is preferred at higher SiO_2/Al_2O_3 and lower Na_2O/SiO_2 ratios in the gel (Feijen *et al.*, 1994). Of these ratios, the effect of the SiO_2/Al_2O_3 ratio on the synthesis of zeolites is the most widely investigated and is discussed in detail below.

SiO₂/Al₂O₃ ratio

As indicated by Jacobs and Martens (1987), the concentration of aluminium in the zeolite gel can influence the rate of crystallization of that zeolite. For ZSM-5, the higher the aluminium content, the lower the rate of crystallization and thus the lower the percentage XRD crystallinity of the batch for a given synthesis time and temperature (Mahada *et al.*, 1999). In addition, different SiO_2/Al_2O_3 molar ratios can produce different crystal shapes of ZSM-5 zeolite (Jacobs and Martens, 1987; Kim *et al.*, 1998). Di Renzo (1998) also reported that for ZSM-5 the higher the aluminium content, the lower the rate of crystallization and the smaller the crystal sizes, which

could be beneficial in some catalytic applications. Suzuki *et al.* (1986) found that in the synthesis of ZSM-5 zeolites, the sizes of the crystals formed increased from 1 μm to 3 μm in diameter when the SiO_2/Al_2O_3 ratio was increased from 52 to 360. Similarly, Kim *et al.* (1998) reported that the average particle sizes increase from 0.65 μm to 2.01 μm for their synthesis of ZSM-5 when the SiO_2/Al_2O_3 ratio increased from 50 to 492 (see Figure 2.4). Xu *et al.* (1995a)

Si/Al = 100

Si/Al = 200

Si/Al = 242

Si/Al = 488

Si/Al = 984
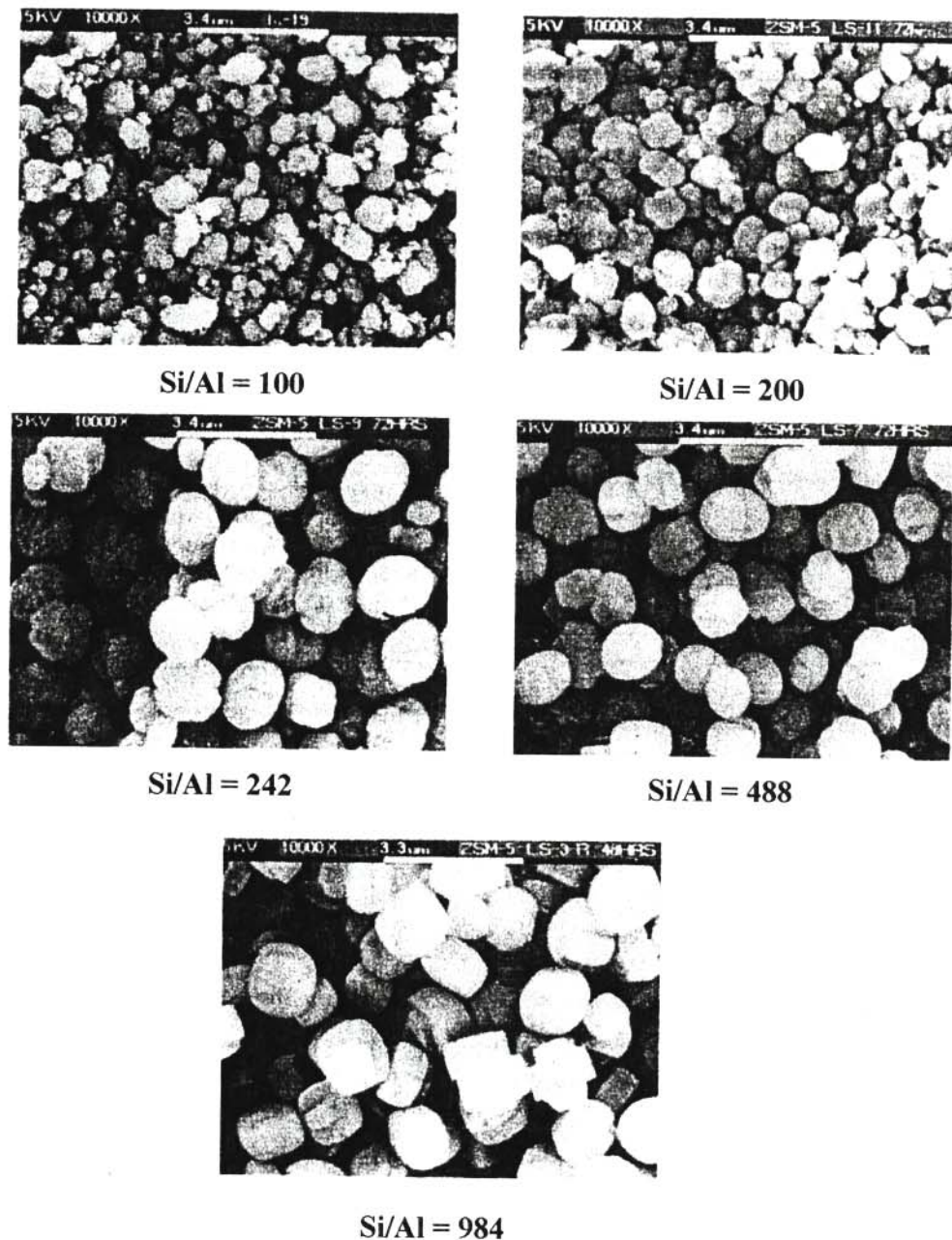
Figure 2.4 Scanning electron micrographs of ZSM-5 with various SiO_2/Al_2O_3 ratios at the same magnification, X 10 000 (taken from Kim *et al.*, 1998).

also observed that the morphology of the zeolite ferrierite depended on the SiO_2/Al_2O_3 ratio of the reaction mixture. At the SiO_2/Al_2O_3 ratio of 10, a sheet-like morphology was obtained whereas a hexagonal morphology was detected at the SiO_2/Al_2O_3 ratio of 20.

The change in SiO_2/Al_2O_3 ratio is also used as a method for "fine-tuning" the pore openings of zeolites (Smart and Moore, 1995). An increase in the proportion of silicon will (i) slightly decrease the unit cell size and thus the size of the cavities; (ii) decrease the number of cations, thus freeing the channels; (iii) make the zeolite more hydrophobic ("water fearing") in character.

2.3.4 Alkalinity

The pH of the alkaline synthesis mixture, which is generally between eight and twelve, is of key importance for zeolite formation as the OH^- anion fulfills the crucial role of the mineralizing (mobilizing) agent (Feijen *et al.*, 1994). The role of the mineralizing agents is to bring the silicon and the aluminium oxides or hydroxides into solution at an adequate rate. Soluble and useful precursor species have the T-atoms in tetrahedral coordination and contain condensable ligands. In this way a supersaturated state is created which makes nucleation and crystal growth possible (Szostak, 1989). In general, increasing the pH will accelerate crystal growth, and shorten the induction period (period before formation of viable nuclei) by an enhanced reactant concentration.

The dissolution of the gel, promoted by the presence of OH^-, proceed via a nucleophilic S_N2 mechanism where the five-fold coordination of silicon in the transition state will weaken the siloxane bonds. This hydrolysis mechanism is depicted in Figure 2.5(a). The condensation
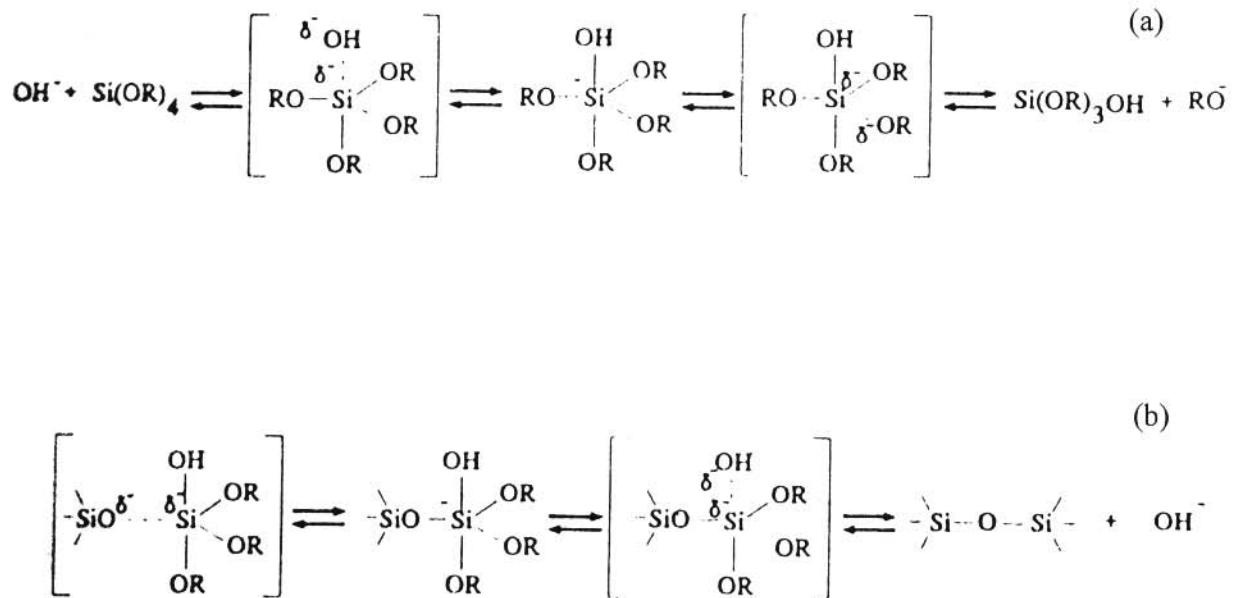
Figure 2.5 (a) Hydrolysis and (b) condensation reaction mechanism of silicate species (taken from Feijen *et al.*, 1994).

occurs via an attack of a nucleophilic deprotonated silanol group on a neutral species, as shown in Figure 2.5(b). This reaction explains the change in pH during zeolite crystallization from aluminosilicate gels (Feijen et al., 1994). It was reported that for the zeolite Eu-1 (Casci and Lowe, 1983) and for ferrierite (Xu *et al.*, 1995a), the pH decreases in the initial stages of hydrothermal synthesis, but after crystallization starts, it increases with increasing crystallinity. The rise in pH is attributed to the incorporation of SiO_2 units in the zeolite framework. After the completion of crystallization, the pH remains constant. It is thus possible to use these changes in pH as a simple and rapid method to follow the course of crystallization (Fegan and Lowe, 1986).

Another important feature of the alkalinity of aluminosilicate gels is that it influences the SiO_2/Al_2O_3 ratio of the crystalline product (Feijen *et al.*, 1994). The average lattice SiO_2/Al_2O_3 ratio shows a tendency to decrease with increasing pH of the synthesis hydrogel. This is readily

explained by a condensation mechanism which involves Si-O⁻ and/or Si-OH groups. An increasing pH reduces the ability of silicon species to condense through enhanced deprotonation. The increasing pH, however, will not influence the type of aluminium species present, as $Al(OH)_4^-$ is the aluminium species most exclusively present in alkaline solutions. The chance of a silicon species condensing with an aluminium species compared to other silicon species will increase with increased pH.

2.3.5 Temperature

In general, reaction temperature has a positive influence on the zeolite formation process; higher temperatures will increase both the nucleation rate and the linear growth rate, and the crystallinity therefore of the sample will normally increase with temperature. There is usually a limit to the temperature that could be used for maximum crystallinity of a pure phase, as would be observed in some of our results in Chapter 5 and Chapter 6, and a disadvantage associated with an increase in temperature is often the formation of a new phase in the required phase. Both nucleation and crystal growth increase with temperature which will have an opposing effect on the final crystal size (Feijen et al., 1994). Jansen and Wilson (1991) have reported that a change in synthesis temperature affects both the crystal growth rate and the crystal size of zeolites formed, that is, the rise in synthesis temperature within a certain ZSM-5 zeolite synthesis field increases both its crystal growth rate and its crystal size.

Other work done on the synthesis of ZSM-5 and ferrierite indicated that for a given synthesis time, temperature affects both the crystal morphology and the crystal size of the zeolites formed (Ramatsetse, 1998). While at lower temperatures the crystals and amorphous material obtained in the synthesis of ZSM-5 without stirring were agglomerated in spheroids, crystals of distinct

shape were, however, obtained at higher temperatures. In the case of ferrierite, few large well-developed rectangular plate-like crystals were already observed amongst the amorphous material after hydrothermal treatment at 150°C where an XRD crystallinity of 1% was obtained, while at higher temperatures (> 150°C), a larger number of smaller rectangular platelets were observed with no observable increase in size with further increases in temperature.

In the above-mentioned studies (Ramatsetse, 1998), the influence of temperature on the percentage XRD crystallinity for the zeolite ZSM-5 and ferrierite was also reported (see Figure 2.6 and Figure 2.7). The percentage crystallinity for the ZSM-5 samples synthesized without stirring increased with increasing temperature up to a constant plateau value. For the ZSM-5 samples prepared with stirring and for the ferrierite samples synthesized with and without
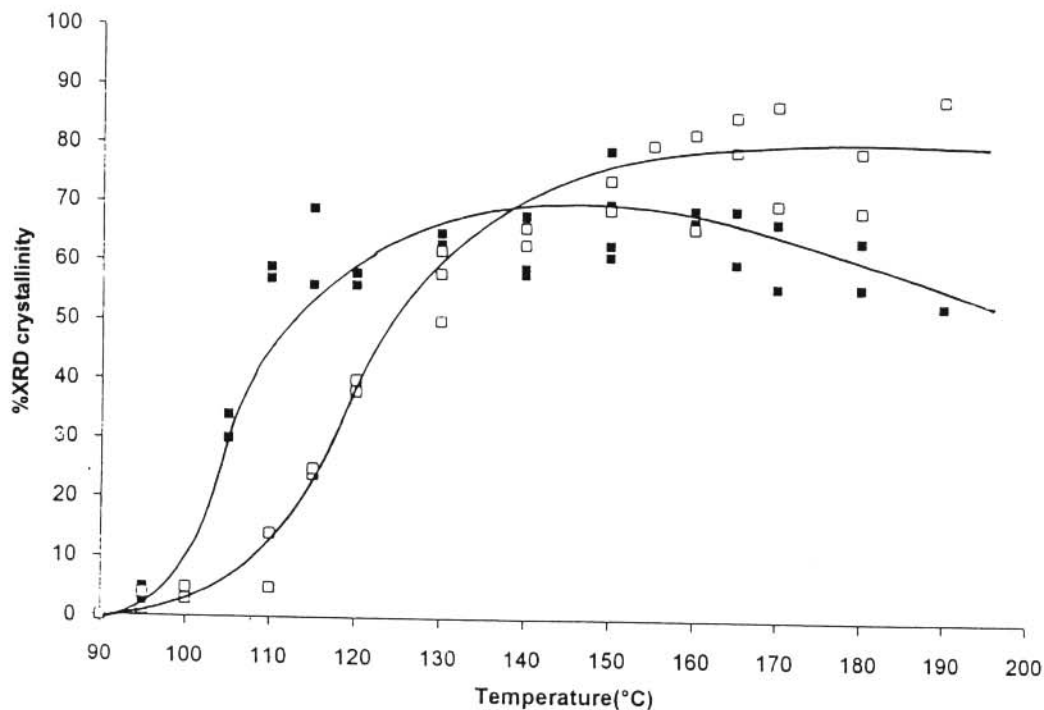
Figure 2.6 Plot of percentage XRD crystallinity of ZSM-5 zeolite-based samples synthesized in an in-house built autoclave versus synthesis temperature prepared with stirring at 1 000 rpm using a magnetic stirrer bar (■) and without stirring (□) (taken from Ramatsetse, 1998).
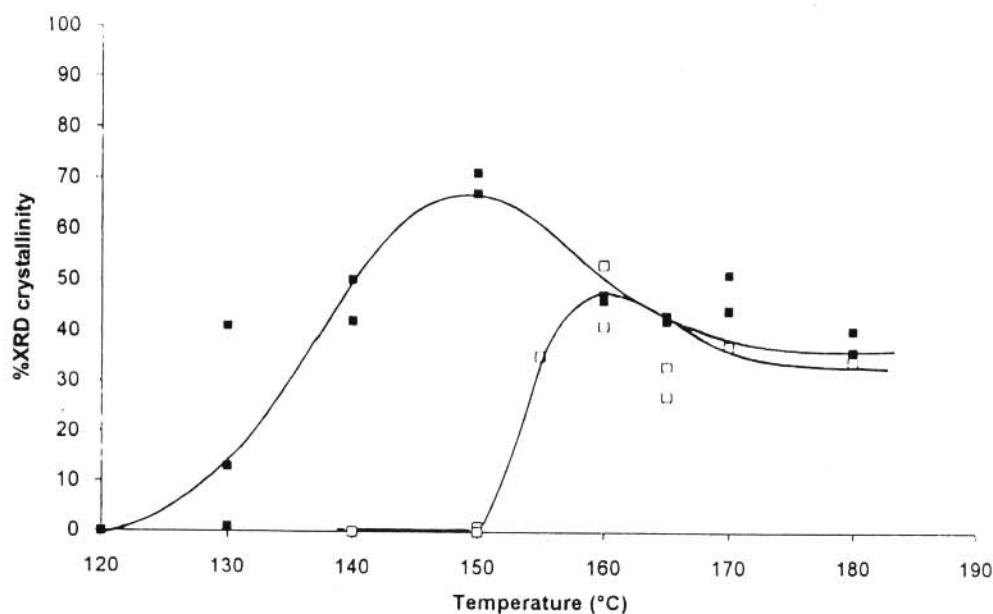
Figure 2.7 Plot of percentage XRD crystallinity of the ferrierite phase of samples synthesized in an in-house built autoclave versus synthesis temperature prepared with stirring with a magnetic stirrer bar at 1 250 rpm (■) and without stirring (□) (taken from Ramatsetse, 1998).

stirring (Figure 2.6 and Figure 2.7), the percentage crystallinity increased with increasing temperature up to a maximum value, followed by a decrease in crystallinity with a further increase in temperature, especially in the case of ferrierite (see Figure 2.7). For the latter zeolite, this decrease in crystallinity was concomitant with the formation of a new zeolitic phase which was subsequently identified by XRD to be α-quartz (see Section 6.2.1.2). For ZSM-5, Jianquan *et al.* (1994) also observed the formation of α-quartz at higher temperatures (e.g. 180°C) for their synthesis in an extremely dense system, called the "kneading method".

Increasing temperatures therefore give rise to denser products as the fraction of water in the liquid phase drops, since it has to stabilize the porous products by filling the pores. The existence of an upper temperature limit for the formation of zeolites is to be expected therefore. The use of non-volatile pore space occupying (filling) species would, in principle, allow the high

temperature synthesis of open, porous structures (Feijen *et al.*, 1994).

An example of the influence of temperature on the type of product that can be obtained at different temperatures is the formation of the zeolite ZSM-5 in zeolite ZSM-11 (Szostak, 1989). When ZSM-11 is crystallized using tetrabutylphosphonium chloride as template at 100°C, no crystalline material is formed before 72 hours. After 72 hours, only the single phase of ZSM-11 is formed. When the temperature is increased above 100°C but below 130°C, the induction time decreases and the rate of crystallization increases. When the temperature is increased up to and above 130°C, however, ZSM-5 is formed.

2.3.6 Reaction time

In general, reaction time has a positive influence on the zeolite formation process; the crystallinity of the sample normally increases with synthesis time. However, as far as time is concerned, zeolite synthesis is governed by the occurrence of successive phase transformations (Ostwald rule of successive phase transformation) (Feijen *et al.*, 1994). The thermodynamically least favourable phase will crystallize first, and will be successively replaced with time by the more stable phases. A typical example is the following crystallization sequence: amorphous → faujasite → Na-P (Gismondine type).

A template-free ZSM-5 zeolite is also affected by the reaction time duration and undergoes phase transformation to a more stable phase. When the template-free ZSM-5 zeolite is hydrothermally treated for a long time, it re-crystallizes into mordenite which can also transform into α-quartz, the more stable phase (Szostak, 1989).

To study the crystallization mechanism of nanocrystalline (crystal sizes in the range of 10 nm to 100 nm) ZSM-5 zeolite formation from supersaturated hydrogels, Van Grieken *et al.* (2000) carried out a kinetic study by varying the synthesis time at the constant temperature of 170°C. Figure 2.8 shows the X-ray diffraction patterns of the as-synthesized solids at different reaction times. The first solid material analyzed was that obtained after 6 hours under hydrothermal synthesis conditions, but as seen from the XRD patterns, it is completely amorphous. The first evidence of crystallinity is detected after 18 hours of reaction time, and the peaks become more intense as the crystallization proceeds up to 24 hours, where the material with a crystallinity of 100% was obtained, with the typical XRD pattern corresponding to the pure MFI structure. Figure 2.9 shows the changes in the crystallinity and the yields of amorphous material and ZSM-5 zeolite with synthesis time. At synthesis times higher than 24 hours the percentage crystal-
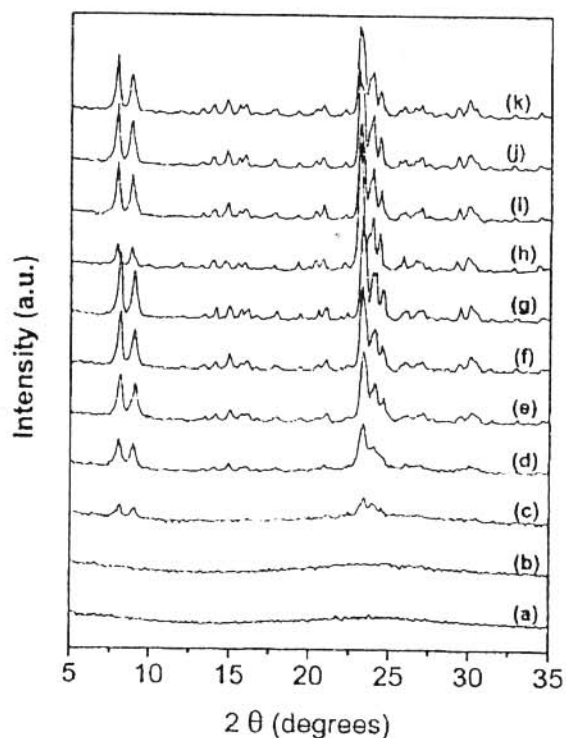
Figure 2.8 XRD spectra of the as-synthesized samples obtained at different reaction times: (a) 6 h, (b) 12 h, (c) 18 h, (d) 20 h, (e) 22 h, (f) 24 h, (g) 48 h, (h) 72 h, (l) 96 h, (j) 108 h and (k) 120 h (taken from Van Grieken *et al.*, 2000).
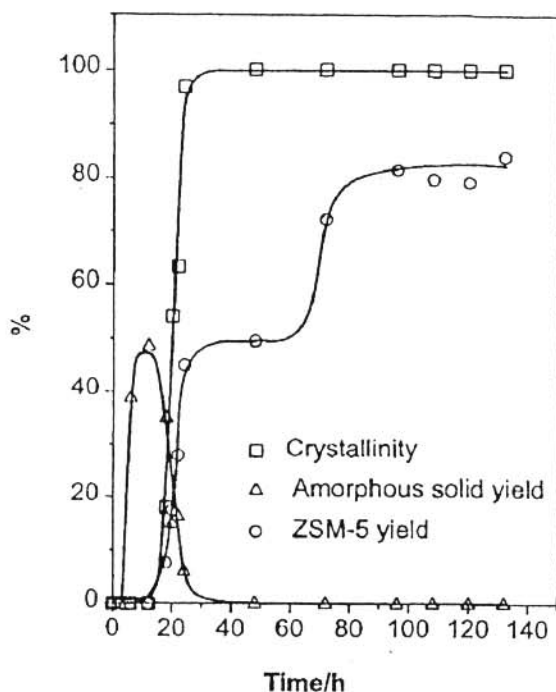
Figure 2.9 Crystallization kinetics and synthesis yield of amorphous solid and ZSM-5 (taken from Van Grieken *et al.*, 2000).

linity remains at 100%, but a step in the percentage yield occurs due to a different zeolitization mechanism. While the initial ZSM-5 crystallization proceeds through solid-solid transformation, which allows the initial amorphous material to be reorganized yielding the crystalline zeolite, after 48 hours the conventional two-step process takes place, starting from the remaining solution, viz. (i) formation of crystalline nuclei, and (ii) growth of these crystalline nuclei by progressive incorporation of soluble species.

It was also shown in this study (Van Grieken *et al.*, 2000) using transmission electron microscopy (TEM) that nanocrystalline ZSM-5 had been synthesized in only 24 hours of hydrothermal crystallization of the clear supersaturated homogeneous synthesis mixture. However, the crystallite sizes increase from 20 nm at 12 hours to 50 nm at 48 hours and increase further to 1 000 nm for a synthesis time of 108 hours.

In a study on the zeolite ferrierite by Xu *et al.* (1995a) it was found that the peak intensities in the diffractogram of the ferrierite sample synthesized for 100 hours were higher than the intensities of the ferrierite sample prepared with 60 hours of hydrothermal synthesis. This implies of course a higher crystallinity for the 100 hours sample than for the 60 hours sample. In other studies on ferrierite synthesis at 150°C and different preparation times up to 150 hours (Ramatsetse, 1998), it was observed that the crystallinity increased up to 79% for the hydrothermal synthesis time of 75 hours and then a decrease in the percentage XRD crystallinity was observed at higher synthesis times due to amorphotization.

2.3.7 **Stirring**

Synthetic zeolites are generally crystallized by heating an aqueous aluminosilicate gel slurry under autogenous pressure, and this process is affected not only by the gel composition but also by the agitation conditions of the slurry. Examples of these are tumbling, rotating, mechanical stirring and magnetic stirring. Some zeolites are crystallized only under stirring conditions, but other zeolites are exclusively obtained as a pure phase without stirring. Siliceous faujasite, zeolite Y, is a typical zeolite which crystallizes under static conditions, and moreover, it is necessary to add seed crystals or to age the gel at low temperature in order to crystallize the pure product (Kasahara *et al.*, 1986). On the other hand, it appears from the literature that all the synthesis methods for ZSM-22 involve agitation of some kind (Olson *et al.*, 1984; Jacobs and Martens, 1987; Simon *et al.*, 1994; Asensi *et al.*, 1998).

According to Jacobs and Martens (1987), in synthesizing high-silica zeolites, the stirring rate is an important parameter for the overall yield of crystalline material, because the amounts of crystalline material obtained with stirring are in most cases higher (up to 50%) than those

obtained under the unstirred conditions. These results are partly in agreement with other studies on the synthesis of ZSM-5 and ferrierite with and without stirring at different temperatures (Ramatsetse, 1998). The results for ZSM-5 show that with stirring, higher percentage XRD crystallinities were obtained at lower temperatures than for synthesis without stirring. However, at higher temperatures, it is the other way round (see Figure 2.6). Samples synthesized without stirring are more crystalline than those synthesized with stirring at the same temperature for temperatures above $140^{\circ}C$.

In the synthesis of ferrierite, the crystallinity was found to increase for batches prepared with stirring relative to preparations carried out without stirring up to a temperature of $150^{\circ}C$ (see Figure 2.7). Furthermore, the crystallization without stirring starts at significantly higher temperatures. With stirring, an average of 18.3% XRD crystallinity was already obtained at $130^{\circ}C$ while the first signs of crystallinity for the static preparation was at $150^{\circ}C$ (an average of 0.5% XRD crystallinity).

It was also observed in these studies (Ramatsetse, 1998) that stirring affects the morphology of the synthetic zeolites. The stirred ZSM-5 batches formed spheroids throughout the temperature range investigated (up to $190^{\circ}C$), while the unstirred samples form spheroids only at lower temperatures and crystals of definite morphology are obtained at temperatures higher than $150^{\circ}C$. For the ferrierite synthesis it was observed that although stirring increases the percentage XRD crystallinity, relative to the samples synthesized without stirring at the same temperature, it resulted, however, in broken up crystals.

Beschmann *et al.* (1994) synthesized ZSM-5 samples with stirring at 100 rpm or under static conditions, the aim being to obtain crystals of different sizes. The stirred samples gave smaller

crystals while the unstirred samples gave larger crystals (see Figure 2.10). Thus, stirring rates significantly affect crystal size. The effect corresponds to the formation of large zeolite crystals in viscous systems, where convective motion is hindered and mass transfer is diffusion controlled (Di Renzo, 1998).

(a)   (b)
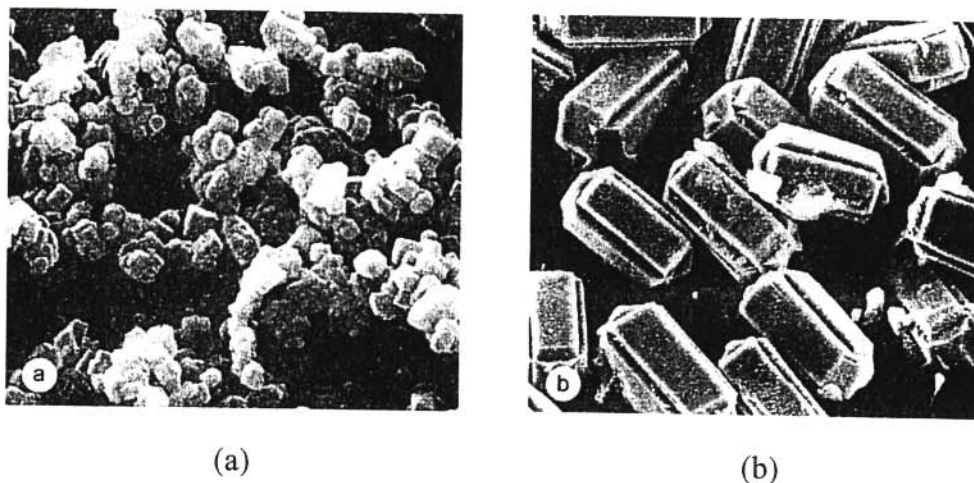
Figure 2.10 SEM micrographs of ZSM-5 zeolite samples synthesized: (a) cubic morphology obtained with stirring and (b) twinned hexagonal morphology obtained under static conditions (taken from Beschmann *et al.*, 1994).

It should be mentioned, however, that in most of the references on zeolite synthesis, it appears that the experiments were conducted in unstirred autoclaves.

2.3.8 **Seeding**

Seeding is a technique in which the supersaturated system is inoculated with small particles of the material to be crystallized. These seed particles (crystals) will increase in size as fresh crystalline material is deposited on them. By this operation the nucleation stage is in fact by-passed and total elimination of the induction period can be achieved. As the surface area

provided by the seed crystals is larger than the ones provided by the fresh nuclei, the seeding technique provides a favourable condition for measuring linear growth rate (Feijen *et al.*, 1994).

Bronić *et al.* (1999) also reported that seeding is a powerful technique for the control of zeolite synthesis pathways, and hence it is frequently used in studies of the kinetics and mechanism of zeolite crystallization. The most pronounced effects of seeding are shortening of the induction time and increasing of the crystallization rate. Such results were obtained by Kibby *et al.* (1974) for the synthesis of the zeolite ferrierite at 130°C (see Figure 2.11). In the seeded synthesis, crystallization was completed within 2 hours, while in the absence of seed, crystallization started later and took longer to complete. These effects were thought to result from the increased surface area available for crystal growth due to the presence of the seed, with the seed crystals growing at the expense of the gel phase (Thompson and Dyer, 1985). However, a study of the measurements of the crystal sizes showed that the seed crystals grow at a rate which differs only slightly from the rate of crystal growth in the unseeded system (Zhdanov, 1971).
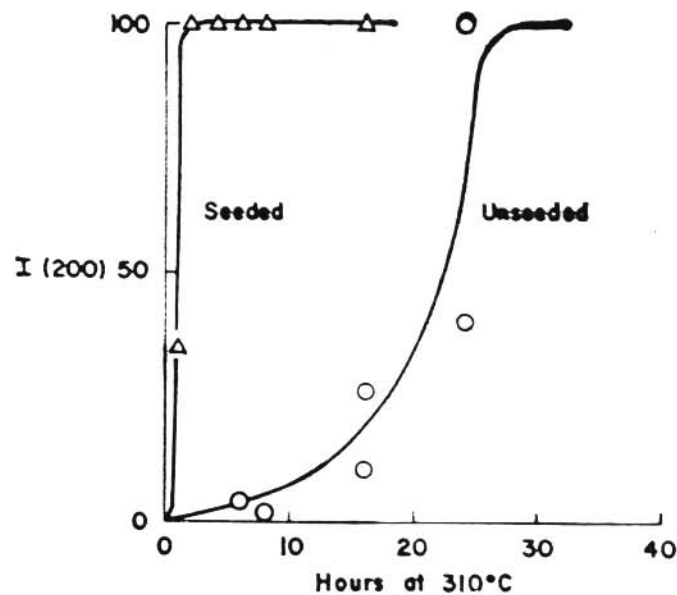
Figure 2.11 Kinetics of ferrierite crystallization (I (200) = % crystallinity) (taken from Kibby *et al.*, 1974).

Some other effects have also been observed in seeded zeolite crystallization systems. Koizumi and Roy (1960) found that some zeolites, like scolecite, can only be crystallized in the presence of a seed. Kacirek and Lechert (1975) found that the presence of zeolite X seed crystals cause crystallization of pure zeolite Y from a reaction mixture, while crystallization of zeolite P took place from the reaction mixture when seed crystals were not present. Similarly, Warzywoda and Thompson (1991) indicated that the presence of zeolite A seed crystals cause crystallization of pure zeolite A from a mixed Na/K-aluminosilicate gel ($K_2O/(Na_2O + K_2O) = 0.5$). In the absence of the seed crystals, the system resulted in a mixture of zeolite K-F (~95%) and zeolite A (~5%). On the other hand, crystal agglomeration was noted to occur when zeolite A seed crystals were put into an agitated system containing an amorphous gel and when fresh reagents were added to an ongoing crystallization.

As indicated by Warzywoda et al. (1991) and Bronić et al. (1999), the addition of seed crystals of different types of zeolites into a clear aluminosilicate solution may cause different nucleation phenomena:

(i)   the initial breeding may occur in silicate systems with dried seeds;

(ii)   the phenomenon of polycrystalline breeding was observed when relatively large hydroxy sodalite seeds were put into a clear aluminosilicate solution;

(iii)   surface nucleation was observed on zeolite A seed surfaces in a clear solution environment.

Bronić et al. (1999) concluded that the presence of the seed crystals facilitates not only growth of the seed mass, but that more complex phenomena also occur. Especially interesting is that the evolution of seed crystals is quite different in a clear aluminosilicate solution than under the conventional synthesis conditions in which the seed and the gel are in close physical contact. To

study the simultaneous action of seed crystals on both the clear solution and the gel phase, Dutta and Bronić (1994) designed the membrane reactor. The permeable membrane separates the gel from the seed, but allows free passage of the reactive species (aluminate and silicate anions, OH^- and Na^+) present in the solution. Based on the study of the influence of zeolite Y seed crystals on the crystallization of zeolite Y and zeolite P from different reaction compositions in the membrane reactor, the authors arrived at several conclusions. The nuclei do not travel through the membrane with 2 000Å pores, indicating a limitation in their sizes and that the crystal growth occurs via a solution-mediated system. From a synthetic viewpoint, the possibility of independent nucleation of two different zeolites was shown, which were separated by the membrane but connected by a common reaction solution.

Ageing can also play the role of seeding. Gonthier and Thompson (1994) indicated that numerous studies have been conducted in which the mixed amorphous gel solution was aged at lower temperature prior to reacting at elevated temperatures. The role of ageing is that some amorphous gel solutions appear to need time during which the solution can form nuclei, even though at dramatically reduced rates, which can then become activated at elevated temperatures. These steps are sometimes necessary for successful crystallization, as in the case of zeolite Y, which can sometimes result in essentially complete crystallization at room temperature, or can at times result in a bimodal distribution of crystal sizes, or at other times produce no effect at all.

The magnitude of the temperature dependent parameters will determine the outcome of the ageing process. However, when nuclei are formed during room temperature ageing, the solution begins its high temperature period of the process as though one had added seeds. Thus, one notes the strong similarity between physically adding seed crystals, ageing solutions, which are known to form nuclei at room temperature, and adding nuclei-sized entities created elsewhere

(sometimes called "directing agents") to a fresh gel solution which were the result of a brief hydrothermal treatment sufficient only to create nuclei-sized entities.

2.4. ZEOLITE ZSM-5

In this section we will focus on the zeolite ZSM-5 in more detail, giving a brief historical background account to its development as an industrial catalyst, its structural properties and brief descriptions of the different methods available for the synthesis of this zeolite.

2.4.1 Historical background

ZSM-5 was first synthesized in 1965 by Landolt and Argauer (Degnan *et al.*, 2000). Their discovery was a direct result of Mobil's investigation of quaternary amines as structure-directing agents in zeolite synthesis. Because it was synthesized in very small quantities (less than 5 g), ZSM-5 remained a laboratory curiosity until 1967 when it was first evaluated for processing waxy gas oils. It was soon determined to be a very shape-selective material that cracked only normal or slightly branched paraffins. For much of the 1960's most of the research on ZSM-5 was directed toward the development of new dewaxing catalysts.

It is not surprising that efforts to assess the potential of ZSM-5 were delayed. Zeolite Y-based cracking catalysts were commercially introduced in 1964. During the 1960's a significant proportion of Mobil's catalytic cracking research and development effort was directed at improving the stability and effectiveness of these new zeolite Y-based catalysts, including detailed studies on ion exchange with rare earth cations.

When ZSM-5 was first evaluated as a cracking catalyst in the Mobil laboratories, its initial evaluation was quite unremarkable (Degnan *et al.*, 2000). A blend of 10% rare earth (e.g. La or Ce) exchanged zeolite Y (REY) and unsteamed 5% ZSM-5 in a fixed fluid bed gave the same octane improvement as REY alone. Separate experiments aimed at assessing the effect of processing wide cut FCC gasoline over ZSM-5 also showed that gasoline research octane was not affected. However, additional research showed that the heavier fraction of FCC gasoline (boiling above 82°C) could be separately upgraded over ZSM-5 and that the octane rating did increase when this was blended back with the lighter gasoline.

Research on ZSM-5 in cracking applications began to gain momentum in the early 1970's. By then, several studies with small quantities of ZSM-5 showed that mildly steamed ZSM-5 did in fact improve the gasoline octane number, but the mechanism by which this was occurring was not yet understood. Nevertheless, several key properties of ZSM-5 had to be evaluated prior to even considering it for service in Thermofor catalytic cracking (TCC) and FCC units. These included steam stability, metal resistance and selectivity maintenance (Degnan *et al.*, 2000).

2.4.2 Structural properties

ZSM-5 has the formula $M_{x/n}[(AlO_2)_x(SiO_2)_{96-x}].16H_2O$ and has the pentasil units as its building blocks; the pentasil units form chains which in turn are interlinked to form the three dimensional framework with ten-membered ring openings of approximately 5.5Å diameter. The Si-Al ordering within the tetrahedral framework is difficult to determine by conventional structural methods, but one of the guidelines has been that two aluminium atoms cannot be in adjacent tetrahedral sites (Lowenstein's rule) (Venuto, 1994).

In the structure of the ZSM-5 zeolite (Figure 2.12), each pair of double five rings (a) is hydrolyzed on the Si-O-Si bond to form opened double five ring species (b). The opened double five ring species dimerize by loosing water to form the dimeric secondary building units (SBU's) (c).

Figure 2.12 Formation of ZSM-5 zeolite via structure built up nucleated by the SBU's. Growth is through addition of TO_2 (where T = Si or Al) units to form the final crystalline structure. The process is always in equilibrium with the silicate species (taken from Szostak, 1989).

These dimers polymerize by the addition of free silicates to form chain building blocks (d). These chains are linked together through their oxygens by further addition of silicates to form a sheet (e). The sheets are stacked together through their inversion centers, also by the addition of silicates, to form ZSM-5 (f). If the sheets are joined through their mirror planes, they result in the formation of ZSM-11 (Szostak, 1989).

In both ZSM-5 and ZSM-11, the largest aperture into any enclosed volume is formed by the ten-membered oxygen rings (Flanigen, 1991; Szostak, 1989). There are two types of ten-membered oxygen rings. The first type is formed when those rings are joined together to form a straight channel. These are found in both ZSM-5 and ZSM-11. The second type is formed when those rings are joined together to form a sinusoidal channel which is found in ZSM-5 only (Kokotailo et al., 1978). In ZSM-5, the first type of channel is the dominant diffusion path (Haag, 1994).

The size of the pores forming the straight channel of ZSM-5 is 5.4Å X 5.6Å and that of the sinusoidal channel is 5.1Å X 5.5Å. Where these two channels intersect, a free volume of about 9Å in diameter is formed and this space is significant for catalysis. These two types of channels in ZSM-5 cancel out the counter-diffusion problems encountered in most zeolites and create "molecular traffic control". The larger molecules diffuse through the straight channels while the smaller ones can also diffuse through the sinusoidal channels (Venuto, 1994).

Thus, apart from the inversion centers and mirror planes, the difference between ZSM-5 and ZSM-11 can be observed from the difference in their hollow tube representation (see Figure 2.13). The hollow tube representations provide easy visualization of the difference in the pore system of these two zeolites (Szostak, 1989).
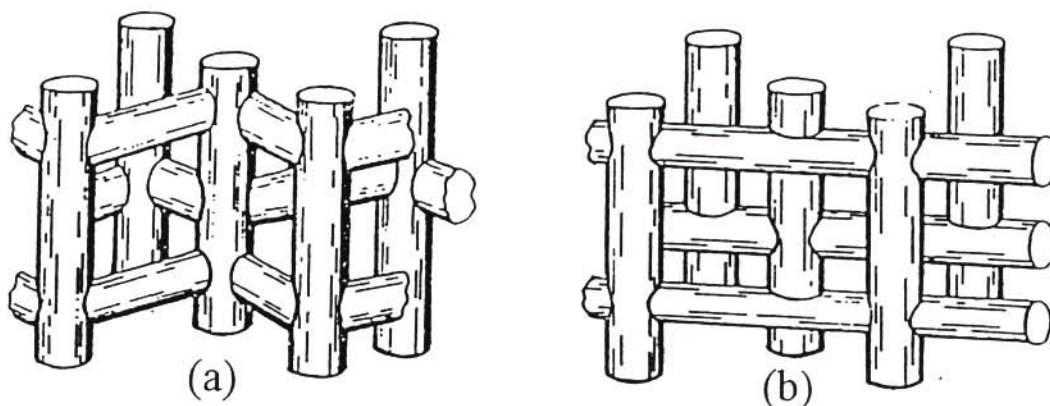
Figure 2.13 Hollow tube representation of the ten-membered ring zeolites: (a) ZSM-5 and (b) ZSM-11 (taken from Szostak, 1989).

2.4.3 Synthesis of ZSM-5

According to Derouane *et al.* (1981), increasing attention was devoted during the 1970's to the synthesis and the properties of new zeolitic materials crystallized in the presence of organic cations. Amongst these materials, zeolite ZSM-5 has received the greatest attention, not only because of its exciting catalytic properties for a variety of reactions (methanol to gasoline conversion, xylene isomerization, distillate dewaxing, ethylbenzene synthesis, upgrading of Fischer-Tropsch synthesis fractions, etc.), but also because it was the initial member of a large family of materials, the pentasil family, differing not only by their aluminium content, but also by a continuous change in their crystallographic structure (such as encountered when considering the ZSM-5 to ZSM-11 series) or inclusion of other elements such as iron, boron, arsenic, chromium, etc., substituting the aluminium atoms in the tetrahedra.

A great variety of synthesis procedures have been reported in the patent literature. Organic cations most usually employed are tetraalkylammonium (TAA) salts or bases (or their

precursors), amongst which the derivatives of tetrapropylammonium (TPA) and tetrabutyl-ammonium (TBA) seem preferable for the synthesis of ZSM-5 or ZSM-11 materials. A huge amount of research has also been carried out on the synthesis of the "aluminium-free" isomorph of ZSM-5, silicalite, where no aluminium source is intentionally added to the synthesis mixture.

Table 2.1 gives a summary of some ZSM-5 synthesis procedures reported in the literature (only recipes that give the amounts of all the reagents used in the procedure are listed in the table). As indicated in Table 2.1, it is generally found that although other templates can be used (e.g. 1,6-hexanediamine (C₆DN) (Jianquan *et al.*, 1994) and pyrrolidine (Suzuki *et al.*, 1986)), the template most commonly used for ZSM-5 synthesis is the tetrapropylammonium ion (TPA-Br or TPA-OH). Otero Areán *et al.* (2000) synthesized a template-free ZSM-5.

Although ZSM-5 is usually first synthesized in the sodium form (Na-ZSM-5), Beschmann *et al.* (1994) reported a method in which ZSM-5 was directly synthesized in ammonium form without any post-synthesis treatment. The alkali metal was substituted by ammonium in the synthesis gel in order to act as counter ion in the synthesized zeolite. On calcination it produced H-ZSM-5.

Fumed silica (Aerosil) is frequently used as the silica source amongst the synthesis methods summarized, but other sources such as silicic acid, water glass, tetraethylorthosilicate and colloidal silica (e.g. Ludox AS-40) have also been applied successfully. Different silica sources could result in differences in the product ZSM-5 formed. For example, Jacobs and Martens (1987) used the same synthesis composition but different silica sources, namely Aerosil and water glass, and obtained ZSM-5 zeolites with totally different morphology. The synthesis procedures summarized also show a large variety of aluminium sources that can be used, namely aluminium hydroxide, sulfate, nitrate, triisopropylate and sodium aluminate.

Table 2.1 ZSM-5 synthesis procedures

Si source	Al source	Template	Molar composition	Temp (°C)	Time (h)	Stirring (rpm)	Morphology	Particle size (μm)	Reference
Precipitated silica	Aluminium hydroxide	TPA-OH	$32SiO_2{:}Al_2O_3{:}3.96Na_2O{:}0.57(TPA)_2O{:}2035H_2O$	170	144	Unstirred			Anderson et al. (1979)
Fumed silica (Aerosil)	Sodium aluminate	TPA-OH	$60SiO_2{:}Al_2O_3{:}0.3Na_2O{:}24(TPA)_2O{:}1550H_2O$	150	144	Stirred	Rectangular plates	4 X 2	Jacobs et al. (1981)
Microspheroidal silica	Sodium aluminate	TPA-Br	$24SiO_2{:}Al_2O_3{:}3.6Na_2O{:}3(TPA)_2O{:}180H_2O.$	120	2 – 576	Unstirred	Twinned cubic to spheroidal	0.10 – 0.05	Padovan et al. (1984)
Silicic acid	Aluminium sulfate	TPA-Br	$84SiO_2{:}Al_2O_3{:}15.8Na_2O{:}9.5(TPA)_2O{:}31C_3H_9N{:}0.02H_2SO_4{:}3362H_2O$	160	20 or 44	Unstirred			Copperthwaite et al. (1986)
Water glass	Aluminium sulfate	Pyrrolidine	$145SiO_2{:}Al_2O_3{:}45Na_2O{:}99pyrrolidine{:}38H_2SO_4{:}5797H_2O$	150	7 – 40	Stirred	Cubic and elliptical	0.7 – 3.0	Suzuki et al. (1986)
Water glass	Aluminium sulfate	TPA-Br	$145SiO_2{:}Al_2O_3{:}45Na_2O{:}8(TPA)_2O{:}38H_2SO_4{:}5797H_2O$	150	7 – 40	Stirred	Twinned cubic	3.0 – 10.0	Suzuki et al. (1986)
Fumed silica (Aerosil)	Aluminium nitrate nonahydrate	TPA-Br	$72SiO_2{:}Al_2O_3{:}14.4Na_2O{:}90(TPA)_2O{:}1430glycerol{:}10500H_2O$	150	72	Rotated (50)	Elongated hexagonal		Jacobs and Martens (1987)
Fumed silica (Aerosil)	Sodium aluminate	TPA-Br	$42SiO_2{:}Al_2O_3{:}6.09Na_2O{:}1.55(TPA)_2O{:}1553H_2O$	150	72	Rotated (50)	Twinned cubic		Jacobs and Martens (1987)
Fumed silica (Aerosil 200)	Aluminium hydroxide	TPA-Br	$60SiO_2{:}xAl_2O_3{:}9Na_2O{:}3(TPA)_2O{:}3000H_2O$, x = 0.4, 0.5, 0.67 or 1.0	150	72	Stirred			Nicolaides et al. (1991)
Silica sol	Aluminium nitrate nonahydrate	TPA-Br	$350SiO_2{:}Al_2O_3{:}2.5Na_2O{:}17.5(TPA)_2O{:}14350H_2O$	90	20 – 400	Magnetic stirring	Plate-like		Yi and Ihm (1993)
Colloidal silica (Ludox AS-40)	Aluminium triisopropylate	TPA-Br	$48SiO_2{:}Al_2O_3{:}1.25(TPA)_2O{:}96NH_3{:}960H_2O$	185	168	Stirred (100) / Unstirred	Cubic / Twinned hexagonal	0.15 X 0.15 X 0.15 / 50 X 20 X 20	Beschmann et al. (1994)

Table 2.1 Continue

Si source	Al source	Template	Molar composition	Temp (°C)	Time (h)	Stirring (rpm)	Morphology	Particle size (μm)	Reference
Alumino-silicate	Alumino-silicate	C_6DN	$SiO_2:xAl_2O_3:0.0379Na_2O:0.0216C_6DN$	110-200	67 – 303	Unstirred	Twinned cubic		Jianquan et al. (1994)
Water glass	Aluminium sulfate 16-hydrate	TPA-Br	$60SiO_2:xAl_2O_3:63Na_2O:2.0(TPA)_2O:60NaCl:50H_2SO_4:3066H_2O$, x = 0, 0.26, 0.34, 0.5, or 1.0	Programmed up to 210	2	Mechanical stirring (1500)			Ahmed et al. (1996)
Colloidal silica (Ludox AS-40)	Sodium aluminate	TPA-Br	$100SiO_2:xAl_2O_3:(6.9 - 15)Na_2O:(1.5 - 2.5)TPA_2O:(3000 - 5500)H_2O$ x = 0.2, 0.4, 0.5, 0.8 or 1.0	100	21 – 52	Stirred (350)	Twinned cubic to spheroidal	2.01 – 0.71	Kim et al. 1998
Fumed silica	Sodium aluminate	Template-free	$50SiO_2:Al_2O_3$	170	65	Unstirred			Otero Areán et al. (2000)
Tetraethyl-orthosilicate	Aluminium sulfate 18-hydrate	TPA-OH	$60SiO_2:Al_2O_3:10.7(TPA)_2O:650H_2O$	170	6 – 120	Unstirred	Elongated hexagons	0.02 – 1.0	Van Grieken et al. (2000)

The SiO$_2$/Al$_2$O$_3$ ratio in the hydrogel of the methods summarized range from 24 to 540, but Ahmed *et al.* (1996), in their rapid crystallization technique, reported the synthesis of high-silica ZSM-5 at much higher ratios such as 6522 and also of silicalite which was prepared without the addition of aluminium. It was also reported by these authors, and by Hardenberg *et al.* (1992), that lower SiO$_2$/Al$_2$O$_3$ ratios were obtained in the product than in the precursor gel, meaning that more silica species remain in solution. This is also in agreement with the published results of Yi and Ihm (1993). In contrast to the last three groups of researchers, Suzuki *et al.* (1986) reported a higher SiO$_2$/Al$_2$O$_3$ ratio in the product than in the hydrogel for their method of synthesis. No explanations, however, were given by these authors for this observation. Kim *et al.* (1998) reported a change in morphology from twinned cubes to spheroids with a decrease in SiO$_2$/Al$_2$O$_3$ ratio.

Synthesis temperatures for ZSM-5 range from 90°C to 185°C, but Ahmed *et al.* (1996) even employed temperatures as high as 210°C in their synthesis of high-silica ZSM-5 with the rapid crystallization technique. In their method, the temperature was programmed from room temperature up to 210°C within 2 hours and was cooled down immediately after the maximum temperature was reached. Although Jianquan *et al.* (1994) investigated the synthesis of the zeolite over the temperature range of 110°C to 200°C, they obtained the highest crystalline ZSM-5 at 110°C. They indicated that higher temperatures (e.g. 200°C) are unfavourable for the formation of pure ZSM-5. Furthermore, from all these methods, it is obvious that the lower the synthesis temperatures, the longer the synthesis time required. In this regard, Yi and Ihm (1993) indicated that an induction period around 100 hours was required for their synthesis of ZSM-5 at 90°C, and obtained maximum crystallinity only after 260 hours, while other authors reported maximum crystallinity after 72 hours at higher temperatures.

Another obvious conclusion that can be reached from the methods and results summarized in Table 2.1, which has already been indicated above, is that high-silica ZSM-5 zeolites are prepared in shorter times than those with higher aluminium content. For example, Suzuki et al. (1986) reported the synthesis of ZSM-5 within 40 hours with a SiO_2/Al_2O_3 ratio of 145 at 110°C while Anderson et al. (1979) made use of a synthesis time of 144 hours at 170°C for their synthesis of ZSM-5 with a SiO_2/Al_2O_3 ratio of 32. A number of authors used a synthesis time of 72 hours at a temperature of 150°C (Jacobs and Martens, 1987; Nicolaides et al., 1991). Padovan et al. (1984), who did the synthesis at 120°C and at different times up to 576 hours, also reported highest crystallinity at 72 hours. Interestingly, however, it was also reported by Padovan et al. (1984) that for the meta-xylene isomerization reaction catalyzed by the acid form of the zeolite, the activity rises progressively with synthesis time of the zeolite. Their results could be explained in terms of the crystal sizes of the zeolites which increased up to 72 hours (0.1 μm) and after which they decreased to 0.05 μm for the synthesis time of 576 hours.

The reported methods indicate that ZSM-5 can be successfully synthesized under both static or agitated conditions. The mode of agitation varies from overhead mechanical stirring to stirring with a magnetic stirrer bar at rates of 100 rpm to 1 500 rpm or by rotation of the autoclave at 50 rpm.

Different morphologies of the formed ZSM-5 are reported by the different authors, and this strongly suggests that starting materials and synthesis conditions and procedures play a role in the final morphology observed. Padovan et al. (1984) reported twinned cubes at shorter synthesis times which transform into spheroids at longer times. Kim et al. (1998) also reported a change from twinned cubes to spheroids, but with a decrease in SiO_2/Al_2O_3 ratio in their case. Other morphologies reported are rectangular plate, elliptical, cubic and elongated hexagonal

structures.

A variety of reactor types seem suitable for the synthesis of ZSM-5. Reactors ranging from sealed glass tubes (Padovan et al., 1984), polypropylene bottles with glass capillaries for reflux (Yi and Ihm, 1993), stainless steel autoclaves (Copperthwaite et al., 1986; Suzuki et al., 1986; Ahmed et al., 1996) to a teflon-lined stainless steel autoclave (Otero Areán et al., 2000; Van Grieken et al., 2000) were used. The sizes of the autoclaves used ranged from 34 ml (Copperthwaite et al., 1986) to 30 litres (Kim et al., 1998). Most of the laboratory syntheses, however, were performed in 1 litre autoclaves. Although most of the preparations were carried out under autogenous pressure, one method specified pressurizing the system with nitrogen before heating (Ahmed et al., 1996) while atmospheric pressure synthesis was also reported (Yi and Ihm, 1993; Kim et al., 1998).

Ahmed et al. (1996) reported the adjustment of the pH from > 13.5 to 9.7 or 10.3 by the addition of sulfuric acid to obtain a homogeneous hydrogel. Their results showed that higher pH (> 10.3) facilitate the formation of quartz in ZSM-5. Jacobs and Martens (1987) also used sulfuric acid in their dilute method to adjust the pH to 11.

Although some of the researchers (Anderson et al., 1979; Jacobs et al., 1981) did not age the precursor gels before crystallization started, others did (see also Section 2.3.8). Ahmed et al. (1996) reported that the hydrogel was aged for 48 hours at room temperature for some of their samples, while other authors only reported the mixing of the final reaction mixture for different times at room temperature. Beschmann et al. (1994), for example, mixed it for 180 seconds while Yi and Ihm (1993) mixed it for 1 hour.

Although in most of the studies the product is separated from the mother liquor by filtration (Anderson *et al.*, 1979; Jacobs *et al.*, 1981; Suzuki *et al.*, 1986), Yi and Ihm (1993) separated them by both filtration and centrifugation. In one of the reports, only centrifugation was used (Van Grieken *et al.*, 2000) while for the larger scale synthesis of Kim *et al.* (1998), a filter press unit was utilized. There was no need to separate the product from its mother liquor as usual in the extremely denser system of Jianquan *et al.* (1994), which was called the "kneading method".

ZSM-5 is usually calcined in air at temperatures ranging from $500^{\circ}C$ to $630^{\circ}C$ for different calcination times ranging from 2 hours to 20 hours. However, Jacobs *et al.* (1981) carried out the calcination in nitrogen. There is no indication in any of the above-mentioned procedures of the influence of the different calcination temperatures and times on the quality of the product formed.

2.5 ZEOLITE FERRIERITE

As was the approach taken with ZSM-5, a short historical background, structural characteristics and typical examples of synthetic procedures will now be given in this section for the zeolite ferrierite.

2.5.1 Introduction

Natural ferrierite was discovered by R.P.D. Graham in 1918 and named in honour of W.F. Ferrier of the Canadian Geological Survey (Staples, 1955). By 1955, the only locality reported for ferrierite had been the north shore of Kamloops Lake in British Columbia where it occurred as spherical aggregates of radiating blades enclosed in chalcedony. Since then other occurrences

of ferrierite have been reported in Bulgaria, Italy, Yugoslavia, Japan and the western USA (Kibby *et al.*, 1974). It was found in cavities of volcanic rocks and was associated with quartz (chalcedony) or calcite. The presence of 3% magnesium in natural ferrierite made it unusual amongst the zeolites. That is why until 1974 it was referred to as a magnesium zeolite.

Powder X-ray data for the mineral ferrierite were reported by Staples (1955) and crystal structures were determined by Vaughan (1966) and Kerr (1966). Ferrierite's unit cell is orthorhombic with dimensions a = 19.16Å, b = 14.13Å and c = 7.49Å, and its composition is approximately $Na_2Mg_2Al_6Si_{30}O_{72}.18H_2O$ (Kibby *et al.*, 1974). Substitutions of Ca^{2+}, Fe^{2+} and K^+ in place of Na^+ and Mg^{2+} as cation in the ion exchange positions are also found in the mineral ferrierites. The monoclinic structure was also reported by Gramlich-Meier *et al.* (1985). The framework structure of the monoclinic ferrierite deviates slightly and yet significantly from orthorhombic symmetry. In contrast to the structure of the more abundant orthorhombic ferrierite, monoclinic ferrierites from Altoona show no T-O-T angles of 180°.

A representation of the ferrierite structure is shown in Figure 2.14. The structure contains dense layers of interlinked five-membered rings of TO_4 tetrahedra, perpendicular to the *a*-axis, which
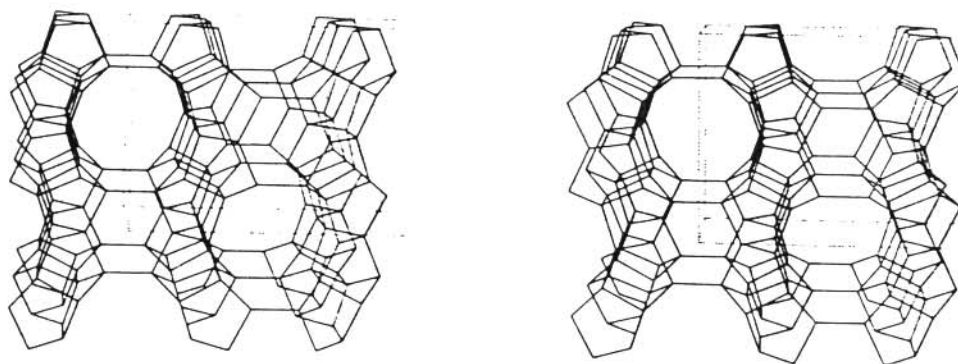
Figure 2.14 Ferrierite framework viewed along [001] (taken from Meier and Olson, 1987).

are separated by six-membered ring channels, eight-membered ring channels and ten-membered ring channels. The eight-membered ring channels run in the [010] (*b*-axis) direction and intersect both six-membered ring channels and ten-membered ring channels, which run in the [001] (*c*-axis) direction. Cavities of 6Å to 7Å diameters are formed by the intersection of six-membered ring channels and eight-membered ring channels. There are two of these per unit cell which contain the magnesium ions in mineral ferrierites. The free diameter of the main ten-membered ring channels (two per unit cell) is 4.2Å X 5.4Å, hence ferrierites are considered as medium pore zeolites (Venuto, 1994).

Since the 1970's several publications have appeared describing the preparation of the synthetic ferrierite zeolite (see Section 2.5.2). Unlike the natural ferrierite, whose SiO_2/Al_2O_3 ratio varies around an average value of twelve, the synthetic zeolites can have SiO_2/Al_2O_3 ratios of higher than twelve. For example, the SiO_2/Al_2O_3 ratio of the ferrierite synthesized by Harrison *et al.* (1987) was found to be 30, whereas the highest SiO_2/Al_2O_3 ratio reported was 190 (Jacobs and Martens, 1987).

2.5.2 **Synthesis of ferrierite**

Ferrierite was first synthesized unknowingly by Coombs *et al.* (1959) from mixed sodium-calcium compositions heated hydrothermally to 330°C. With sodium or calcium alone, only mordenite and analcime were found. However, a calcium-free ferrierite from a water-rich mordenite preparation method containing excess sodium oxide was later reported, as well as the coexistence of sodium ferrierite with mordenite, quartz and analcime. Barrer and Marshall (see Kibby *et al.*, 1974) synthesized a strontium zeolite in 1964 which they later identified as ferrierite and it was reported that both calcium and strontium ferrierites can be synthesized from

oxide mixtures with composition: $7SiO_2:Al_2O_3:CaO(SrO)$.

Table 2.2 gives a summary of some ferrierite synthesis procedures reported in the literature.

In summary, it is shown that the zeolite ferrierite could be synthesized with and without a structure-directing template. Different organic nitrogen compounds can be used as templates for its synthesis. Nanne *et al.* (1980) indicated that piperidine is the best template for their particular synthetic procedure. If instead, closely related heterocyclic nitrogen compounds, such as pyrrole, amidazol, pyridine or pyrrolidine are used, either no ferrierite is formed at all or the ferrierite obtained is highly contaminated with other zeolitic and/or amorphous material. However, other authors (Wenyang *et al.*, 1989; Dutta *et al.*, 1992; Xu *et al.*, 1995a) later reported the successful use of ethylenediamine, pyridine and pyrrolidine as templates. Kibby *et al.* (1974) made attempts to prepare a hydrogen ferrierite directly by using tetramethylammonium (TMA) ions in the synthesis. Their results showed that a complete substitution of TMA ions for sodium ions was not successful, but mixed TMA-Na-ferrierites did crystallize with about one-third of the sodium ions replaced by TMA ions.

Ludox (both AS-40 and HS-30) is commonly used as the silica source, but water glass (Nanne *et al.*, 1980) and silica gel (Grandvallet *et al.*, 1992) can also be utilized. From Table 2.2 it is observed that sodium aluminate and sodium sulfate are the most commonly used aluminium sources. Dutta *et al.* (1992) reported the successful template-free synthesis of ferrierite using aluminium oxide.

The SiO_2/Al_2O_3 ratio in the different recipes studied range from 7.5 to 187. Wenyang *et al.* (1989) indicated that the molar SiO_2/Al_2O_3 ratio of the reaction mixture will influence which

Table 2.2 Ferrierite synthesis procedures

Si source	Al source	Template	Molar composition	Temp.(°C)	Time (h)	Morphology	Particle size (μm)	Reference
Colloidal silica (Ludox AS-40)	Sodium aluminate	Template-free	$8SiO_2:Al_2O_3:Na_2O:1462H_2O$	290-325	40 – 119	Octagonal platelets	10 – 100	Kibby et al. (1974)
Water glass	Aluminium sulfate	Piperidine	$(23.4 – 187.0)SiO_2:Al_2O_3: (2.5 - 42.8)Na_2O:(4.3 - 11.2)Na_2SO_4:(9.7 - 73.4)$piperidine:$(485 - 3876)H_2O$	150	113			Nanne et al. (1980)
Water glass	Aluminium sulfate	Ethylenediamine	$(15 - 50)SiO_2:Al_2O_3:(1 - 8)Na_2O:(20 - 45)$ethylenediamine:$(40 – 420)(C_2H_2)_3N$	150 – 200	1 – 96			Wenyang et al. (1989)
Silica gel	Aluminium sulfate 18-hydrate	Pyridine	$93.5SiO_2:Al_2O_3:7.4Na_2O:19.6Na_2SO_4: 30$pyridine:$1938H_2O$	150	75			Grandvallet et al. (1992)
Colloidal silica (Ludox AS-40)	Sodium aluminate	Pyrrolidine	$20SiO_2:Al_2O_3:1.2Na_2O:12.6$pyridine:$398H_2O$	165	11 – 80			Dutta et al. (1992)
Silica sol (Ludox HS-30)	Aluminium oxide	Template-free	$15SiO_2:Al_2O_3:1.5Na_2O:1500H_2O$	220	11 –1000			Dutta et al. (1992)
Colloidal silica (Ludox HS-30)	Sodium aluminate	Template-free	$(10$ or $20)SiO_2:Al_2O_3:1.6Na_2O: (400$ or $431)H_2O$	175	20 – 100	Eliptical	100	Xu et al. (1995a)
Colloidal silica (Ludox HS-30)	Sodium aluminate	Pyrrolidine	$(10$ or $20)SiO_2:Al_2O_3:1.6Na_2O: 12$pyrrolidine:$(400$ or $431)H_2O$	175	20 – 100	Rectangular sheet-like Hexagonal	16 X 12 / 22 X 12 X 12	Xu et al. (1995a)

zeolite will form. In their non-aqueous method, both the SiO_2/Al_2O_3 and $(CH_3CH_2)_3N/Na_2O$ ratios were varied. At a SiO_2/Al_2O_3 ratio of 18 and for $(CH_3CH_2)_3N/Na_2O$ ratios ranging from 8 to 20, only ferrierite was obtained. At higher $(CH_3CH_2)_3N/Na_2O$ ratios, the amorphous content of the product increased with increasing $(CH_3CH_2)_3N/Na_2O$ ratios. With a SiO_2/Al_2O_3 ratio of 35, ferrierite was again synthesized but with $(CH_3CH_2)_3N/Na_2O$ ratios below 15. For $(CH_3CH_2)_3N/Na_2O$ ratios between 15 and 20 the product was ZSM-5, and amorphous material was obtained at even higher $(CH_3CH_2)_3N/Na_2O$ ratios. At higher SiO_2/Al_2O_3 ratio (around 70), only ZSM-5 was obtained within the range of $(CH_3CH_2)_3N/Na_2O$ ratios investigated.

Xu *et al.* (1995a) indicated that in their templated method for the synthesis of this zeolite, the morphology obtained depends on the SiO_2/Al_2O_3 ratio of the reaction mixture. At the SiO_2/Al_2O_3 ratio of 10, a rectangular sheet-like morphology was obtained and a hexagonal morphology was detected at the SiO_2/Al_2O_3 ratio of 20.

As seen in Table 2.2, the synthesis temperatures ranged from $150^{\circ}C$ to as high as $325^{\circ}C$. However, it is also evident that higher temperatures are needed for the untemplated methods. Dutta *et al.* (1992) synthesized templated ferrierite at $165^{\circ}C$ for 80 hours and the template-free ferrierite at $220^{\circ}C$ for 648 hours. Furthermore, it is also clear that lower temperatures on average need higher synthesis time for complete crystallization. Wenyang *et al.* (1989) indicated that an increase in synthesis temperature causes a decrease in the nucleation time and an increase in the crystallization rate. Xu *et al.* (1995a), who employed synthesis times up to 100 hours, with both a templated and an untemplated method, indicated that the longer the synthesis time, the higher the percentage XRD crystallinity. In the method used by Kibby *et al.* (1974), use was made of the highest temperatures reported for the synthesis of ferrierite. Mordenite was obtained as the major phase below $290^{\circ}C$ and analcime crystallized as the major phase above $325^{\circ}C$.

Furthermore, even at the temperatures between 290°C and 325°C, ferrierite with traces of mordenite and/or analcime were obtained.

Most authors did not report the morphology of their synthesized ferrierites, exept for Kibby *et al.* (1974) who reported an octagonal morphology with crystallite sizes ranging from 10 μm to 100 μm, and Xu *et al.* (1995a) who also indicated that the ferrierite obtained from their template-free method gave egg-shaped crystals with an average size of 100 μm while mixed morphologies were obtained for the templated method. Rectangular sheet-like and hexagonal crystals with the average sizes of 16 μm X 22 μm and 22 μm X 12 μm X 12 μm respectively, were found in the latter method.

Different reactors were used by the various research groups and these ranged from pyrex tubes inserted in a hydrothermal bomb (Kibby *et al.*, 1974), a 250 ml stainless steel autoclave (Wenyang *et al.*, 1989), a Parr teflon-lined acid digestion bomb (Dutta *et al.*, 1992) to a 110 ml teflon-lined stainless steel autoclave (Xu *et al.*, 1995a). Kibby *et al.* (1974) indicated that the diameter of the pyrex tubes used have a significant influence on the yield of the ferrierite crystals. At first they used a tube with an inner diameter of 6.6 cm and obtained mainly an amorphous phase. When the diameter of the tube was halved to 3.3 cm, high yields of ferrierite were formed with very little amorphous material. It was believed that nucleation of ferrierite crystals started at the walls of the pyrex tube containing the gel. Perhaps this is due to the lower surface area of the pyrex tube, which then lead to a higher amount of nuclei per area, under the same reaction conditions, to get the reaction going.

Crystallization of the reaction mixtures for ferrierite synthesis are usually carried out under autogenous pressure. In the case of the anhydrous method by Wenyang *et al.* (1989), all

preparations were done under the protection of dried nitrogen. Although most authors did not mention ageing of the precursor gel before it is hydrothermally treated, Nanne *et al.* (1980) aged it for 15 minutes with stirring before crystallization commenced.

It can also be noted from Table 2.2 that none of the reported methods indicated that agitation of the reaction mixture was employed during the synthesis.

The concentration of the hydroxide ions used in the precursor gel for the synthesis of ferrierite also varies. Xu *et al.* (1995a) reported the adjustment of the pH to about 12 by the addition of sodium hydroxide. Dutta *et al.* (1992) indicated that for their untemplated method, increasing the OH^-/SiO_2 ratio by 16% speeded up the crystallization process, but also resulted in the crystallization of mordenite, whereas lowering the OH^-/SiO_2 ratio by the same amount resulted in the zeolite crystallization only after 1 000 hours of heating.

Calcination temperatures used for the removal of the template from the ferrierite products are usually around 500°C for 3 hours to 4 hours in air, except for Xu *et al.* (1995a), who used nitrogen at 550°C for 4 hours, followed by oxidation in air at 550°C for another 4 hours.

CHAPTER THREE

CHARACTERIZATION OF ZEOLITES

3.1 INTRODUCTION

Before a zeolite can be used for a certain application it is necessary to characterize that zeolite to determine if it has the desired properties for the specific application. If not, another synthesis method should be used, or the zeolite must be modified, in order to meet the specifications. Zeolite synthesis, modification, characterization and application are thus strongly related, as is schematically indicated in Figure 3.1 (Van Hooff and Roelofsen, 1991).
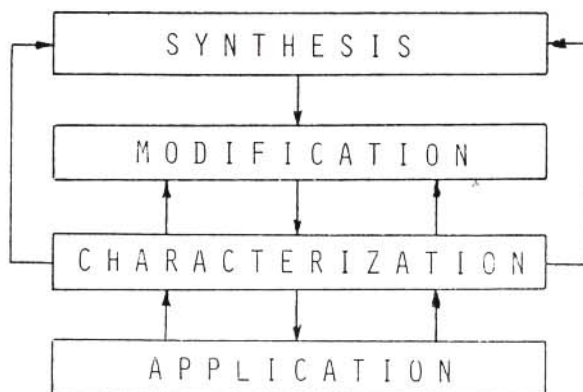
Figure 3.1 Importance of zeolite characterization (taken from Van Hooff and Roelofsen, 1991).

Of course, not all the properties of a zeolite are of the same importance for every application. This aspect is illustrated in Figure 3.2 in which it is indicated which characteristics are of special importance for the main applications shown in the figure for the three different zeolites listed. For example, for the application of zeolite A as an adsorbent or ion-exchanger in detergents, pore

IMPORTANT CHARACTERISTIC	TYPE OF ZEOLITE		
	ZEOLITE A	ZEOLITE Y	ZSM-5
STRUCTURE STRUCTURAL DEFECTS		◌	●
PORE-SIZE	●	◌	●
CHEMICAL COMPOSITION	●	●	●
FRAMEWORK Si/Al RATIO		●	◌
ACIDITY		●	●
STABILITY		●	◌
MORPHOLOGY PARTICLE SIZE	●	◌	●
IMPORTANT APPLICATION	ADSORBENT ION EXCHANGER IN DETERGENTS	CRACKING CATALYST	SHAPE SELECTIVE CATALYST

Figure 3.2 Most important characteristics of three well-known zeolites and their major applications (taken from Van Hooff and Roelofsen, 1991).

size, chemical composition, particle size and morphology are extremely important, while acidity and stability play a minor role. These latter characteristics, however, are of crucial importance for the application of zeolite Y as a cracking catalyst. For this reason, specific characterization methods are used for the evaluation of the zeolites in relation to the application for which the specific property is important.

As indicated in Figure 3.2, the main characteristics of zeolites are their structure, pore size and pore volume, SiO_2/Al_2O_3 ratio, acidity, morphology and crystallite size. The characterization of the structure is mainly done by XRD, but nuclear magnetic resonance spectroscopy (NMR) and

infrared spectroscopy (IR) or Fourier transform infrared spectroscopy (FTIR) also give additional information. A tremendous amount of research effort has gone into the characterization of the acidity of zeolites and several experimental methods, such as chemical titration, FTIR, NMR and X-ray photoelectron spectroscopy (XPS) and thermal methods, are currently used by researchers in this field (Costa *et al.*, 2000). Temperature programmed desorption (TPD) of ammonia is also one of the methods commonly used for the determination of the acidity of zeolites. Pore volume, surface area and pore size distribution can be determined by the Brunauer, Emmett and Teller isotherm (BET) (Van Grieken *et al.*, 2000), and Van Hooff and Roelofsen (1991) also indicated that Xe-NMR spectroscopy can be used to obtain information on the pore system and pore sizes of zeolites.

Particle size determination of zeolites is based on sieving or sedimentation. By the dry sieving method, particles larger than 5 µm can be determined, while the Coulter counter sedimentation method is suitable for particles down to 0.5 µm (Van Hooff and Roelofsen, 1991).

In the sections that follow some of the techniques described above and their applicability in the determination of certain properties of the zeolitic materials will be reviewed in more detail.

3.2 INFRARED SPECTROSCOPY

IR or FTIR spectroscopy can generally be used to detect the different building units in zeolites or species present in them. Szostak (1989) indicated that IR spectroscopy has been extensively utilized to determine the presence of the different five-membered ring structures for zeolites of the pentasil family. IR spectroscopy can also be used to indicate the presence of the template in the zeolite. For instance, the peak indicating the presence of tetrapropylammonium bromide as a

template in the zeolite ZSM-5 can be shown by observing the CH_2 and CH_3 absorptions extending from 3 100 cm^{-1} to 2 850 cm^{-1}. After calcination, these peaks disappear since the template has been removed (Bordiga et al., 1996).

FTIR spectroscopy can also be used to determine the strength of the acid sites in the zeolites. Woolery et al. (1986) obtained FTIR spectra of six H-ZSM-5 samples ranging in SiO_2/Al_2O_3 ratios from 70 to 26 000. At relatively low SiO_2/Al_2O_3 ratios, two ν_{OH} bands are observed at 3 740 cm^{-1} and 3 610 cm^{-1}, which are due, respectively, to terminal SiOH groups (required to terminate the finite crystalline lattice) and the Brønsted acid sites associated with the aluminium tetrahedra. The higher value for the silanol group indicates that the O-H bond is much stronger (and the proton less acidic) than in the case of the Brønsted acidic O-H (Van Santen and Kramer, 1995). As the SiO_2/Al_2O_3 ratio increases, the 3 610 cm^{-1} band intensity diminishes. However, concomitant with the loss of this band is the appearance of a new broad band centered at ~3 500 cm^{-1}. The intensity of this band increases in a consistent fashion as the aluminium content decreases (see below). In addition, at the higher SiO_2/Al_2O_3 ratios of 600 and 26 000, the intensity of the 3 740 cm^{-1} band increases significantly. Thus, as the aluminium content is systematically decreased in ZSM-5, two new hydroxyl species are formed, which, due to the absence of sufficient aluminium, must be associated with silicon atoms.

One of these SiOH species is essentially unrestricted, that is, free from structural perturbation from the zeolite, and thus appears vibrationally accidentally degenerate with the terminal SiOH groups. A second SiOH entity is formed which is, however, greatly affected by the zeolite: a high degree of hydrogen bonding appears to be present, which lowers the frequency of ν_{OH} to ~3 500 cm^{-1} and significantly broadens the band (Woolery et al., 1986).

A third hydroxyl band occurring at ~3 680 cm^{-1} is also observed in the intermediate SiO$_2$/Al$_2$O$_3$ ratio samples. Significant overlap with the other OH bands precludes correlation of this band intensity with aluminium content. It may well be present in the 600 and 26 000 samples, but is obscured by the very intense 3 735 cm^{-1} band.

FTIR analysis of adsorbed pyridine also allows to distinguish between the Brønsted and the Lewis acid sites present. An example of such a study is that by Emeis (1993) who indicated that in the adsorption of pyridine on zeolites, IR adsorption bands appear at 1 455 cm^{-1} which are assigned to pyridine associated with Lewis acid sites and at 1 545 cm^{-1} for pyridine adsorbed on Brønsted acid sites.

3.3 TEMPERATURE PROGRAMMED DESORPTION

Acidity is one of the most important properties of zeolites which make them very useful as solid acid catalysts. The catalytic properties, such as activity and selectivity, depend not only on the number of the acid sites, but also on their specific activities. It is clear that this activity is related to the acid strength of these sites.

The Brønsted equations have been used to describe the relation between the rate of homogeneously acid-catalyzed reactions and the acid strength of the catalysts. A similar relationship for heterogeneous acid-catalyzed reactions has been sought for a long time by researchers working in this field (Costa *et al.*, 2000). The major problem has been that, in any given heterogeneous catalyst, a wide range of acid strengths can be found on the surface, due to the different structure, topology and chemical composition around each acid site. This makes the estimation of acid site strength distributions somewhat difficult. Furthermore, it is not easy to

establish a unique scale of acidity similar for instance to the pK_a for solutions.

TPD of ammonia is a commonly used technique for the determination of the number and strength of the acid sites (Kwak and Sachtler, 1994; Costa *et al.*, 2000). Numerical procedures to perform digital deconvolution of the curves obtained by single TPD experiments into the related mono-energetic component curves can be carried out. This method allows the estimation of the acid site strength of the sites on a catalyst surface using the activation energy for ammonia desorption as a measure of acidity of any given site (Costa *et al.*, 2000).

Beyond the determinant factor of framework composition of the zeolites, also the spatial distribution of the acid sites across the framework is important, i.e., for a given composition, the structure type will modify the surface properties. In order to systematize a Brønsted-type approach to heterogeneous catalysis, it is extremely interesting to know if the same kind of correlation between the activity and the acidity can be found for acid-catalyzed reactions over acid catalysts with different structures, and to compare the corresponding parameters.

For the semi-quantitative assessment of the strength of the acid sites through the technique of peak deconvolution and the determination of the value of the density of acid sites, Le and Le Van Mao (2000) studied the desorption of gaseous ammonia with gas chromatography (GC) using a thermal conductivity detector and by carrying out a back titration with an acid solution. The molar ratio, $R_{ac/Al}$, was defined as the ratio of number of moles of acid sites to that of the number of moles of aluminium in the zeolite. These authors studied both an H-ZSM-5 zeolite and a desilicated H-ZSM-5 (H-DZSM-5) zeolite. For the H-DZSM-5 sample, it was shown, using the ammonia TPD acid back-titration method, that the acid site density is 1.05×10^{-3} mol/g of zeolite, which corresponds to an increase of about 35% with respect to the parent H-ZSM-5

zeolite. For both parent H-ZSM-5 and H-DZSM-5 zeolites, the $R_{ac/Al}$ ratio was found to be equal to 1.0, meaning that all the acid sites of this zeolite are accessible to the ammonia molecules. The ammonia TPD profile was similar to that of the parent H-ZSM-5. This indicated similar distributions in terms of acid site strength.

Kwak and Sachtler (1994) characterized ZSM-5 by TPD of ammonia and two major peaks were detected. A peak at 270°C resulting from the desorption of ammonia from weak acid sites and a peak at 500°C arising from the desorption from strong Brønsted acid sites.

3.4 NUCLEAR MAGNETIC RESONANCE SPECTROSCOPY

The impact of solid-state NMR as a powerful tool for the studying of zeolites has been dramatic since the pioneering work of Lippmaa, Engelhardt and co-workers in the early 1980's (Lippmaa *et al.*, 1980; Lippmaa *et al.*, 1981). They dealt for the first time with high-resolution solid-state ^{29}Si NMR spectroscopy of zeolites, which led to a tremendous progress been made with regard to enhanced resolution, sensitivity and improved multinuclear capabilities. Solid-state NMR spectroscopy is nowadays a well established technique for the characterization of zeolites and related materials with respect to structure elucidation and catalytic behaviour.

Solid-state NMR provides some advantages as compared to XRD, since amorphous materials as well as crystalline materials can be studied (Stöcker, 1994). In addition, silicon and aluminium have almost the same scattering factors, which means no discrimination between these two nuclei can be achieved by XRD. While XRD provides information about the long-range ordering and periodicities, the NMR techniques allow investigations on the short-range ordering (local environment) and structure. Powder XRD reveals only limited information with respect to

zeolite lattice structures and only single crystal XRD could be used to elucidate zeolite structures. However, XRD is a complementary technique to solid-state NMR, and the use of both methods is still a powerful combination with regard to zeolite characterization.

The following types of NMR spectroscopy are used for the characterization of zeolites:

^{13}C NMR

Van Hooff and Roelofsen (1991) indicated that studies of the structure and position of organic species present in zeolites synthesized with organic templates are of great interest for elucidating the process of zeolite formation. High-resolution solid-state ^{13}C NMR, using cross-polarization (CP) and magic angle spinning (MAS), has great potential in such investigations. The isotopic ^{13}C chemical shift is highly sensitive to the environment of the carbon nucleus, and the ^{13}C NMR spectra in general display narrow and well resolved peaks for each kind of distinct carbon atom of the organic guest molecule in the zeolite.

^{1}H NMR

While the proton-proton dipolar interaction in dehydrated zeolites are relatively small owing to the large proton-proton distances, ^{1}H NMR spectroscopy of zeolites is complicated by hetero-nuclear dipolar interaction of the protons with the quadrupolar ^{27}Al nuclei, and the generally narrow range of proton chemical shifts. Nevertheless, ^{1}H MAS NMR spectroscopy, at high magnetic fields and fast spinning rates, of carefully dehydrated samples provides sufficient spectral resolution to identify different proton sites in zeolites, and to characterize, quantitatively, their distribution in the zeolite structure. Four distinct types of protons can be identified by their chemical shifts: terminal SiOH, bridging hydroxyl groups (SiO(H)Al), AlOH due to non-framework aluminium and ammonium ions (Engelhardt, 1991).

^{29}Si NMR

Woolery *et al.* (1986) showed that when using the MAS ^{29}Si NMR spectra of the NH_4^+-exchanged, Na^+-free form of ZSM-5 with SiO_2/Al_2O_3 ratios of 600 and 26 000, the resonance observed at $\delta = 113$ ppm (δ = chemical shift) is due to $Si(OSi)_4$, while the peak at $\delta = 103$ ppm is typical of $Si(OH)(OSi)_3$. Quantification of the two [29]Si signals for the sample with a SiO_2/Al_2O_3 ratio of 26 000 reveals that ~7% of the silicon is present as SiOH. Given an average crystallite size of 0.5 μm for this sample, the number of SiOH groups required to terminate the crystal lattice is only about 0.4%, which is over an order of magnitude less than that observed. Previously it has been reported by Boxhoorn *et al.* (1984) that ZSM-5 in the as-synthesized form ($SiO_2/Al_2O_3 = 280$) has a very high silanol (or more correctly silanoxy, where the counter ion could be H^+, Na^+ or TPA^+) content of ~18%, which is essentially eliminated upon calcination. In contrast to the results obtained by Boxhoorn and co-workers, Woolery *et al.* (1986) observed a substantial silanol signal after removal of the organics and of Na^+.

A number of review papers have been published during the 1980's summarizing the structural information and relationships available from the ^{29}Si NMR spectroscopic data on zeolites (Fyfe *et al.*, 1983; Klinowski, 1991). One of the most important results by Lippmaa, Engelhardt and co-workers (Lippmaa *et al.*, 1980; Lippmaa *et al.*, 1981) was establishing the relationship between the [29]Si chemical shift sensitivity and the degree of condensation of the silicon-oxygen tetrahedron, that is the number and type of tetrahedrally coordinated atoms (T-atoms) connected to a given SiO_4 unit. The degree of condensation is symbolized by Si(nAl), where n = 0, 1, 2, 3 or 4 and indicates the number of aluminium atoms sharing oxygens with the SiO_4 tetrahedron under consideration. Furthermore, the [29]Si chemical shift is influenced by the Si-O-T bond angle and silicon-oxygen bond length, which means, that chemically equivalent but crystallographically non-equivalent silicon nuclei may have different chemical shifts.

^{27}Al NMR

It is known that ^{27}Al NMR spectroscopy is able to distinguish between tetrahedrally and octahedrally coordinated aluminium atoms. From the literature data it can be concluded that the NMR peak due to tetrahedral aluminium is located in the region of 50 ppm to 60 ppm, while the octahedral aluminium shows a peak at $\delta = 0$ ppm, when the chemical shifts are measured with respect to $Al(H_2O)_6^{3+}$ as the external reference (Debras *et al.*, 1986).

The ^{27}Al NMR chemical shifts in zeolites are generally in the region of 50 ppm to 60 ppm which will then indicate that most of the aluminium atoms are in tetrahedral coordination in the framework. The octahedral aluminium species are only detected in dealuminated samples. However, in some precursors, octahedral aluminium is also detected and its amount increases with increasing aluminium content. The NMR peak width is larger for the precursors than for the calcined samples.

The total integrated ^{27}Al NMR peak intensity of a spectrum increases with increasing ^{27}Al per unit cell for precursors and calcined products. Unfortunately, the method is not sensitive enough to detect < 0.2 ^{27}Al per unit cell with sufficient accuracy (Debras *et al.*, 1986).

^{23}Na NMR

When the precursor and calcined zeolites are characterized by ^{23}Na NMR spectroscopy, it was observed that the experimental points are rather scattered and thus ^{23}Na NMR spectroscopy is not suitable for precise quantitative analysis. This is probably due to the quite different electric field gradients experienced by the sodium ions in the precursors and in the calcined samples. It is well known that some intensity can be lost because the NMR peaks can be broadened beyond detection (Debras *et al.*, 1986; Engelhardt, 1991).

¹²⁹Xe NMR

Fraissard and Ito (1988) developed ¹²⁹Xe NMR spectroscopy as a method to obtain information on the pore system and sizes of zeolites. Due to the relatively large diameter of the xenon atom (4.36Å), information is only obtained on the larger pores. An expression for the chemical shift of xenon adsorbed in porous materials was also given:

$$\delta = \delta_0 - \delta_e - \delta_m - \delta_{(xe-z)}.\rho_z - \delta_{(xe-xe)}.\rho_{xe}$$

This relation shows that the observed chemical shift is the sum of the chemical shifts originating from the reference (δ_0); electric field (δ_e); magnetic field (δ_m); interaction of the xenon atoms with the zeolite ($\delta_{(xe-z)}\rho_z$) (where ρ_z is related to the zeolite structure); mutual interactions between the xenon atoms ($\delta_{(xe-xe)}\rho_{xe}$) (where ρ_{xe} is the concentration of the xenon atoms, in the pores).

¹²⁹Xe NMR has also been applied in various other investigations such as:

(i)   study of coke formation during catalytic cracking (Ito *et al.,* 1988);

(ii)   study of the formation of nickel particles upon reduction of Ni^{2+}-exchanged zeolite Y (Scharpf *et al.,* 1986).

¹⁷O NMR

Since oxygen is the main constituent of the zeolite framework, the possibilities for carrying out detailed ¹⁷O NMR spectroscopic studies in the solid state are particularly attractive. However, the ¹⁷O isotope has a very low natural abundance and a quadrupole moment which renders the observation of ¹⁷O NMR very difficult without extensive ¹⁷O enrichment of the sample (Engelhardt, 1991).

3.5 ATOMIC ABSORPTION SPECTROSCOPY

Atomic absorption spectroscopy (AAS) is used to determine the amount of elements, such as aluminium, silicon, sodium, etc., present in zeolites. An example of this technique is given by Kotrel *et al.* (1999), who analyzed for aluminium and sodium in ZSM-5, zeolite β and zeolite Y by first dissolving the zeolites in hydrofluoric acid. The resulting solutions were analyzed by AAS using the inductively coupled plasma technique for Al^{3+} and the flame technique for Na^+.

Park *et al.* (2000) synthesized zeolitic materials (with cancrinite and sodalite as major phases) from fly ash using both the molten-salt method and the conventional hydrothermal method. Using AAS, they determined the mass of the elements silicon, aluminium and iron in the fly ash, which is not incorporated in the formed zeolitic materials.

3.6 BET SURFACE AREA

The Brunauer, Emmett and Teller isotherm (BET) is one of the common methods used to characterize zeolites in terms of surface area and pore volume.

Van Grieken *et al.* (2000) used BET to determine the surface area and pore volume of nanocrystalline ZSM-5 zeolites. A decrease in the surface area from 711 m^2/g to 469 m^2/g was obtained with an increase in synthesis time from 6 hours to 24 hours, which go hand in hand with an increase in percentage XRD crystallinity from 0% to almost 100%. The isotherms corresponding to the initially formed amorphous solids indicated that these materials are mainly mesoporous, with a large amount of nitrogen being adsorbed at higher p/p_o. These materials possess a total pore volume, measured at a p/p_0 ratio of 0.99, around 1 ml/g, although the

presence of an important amount of micropores in these non-crystalline materials was also observed (~0.10 ml/g). The interparticle voids present in such samples of low crystal sizes lead to the high total volume. Once the solid reaches crystallinities above 50%, the nitrogen adsorption is practically completed at p/p_0 values lower than 0.1, denoting the increased contribution of the microporosity. The highly crystalline material shows a pore volume of about 0.17 ml/g in close agreement to that corresponding to the pure MFI structure. Thus, a significant decrease in the total pore volume of these samples is observed as the crystallinity increases.

Using the Barret, Joyner and Halenda method of pore size distribution determination (BJH model), the amorphous materials were found to show a maximum pore diameter centered around 120Å to 140Å, corresponding to the presence of mesoporosity, which disappears completely as the crystallization process proceeds to give higher crystallinity materials (Van Grieken *et al.*, 2000).

In contrast to the results of Van Grieken and co-workers, Ahmed *et al.* (1996) indicated that the surface area of the zeolite ZSM-5 increases with an increase in crystallinity and they obtained a maximum of 330 m^2/g. It should be noted, however, that the ratio of the intensities of the IR bands at 550 cm^{-1} and at 450 cm^{-1} were used as a measure of the crystallinity of the samples prepared. Le and Le Van Mao (2000) reported surface areas of 364 m^2/g and 370 m^2/g for 100% crystalline ZSM-5 samples.

3.7 X-RAY POWDER DIFFRACTION

According to Baerlocher and McCusker (1994), zeolites are notoriously difficult to synthesize in a form suitable for single crystal analysis. As a result, zeolites and powder diffraction analysis

have been intimately associated with one another from the beginning of the modern zeolite science. Murthy and Reidinger (1996) also reported that for zeolite characterization by XRD, the samples must be powders and the minimum amount of material required is a few milligrams. However, greater accuracy is achieved if up to a gram of the sample is available.

Because of their complexity, zeolites have proved to be a challenge for the powder method and have thereby helped to promote the progress in the method itself. Although powder diffraction instrumentation and methodology have made substantial progress during the last decades, many zeolite problems are still pushing the limits of the method. In fact, they have gained the reputation of being worse-case test examples for new developments in powder diffraction data analysis (Baerlocher and McCusker, 1994).

The principal limitation of powder data is the fact that three dimensional diffraction data are projected onto one dimension with a corresponding loss of information. Single crystal refinements are usually over-determined (ratio between observations and variables) by a factor of 10. For zeolite refinements with powder data, this ratio often comes dangerously close to 1. In the former case, it is not disastrous if some of the observations are in error, or if the model used has deficiencies. The over-determination will help to pinpoint any shortcomings. With powder data, however, such errors can easily lead to seriously wrong results, and a person working with powder data must always be aware of this fact (Baerlocher and McCusker, 1994).

XRD is commonly used for the determination of the correct structure and purity of the synthesized zeolite, and for evaluating zeolite crystallinities. The structure and purity are obtained by using the X-ray pattern of the crystalline substance, which can be thought of as a "finger print" that each crystalline material has within limits, viz. a unique diffraction pattern

(Murthy and Reidinger, 1996). If all observed peaks can be found in the simulated pattern and have similar intensities, the crystal structure of the zeolite under investigation is the same as the structure that is used for the pattern simulation. If extra peaks are observed or peaks are missing, this is an indication that other crystalline phases are present, or the structure is different (Van Hooff and Roelofsen, 1991).

Diffraction peak intensities can be used to determine the crystallinity of the zeolite sample (Van Hooff and Roelofsen, 1991). For this purpose the intensity of one particular peak (or a number of peaks) are compared with the intensity of the same peak (or peaks) of a standard sample. The X-ray crystallinity then can be calculated from Equation 3.1:

$$\%\text{XRD crystallinity} = \frac{\text{Intensity of sample peak/s}}{\text{Intensity of same peak/s of standard}} \times 100 \qquad (3.1)$$

Szostak (1989) reported that the peaks chosen are selected specifically in order to obtain peaks which are the least affected by the degree of hydration of the sample and minimally affected by other factors. The percentage crystallinity can also be determined by examining the area of the peaks (see Equation 3.2):

$$\%\text{XRD crystallinity} = \frac{\text{Area/s of peak/s of sample}}{\text{Area/s of peak/s of standard}} \times 100 \qquad (3.2)$$

The width of the diffraction peaks also gives information about the average crystallite size of the investigated zeolite sample (Van Hooff and Roelofsen, 1991). The relationship between the crystallite size (t) and peak width (B) is given by Equation 3.3, where θ is the incident angle and λ the wavelength of the X-ray radiation.

$$t \text{ (in } \mu m) = \frac{0.9 \, \lambda \text{ (in } \mu m)}{B \cos \theta} \qquad (3.3)$$

Due to the peak broadening effect, it is not advisable to use peak intensities in measuring X-ray crystallinities for crystallites smaller than 0.3 μm (Van Hooff and Roelofsen, 1991).

X-ray diffraction can thus give information about crystal structure, degree of crystallinity and crystallite size. It is, however, impossible to obtain information about the presence of structure defects by this method. This can be done by high-resolution electron microscopy (HREM) (Van Hooff and Roelofsen, 1991). Although XRD is a commonly used method for the evaluation of zeolites, there are some problems associated with this method. The intensities of the low angle peaks are influenced by the type of counter ion, by the shape and size of the crystals and by the sorbates present, which may result in erroneous estimations (Hardenberg *et al.*, 1992).

For the characterization of ZSM-5, Szostak (1989) indicated that the four peaks corresponding to the 2θ range of 22.5° to 24° have been used with relative success. Suzuki *et al.* (1986) obtained the crystallinity of ZSM-5 by using the peak intensity at 23° 2θ. Typical diffractograms of ZSM-5 and silicalite are shown in Figure 3.3.

Hardenberg *et al.* (1992) determined the XRD crystallinities of ZSM-5 zeolites by the following three methods:

(i)   sum of the intensities of the five major peaks;

(ii)   sum of the intensities of the peaks between 22° 2θ and 25° 2θ;

(iii)   intensity of the peak at 23.1° 2θ.
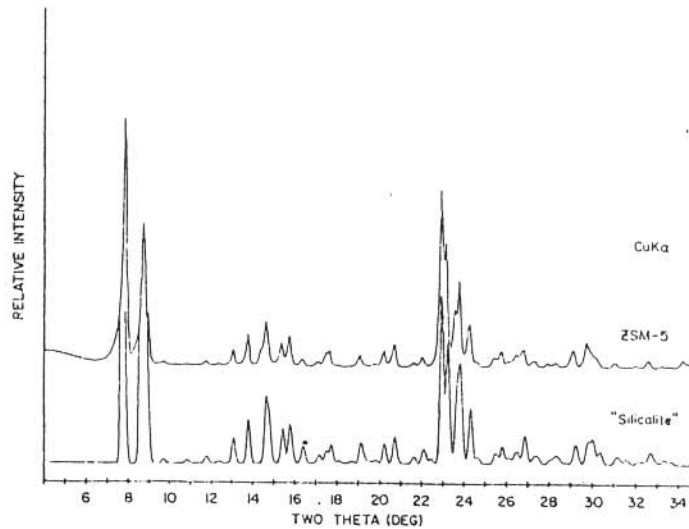
Figure 3.3 The diffractograms of ZSM-5 and silicalite (taken from Olson *et al.*, 1880).

These results were then compared with those obtained by *n*-hexane cracking as a CTR for the same zeolites (see Figure 3.4). The results indicated that either the XRD crystallinities are underestimated or the CTR crystallinities are over-estimated. Furthermore, the results also showed that there is a close correlation between methods (ii) and (iii) and the CTR, even at the
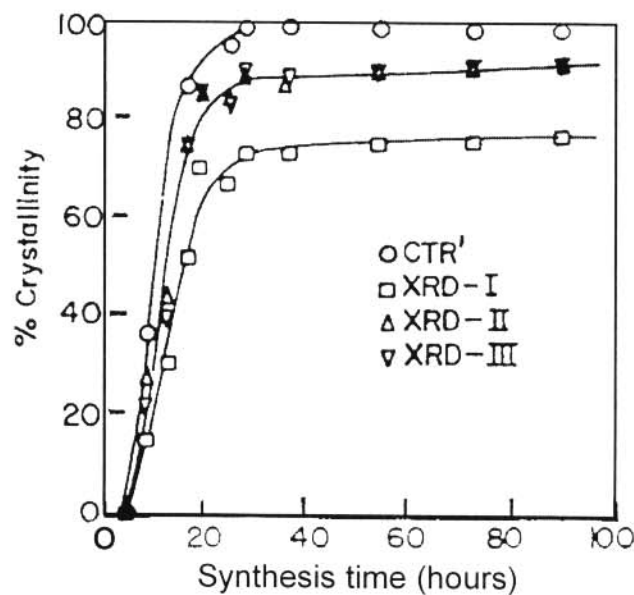
Figure 3.4 Plot of percentage crystallinity, calculated in three different ways, versus synthesis time for ZSM-5 zeolites with a SiO_2/Al_2O_3 ratio of 90 (taken from Hardenberg *et al.*, 1992).

low percentage crystallinities, and that method (i) gives the lowest values. Method (iii) gave slightly lower results than method (ii). Due to the closer agreement between (ii) and the CTR, Hardenberg *et al.* (1992) concluded that of the three XRD methods, the summation of the intensities of the peaks between 22° 2θ and 25° 2θ is the preferred one.

Wenyang *et al.* (1989) used XRD as one of the techniques to characterize the zeolite ferrierite. The percentage crystallinity was calculated by measuring the summation of the intensities of the seven peaks at the 2θ values of 9.3°, 22.3°, 22.5°, 23.5°, 24.4°, 25.2° and 25.6°, as compared to a highly crystalline material obtained from the same batch composition.

The percentage XRD crystallinity of the zeolite ferrierite was also calculated by using the sum of the intensities of all the peaks between 22° 2θ and 26° 2θ (Ramatsetse, 1998). This summation was divided by the sum of the intensities of the same peaks of the reference sample and the quotient thereof was multiplied by one hundred.

3.8 SCANNING ELECTRON MICROSCOPY

SEM is used primarily for the study of surface topography of solid materials (Reimschuessel *et al.*, 1988). It permits a depth of field far greater than optical or transmission electron microscopy. However, the resolution of SEM is about 30Å, approximately two orders of magnitude greater than the optical microscope and one order of magnitude less than the transmission electron microscope (TEM). Thus, SEM bridges the gap between the other two techniques. Any solid material can be studied. Sample size is limited to specimens less than about 10 cm in diameter.

SEM has been applied to the study of fibrous materials, ceramics, composites, metals, catalysts, polymers and biological materials. Information may be obtained by examination of both the natural surface of materials and that exposed by either fracture or sectioning. Rough topographic features, void content and particle agglomerations are easily revealed as well as compositional (phase) differences within a material (Reimschuessel et al., 1988).

SEM is the most versatile technique for the study of the morphology and particle size distribution of zeolites, since the size and morphology of the zeolite particles influence their properties. A typical example is the size and shape required for the application of Na-zeolite A as a builder in detergent formulations. The particle size should be in the range of 1.0 μm to 10 μm and the edges of the cubic zeolite crystals should be rounded off (Reimschuessel et al., 1988).

Using SEM, Concepción et al. (1996), observed that the crystals of certain zeotypes (MgAPO-5) may be of hexagonal morphology, which were either platelets or long prisms, varying in size depending on the crystallization conditions. The crystals of zeolite ZSM-23 have a rice-like morphology (about 6 μm in length and 3 μm in width) (Xu et al., 1994).

In a previous investigation (Ramatsetse, 1998), ZSM-5-based samples were synthesized with and without stirring and characterized by SEM. The SEM analyses showed that with this particular ZSM-5 synthesis recipe (see Section 2.4.2), and without stirring, spheroidal agglomerates of amorphous and zeolitic materials are obtained for synthesis temperatures up to 150°C and crystallinity up to 74%. The diameters of those spheroids increased to 5 μm with increasing temperature, up to 150°C. At higher temperatures, individual crystals were observed, which appear to grow out of the spheroids. Examples of these structures are shown in Figure 3.5. With
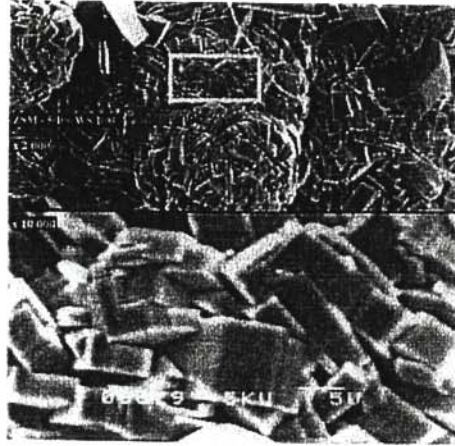
Figure 3.5. SEM micrograph of a ZSM-5 sample synthesized without stirring at 180°C (taken from Ramatsetse, 1998).

stirring of the reaction mixture, only the spheroidal morphology was observed, even at synthesis temperatures as high as 190°C. The diameters of these spheroids were less than 1 μm.

In contrast to the results obtained with ZSM-5 described above, Ramatsetse (1998) also showed that with the ferrierite synthesis recipe used (solid silica gel, Grandvallet *et al.*, 1992), ferrierite crystallites could already be observed at considerably lower percentage crystallinities (e.g. as low as 1%) for the syntheses both with and without stirring. The crystals obtained with stirring of the reaction mixture showed evidence that they were broken up or crushed to a certain extent by the magnetic stirrer bar.

3.9 TRANSMISSION ELECTRON MICROSCOPY

TEM can be used to study the structure and morphology of materials by examining the diffracted and transmitted electron intensities (Reimschuessel *et al.*, 1988). With the scanning attachment the microscope is operated in the scanning transmission electron microscope (STEM) mode.

This is used for image analysis and for elemental microanalysis of areas as small as 5 nm in size. Most solid materials can be studied, but because of technical constraints and because of the large scattering of the electrons in the solids, sample sizes are limited to no more than 3 mm in diameter and less than 0.2 µm in thickness. Obtaining a thin sample, which will be transparent to the electron beam, is a critical aspect of TEM. Characterization of powder samples can be obtained by combining TEM and STEM capabilities. Particle size distributions are obtained from the digitized STEM image and energy dispersive electron X-ray spectroscopy (EDS) is used to obtain elemental composition information.

Van Grieken *et al.* (2000) used TEM to follow the steps undergone by ZSM-5 during zeolitization. They were able to observe the primary particles forming the amorphous materials (Figure 3.6(a)), the spheroidal secondary particles forming the nanocrystalline (20 nm) ZSM-5
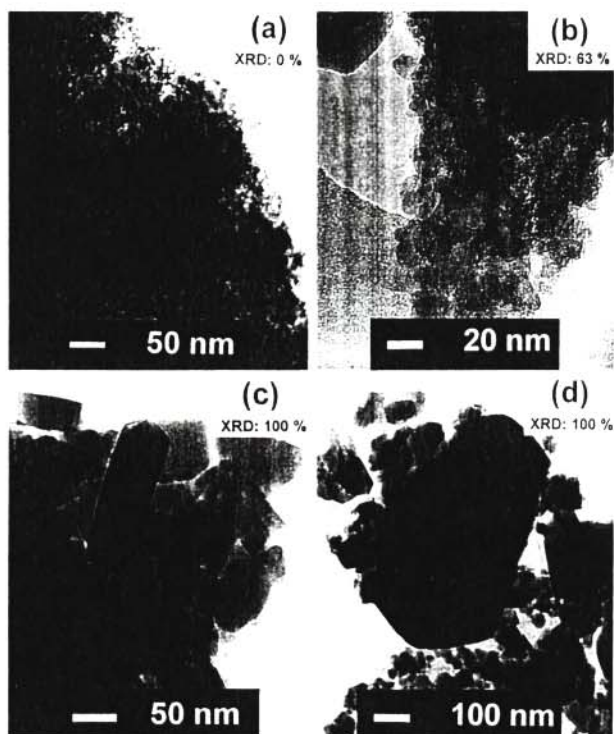
Figure 3.6 TEM images of ZSM-5-based samples with different crystallinities: (a) t = 12 h, (b) t = 22 h, (c) t = 48 h and (d) t = 108 h (taken from Van Grieken *et al.*, 2000).

(Figure 3.6(b)). In the last stages of the crystallization process, the zeolitization of these secondary particles yields ZSM-5 crystallites with sizes in the range of 50 nm and mostly of a cubic shape (Figure 3.6(c)). After 108 hours of synthesis, larger crystals with sizes up to 1 000 nm were observed (Figure3.6 (d)).

3.10 ALKANE CRACKING AS A CATALYTIC TEST REACTION

CTR is a technique in which the activity of a catalyst is evaluated by performing a probe reaction. Different reactions can be used, such as the isomerization of xylene (Copperthwaite *et al.*, 1978) and paraffin cracking (Nicolaides *et al.*, 1989). The latter authors reported the use of *n*-hexane cracking as a CTR, in combination with XRD analysis, in evaluating the yield of crystalline material obtained from batches of ZSM-5 zeolites with different aluminium content, prepared under both static and stirred conditions. *n*-Hexane cracking was chosen as the test reaction since it was indicated previously (Olson *et al.*, 1980) that the observed catalytic activity of ZSM-5 for *n*-hexane cracking at 538°C is linearly proportional to the tetrahedral aluminium content of the zeolite, whereas amorphous SiO_2-Al_2O_3 has almost negligible *n*-hexane cracking activity at the same temperature. Zeolite crystallization under static conditions and high aluminium concentrations lead to samples with non-ion-exchangeable sodium ions and lower than expected catalytic activities. The samples synthesized with stirring, however, could undergo almost complete ion exchange (with trace amounts of residual sodium). For these samples, a linear correlation was observed between *n*-hexane cracking activity and the percentage aluminium in the zeolite.

3.11 MECHANISMS FOR THE CRACKING OF ALKANES

A summary of the different cracking mechanisms for alkanes and the product distributions obtained over solid acid catalysts is given below.

In a major breakthrough in 1984, Haag and Dessau reported on the monomolecular cracking mechanism of alkanes catalyzed by solid acids, such as zeolites. It is now widely accepted that this mechanism occurs at high reaction temperatures by the direct attack of a Brønsted acid site on a C-C bond, forming a surface "carbonium ion type" activated complex (Corma and Orchillés 2000; Kotrel *et al.*, 2000). This mechanism, now known as the Haag-Dessau mechanism or protolytic monomolecular cracking, is illustrated in Figure 3.7.
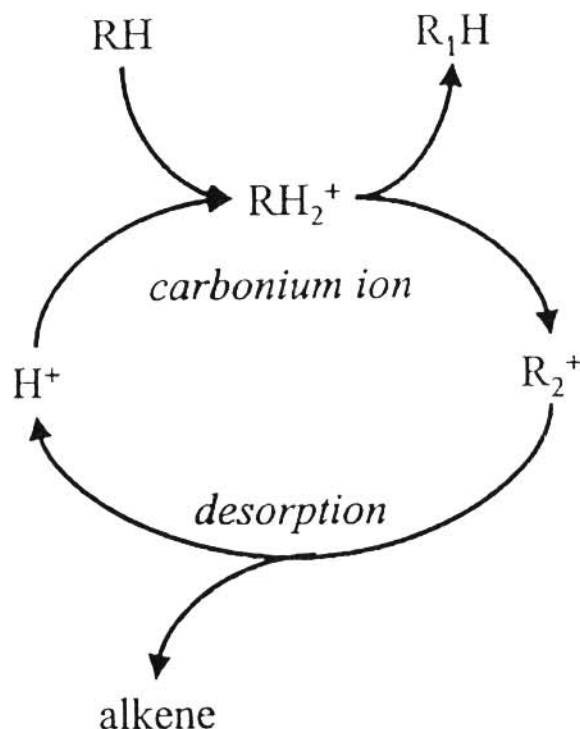
Figure 3.7 The Haag-Dessau cracking mechanism for alkanes (RH) proceeding via a carbonium ion transition state (taken from Kotrel *et al.*, 2000).

The Haag-Dessau mechanism of alkane cracking emerged from the product distribution data observed in the cracking of 3-methylpentane or *n*-hexane catalyzed by acid solids (H-ZSM-5, zeolite Y or silica-alumina) at 350°C to 550°C over a wide range of conversions. Haag and Dessau (1984) observed simple distributions of products formed from each alkane when they extrapolated their data to zero conversion – the products included substantial yields of dihydrogen, methane, and ethane (in addition to alkenes and some higher alkanes). They proposed the reaction scheme shown in Figure 3.8 for the initiation step in the cracking of these alkanes. Reaction (a) results from bond breaking indicated by line (a), etc. The carbenium ions formed react further, being deprotonated to give alkenes, and may subsequently undergo isomerization, disproportionation, and alkylation.
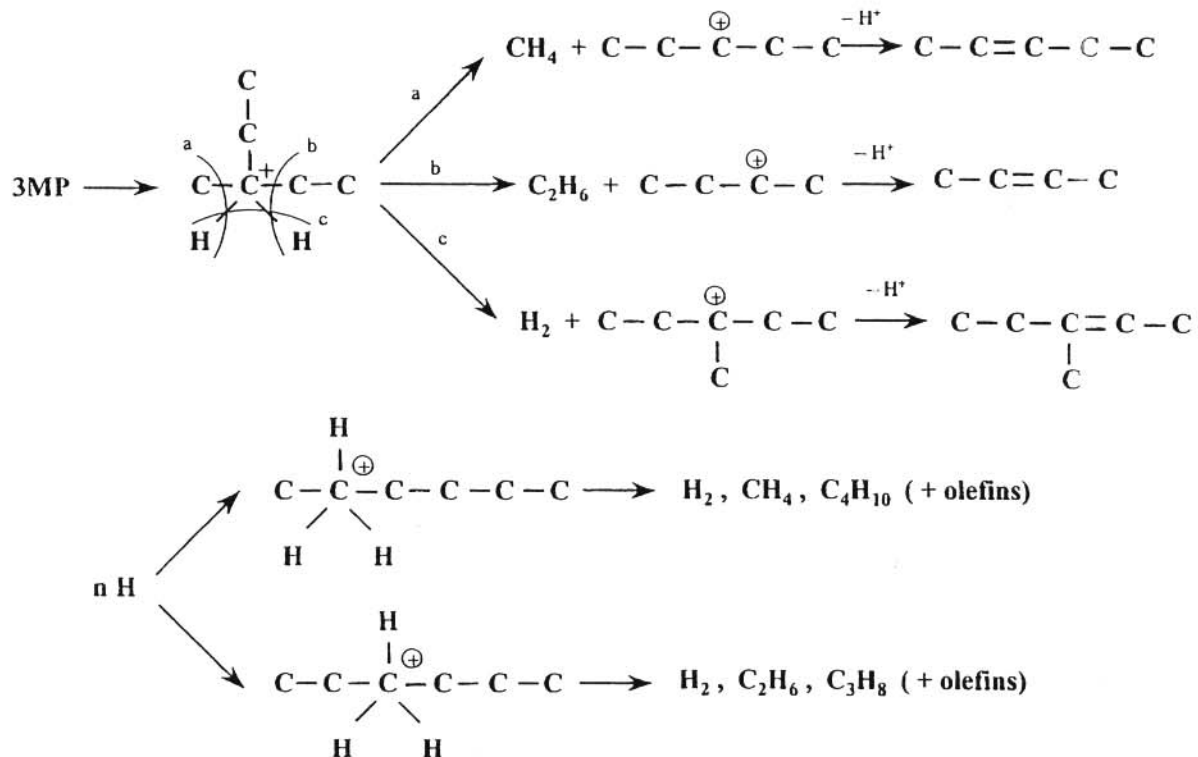
Figure 3.8 Protolytic cracking of 3-methylpentane (3MP) and *n*-hexane (nH) via pentacoordinated carbonium ions (taken from Corma and Orchillés, 2000).

The "carbenium-like" ion left on the surface can also abstract a hydride from the reactant alkane, forming an alkane and another carbenium ion which can crack by β-scission (cleavage of the C-C bond located β to the trivalent positively charged carbon atom) to give a smaller carbenium ion and another alkene (Figure 3.9) (Kotrel *et al.*, 2000). This is a chain reaction, appearing to be autocatalytic. The carbenium ion on the solid acid surface can also result from the protonation of alkenes.
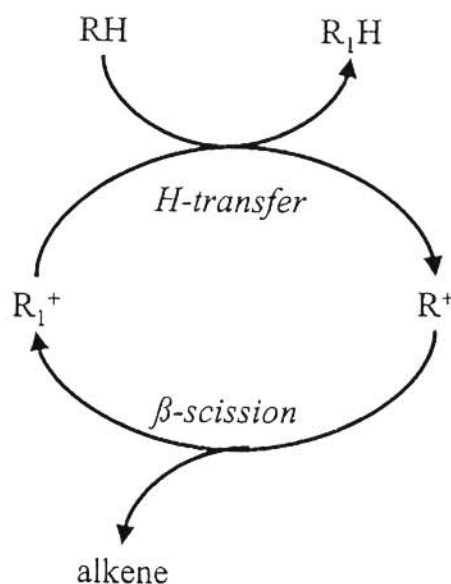
Figure 3.9 Classical cracking mechanism for an alkane molecule (RH) consisting of a hydride transfer step to a smaller carbenium ion (R_1^+) followed by β-scission (taken from Kotrel *et al.*, 2000).

After hydride transfer has occurred and the carbenium ion is formed, it is reported that it is difficult to visualize a β-scission without involving a primary carbenium ion, which is highly unstable. In this way Sie (1992) has proposed a mechanism for the cracking of carbenium ions that avoids the formation of primary carbernium ions and involves the participation of protonated cyclopropane ring structures. This mechanism is shown in Figure 3.10. Typical products are propene and isobutane.

83
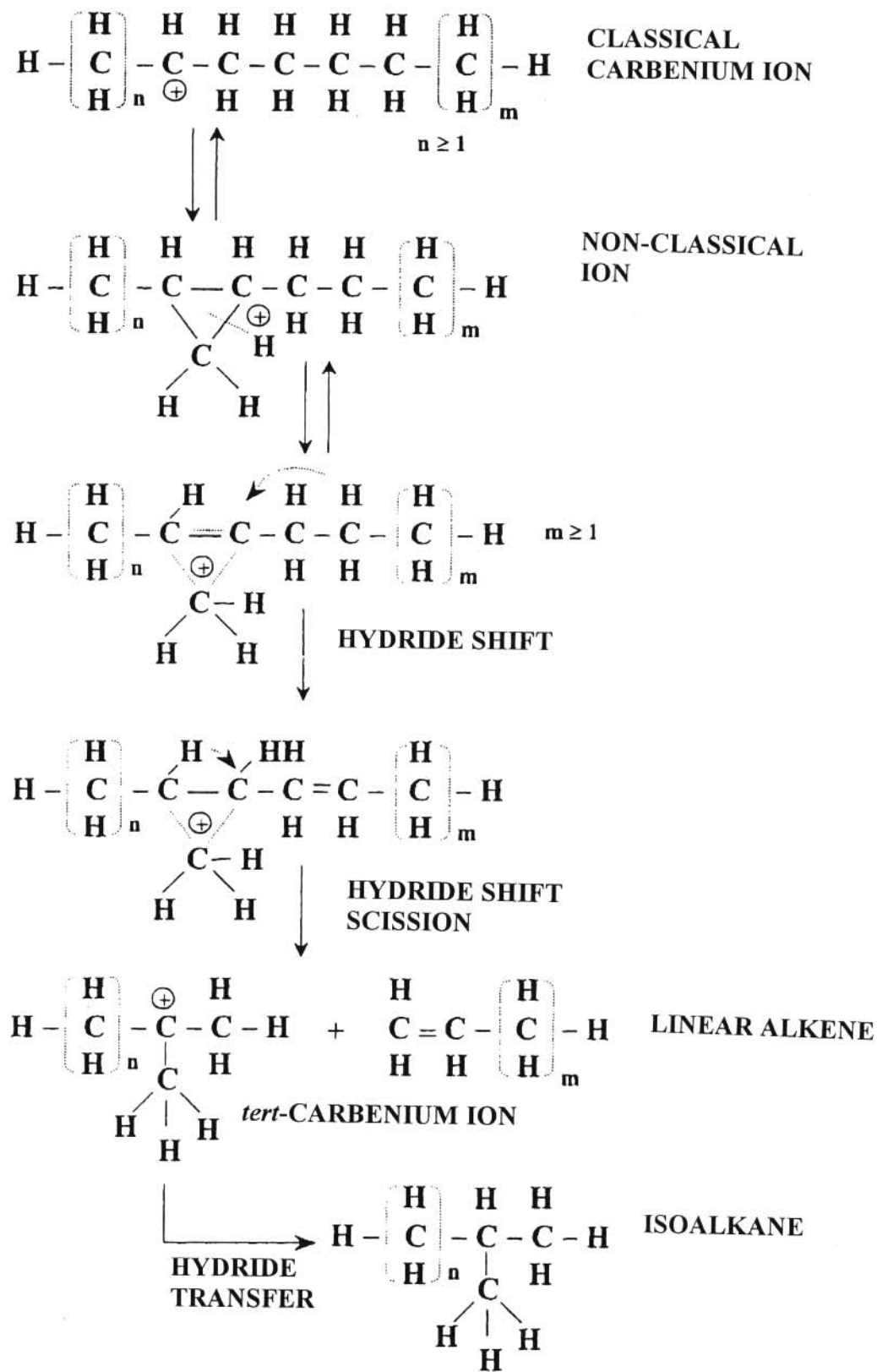
Figure 3.10 Proposed mechanism of acid catalysed cracking of a normal paraffin (taken from Corma and Orchillés, 2000).

This mechanism not only avoids participation of primary carbenium ions, but can also explain the high yield of isoalkanes obtained during the cracking of *n*-alkanes .

There is no doubt that the product distribution obtained during cracking of alkanes will depend on the relative contributions of the protolytic and β-scission mechanisms on C-C rupture. Then, if most of the cracking occurs through a bimolecular β-scission mechanism, high yields of branched products will be obtained. Corma *et al.* (1997) indicated that when reactants with more than four carbon atoms are used, it becomes impossible to determine the exact contribution of the protolytic and β-scission mechanisms to the final product distribution obtained if only product distribution data are used in the procedure.

On the contrary, with shorter chains, protolytic cracking dominate and methane, ethane and even ethylene and H_2 are produced. As an example, different authors (Bandiera and Taarit, 1990; Kwak and Sachtler, 1994; Kwak *et al.*, 1994) detected equimolar amounts of methane and ethene at low propane conversions over H-ZSM-5 catalyst, observing a 63% cracking probability and a 37% dehydrogenation probability. These values are consistent with the almost statistical cleavage of the carbonium ion formed by protonation of propane at the central carbon atom, which has two possibilities to cleave into methane and an ethyl cation or one possibility to cleave into dihydrogen and propene (Cheung *et al.*, 1996).

The catalyst and operation variables can also have an influence on the reaction mechanism. Haag and Dessau (1984) found that the activation energy was higher for the protolytic than for the β-scission mechanism. Thus, it can be expected that the monomolecular mechanism will predominate at higher temperatures. Moreover, the monomolecular character of the protolytic

and bimolecular nature of β-scission will make the former predominant at low partial pressures of hydrocarbon and lower levels of conversion.

Furthermore, it appears that bimolecular hydride transfer leading to a β-scission mechanism involves a larger transition state than the unimolecular protolytic cracking. Thus, appears that the pore size of the zeolite used as the catalyst can introduce a shape selectivity effect that will control the relative extent of the protolytic and β-scission mechanisms (Corma and Orchillés, 2000). On the other hand it must be taken into account that bimolecular mechanisms are favoured at higher site density and higher adsorption capacity. Thus, an increase of the framework SiO_2/AlO_3 ratio of zeolite will have negative effect on the rate of bimolecular cracking. All of these will certainly be reflected by the product distribution obtained.

CHAPTER FOUR

EXPERIMENTAL

4.1 INTRODUCTION

In this chapter we describe the reagents and their grades, as well as the equipment used to carry out the experiments reported in this thesis. The seven different methods utilized for the synthesis of the two zeolites of interest, namely zeolites ZSM-5 and ferrierite, are also reported in detail. Also described are the characterization techniques employed in this project, viz. XRD, SEM and CTR's.

4.2 REAGENTS

In this section (see Table 4.1) we list the reagents used and their purity or composition in wt%.

Table 4.1 Reagents used, their purity or composition, and supplier

Reagents	Purity or composition (wt%)	Supplier
Aluminium sulfate 14-18 hydrate	98	Aldrich
Ethanol	96	
Glycerol	99+	
Ludox HS-30	30	
n-Propylamine	99+	
Piperidine	99.5+	
Pyridine	99+	
Pyrrolidine	99.5+	
Silicic acid	----[a]	
Sodium silicate solution (water glass)	SiO_2, 27; NaOH, 14	
Aluminium sulfate 18-hydrate	100 to 110	Reidel-de Haën
Sodium aluminate	Al_2O_3, 50 to 56; Na_2O, 40 to 45; Fe_2O_3; 0.05	

Table 4.1 continue

Aluminium hydroxide	99	Merck
n-Hexane	99+	
Quartz	----[a]	
Tetrapropylammonium bromide	99+	
Sodium hydroxide	99+	BDH
Sodium sulfate	99	
Silver nitrate	99.8	
Aluminium nitrate nona-hydrate	99+	Fluka
Ammonium chloride	99.5+	
Ammonia solution	25	Uni-Lab
Sulfuric acid	90 to 91	Rochelle Chemical
Sodium chloride	99.5+	N.T. Laboratory
Aerosil 200	----[a]	Degussa
Silica gel (S342)	----[a]	Grace (Germany)
Air	99.999	Afrox
Hydrogen	99.999	
Nitrogen	99.999	
Propane	Propane, 94.154; ethane, 2.204; butane, 3.642	

[a]Not available

For the synthesis and washing of zeolites, deionized water was essential. This was obtained by using a Microsep Milli-Q water supplier which uses reverse osmosis and a polishing method to give reagent grade ultrapure water of 18 MΩ cm^{-1} resistivity at 25°C.

4.3 SYNTHESIS OF ZEOLITES

The aim of this project was to investigate whether autoclaves of different construction (top stirring or bottom stirring) will give similar results in terms of crystallinity, morphology, crystallite size, etc., and also to study the effect of reaction temperature and stirring conditions on the synthesis of the zeolites ZSM-5 and ferrierite, using the different autoclave systems and different synthesis recipes. Details on the autoclaves and recipes used are given below.

4.3.1 **Autoclaves**

Two types of autoclaves were used for the syntheses of the zeolites. One was a 1 000 ml Parr autoclave (type 4531). This reactor is fitted with a magnetic drive and a turbine type impeller, which allows for top-stirring of the reaction mixture, a removable reaction vessel, heavy duty drive and temperature controller (type 4842) with expansion module. The rate of stirring can be varied up to 800 rpm. With this commercial autoclave, the hydrothermal synthesis reaction can be carried out under autogenous pressure up to 140 bar and at temperatures up to $350^{\circ}C$.

The other autoclave used was a 350 ml in-house built stainless steel autoclave whose construction was described in detail elsewhere (Ramatsetse, 1998). The stirring in this autoclave was carried out from the bottom using a magnetic stirrer bar and a Heidolph MR 300K hotplate/stirrer which could reach an indicated 1 250 rpm. The autoclave was fitted with a 0 to 25 bar stainless steel pressure gauge (WIKA, 23-2-63).

The hydrothermal syntheses of the zeolites were performed both with and without stirring. With the in-house built autoclave, the ZSM-5 syntheses with stirring were performed using a 25 mm X 6 mm magnetic stirrer bar with the hotplate/stirrer set at 1 000 rpm. For the ferrierite syntheses in the in-house built autoclave, the reaction mixtures were stirred with a 52 mm X 8 mm magnetic stirrer bar with the stirrer at the setting of 1 250 rpm. For the preparation of the reaction mixtures, the stirring was carried out using a 25 mm X 6 mm magnetic stirrer bar, unless otherwise stated.

At the end of the hydrothermal treatment, the products obtained were filtered using a 14 cm diameter porcelain buchner funnel which was fitted with a glass microfibre filter paper

(Whatman GF/C) of 12.5 cm in diameter. The solids were extensively washed with deionized water until the filtrates were free of bromide, sulfate or hydroxide ions, which can be detected by the addition of silver nitrate to the filtrates. The products were then dried overnight (about 12 hours) in a drying oven (Labotec Ecotherm) at 110°C for the ZSM-5 materials and 120°C or 130°C for the ferrierite products.

To clean the autoclave between consecutive batches, washing was accomplished using 1 M sodium hydroxide solution for 1 hour at 150°C under autogenous pressure. After cooling, the autoclave was thoroughly rinsed with deionized water before loading the next reaction mixture.

4.3.2 Synthesis of ZSM-5-based materials

Four different recipes were used for the synthesis of the zeolite ZSM-5. Three of these methods were according to the literature (Copperthwaite *et al.*, 1986; Jacobs and Martens, 1987; Nicolaides *et al.*, 1991), whilst the fourth was a modified literature method in which water glass was used as the silica source instead of fumed silica (Aerosil 200). Details of all these recipes are given in Section 4.3.2.1 to Section 4.3.2.4 below. The amounts of each reagent used in each recipe were either increased or decreased by a constant factor depending on the differences in volume of the autoclave used in the publication and our own autoclaves.

For the removal of the template, tetrapropylammonium bromide, the dried solids were placed in a furnace (Carbolite type S30 fitted with a 2AU ESF Eurotherm) for calcination. During the calcination, the temperature was increased from room temperature in steps of 75°C, at 15 minute intervals, until the temperature reached 450°C, then increased to 550°C and maintained there for one hour, followed by a final increase to 630°C, at which temperature the samples were kept for

3.5 hours.

4.3.2.1 *ZSM-5 synthesis method 1 (Aerosil 200)*

One of the methods used for the synthesis of zeolite ZSM-5 in this project was that reported by Nicolaides *et al.* (1991) which utilized fumed silica as the silica source.

Three types of solutions were prepared. Solution A, which was a sodium aluminate solution, was prepared from 8.95 g of sodium hydroxide and 1.35 g of aluminium hydroxide to which 37.5 ml of deionized water was added. The mixture was heated and stirred until a clear solution was obtained. Solution B was prepared by mixing 14.85 g tetrapropylammonium bromide with 37.5 ml of deionized water with stirring, but without heating, until the solids had dissolved. "Solution C", which was essentially a silica slurry, was prepared from 40.20 g of fumed silica (Aerosil 200) to which 325 ml deionized water was added under vigorous stirring, using a domestic blender, until a smooth slurry was obtained.

To the slurry ("solution C"), solution A and then solution B were added respectively under vigorous stirring using the domestic blender. An additional 220 ml deionized water was added to the final mixture and transferred to the Parr autoclave and subjected to the hydrothermal synthesis under the hydrothermal reaction conditions given in the relevant sections in Chapter 5. The molar composition of the gel was:

$$77SiO_2:Al_2O_3:13Na_2O:3(TPA)_2O:3\ 978H_2O$$

4.3.2.2 *ZSM-5 synthesis method 2 (water glass)*

The method of Nicolaides *et al.* (1991) was modified by using water glass as both the silica and sodium hydroxide sources for the synthesis of ZSM-5.

Three types of solutions were prepared. Solution A, which was an aluminate solution, was prepared from 0.45 g of aluminium hydroxide to which 12.5 g of deionized water was added. The mixture was heated and stirred until it boiled. In this case no clear solution was obtained. Solution B was prepared by mixing 4.50 g of tetrapropylammonium bromide with 12.5 g of deionized water with stirring, but without heating, until the solids had dissolved. Solution C was prepared from 49.63 g of water glass to which 108.33 g of deionized water was added under vigorous stirring, using a 52 mm X 8 mm magnetic stirrer bar, until a homogeneous solution was obtained.

To solution C, solution A and then solution B were added under vigorous stirring using the magnetic stirrer bar. An additional 44.05 g of deionized water was added. This modified recipe resulted in a reaction mixture with a molar composition of:

$$77SiO_2:Al_2O_3:30Na_2O:3(TPA)_2O:3\ 978H_2O$$

This was then transferred to the in-house built autoclave. The hydrothermal synthesis was carried out at different temperatures (ranging from 90°C to 210°C) for 72 hours either with or without stirring.

4.3.2.3 *ZSM-5 synthesis method 3 (silicic acid)*

The next method used was the one reported by Copperthwaite *et al.* (1978) and by Whittingham

(1995). In this method silicic acid was used as the silica source.

This recipe involved the preparation of two types of solutions. Solution A was prepared from 16.0 g silicic acid, 4.0 g sodium hydroxide and 8.0 g of tetrapropylammonium bromide to which 40 ml deionized water were added. The mixture was stirred (with the 52 mm X 8 mm magnetic stirrer bar) until a homogeneous solution was obtained. To this solution, 8 ml of *n*-propylamine was added, again with vigorous stirring. Solution B was prepared by mixing 2.0 g of aluminium sulfate 14-18-hydrate with 8 ml of deionized water with stirring until the solids had dissolved. To this solution, 0.4 ml of sulfuric acid was added, once more with vigorous stirring.

To solution A, solution B was then added under vigorous stirring using the magnetic stirrer bar. Additional deionized water was added to the final mixture until a volume of 200 ml was obtained. The mixture was stirred further for 10 minutes and then transferred to the autoclave. The syntheses were performed at different temperatures (80°C to 210°C) with stirring or without stirring for 44 hours. The molar composition of the gel was:

$$84SiO_2:Al_2O_3:15.8Na_2O:9.5(TPA)_2O:31C_3H_9N:0.02H_2SO_4:3\,362H_2O$$
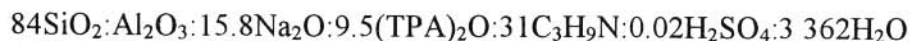
4.3.2.4 *ZSM-5 synthesis method 4 (Aerosil 200 and glycerol)*

The fourth method used for the synthesis of ZSM-5-based materials in this project was the one reported by Jacobs and Martens (1987). This method also uses fumed silica, as in synthesis method 1, but glycerol and an ammonia solution (25%) were used as additional reagents, and aluminium nitrate nona-hydrate was used instead of aluminium hydroxide.

For this recipe, three types of solutions were prepared. "Solution A", which was a silica slurry, was prepared from 2.70 g fumed silica (Aerosil 200) to which 85.10 g deionized water was added under vigorous stirring, using a domestic blender, until a smooth slurry was obtained. Solution B was prepared by mixing 30.20 g of tetrapropylammonium bromide with 28.40 g of deionized water, with stirring, until the solids had dissolved. To this solution 83.30 g of glycerol were added, also with stirring. Solution C was a sodium aluminate solution prepared from 0.70 g of sodium hydroxide and 0.50 g of aluminium nitrate nona-hydrate to which 5.5 g of deionized water were added. The mixture was stirred until the solids had dissolved. To this solution 0.60 g ammonia solution (25%) was added, also with stirring.

To the slurry ("solution A"), solution B and then solution C were added under vigorous stirring. The final mixture was transferred into the autoclave and the synthesis was conducted at different temperatures ($90^{\circ}C$ to $210^{\circ}C$), with or without stirring for 72 hours. The mixture had a molar composition of:

$$72SiO_2:Al_2O_3:14.4Na_2O:90(TPA)_2O:1\ 430glycerol:10\ 500H_2O$$

4.3.3 Synthesis of ferrierite-based materials

The zeolite ferrierite was synthesized using three different literature methods which utilize three different silica sources (Nanne *et al.*, 1980; Grandvallet *et al.*, 1992; Xu *et al.*, 1995a).

4.3.3.1 *Ferrierite synthesis method 1 (silica gel, S432)*

One of the methods used for the synthesis of ferrierite was a patented procedure by Grandvallet *et al.* (1992). This synthesis was performed in the Parr autoclave in order to compare the results

with those obtained earlier (Ramatsetse, 1998) under similar conditions in the in-house built autoclave. The silica gel used in this synthesis was specified to be 98% between 315 μm and 500 μm.

This method involved the following: Solution A was a hydroxide solution prepared from 5.40 g of sodium hydroxide and 100 g of deionized water. Solution B was prepared from 25.60 g of sodium sulfate, 6.14 g aluminium sulfate 18-hydrate and 100 g of deionized water. Solution C was prepared from 21.80 g of pyridine and 115.20 g of deionized water. Solution A was added to 54.40 g silica gel (S432), whilst stirring, until a homogeneous mixture was obtained, followed by the addition of solution B and then finally solution C, with continuous stirring. In order to ascertain the influence of temperature on the crystallinity of the ferrierite samples formed, different batches were prepared under autogenous pressure for 75 hours and the temperature was varied from 120°C to 200°C, and the synthesis were conducted with or without stirring. The mixture had a molar composition of:

$$93.5SiO_2:Al_2O_3:7.4Na_2O:19.6Na_2SO_4:30pyridine:1\,938H_2O$$
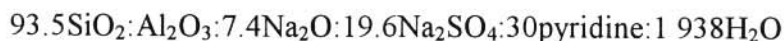
All the samples synthesized were dried overnight at 120°C and calcined in air to remove the template. During the calcination, the temperature was increased from room temperature in steps of 75°C, at 15 minute intervals, until the temperature of 450°C was reached and then increased to 500°C and maintained at this temperature for 3 hours.

Synthesis with seeding

The above-mentioned method was again used to synthesize the zeolite ferrierite in the presence of ferrierite seeds. These syntheses were performed in the in-house built autoclave using different masses (0.5 g and 1.0 g) of the ground seed. In each case the seed was added as the last

reagent to the reaction mixture, with stirring using the domestic blender. The seed used was a zeolite ferrierite with XRD crystallinity of 88% synthesized according to the method used by Nanne *et al.* (1992) where water glass was used as the silica source (see Section 4.3.3.2).

The reaction mixtures were hydrothermally treated without stirring at different temperatures ranging from 120°C to 200°C using either 0.5 g or 1.0 g of seed which was finely ground. The procedure, where 1.0 g was used was repeated with stirring using the 52 mm X 8 mm magnetic stirrer bar at a setting of 1 250 rpm.

Investigation of the cracks observed

It was suspected that the hydrothermal treatment and/or the sodium hydroxide were the causes of the formation of cracks found on the particles of silica gel (S432) during the synthesis of the ferrierite using this method. To investigate this, eight batches of silica gel (S432) were treated in different ways in the Parr autoclave.

Two identical batches were prepared by mixing 54.40 g of silica gel (S432) with 315 ml of deionized water. One was stirred and the other was not stirred. The third batch was prepared with 5.40 g of sodium hydroxide as the additional reagent. The fourth batch was prepared similarly to the third batch with the exception that 21.8 g of pyridine was added to the reaction mixture. These four batches were similarly treated under autogenous pressure at 150°C in the stirred reactor at 300 rpm, except one of the first two identical batches which was not stirred.

The additional four batches were prepared and placed in the autoclave in the same way as the previous four batches, except that they were treated at 120°C without stirring, and for one of the duplicate batches, a stirring rate of 300 rpm was used.

Particle size of silica gel

The effect of particle size of the silica gel (S432) on the percentage XRD crystallinity and morphology of the zeolite ferrierite synthesized under the above-mentioned method was also investigated. For these experiments silica gel (Grace S432) of particle sizes around 2 mm was ground and screened to smaller particle size fractions in the diameter ranges of 150 μm < d < 300 μm, 300 μm < d < 500 μm, 500 μm < d < 800 μm and 800 μm < d < 2 000 μm. The sieving was carried out using an Endecotts test sieve shaker (Endecotts, E.F.L. 1MK11, 3366) for a period of 30 minutes.

For the study of the effect of silica particle size, batches were synthesized without stirring at a constant synthesis temperature of 150°C and autogenous pressure in the Parr autoclave.

4.3.3.2 *Ferrierite synthesis method 2 (water glass)*

Another method used for ferrierite synthesis was according to the patented procedure developed by Nanne *et al.* (1992). This series of syntheses was carried out in the Parr autoclave only. This recipe was used in order to obtain a highly crystalline sample (as determined in previous studies (Ramatsetse, 1998)) to be used subsequently as seed.

Three types of solutions, namely solutions A, B and C, were prepared. Solution A was a water glass solution prepared from 205.22 g of water glass and 120 g of deionized water. Solution B was prepared from 31.96 g of piperidine and 120 g of deionized water. Solution C was prepared from 6.82 g of aluminium sulfate 18-hydrate, 2.50 g sulfuric acid and 120 g of deionized water. Solution B was added to solution A while stirring with a magnetic stirrer bar until a

homogeneous mixture was obtained, and finally solution C was added with continuous stirring. The mixture had a molar composition of:

$$90SiO_2:Al_2O_3:35Na_2O:3H_2SO_4:37\text{piperidine}:2\,612H_2O$$

In this investigation, samples were synthesized with top-stirring at 500 rpm, under autogenous pressure for 113 hours at a constant temperature of $150^{\circ}C$.

The as-synthesized ferrierite samples were thoroughly washed by mixing the solid product with water and overhead stirring for 1 hour followed by decantation of the water after the solid had settled. This process was continued until the water was free from sulfate as well as hydroxide ions, as determined by the addition of silver nitrate to the decanted aqueous phase. The drying and calcination was the same as that of the previous method, except that in this case the samples were calcined twice in air at $500^{\circ}C$ for 3 hours in order to completely remove the template (piperidine).

4.3.3.3 *Ferrierite synthesis method 3 (Ludox HS-30)*

Ferrierite zeolite-based materials were also synthesized using Ludox HS-30 as a silica source according to the method by Xu *et al.* (1995a). In this investigation only the in-house built autoclave was used.

The preparation of the reaction mixture involved four types of solutions. Solution A was a sodium aluminate solution prepared from 0.5 g of sodium chloride, 3.85 g sodium aluminate and 27.37 g of deionized water. Solution B was prepared from 47.09 g Ludox HS-30 and 54.74 g of deionized water. Solution C was prepared from 27.06 g pyrrolidine and 27.37 g of deionized water. Solution D was prepared from 0.73 g sodium hydroxide and 18.27 g of deionized water.

Solution A was added to solution B whilst stirring with the magnetic stirrer bar until a homogeneous mixture was obtained, followed by solution C and finally solution D. The molar composition of the reaction mixture was:

$$13SiO_2:Al_2O_3:6Na_2O:20pyrrolidine:473H_2O$$
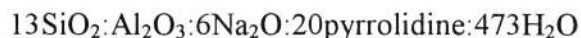
In order to ascertain the influence of temperature on the crystallinity of these ferrierite samples, different ferrierite samples were synthesized under autogenous pressure for 80 hours at different temperatures ranging from $120^{\circ}C$ to $200^{\circ}C$. In this investigation the influence of stirring rate was also considered. Samples were therefore prepared with and without stirring.

In this method all the ferrierite samples were dried at $130^{\circ}C$ overnight and calcined twice in air at $550^{\circ}C$ for 4 hours to remove the template (pyrrolidine). During the calcination, the temperature was increased from room temperature in steps of $75^{\circ}C$, at 15 minute intervals, until it reached $450^{\circ}C$, and by $100^{\circ}C$ to $550^{\circ}C$ and left at $550^{\circ}C$ for 4 hours.

4.4 CHARACTERIZATION OF THE ZEOLITE PRODUCTS

All samples synthesized were characterized by XRD and most of them by SEM. CTR's were also employed to determine the catalytic activity of some of the ZSM-5-based samples. *n*-Hexane cracking and propane cracking were chosen as the CTR's. The use of CTR's was undertaken since they are good supplementary techniques to XRD for the more complete characterization of the zeolitic materials produced.

4.4.1 **X-ray powder diffraction**

X-ray powder diffraction analyses of all the samples synthesized were carried out with a Siemens PW17 based diffractometer using CuK_α radiation. The procedure followed during the sample preparation and analysis were as previously described (Ramatsetse, 1998). Percentage relative XRD crystallinities were calculated from the sum of the major peak intensities relative to that of a highly crystalline reference sample multiplied by hundred, which was the method previously used by Ramatsetse (1998) and Nicolaides (1999) (see also Section 3.7). The standard used for the ZSM-5-based materials was a highly crystalline ZSM-5 sample synthesized during the course of this project by using the silicic acid method (Section 4.3.2.3), and for the ferrierite samples a highly crystalline ferrierite synthesized by Dr C.P. Nicolaides, using the patented method by Nanne *et al.* (1980). The XRD diffractogram of the ZSM-5 reference sample is given in Figure 5.24). Figure 4.1 below is the XRD diffractogram of the ferrierite reference done on the same diffractometer.
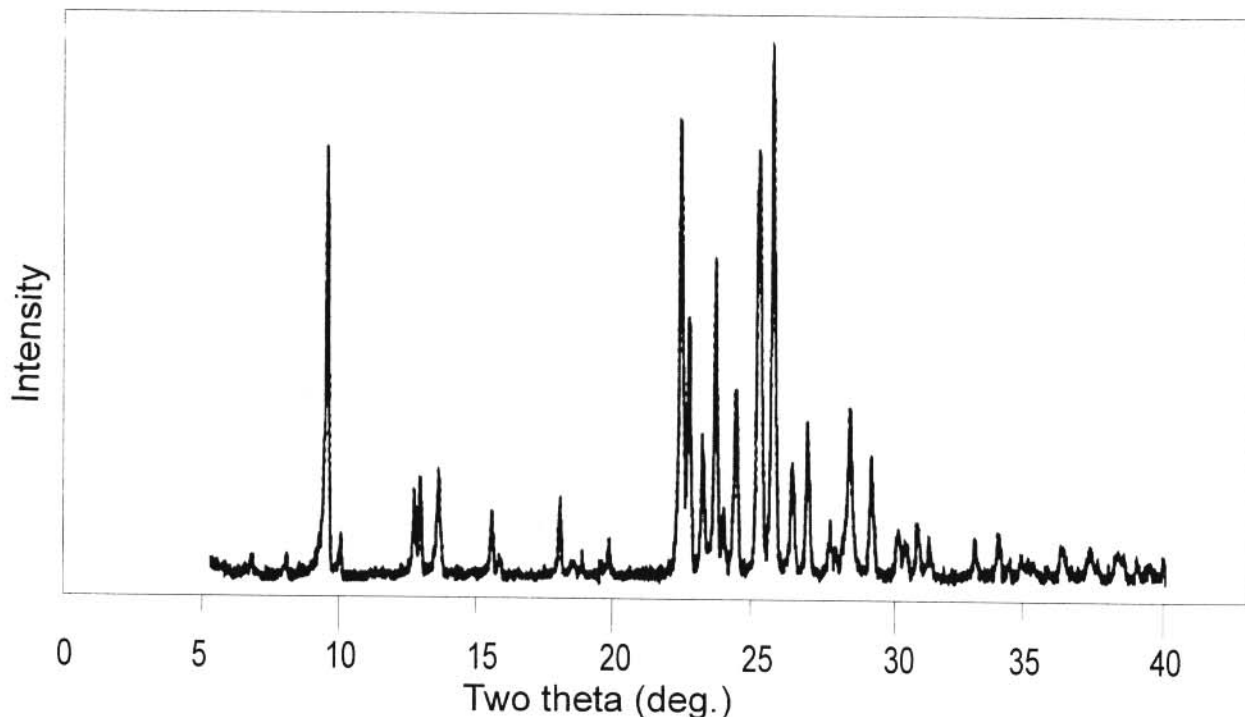
Figure 4.1 XRD diffractogram of the ferrierite reference sample used in this study.

4.4.2 Scanning electron microscopy

Morphological analyses of the synthesized samples were carried out using an Hitachi 450 scanning electron microscope. The samples were viewed at an accelerating voltage of 5 kV and using the lowest beam current in order to avoid sample damage. The procedure for the sample preparation and analysis was identical to that described earlier (Ramatsetse, 1998). In addition to the above method for sample preparation, an ultrasonic method was also used which is outlined below.

Small amounts of the zeolitic material (about 0.1 g) were transferred into a test tube. About 5 ml of ethanol were added to each tube which was placed in an ultrasonic bath (Bramsonic 5200) for about 30 seconds to separate the sample particles and produce a suspension of fine particles. Small amounts of the suspension were extracted with a 2 ml disposable polyethylene pasteur pipette and transferred onto a conducting adhesive carbon tab (12 mm in diameter) which were attached to an aluminium stub. The alcohol was allowed to evaporate in an oven at 60°C. The mounted samples were gold-coated in a BIO-RAD high resolution cold sputter coater.

4.4.3 Catalytic test reactions

The catalytic activity of selected ZSM-5-based samples of different percentage crystallinities, synthesized according to the Aerosil method described in Section 4.3.2.1, was evaluated using propane and n-hexane cracking as the CTR's. Selected samples were chosen from the series of batches synthesized with and without stirring in the Parr autoclave as well as those synthesized with stirring in the in-house built autoclave, with all samples having the same SiO_2/Al_2O_3 ratio in the starting gel (see Table 4.2). These samples were first ion exchanged with ammonium chlo-

Table 4.2 H-ZSM-5-based materials synthesized under different conditions using the Aerosil 200 method, evaluated by catalytic test reactions

Batch no.	Autoclave	Stirring rate (rpm)	%XRD crystallinity
493	Parr	100	2
510		100	18
511		100	27
513		100	51
519		100	63
520		100	78
242	Parr	WS[a]	5
244		WS[a]	13
71		WS[a]	39
250		WS[a]	58
258		WS[a]	80
11	In-house	1 000	5
43		1 000	33
29		1 000	54
18		1 000	65

[a]WS = without stirring

ride (see Section 4.4.3.1 below) to form H-ZSM-5 before being subjected to catalytic evaluation using *n*-hexane and propane cracking as CTR's.

4.4.3.1 *Ion exchange to obtain H-ZSM-5*

Each calcined product was converted to the ammonium form by ion exchange at room temperature with 1 M ammonium chloride solution. The solid (zeolite) and the solution (10 ml of solution/g of solid) were placed in a beaker and gently stirred for 1 hour using an overhead stirrer. The impeller was suspended on top of the solid so as not to crush the particles. The

ammonium solution was then decanted, fresh solution added and the ion exchange procedure was repeated three times. The ammonium form of the zeolites was then washed with deionized water until the filtrates were free of chloride ions, as tested by the addition of silver nitrate to the filtrate. The final step in the preparation of the zeolite was its conversion into the acidic form by the calcination of the ammonium form of the zeolites or zeolite-based materials at 550°C for three hours in air to give the H^+-form of ZSM-5.

4.4.3.2 *Catalytic reactor*

The reactor and heating metal jacket used were constructed at the mechanical workshop of the University of the Witwatersrand. A tubular stainless steel reactor (see Figure 4.2), 10 mm internal diameter and 260 mm in length, was loaded with the catalyst. The particle sizes of the catalysts used were 300 μm < d < 500 μm obtained by sieving. For *n*-hexane cracking, 0.1 g of the catalyst was mixed with 3.7 g of quartz to act as catalyst diluent. For the propane cracking experiments, 0.5 g of catalyst was mixed with 2.0 g of silica gel (S432).

The procedure for the packing of the reactor is as follows: the bottom part of the reactor was packed with glass wool (Fluka), followed by the stainless steel balls, then with another thin layer of glass wool. The stainless steel balls and the two thin layers of glass wool occupied about 74 mm in height from the bottom part of the reactor. The catalyst bed was put on top of the second glass wool layer. This occupied a height of about 85 mm of the middle part of the reactor. A third thin layer of glass wool then covered the top part of the bed. Next the controlling thermocouple, that passed through the lid of the reactor, was inserted through the top layer of glass wool into the catalyst bed in such a way that the tip was in the middle of the bed, as determined by prior measurements. Then the top layer of stainless steel balls was added. The lid
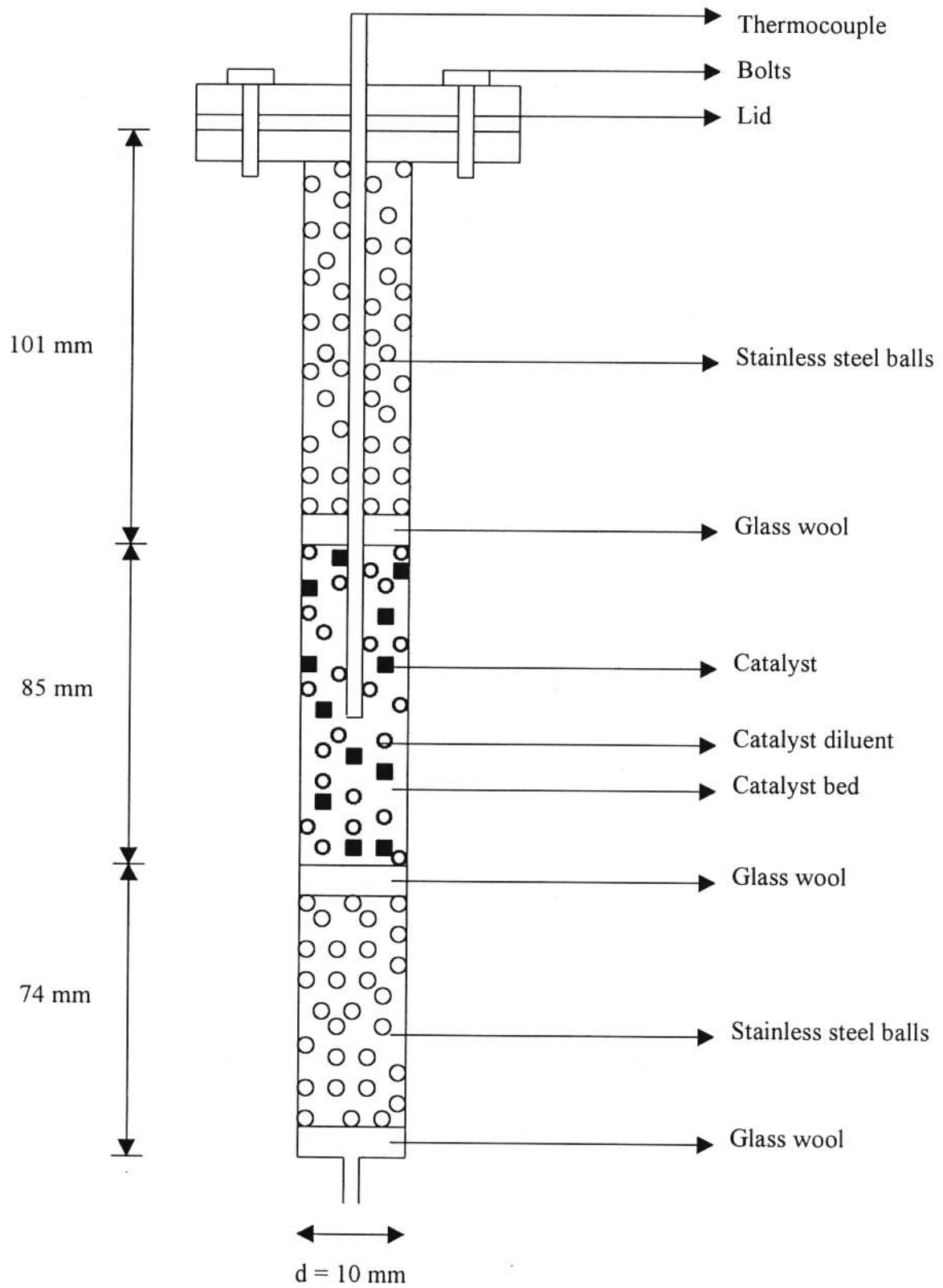
Figure 4.2 Packing of the catalytic reactor.

was put in place and the reactor was then closed by tightening the bolts.

The stainless steel nuts used to screw the lid to the reactor were smeared with an assembly paste (Swift White, Molyokote, type D). The reactor was tightly held within a clamp in order to fasten the nuts, first with a spanner and then with a torque wrench after which it was placed in the heating metal jacket of the reactor system.

A schematic representation of the reactor set up is given in Figure 4.3. The tubing leading to the gas chromatograph (GC) was heated at 200°C by a temperature controlled heating tape. Both the tubing and the reactor were covered by a thermal blanket (Fiberfrax Durablanket) in order to assist with insulation. The thermal blanket was in turn covered by aluminium foil.
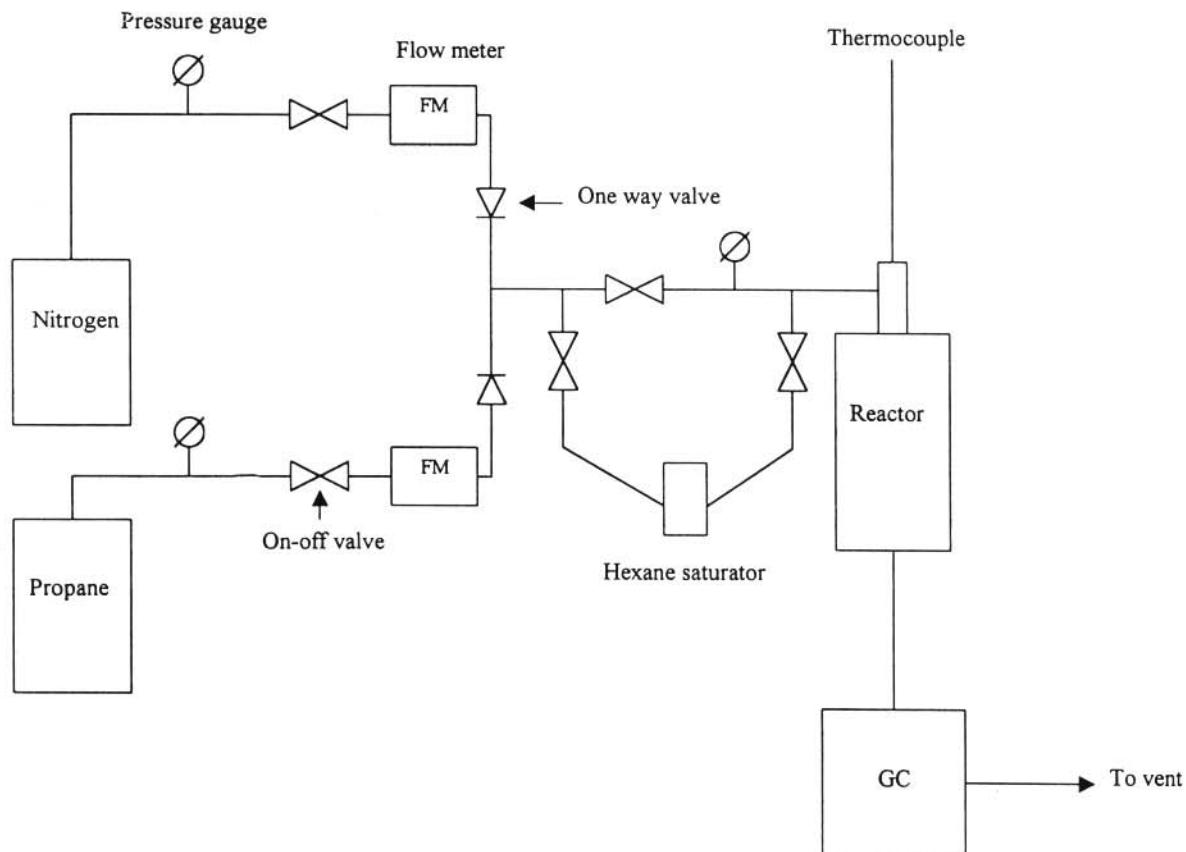
Figure 4.3 The catalytic reactor system.

After loading of the catalyst, the system was first purged with flowing nitrogen at 20 ml per minute while the temperature of the reactor was raised up to 500°C. For the *n*-hexane cracking experiments, the nitrogen stream (at 20 ml/min) was saturated with *n*-hexane at 0°C and sampling for GC analysis was after 22 minutes (time-on-stream (TOS) = 20 minutes). In the case of propane cracking, the nitrogen stream was mixed with propane at a volmetric ratio of 1:1 and sampling was after 5 minutes (or after 3 minutes on-stream). The higher TOS for *n*-hexane cracking is due to the larger volume of the hexane saturator to be flushed.

A Varian 330 GC with a Porapak Q column and flame ionization detector was used for the analysis of the products for both CTR's. The GC column's temperature was raised to 36°C in 10 minutes followed by an increase to 120°C in 15 minutes, and kept at 120°C for 5 minutes and was finally raised to 200°C in 15 minutes and kept there for 25 minutes. Throughout each run, the temperature of the injector and of the detector was kept at 150°C and that of the auxilliary at 220°C.

4.4.3.3 *Calculations*

As an example, the calculations of the catalytic results obtained from *n*-hexane cracking over the 78% XRD crystallinity H-ZSM-5 catalyst are given below. A chromatogram is shown in Figure 4.4 where the reactant and the product peaks have been identified and labelled. Table 4.3 is the corresponding print-out of the GC results. The first peak in the chromatogram is the methane peak (C_1) which elutes after 1.5 minutes. The second peak is ethene ($C_2^=$), and the third peak is ethane (C_2^-). These are then followed by the propene ($C_3^=$) and propane (C_3^-) peaks. The next group of peaks retained for 16.76 minutes to 17.63 minutes is the mixture of *iso*-butene, the *n*-butenes and butanes (C_4's). Complete separation of all the isomers cannot be achieved with the
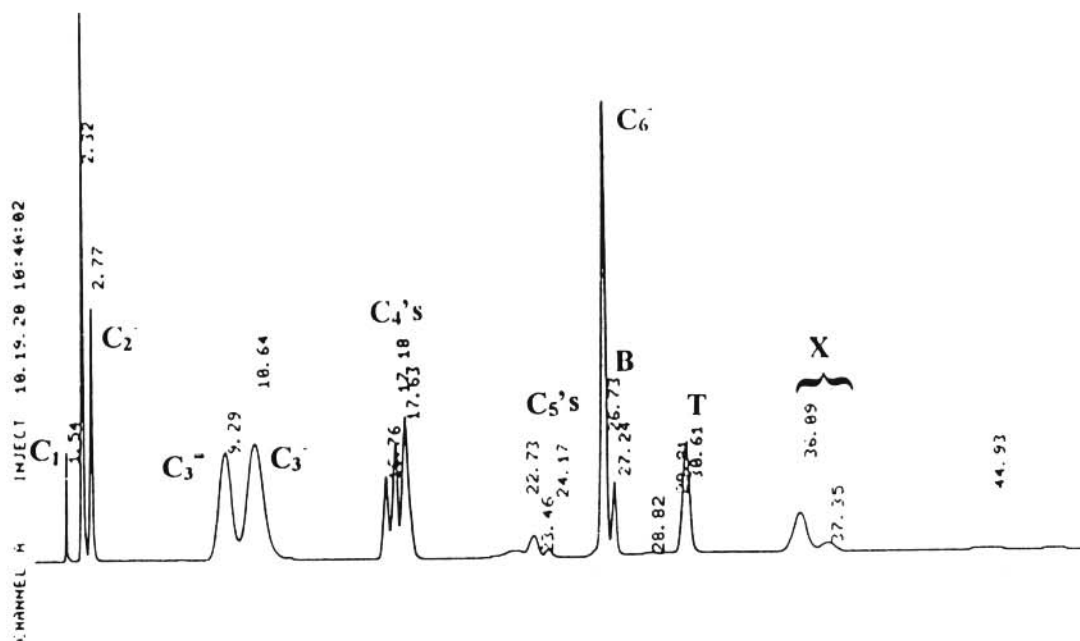
Figure 4.4 Gas chromatogram of products obtained from *n*-hexane cracking over the 78% crystallinity H-ZSM-5 sample (synthesized with stirring in the Parr autoclave).

Table 4.3 Print-out of the results from the chromatogram of the products obtained from *n*-hexane cracking over the 78% crystallinity H-ZSM-5 sample (synthesized with stirring in the Parr autoclave)

```
                                    10.19.20 10:40:02

FILE   1.      METHOD  0.      RUN   7      INDEX   7

PEAK#      AREA%       RT        AREA BC

    1       1.007      1.54       7347 01
    2       9.404      2.32      68578 08
    3       5.477      2.77      39940 05
    4      11.798      9.29      86042 02
    5      17.031     10.64     124200 03
    6       3.41      16.76      24866 02
    7       4.847     17.18      35350 02
    8       8.578     17.63      62558 03
    9       1.341     22.73       9782 02
   10       1.865     23.46      13598 02
   11       0.488     24.17       3559 03
   12      17.417     26.73     127020 02
   13       2.854     27.24      20811 03
   14       0.187     28.82       1365 02
   15       0.115     29.81        838 02
   16       7.317     30.61      53360 03
   17       4.993     36.09      36412 02
   18       1.2       37.35       8754 03
   19       0.671     44.93       4895 01

TOTAL    100.                  729275
```

Porapak column. Similarly the next group of peaks retained from 22.73 minutes to 24.17 minutes is the mixture of pentene and pentane isomers (C_5's). The next peak is that of the unreacted n-hexane (C_6). The last three groups of peaks after n-hexane are therefore benzene, toluene and xylene (BTX) which are all denoted as C_{6+} (or heavier) in Chapter 5. It should be noted here, that kinks in the chromatograms, particularly at the high retention times, as can be seen in Figure 4.4, and which were seen as peaks by the intergrator, were excluded from our calculations of percentage conversion and percentage selectivity.

The percentage conversion is the percentage of n-hexane converted to products and is calculated by subtracting the percentage of the area of the unreacted n-hexane from 100 as indicated in Equation 4.1. From Table 4.3, and excluding the kinks at 44.93 minutes,

$$\%\text{Conversion} \quad = \quad (100 - \%n\text{-Hexane}) \tag{4.1}$$

$$= (100 - 17.5)\%$$

$$= 82.5\%$$

Assuming first-order kinetics for the monomolecular cracking of n-hexane, the activity of the catalyst is calculated by using the formula given in Equation 4.2,

$$\text{Activity} \quad = \quad -\ln(1-x) \tag{4.2}$$

where x is the fractional conversion, resulting in an activity of 1.74 for the catalyst under consideration.

The percentage selectivity (in mass%), to a particular product C_y, is calculated using

$$\text{Selectivity} \quad = \quad \frac{\text{Mass\% of product } C_y}{\%\text{Conversion}} \quad X \quad 100 \tag{4.3}$$

For example, the selectivity to C_3^- in this experiment is 20.8%.

Product spectrum (in mole%), to a particular product C_y, is calculated as follows:

$$\text{Mole\% } C_y = \frac{\text{Mass\% of product } C_y}{\text{Molar mass of } C_y} \quad X \quad \frac{100}{\text{Total moles of product formed}} \quad (4.4)$$

In the propane conversion experiment, the excess propane caused difficulty with the separation of propene and propane and the conversion could not be calculated from the decrease in the mass percentage of propane. Furthermore, the propane source contains ethane (2.204%) and butanes (3.642%) as impurities, and it is expected that the C_4's will react at a higher rate than the propane to give the lower alkanes, C_1 to C_3. For these reasons the percentage conversion of propane (with impurities) over the different H-ZSM-5-based materials investigated was calculated as follows:

$$\%\text{Conversion} = \frac{[\%(C_3^- + C_4\text{'s) in}] - [\%(C_3^- + C_4\text{'s) out}]}{[\%(C_3^- + C_4\text{'s) in}]} \quad X \quad 100 \quad (4.5)$$

CHAPTER FIVE

RESULTS AND DISCUSSION ON THE SYNTHESIS, CHARACTERIZATION AND CATALYTIC PROPERTIES OF ZSM-5-BASED MATERIALS

5.1 INTRODUCTION

In a previous investigation (Ramatsetse, 1998), we examined the influence of the hydrothermal synthesis temperature and stirring rate on the percentage crystallinity and morphology of ZSM-5-based materials which were prepared according to a known synthesis method and in an in-house built autoclave (see Section 2.3.5 and Section 2.3.7). In this project, our first aim was to investigate whether the conclusions reached previously on the influence of the hydrothermal synthesis temperature and stirring rate are generally applicable to the case where a commercial Parr autoclave is used, with and without overhead stirring (instead of the bottom stirring using a magnetic stirrer bar). The results from these series of experiments conducted in the Parr autoclave are given and discussed in this chapter. Also reported in this chapter are the results obtained and conclusions reached on using different ZSM-5 synthesis recipes and their effect on (i) the percentage crystallinity, (ii) its controllability and reproducibility, (iii) the zeolite morphology, and (iv) the crystallite size, all as a function of synthesis temperature and stirring, as determined using XRD and SEM analyses. A comparison between these results and those obtained previously (Ramatsetse, 1998) is also presented. For this purpose, the previously

reported percentage crystallinities were re-calculated using the higher crystallinity standard used in the present investigation (see Section 4.4.1) in order to allow for more accurate comparisons.

In terms of the catalytic evaluation of the materials prepared, some of the ZSM-5 zeolite-based materials prepared with stirring in the in-house built and in the Parr autoclave with and without stirring were ion exchanged to obtain H-ZSM-5-based materials and *n*-hexane cracking and/or propane cracking were then used as the catalytic test reactions (CTR's). This was done in order to investigate whether the samples synthesized with and without stirring and with almost the same percentage XRD crystallinities exhibit similar catalytic behaviour, and in addition, to ascertain the differences or similarities in catalytic performance between the samples synthesized using the same recipe but in different autoclaves (different volumes and different stirring mechanisms, see below).

For the purpose of this thesis, zeolite-based materials of XRD crystallinity < 30% are considered as substantially amorphous, while partially crystalline material are taken as those with crystallinities between 30% and 70%, and as highly crystalline, the zeolitic materials with percentage XRD crystallinities of > 70% (Nicolaides, 1996; Nicolaides *et al.,* 2002b).

The ZSM-5 zeolite-based materials was synthesized according to the four methods described in Section 4.3.2. All the syntheses reported in this chapter were conducted for a period of 72 hours, except for the method in which silicic acid was used as a silica source, for which a synthesis period of 44 hours was employed. These experiments were carried out at temperatures ranging from just before crystallization commenced, which was usually between 80°C and 90°C, up to 210°C in steps of 10°C. In some cases, intervals of 5°C were used in order to obtain a better

understanding of the relationship between synthesis temperature and crystallinity.

Zeolites synthesized were given batch numbers in a consecutive way according to the time of preparation. These are given in order to show at what stage in the project any specific synthesis had been performed. Batch numbers and reaction temperatures are also indicated on the SEM micrographs shown below. The acronym "WS" refers to synthesis without stirring.

5.2 THE EFFECT OF TYPE OF AUTOCLAVE

In this part of the investigation, the recipe previously used for the synthesis of the ZSM-5-based materials in the in-house built autoclave, viz. the Aerosil 200 method, was employed for the series of syntheses performed in the commercial Parr autoclave (see Section 4.3.2.1, and Nicolaides *et al.*, 1991). The main difference between these autoclaves is that the Parr autoclave has a top stirrer made up of impellers while with the in-house built autoclave a magnetic stirrer bar is used. Furthermore, the Parr autoclave has a volume of 1 000 ml in comparison with the 350 ml of the in-house built autoclave. These experiments can also be viewed as an investigation into the scale-up of the recipe. The batches were synthesized with and without stirring for 72 hours in the temperature range of 90°C to 210°C. The effect of stirring rate in the Parr autoclave on the percentage crystallinity of the ZSM-5-based materials was also investigated.

5.2.1 Synthesis without stirring (Parr autoclave)

In this investigation, at least two batches were prepared at each synthesis temperature.

XRD analysis

Examples of the X-ray diffractograms of some of the ZSM-5 zeolite-based materials prepared without stirring in the Parr autoclave are shown in Figure 5.1. Figure 5.1(a) is the diffractogram of one of the samples which was hydrothermally synthesized at 90°C. The hump in the diffractogram at around 23° 2θ, which is characteristic of amorphous materials (Nicolaides, 1996), shows that the product is X-ray amorphous. In Figure 5.1(b), which is the diffractogram of the sample prepared at 100°C, small peaks are observed on top of the hump. At 130°C, the characteristic peaks of ZSM-5 become more evident, as shown in Figure 5.1(c). The positions of these peaks are at the same angles as the major peaks for ZSM-5 (Von Ballmoos and Higgins, 1990; Nicolaides, 1999). It can further be observed from the X-ray diffractograms that on average the peak intensities increase with increasing reaction temperature up to 200°C (see Figure 5.1(d) and Figure 5.1(e)), and at the same time the hump appearing in the diffractogram of the amorphous material diminishes at the higher synthesis temperatures, i.e. as the percentage crystallinity increases.

At 210°C, which is the maximum temperature investigated in our studies, a decrease in the intensities of the characteristic peaks of ZSM-5 is observed. This could possibly be due to dissolution of the crystallites at these higher temperatures. Figure 5.1(f) is the diffractogram of one of the samples synthesized at 210°C where this decrease in the peak intensities can be readily observed.

The calculation of the percentage XRD crystallinity of the ZSM-5 zeolite samples was done according to the previously published method (see Section 4.4.1) and the values obtained for the samples synthesized at different temperatures are listed in Table 5.1 and presented graphically in Figure 5.2. This plot gives an S-shaped curve for the percentage XRD crystallinity as a function
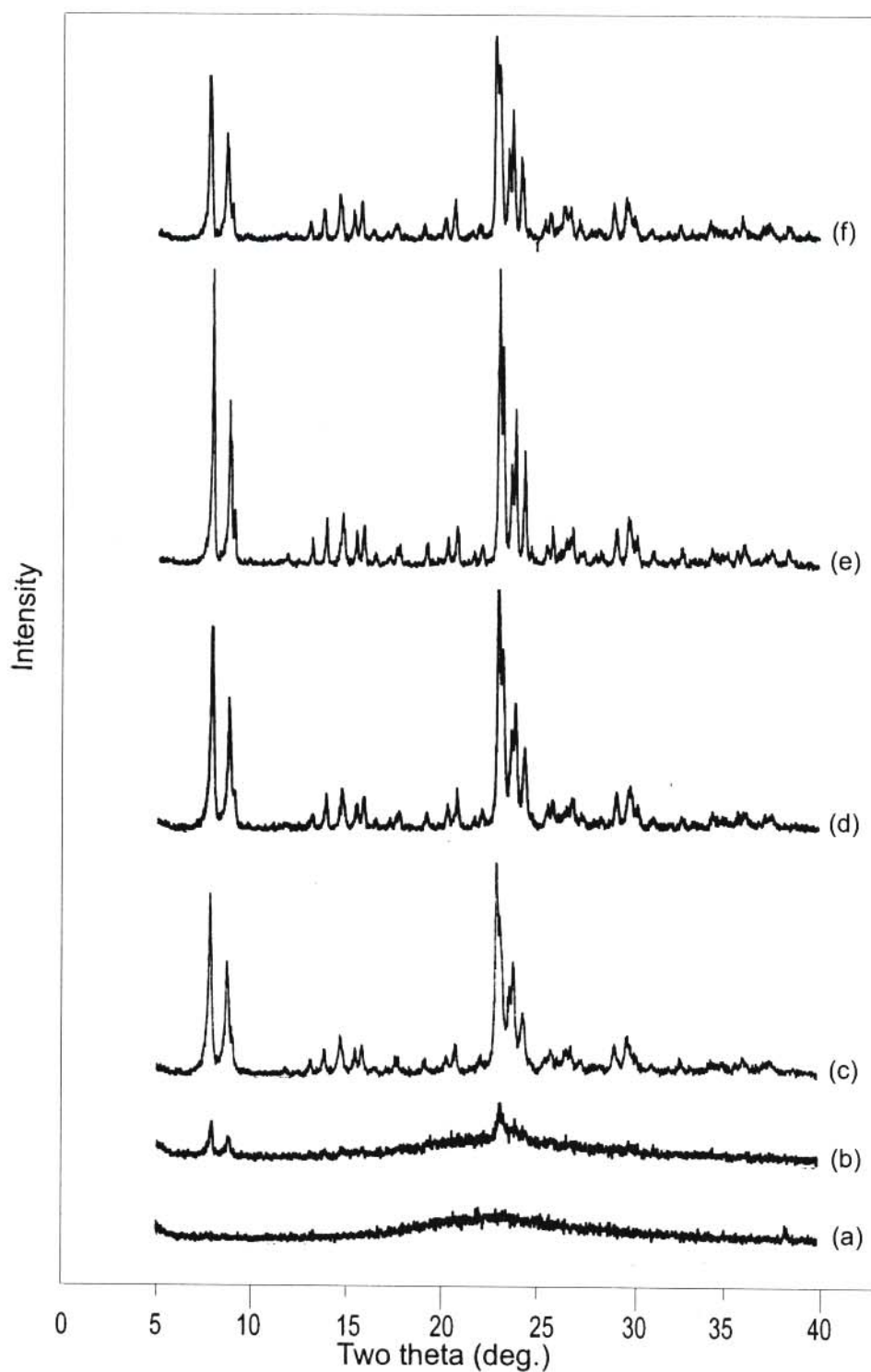
Figure 5.1 X-ray diffractograms of the ZSM-5-based samples synthesized without stirring in the

Parr autoclave using the Aerosil 200 method at different temperatures: (a) 90°C (batch no. 241),

(b) 100°C (batch no. 242), (c) 130°C (batch no. 248), (d) 150°C (batch no. 252), (e) 200°C (batch

no. 159), and (f) 210°C (batch no. 266).

Table 5.1 Percentage XRD crystallinity of the ZSM-5-based samples synthesized without stirring in the Parr autoclave using the Aerosil 200 method at different temperatures

Batch no.	Synthesis temperature (°C)	%XRD crystallinity	Mean	Standard deviation
240	90	0		
341	90	0	0	0.0
242	100	5		
243	100	3	4	1.4
244	110	13		
245	110	9	11	2.8
246	120	17		
247	120	24	21	5.0
248	130	59		
249	130	62	61	2.1
250	140	63		
251	140	67	65	2.8
252	150	68		
253	150	68	68	0.0
256	160	75		
258	160	80	78	3.5
254	170	80		
255	170	74	77	4.2
257	180	81		
259	180	86	84	3.5
157	190	83		
158	190	74	78	4.7
261	190	76		
159	200	94		
263	200	75	85	13.4
160	210	84		
266	210	65	75	13.4

of hydrothermal synthesis temperature. The inflection point for this curve is reached at about 125°C. This is followed by a further increase in percentage XRD crystallinity with increasing temperature up to approximately 200°C where the average percentage crystallinity was found to be 85%. Above 200°C, the percentage XRD crystallinity decreased with increasing synthesis
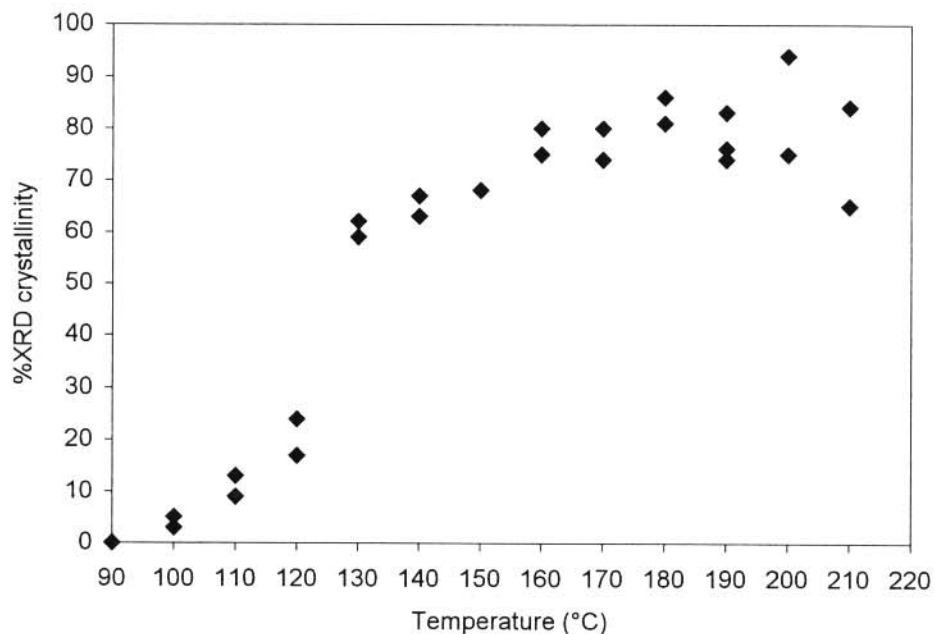
Figure 5.2 Plot of percentage XRD crystallinity versus synthesis temperature for ZSM-5-based samples synthesized without stirring in the Parr autoclave using the Aerosil 200 method.

temperature to an average value of 75% at 210°C.

Interestingly, although the standard deviations indicate good reproducibility amongst the duplicate samples at each temperature up to 190°C, this was not the case at the higher temperatures. At 200°C and 210°C the standard deviations are both 13.4. The highest crystallinity of 94% was obtained with one of the samples prepared at 200°C, but the duplicate sample prepared at this temperature has a crystallinity value of 75%. Most importantly, in terms of the synthesis of samples spanning the whole crystallinity range, it can also be observed that samples of intermediate percentage crystallinities, i.e. between 25% and 55%, could not be obtained (using this synthesis method and as a function of reaction temperature) since these crystallinities lie on the steep part of the crystallization curve.

SEM analysis

To illustrate the morphology of the ZSM-5-based samples synthesized according to this recipe, and without stirring at different temperatures in the Parr autoclave, SEM micrographs of certain representative samples as a function of synthesis temperature are shown in Figure 5.3. The same instrument magnification, namely X 5 000, was used for each sample in order to make a visual comparison of the particle sizes easier.

(a) (b)

(c) (d)
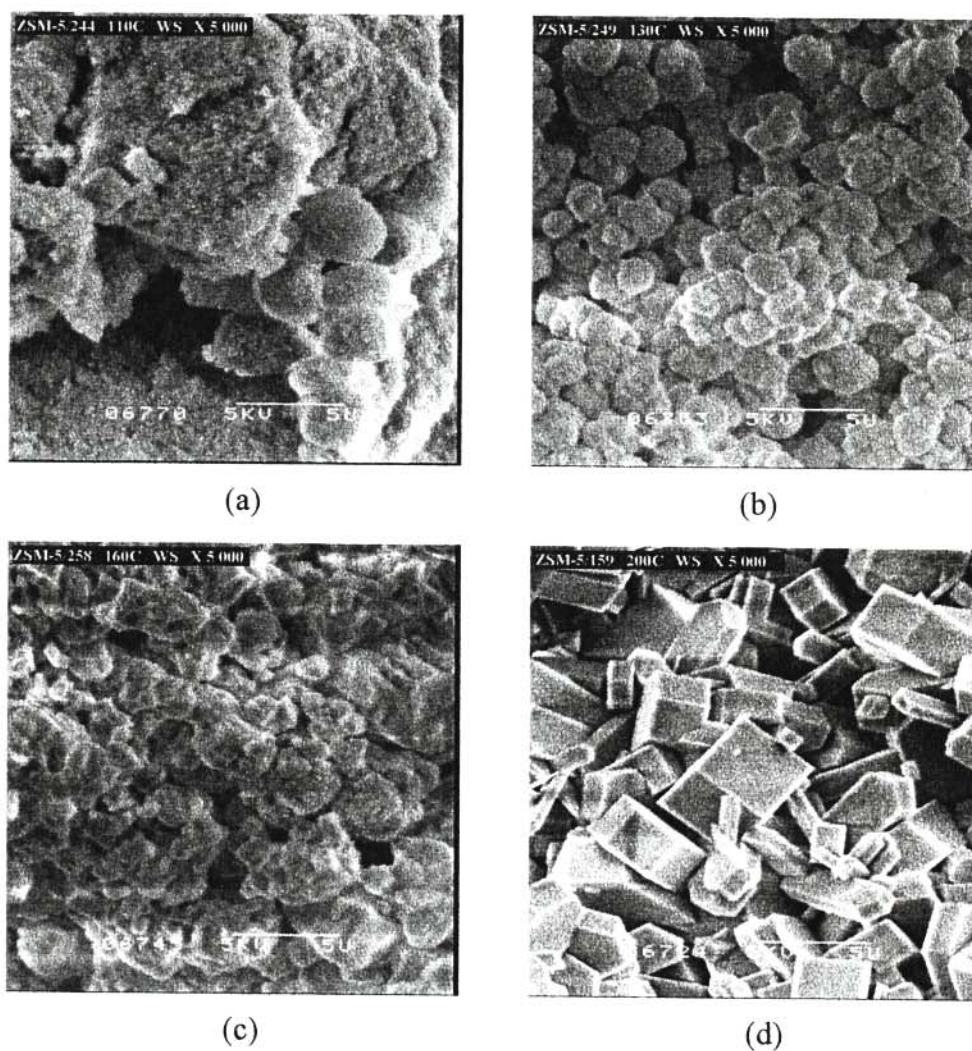
Figure 5.3 SEM micrographs of the ZSM-5-based samples synthesized without stirring in the Parr autoclave using the Aerosil 200 method at different temperatures: (a) 110°C, (b) 130°C, (c) 160°C and (d) 200°C.

Up to 110°C, mainly amorphous materials were observed with only few well-formed spheroids (see Figure 5.3(a)). At temperatures between 110°C and 160°C, spheroidal structures are observed (see Figure 5.3(b) and Figure 5.3(c) which are the micrographs of the samples synthesized at 130°C and 160°C respectively). In the sample prepared at 160°C, some of the spheroids appear distorted and might contain some crystallites within them. The average sizes of these spheroids (where the diameters of about ten spheroids were used for each determination) increase with increasing synthesis temperature between 130°C and 160°C (see Table 5.2). These results are similar to those observed with the samples synthesized without stirring in the in-house built autoclave, except that with the latter samples the sizes of the spheroids were slightly bigger, viz. 3.7 μm at 130°C and 5.1 μm at 150°C (Ramatsetse, 1998). Also in that work, we showed that crystals were already formed in the spheroids at 160°C.

Table 5.2 Influence of synthesis temperature on the average diameters of the spheroids formed in the ZSM-5-based samples synthesized without stirring in the Parr reactor using the Aerosil 200 method

Batch no.	Synthesis temp. (°C)	%XRD crystallinity	Av. diameter (μm)	Standard deviation
249	130	62	2.9	0.7
252	150	68	3.9	0.7
258	160	80	4.0	0.6

The results show that with the Parr autoclave, with increasing temperature up to 160°C and without stirring, higher crystallinity materials are obtained in the form of spheroids, as compared to the results observed in our previous studies. The smaller dimensions of the spheroids obtained in this investigation can be explained in terms of more nuclei being formed leading to the smaller particles, which could possibly be due to the larger volume and hence larger metal surface area at the base of the autoclave. The larger area of the base of the Parr autoclave could therefore be

responsible for the formation of more and isolated nuclei leading to the formation of smaller spheroids.

Polygons of different shapes and sizes are observed only at temperatures above 160°C. Figure 5.3(d) is the SEM micrograph of the 94% XRD crystalline sample synthesized at 200°C. In this micrograph, mainly elongated hexagonal crystals are observed with some cubic structures. The sizes of some of these crystal shapes are tabulated in Table 5.3. Other authors (Beschmann *et al.*, 1994; Van Grieken *et al.*, 2000), who synthesized ZSM-5 without stirring at temperatures above 160°C, also reported hexagon-like crystal structures, while Padovan *et al.* (1984), who carried out the synthesis at lower temperatures (120°C) and without stirring, observed the spheroidal morphology (see Table 2.1, Section 2.4.3). These results are surprisingly in contrast to our previous investigation where the in-house built autoclave was used without stirring and octagons rather than hexagons formed a significant portion of the crystal shapes. This could be a consequence of a higher crystallinity effect due to the smaller in-house autoclave. Thus, diffe-rences are observed in both the type of morphology and spheroid/crystallite sizes, in using the low-volume in-house built autoclave and the large-volume Parr autoclave (both without stirring).

Table 5.3 Morphology and dimensions of the largest crystals formed in the 94% XRD crystalline ZSM-5 sample synthesized without stirring at 200°C in the Parr autoclave (as shown in Figure 5.3(d))

Crystallite morphology	Length (μm)	Breadth (μm)	Thickness (μm)
Cubic	4.0	4.0	3.3
Hexagonal	5.4	1.8	0.7
Hexagonal	----[a]	2.3	0.5
Hexagonal	----[a]	4.7	2.5

[a]Could not be determined from the SEM micrograph.

The results appear to suggest that the volume or surface area of the base of the autoclave also influences the crystallization process, especially in the case of synthesis without stirring, even though the concentration of the reagents is the same. We can conclude that the larger the autoclave surface area at the base, the smaller the particles or spheroids and that crystallites are only observed at relatively higher temperatures. The possibility cannot be excluded, however, that this could also be due to differences in the heating and resultant temperatures in the autoclaves and at the base in particular, if it is assumed that most of the particles gradually sink to the bottom with synthesis time.

5.2.2 Synthesis with stirring (Parr autoclave)

5.2.2.1 Determination of the effect of the stirring rate

ZSM-5 zeolite-based materials were synthesized in the Parr autoclave at different stirring rates ranging from 0 rpm to 800 rpm to determine the possible effect of stirring rate on the percentage XRD crystallinity for this zeolite using this particular ZSM-5 recipe (Aerosil 200, see Section 4.3.2.1). The effect of stirring was investigated at two different temperatures, namely 150°C and 110°C respectively.

Synthesis at 150°C

X-ray diffractograms of some of the samples synthesized at the hydrothermal synthesis temperature of 150°C at different stirring rates are shown in Figure 5.4. These all show the characteristic peaks of ZSM-5 with minimal observable differences in peak intensities.
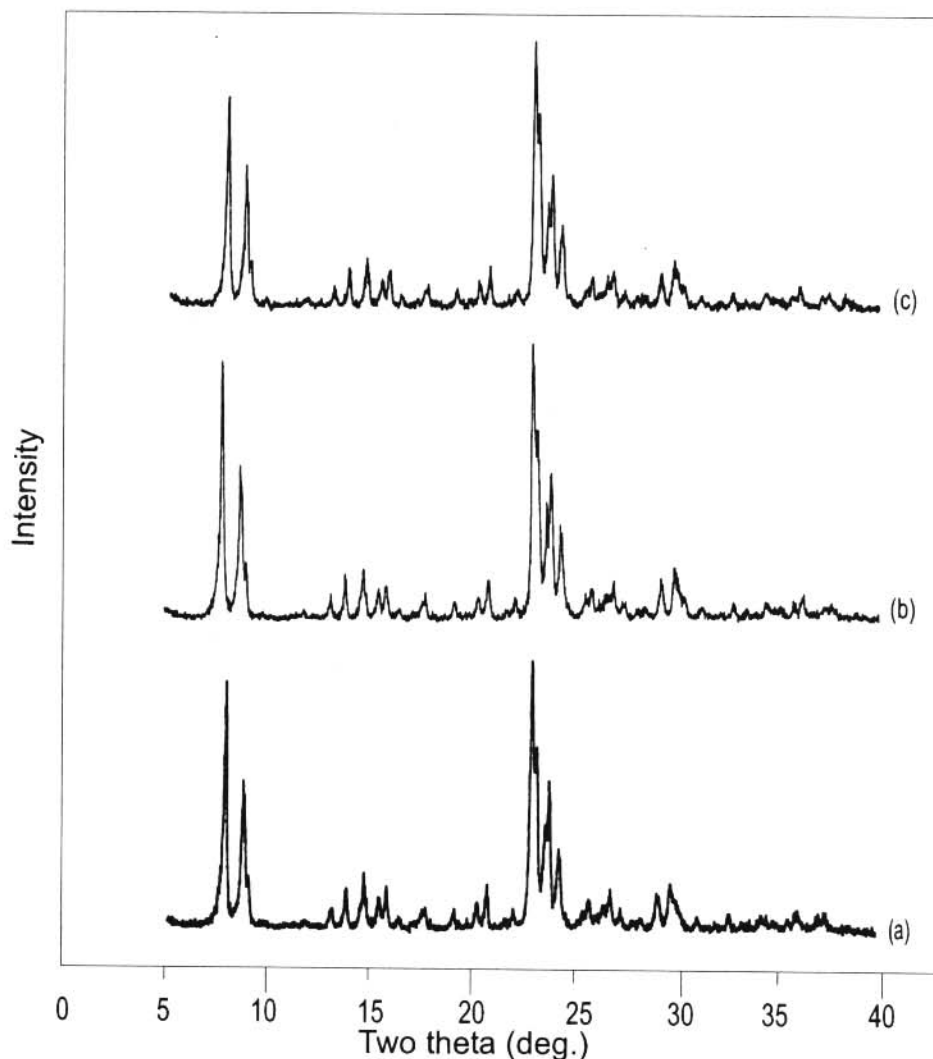
Figure 5.4 X-ray diffractograms of the ZSM-5-based samples synthesized at 150°C in the Parr autoclave using the Aerosil 200 method and at different stirring rates: (a) 0 rpm (batch no. 253), (b) 100 rpm (batch no. 269), and (c) 800 rpm (batch no. 271).

The percentage XRD crystallinities of the samples synthesized at 150°C at different stirring rates are listed in Table 5.4 and graphically presented in Figure 5.5. The plot gives a straight line, within experimental error, with a decline of about 2% over the stirring range of 0 rpm to 800 rpm. These results clearly show that stirring has very little effect on the percentage crystallinity of the ZSM-5 zeolite-based samples synthesized at 150°C using this particular Aerosil 200 ZSM-5 recipe. The small decline in crystallinity with increasing stirring rate range could be attributed

Table 5.4 Percentage XRD crystallinity of the ZSM-5-based samples synthesized at 150°C in the Parr autoclave using the Aerosil 200 method and at different stirring rates

Batch no.	Stirring rate (rpm)	%XRD crystallinity
252	0	68
253	0	68
269	100	70
275	200	72
285	300	67
280	400	67
289	500	69
283	600	72
288	700	65
271	800	66

Figure 5.5 Plot of percentage XRD crystallinity versus stirring rate for ZSM-5-based samples synthesized at 150°C in the Parr autoclave using the Aerosil 200 method.

to the formation of smaller crystallites (see below).

Examples of the micrographs of some of the ZSM-5-based materials synthesized under these conditions are shown in Figure 5.6. Figure 5.6(b), Figure 5.6(c) and Figure 5.6(d) are the SEM micrographs of the samples synthesized at 200 rpm, 400 rpm and 600 rpm respectively. They all show the presence of the spheroidal structures. The average spheroid sizes are 2.2 μm, 2.1 μm and 1.7 μm respectively (see Table 5.5) compared to 3.9 μm for the sample synthesized at 0 rpm (Figure 5.6(a)). These values show that there is a decrease in particle sizes with increasing

(a)   (b)

(c)   (d)

Figure 5.6 SEM micrographs of the ZSM-5-based samples synthesized at 150°C in the Parr autoclave using the Aerosil 200 method and at different stirring rates: (a) 0 rpm, (b) 200 rpm, (c) 400 rpm and (d) 600 rpm.

Table 5.5 Influence of stirring rate on the average diameters of the spheroids formed in the ZSM-5-based samples synthesized at 150°C in the Parr autoclave using the Aerosil 200 method and at different stirring rates

Batch no.	Stirring rate (rpm)	%XRD crystallinity	Av. diameter (μm)	Standard deviation
252	0	68	3.9	0.7
275	200	72	2.2	0.3
280	400	67	2.1	0.7
283	600	72	1.7	0.7
271	800	66	1.5	0.9

stirring rate. It can also be observed that the homogeneity of the particle sizes changes with increasing stirring rate. The spheroids shown in Figure 5.6(a) consist of agglomerates of smaller spheroidal structures. Figure 5.6(b) shows spheroids of almost the same size and with little distortion. Figure 5.6(c) shows large spheroids as well as some small spheroids. In Figure 5.6(d), there are more smaller spheroids than in the previous two cases. These results suggest that some of the bigger spheroids are broken up at the higher stirring rates to form these smaller spheroids.

The fact that stirring does not have a significant influence on the percentage XRD crystallinity at this temperature agrees with the results obtained previously with the in-house built autoclave. According to both of these sets of results (see Figure 2.6, Section 2.3.5 and Table 5.4), there is little difference in the percentage XRD crystallinity of the stirred and unstirred ZSM-5 sample preparations at 150°C. The above-mentioned SEM results show that only distortion of the spheroids with some differences in sizes are observed when the stirring rate is increased. However, since our previous work (Ramatsetse, 1998) indicated a significant difference between stirred and unstirred samples at lower temperatures, the effect of stirring was also examined at 110°C. Stirring is therefore not crucial for the higher-temperature synthesis of ZSM-5 (150°C)

but could be playing an essential role at the low temperature by presumably facilitating the crystallization process through dispersion of the few nuclei formed.

Synthesis at 110°C

As indicated above, the investigation was repeated at 110°C, at which temperature a vast difference in percentage XRD crystallinity was observed between the stirred and the unstirred samples which were synthesized in the in-house built autoclave (see Figure 2.6, Section 2.3.5). In that investigation the average percentage XRD crystallinities of the samples synthesized at 110°C with stirring was found to be 56%, while those of the samples synthesized without stirring was 9.5%. Therefore, this set of experiments was again repeated in the Parr autoclave with stirring rates ranging from 0 rpm to 800 rpm in increments of 100 rpm.

A problem encountered in this investigation involving the low temperature synthesis was that at the higher stirring rates the product was very fine and purification by filtration became problematic. For example, for the sample prepared at 500 rpm, the filter paper disintegrated due to the long filtration time required, and the product analyzed was a mixture of the zeolite-based material and the filter paper, which influenced the XRD results. For this stirring rate, the percentage XRD crystallinity obtained was only 2%. The products of the batches synthesized at 600 rpm and 700 rpm blocked, on the other hand, the pores of the filter papers used. For the sample prepared at 800 rpm (where the percentage crystallinity is 43%), the particles of the product were so small that they went through the filter paper together with the filtrate, even when a double layer of filter paper was used. Sedimentation and centrifugation could also not help to separate the products from the filtrates. After an attempt of more than 80 days to clean the samples, low mass yields were obtained and on calcination black spots were evident in the

samples indicating that the organic template in the pores was still not properly combusted. The batches synthesized at the stirring rates ranging from 0 rpm to 400 rpm did not present any filtration problems.

The X-ray diffractograms of some of the ZSM-5-based samples synthesized at 110°C and at different stirring rates are shown in Figure 5.7. Figure 5.7(a) is the diffractogram of the ZSM-5-based material which was synthesized without stirring. The intensities of the ZSM-5 peaks are low in this diffractogram. In Figure 5.7(b), which is the diffractogram of the ZSM-5-based material synthesized at 100 rpm, the intensities of the characteristic peaks are more pronounced, whilst those for the sample prepared at 700 rpm are even more intense as shown in Figure 5.7(c).
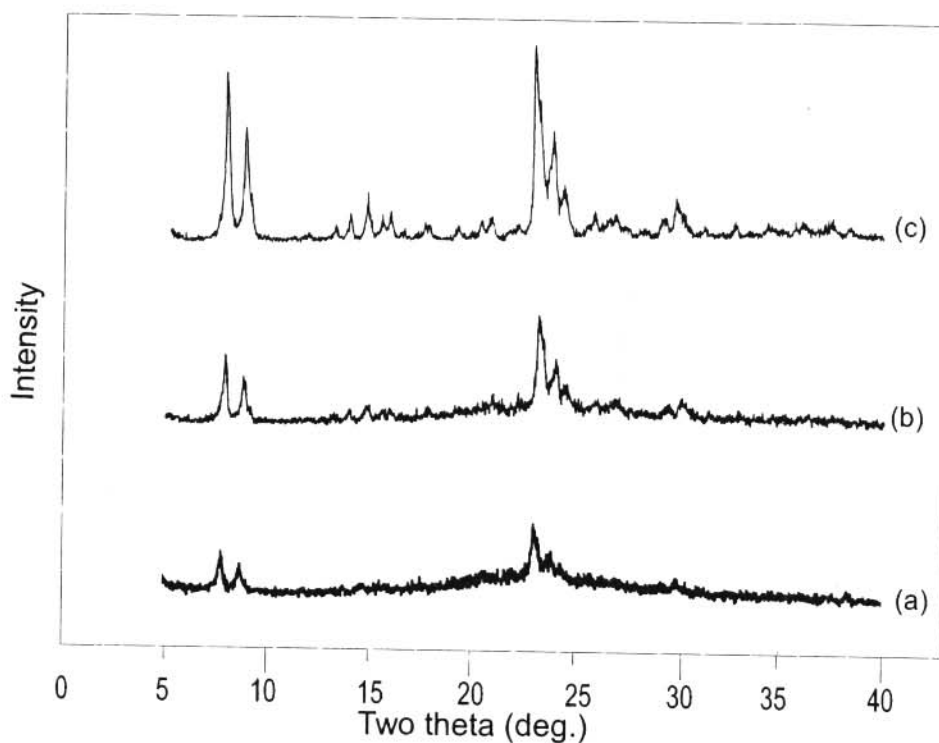
Figure 5.7 X-ray diffractograms of the ZSM-5-based samples synthesized at 110°C in the Parr autoclave using the Aerosil 200 method and at different stirring rates: (a) 0 rpm (batch no. 244), (b) 100 rpm (batch no. 367), and (c) 700 rpm (batch no. 347).

The percentage crystallinity values of the above-mentioned samples are listed in Table 5.6 and graphically presented in Figure 5.8. These show that the percentage crystallinity increases from

Table 5.6 Percentage XRD crystallinity of the ZSM-5-based samples synthesized at 110°C in the Parr autoclave using the Aerosil 200 method and at different stirring rates

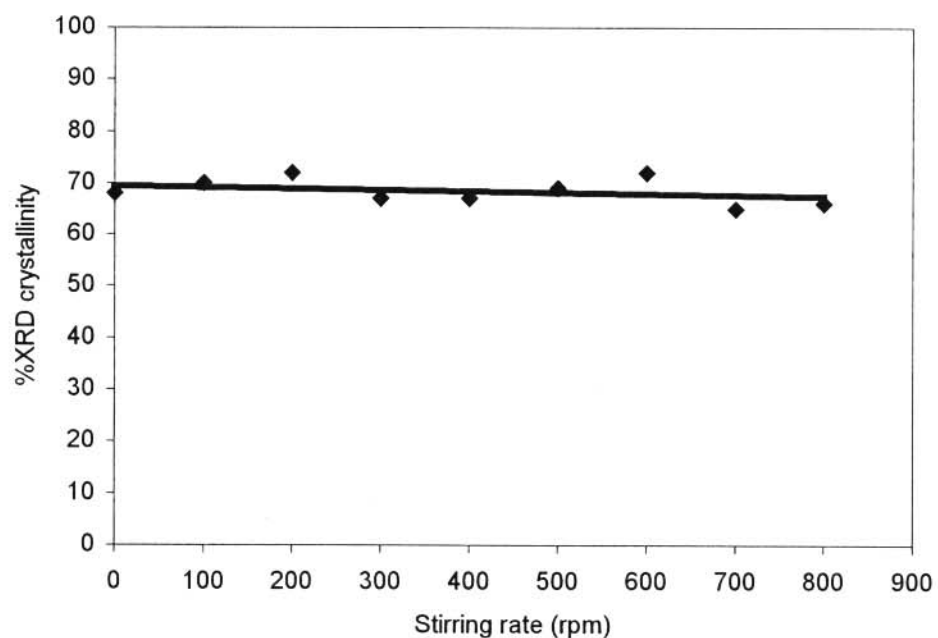| Batch no.	Stirring rate (rpm)	%XRD crystallinity
244	0	13
367	100	24
354	200	15
373	300	14
363	400	19
358	600	49
347	700	53
351	800	43
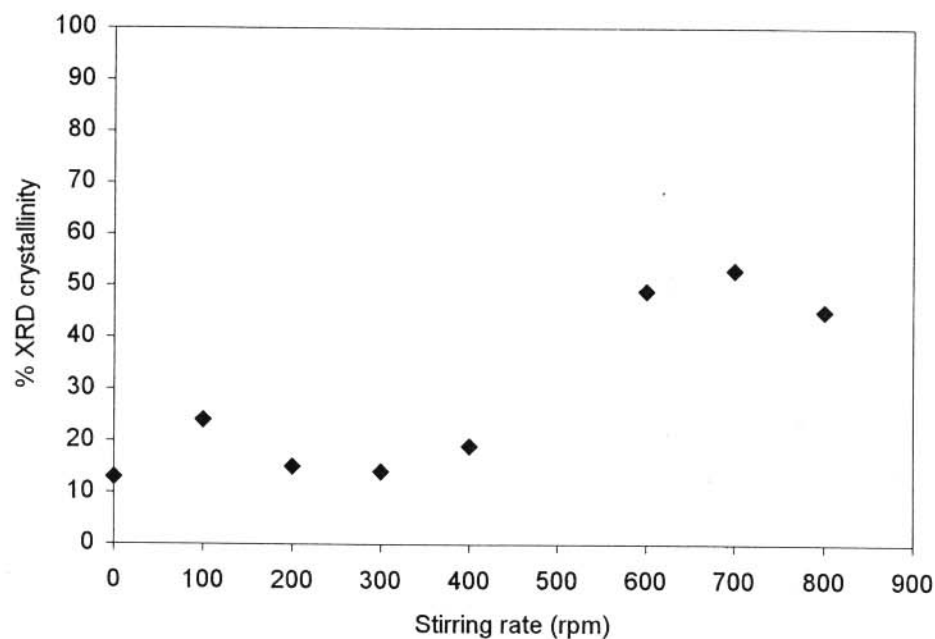
Figure 5.8 Plot of percentage XRD crystallinity versus the stirring rate for ZSM-5-based samples synthesized at 110°C in the Parr autoclave using the Aerosil 200 method and at different stirring rates.

13% for the without-stirring sample to 24% for the preparation at a stirring rate of 100 rpm, and increasing to 53% at the stirring rate of 700 rpm. Since the 100 rpm stirring rate gave the highest percentage XRD crystallinity without giving any filtration problems, it was taken as the most suitable and practical stirring rate to be used in the Parr autoclave for the synthesis of ZSM-5-based materials ranging in crystallinity from the range of the substantially amorphous to that of the highly crystalline.

The effect of stirring rate on the morphology of the ZSM-5-based materials was investigated by SEM. Figure 5.9 shows some of the representative SEM micrographs of the ZSM-5-based materials synthesized at 110°C and at the stirring rates of 100 rpm and 700 rpm respectively. The micrographs clearly indicate that at 100 rpm larger spheroids are formed than at 700 rpm, probably due to distortion by the higher stirring rate. The average diameters of the spheroids so formed are 2.1 µm and 1.2 µm respectively. As was observed with the samples synthesized at 150°C, these results demonstrate that higher stirring rates break down the bigger spheroids to
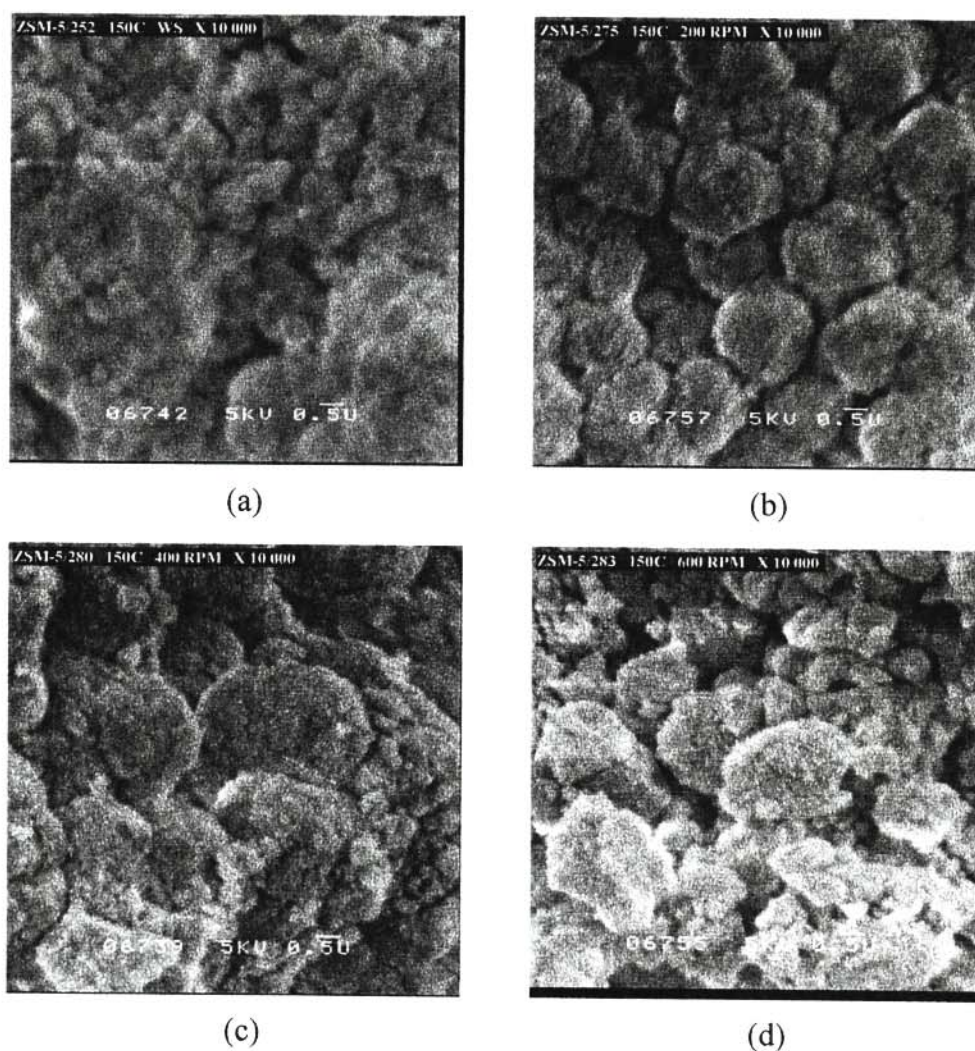

(a)   (b)
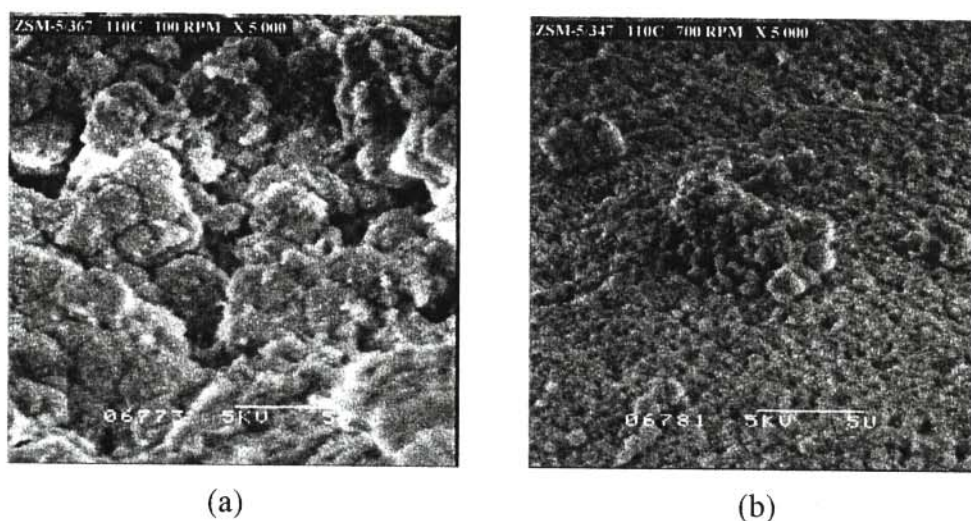
Figure 5.9 SEM micrographs of ZSM-5-based samples synthesized at 110°C in the Parr auto-clave using the Aerosil 200 method and at different stirring rates: (a) 100 rpm and (b) 700 rpm.

smaller ones. Therefore, with increasing stirring rate at 110°C, spheroids of higher crystal-linity but of smaller size are once again obtained. These characteristics could be of importance in catalytic applications (see below).

5.2.2.2 *Synthesis at different temperatures with stirring at 100 rpm (Parr autoclave)*

XRD analysis

The X-ray diffractograms of some of the ZSM-5 zeolite-based materials, and of other phases (see below), prepared with stirring at 100 rpm and at different temperatures are shown in Figure 5.10. Unlike in the case of the unstirred batches, minute spike-like peaks can already be observed on the hump for the samples synthesized at 90°C (Figure 5.10(a)), which indicates a higher per-centage XRD crystallinity at this temperature than for the synthesis without stirring (see Figure 5.1(a)). From 110°C to 130°C, there is a significant increase in peak intensities as is evident from a comparison between Figure 5.10(b) and Figure 5.10(c). On average, a further gradual increase in peak intensities is observed with an increase in synthesis temperature up to 200°C (see Figure 5.10(d) and Figure 5.10(e)). This is followed by a small decline in peak intensities of the characteristic peaks, and the development of additional peaks (e.g. around 26.6° 2θ), as indicated in Figure 5.10(f) which is the diffractogram of the ZSM-5 zeolite-based sample synthesized at 210°C.

XRD analysis of the latter sample was repeated using a Siemens D500 X-ray diffractometer operating with CoK_α radiation in order to identify the additional phase present. The X-ray diffractogram (Figure 5.11) clearly indicates that these additional peaks were due to α-quartz
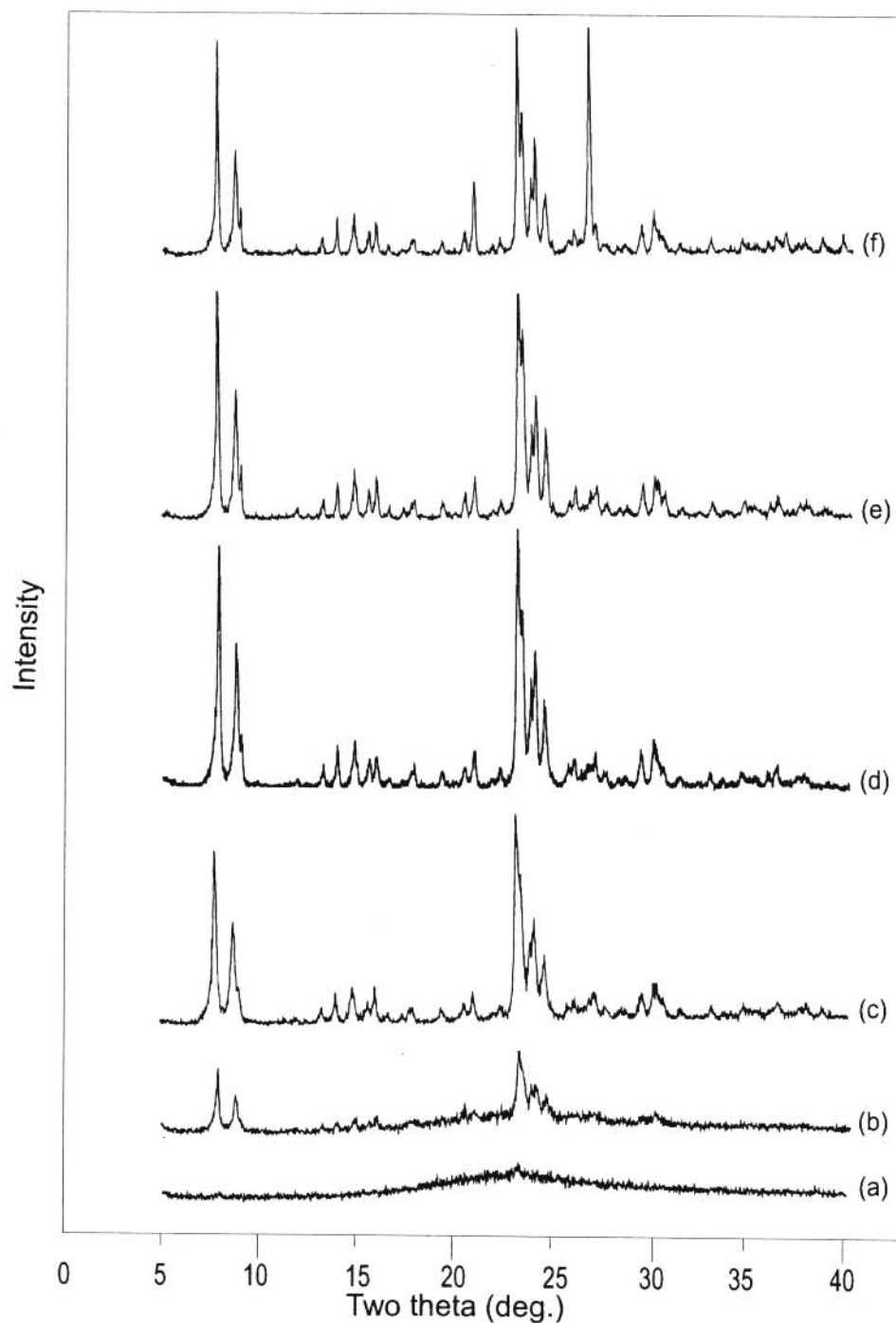
Figure 5.10 X-ray diffractograms of the ZSM-5-based materials (and of other phase at 210°C) synthesized with stirring (at 100 rpm) in the Parr autoclave using the Aerosil 200 method at different temperatures: (a) 90°C (batch no. 493), (b) 110°C (batch no. 510), (c) 130°C (batch no. 512), (d) 150°C (batch no. 269), (e) 200°C (batch no. 521), and (f) 210°C (batch no. 517).

ZSM-5/517 IT2767A
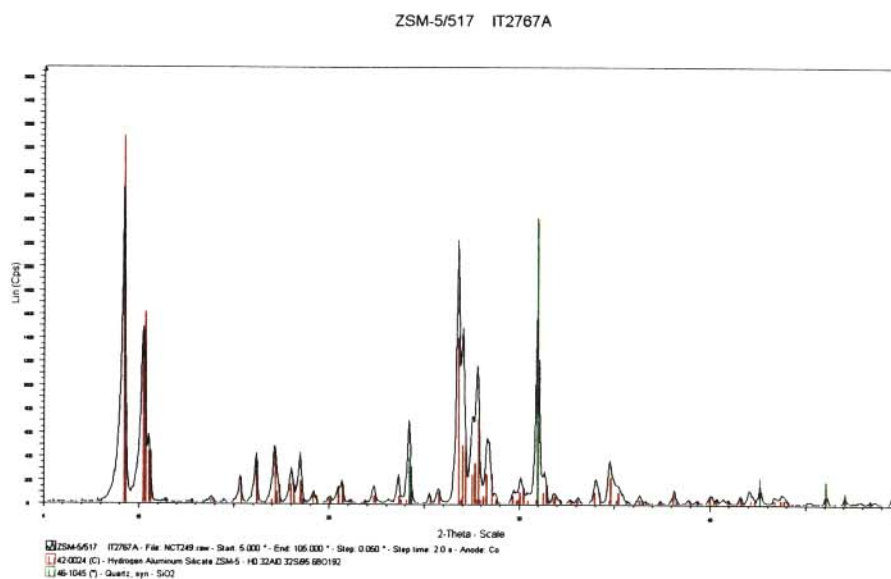
Figure 5.11 Identification of ZSM-5 (red) and α-quartz (green) peaks in the X-ray diffractogram of the sample synthesized at 210°C with stirring at 100 rpm in the Parr autoclave using the Aerosil 200 recipe.

(e.g. peaks at 20.78° 2θ, 26.55° 2θ, 36.46° 2θ and 39.36° 2θ). The formation of α-quartz as an additional phase in ZSM-5 is in agreement with the results obtained before by Dai *et al.* (1986).

The percentage XRD crystallinities of the ZSM-5 phase for the samples synthesized with stirring at 100 rpm and at different temperatures are tabulated in Table 5.7 and graphically shown in Figure 5.12. It should be noted that only the XRD crystallinity of the ZSM-5 phase was evaluated and shown in Table 5.7 and Figure 5.12. This plot gives an S-shaped curve for the percentage XRD crystallinity as a function of hydrothermal synthesis temperature. Its inflection point is reached just before 125°C. For this series of samples, the maximum percentage XRD crystallinity obtained is 79% at 200°C, after which a decline was observed (65% at 210°C). Although no samples were again synthesized with XRD crystallinities in the range of 30% to 50% with this series of experiment, the possibility to obtain such samples is better with this

Table 5.7 Percentage XRD crystallinities of the ZSM-5 phase in the samples synthesized with stirring at 100 rpm in the Parr autoclave using the Aerosil 200 method at different temperatures

Batch no.	Synthesis temperature (°C)	%XRD crystallinity
493	90	2
509	100	2
510	110	18
511	120	27
512	130	59
513	140	51
269	150	70
514	150	63
519	160	63
515	170	67
520	180	78
516	190	76
521	200	79
517	210	65

Figure 5.12 Plot of percentage XRD crystallinity of the ZSM-5 phase versus the synthesis temperature for the samples synthesized with stirring at 100 rpm in the Parr autoclave using the Aerosil 200 method.

stirring mode of synthesis since the crystallization curve shows a more gradual increase in crystallinity with increasing temperature between 100°C and 150°C.

SEM analysis

Figure 5.13 shows the SEM micrographs of some ZSM-5-based samples synthesized with stirring at 100 rpm. Although a percentage XRD crystallinity of 2% was obtained for the sample synthesized at 90°C, spheroids cannot be clearly identified amongst the amorphous materials (see Figure 5.13(a)). Spheroids are observed in the samples synthesized at higher temperatures (see Figure 5.13(b) which is the zeolite-based sample prepared at 160°C). In contrast to the observation made with the samples synthesized without stirring at temperatures higher than 160°C, no definite crystal forms, except for spheroids, could be observed in any of the samples synthesized with stirring at synthesis temperatures ranging from 100°C to 170°C. The diameters of the spheroids formed at temperatures up to 170°C, and spheroidal conglomerates of crystallites at higher temperatures up to 210°C, are listed in Table 5.8, and, on average, there is an increase in their sizes with increasing temperature.

For the sample prepared at 180°C, SEM indicates that there are spheroids as well as crystallites within the spheroids (see Figure 5.13(c)). At higher temperatures (above 180°C) mainly crystals and crystals formed in spheroids could be identified as can be seen in Figure 5.13(d) through to Figure 5.13(f), which are the samples synthesized at 190°C, 200°C and 210°C respectively. On average, the crystallite sizes also increased with increasing synthesis temperature (190°C to 210°C) and the measured values are listed in Table 5.9. Agglomerates of rectangular, hexagonal or coffin-like hexagonal crystals are observed in these micrographs.

(a)

(b)

(c)

(d)

(e)

(f)
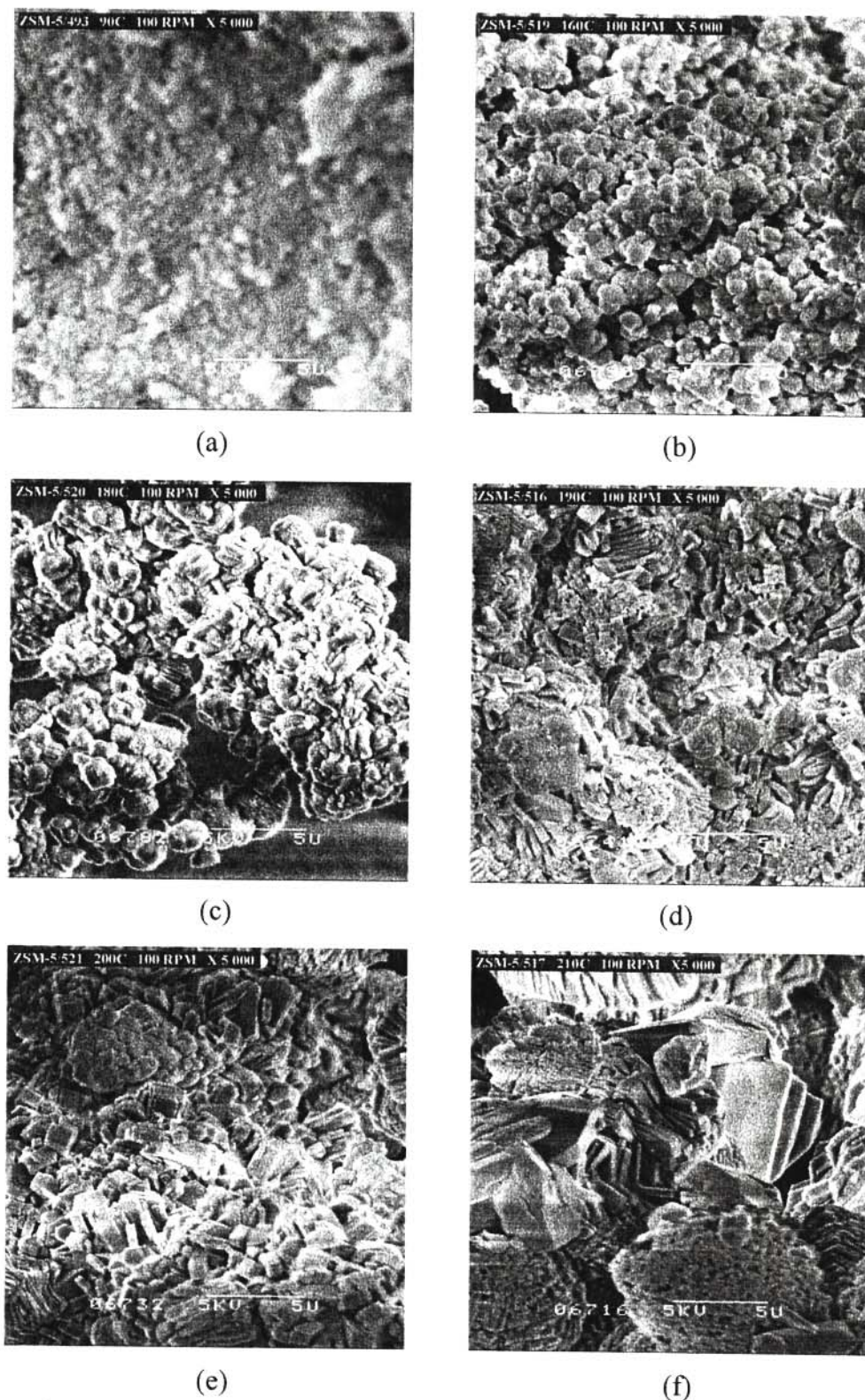
Figure 5.13 SEM micrographs of the ZSM-5-based samples (and of other phase at 210°C) synthesized with stirring at 100 rpm in the Parr autoclave using the Aerosil 200 method at different temperatures: (a) 90°C, (b) 160°C, (c) 180°C, (d) 190°C, (e) 200°C and (f) 210°C.

Table 5.8 Influence of synthesis temperature on the average diameters of the spheroids formed in the ZSM-5-based samples (and of other phase, 210°C), synthesized with stirring at 100 rpm in the Parr autoclave using the Aerosil 200 method

Batch no.	Synthesis temp. (°C)	%XRD crystallinity of ZSM-5 phase	Average diameter (μm)	Standard deviation
512	130	59	0.5	0.2
513	140	51	1.5	0.8
514	150	63	1.0	0.0
519	160	63	1.2	0.2
515	170	67	1.3	0.3
520	180	78	2.1	0.4
516	190	76	2.4	0.9
517	210	65	8.1	0.7

Table 5.9 Influence of synthesis temperature on the dimensions of the hexagons formed in the ZSM-5-based materials (and of other phase, 210°C), synthesized in the Parr autoclave with stirring using the Aerosil 200 method[a]

Batch no.	Synthesis temp. (°C)	%XRD crystallinity of ZSM-5 phase	Length (μm)	Breadth (μm)	Thickness (μm)
516	190	76	2.5	0.5	0.4
521	200	79	2.2	1.5	0.5
			4.5	1.8	0.6
517	210	65	----[b]	1.0	0.05
			4.8	3.9	----[b]

[a]Measured at higher magnifications than those indicated in Figure 5.13.

[b]Could not be determined from the SEM micrograph.

5.2.3 Conclusions

A comparison of the percentage XRD crystallinities of the samples obtained at the different temperatures without stirring in the Parr and the in-house built autoclaves is given in Figure 5.14. It can be concluded that they essentially follow the same S-shaped curve. However, the in-house
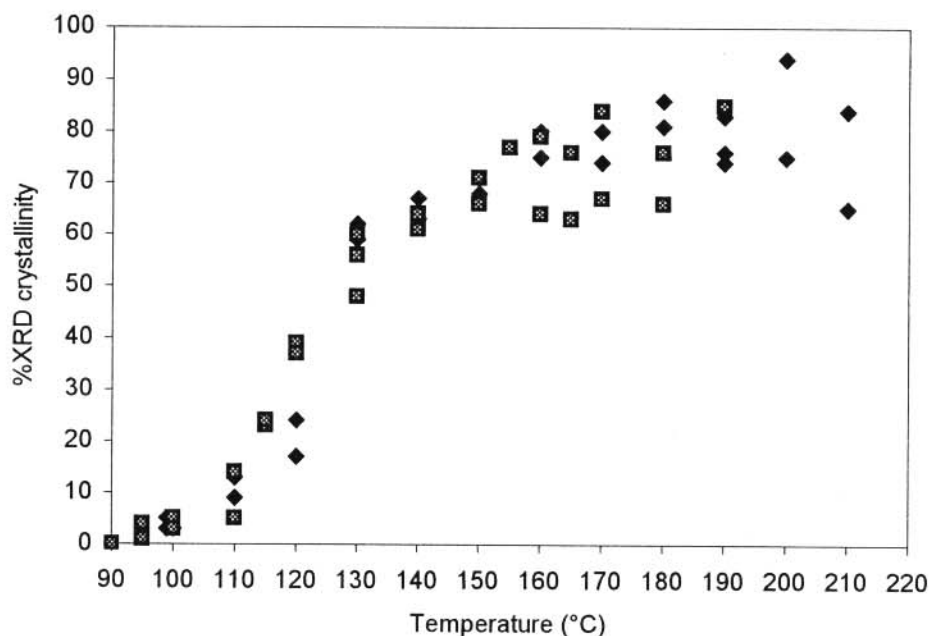
Figure 5.14 Plot of percentage XRD crystallinity versus synthesis temperature for the ZSM-5-based samples synthesized using the Aerosil 200 method without stirring in the in-house built autoclave (▣) and in the Parr autoclave (♦).

built autoclave without stirring at 110°C to 130°C appears to enable us to prepare the elusive 30% to 50% crystallinity range samples. Therefore, the volume or area of the base of the autoclave also appears to be a crucial parameter in the synthesis of this type of materials.

The SEM micrographs of these samples show the formation of spheroids up to 150°C for the in-house built autoclave and up to 160°C for the Parr autoclave. Only above these temperatures, formation of definite crystallites could be observed. The sizes of the spheroids were bigger in the case of the in-house built autoclave than for the Parr autoclave. For instance, at 130°C an average spheroid diameter of 3.7 μm was observed for the samples prepared in the in-house built autoclave while an average of 2.9 μm was obtained for samples synthesized in the Parr autoclave. At higher temperatures (above 160°C) crystals of different morphologies are

observed in the micrographs of the samples obtained from the two different autoclaves. As indicated above, a reason for these differences might be the different volumes of the two autoclaves used and the area of the base of the autoclave. It can be concluded that the bigger the area of the base, the smaller the particle size (spheroids or crystallites).

The plot of percentage XRD crystallinity of the zeolite-based materials prepared with stirring in the Parr autoclave versus the synthesis temperature is shown in Figure 5.15 together with the results previously obtained using the same method, but synthesized in an in-house built autoclave with stirring using a magnetic stirrer bar (Ramatsetse, 1998). Both plots give S-shaped curves for the percentage XRD crystallinity as a function of hydrothermal synthesis temperature. The inflection point for the curve obtained for the samples synthesized with stirring in the in-house
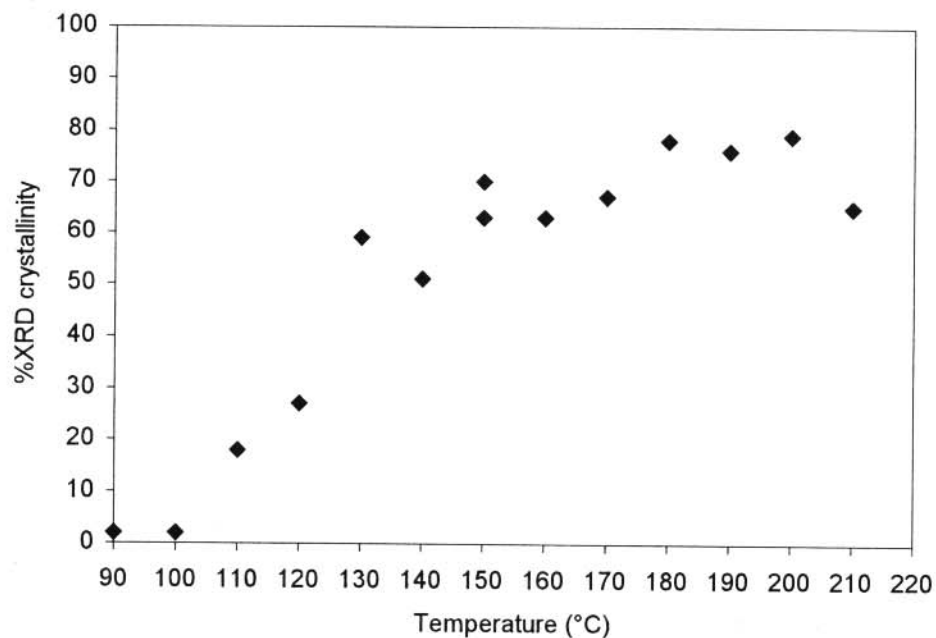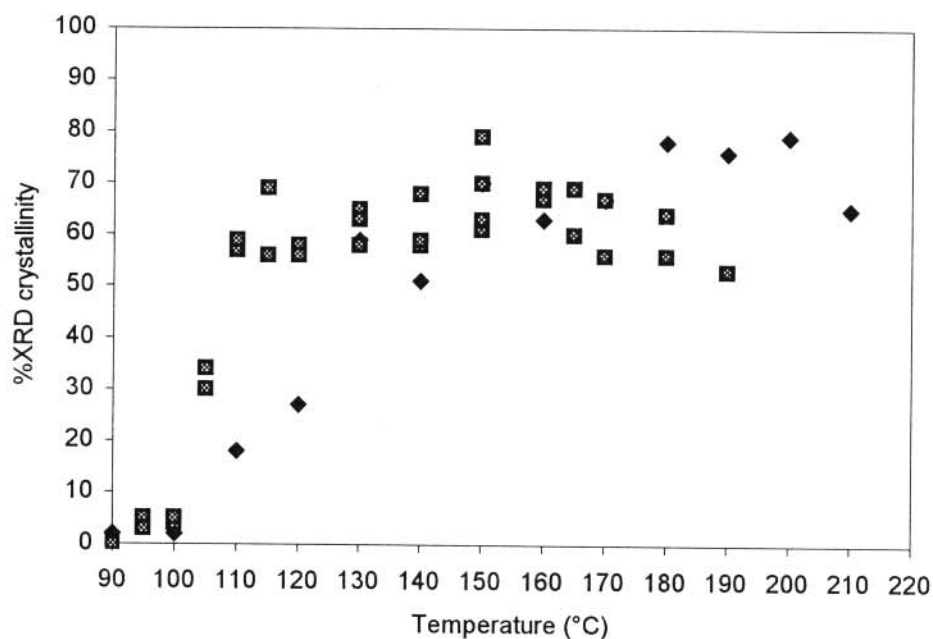

Figure 5.15 Plot of percentage XRD crystallinity of the ZSM-5 phase versus the synthesis temperature for the samples synthesized with stirring using the Aerosil 200 method in the in-house built autoclave at a nominal 1 000 rpm (■) and in the Parr autoclave at 100 rpm (♦).

built autoclave is reached at about 105°C. For this series of samples, maximum XRD crystallinity (average of 65%) is obtained at 150°C. Beyond this temperature, a gradual decline in percentage XRD crystallinity is observed as calculated from peak intensities (51% at 190°C). The curve obtained for the samples synthesized with stirring in the Parr autoclave shows that the inflection point is reached at about 120°C while it was about 125°C for without stirring. For this series of samples, the maximum percentage XRD crystallinity of 79% is obtained at 200°C, after which a slight decline was observed due to the formation of α-quartz. Thus, crystallinity values of between 30% and 50% XRD crystallinity can be obtained in the Parr autoclave with stirring since the crystallization curve shows a more gradual increase in crystallinity with increasing temperature between 100°C and 150°C.

It can be noted that the curve of the series of samples prepared in the Parr autoclave with stirring follows almost the same pattern as the curves obtained for the synthesis in both types of autoclaves without stirring (see Figure 5.14 and Figure 5.15). The possibility cannot be excluded therefore that the stirring rate used in the Parr autoclave (100 rpm) was not an optimum stirring rate, and was probably too low and equivalent to the synthesis under static conditions. That is, the reaction mixture therefore behaves as if it was not stirred, or that it was only partially stirred, and the results resemble those obtained for the unstirred samples.

In contrast to the observation made with the samples synthesized without stirring, the curves for the percentage XRD crystallinities at different synthesis temperatures for the stirred samples from the Parr autoclave and from the in-house built autoclave do not exactly coincide. The in-house built autoclave gives higher percentage XRD crystallinities than the Parr autoclave at lower temperatures (less than 150°C), while at higher temperatures, the reverse behaviour is

observed. The difference in the behaviour of the two autoclaves might have been caused by the difference in their stirring systems. The top stirring impellers of the Parr autoclave are suspended in the reaction mixture above the bottom of the Parr autoclave, while the 25 mm X 6 mm magnetic stirrer bar used in the in-house built autoclave operates at the bottom of this autoclave. This magnetic stirrer of the latter probably crushes and grinds the earliest formed crystals, which then act as nuclei and indirectly seed the reaction mixture which in turn increase the rate of crystallization (Bronić *et al.*, 1999). Hence the higher percentage XRD crystallinities at lower temperatures than for samples synthesized without stirring in the same autoclave and those synthesized in the Parr autoclave.

At higher temperatures (150°C to 190°C), only spheroids were obtained with the in-house built autoclave and no identification of crystal shapes at the maximum magnification possible with the scanning electron microscope used. The lower crystallinities observed with stirring (than without stirring) in the in-house built autoclave is probably due to the smaller crystallite sizes that give rise to lower apparent percentage XRD crystallinity due to peak broadening (Szostak, 1989). Although the percentage crystallinity of samples prepared at higher temperatures in the Parr autoclave with stirring is also lower on average than those synthesized without stirring, this effect is not as significant as it is in the in-house built autoclave. This again emphasizes the importance of the differences in stirring mechanism of the two autoclaves.

Furthermore, in contrast with the results obtained with the in-house built autoclave (see Figure 2.6, Section 2.3.5), the curves for the percentage XRD crystallinities of the syntheses without and with stirring (100 rpm) in the Parr autoclave samples only show a little difference as is illustrated in Figure 5.16. The differences are in the same direction as was obtained for the in-house built autoclave, but less pronounced. This again gives the impression that the rate of
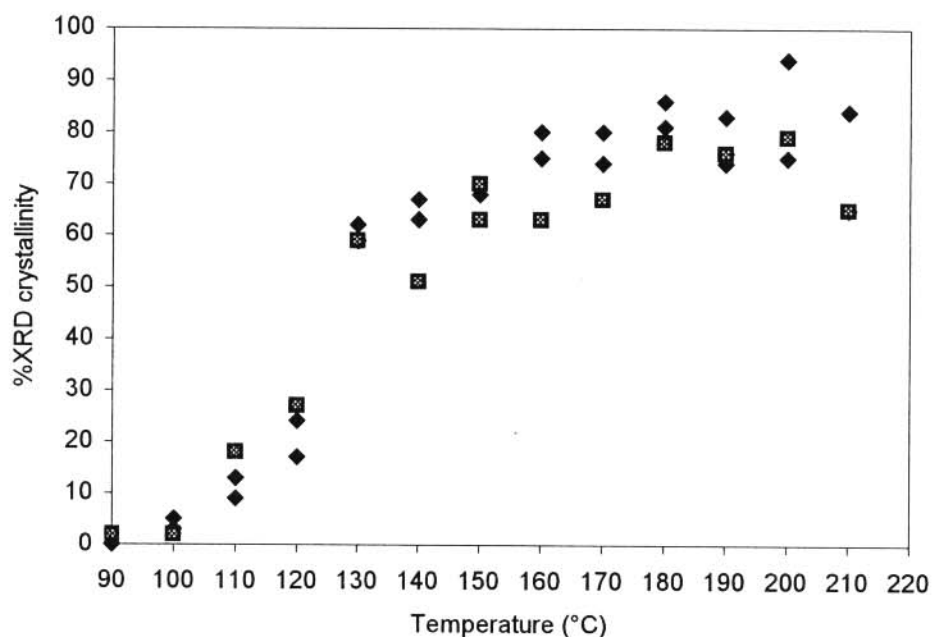
Figure 5.16 Plot of percentage XRD crystallinity of the ZSM-5 phase versus the synthesis temperature for the samples synthesized with stirring at 100 rpm (■) and without stirring (♦) in the Parr autoclave using the Aerosil 200 method.

stirring in the Parr autoclave was lower than it should have been in order to accentuate any effect of stirring, as was observed in Section 5.2.2.1, Table 5.6.

During the course of this project, one batch was synthesized with stirring at 200°C in the in-house built autoclave to investigate if spheroids will still be obtained at this high temperature. It was observed that at 200°C, crystals of definite shapes are clearly visible, some of which are still confined within the spheroidal structures (see Figure 5.17). This strongly suggests therefore that the overall configuration of the autoclaves (i.e. volume, heating, etc.) could also be influencing the crystallization and morphology that can be obtained.

(a)   (b)
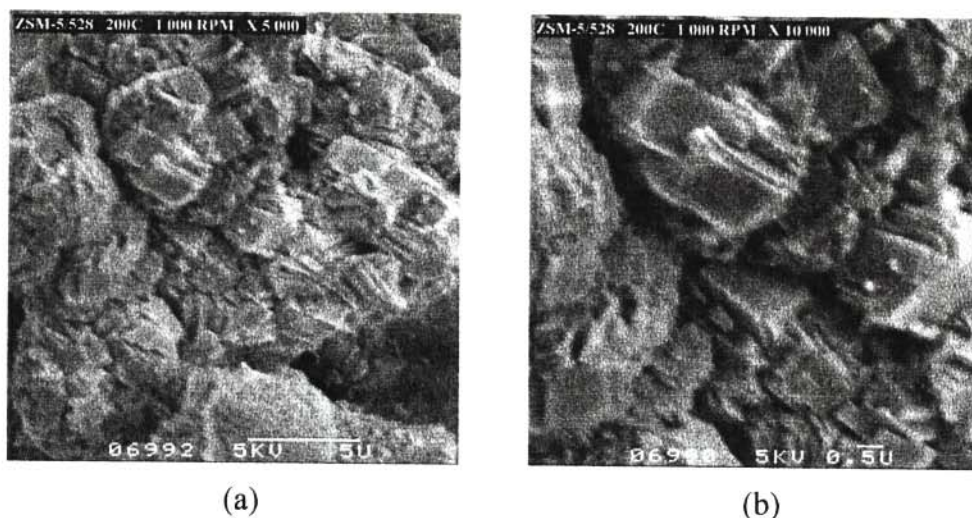
Figure 5.17 SEM micrograph of the ZSM-5 sample synthesized with stirring at 1 000 rpm in the in-house built autoclave using the Aerosil 200 method at 200°C (a) X 2 000 and (b) X 5 000.

5.3 EFFECT OF DIFFERENT SYNTHESIS METHODS (SILICA SOURCES)

In addition to the method where Aerosil 200 was used for the preparation of ZSM-5-based materials, the influence of different silica sources involving different recipes was also investigated. In each of the methods used in this study, the hydrothermal synthesis was carried out both under static and stirred conditions in the in-house built autoclave. For the stirred conditions, the samples were stirred at 1 000 rpm using a 25 mm X 6 mm magnetic stirrer bar. These are the same conditions as previously used in this autoclave for the synthesis of ZSM-5-based samples with Aerosil 200 as the source of silica (Ramatsetse, 1998), and this will allow for comparisons to be made amongst these recipes in terms of percentage crystallinity, its controllability and reproducibility, and morphology of the materials and the spheroid and crystallite sizes obtained.

5.3.1 Water glass

The Aerosil 200 method (Dijkstra *et al.*, 1991; Nicolaides *et al.*, 1991; Ramatsetse, 1998; Nico-

laides, 1999) was adapted and water glass was used instead as the silica source, and with no additional sodium hydroxide being added (see Section 4.3.2.2). The mass of the product obtained with water glass was lower than that from the Aerosil 200 method but the crystals and the spheroids obtained were much larger (see below).

5.3.1.1 *Synthesis without stirring*

XRD analysis

Examples of the X-ray diffractograms of some of the ZSM-5 zeolite-based materials (and of other phases, see below) synthesized without stirring are shown in Figure 5.18. Figure 5.18(a) is the diffractogram of the ZSM-5-based sample which was hydrothermally synthesized at 90°C. In contrast to the synthesis with the Aerosil 200 as the silica source, no hump was observed at around 23° 2θ, but instead one was observed at higher angles at around 38° 2θ. It is known that different amorphous materials can give the hump at different places (Chung and Scott, 1973). A small peak is also observed at 38.4° 2θ. In some of the diffractograms of the amorphous material prepared at lower temperatures with Aerosil 200, a smaller peak was also observed at this angle, see e.g. Figure 5.1(a). We are at this stage, however, unable to make an assignment to this peak. In Figure 5.18(b), which is the diffractogram of the ZSM-5 zeolite-based sample synthesized at 120°C, small peaks at the same angles as the characteristic peaks of ZSM-5 are observed. For the synthesis at 130°C, the characteristic peaks of ZSM-5 are much more evident as shown in Figure 5.18(c). This trend was observed throughout with increasing temperatures up to 180°C as is illustrated in Figure 5.18(e). For the sample prepared at 210°C, additional peaks are, however, observed at 9.7° 2θ, 25.6° 2θ and 26.0° 2θ, which are not the characteristic positions of the α-quartz peaks previously found (see Section 5.2.2.2) as the additional phase for synthesis at high temperatures. These peaks indicate therefore the presence of an additional phase or phases (for

Figure 5.18 X-ray diffractograms of the ZSM-5-based samples, and of other phases, synthesized without stirring using the water glass method at different temperatures: (a) 90°C (batch no. 337), (b) 120°C (batch no. 315), (c) 130°C (batch no. 307), (d) 150°C (batch no. 264), (e) 180°C (batch no. 311), and (f) 210°C (batch no. 362).

the synthesis at this temperature) which we have not identified. From the diffractograms it can also be observed that the hump as well as the peak at 38.4° 2θ diminish at the higher synthesis temperatures as the percentage crystallinity increases, and in addition, the latter peak was not observed at temperatures above $130^\circ C$.

The percentage XRD crystallinities of these samples are listed in Table 5.10. The results indicate that there is no ZSM-5 zeolitic material formed at low temperatures up to $110^\circ C$. From $120^\circ C$ up to $150^\circ C$ there is a gradual increase in percentage XRD crystallinity with increasing synthesis temperature and remains almost constant thereafter up to $180^\circ C$. This is followed by a decline in percentage crystallinity with increasing synthesis temperatures up to $210^\circ C$, which is the highest temperature investigated with this recipe. The decline in percentage crystallinity in terms of the ZSM-5 phase is attributed to the formation of small amounts of additional crystalline phases.

Table 5.10 Percentage XRD crystallinities of the ZSM-5 phase in the samples synthesized without stirring at different temperatures using the water glass method

Batch no.	Synthesis temperature ($^\circ C$)	%XRD crystallinity
337	90	0
332	100	0
323	110	0
315	120	1
307	130	9
480	135	45
302	140	36
368	140	39
481	145	55
264	150	89
353	160	84
303	170	85
311	180	86
319	190	76
327	200	68
362	210	72

SEM analysis

To illustrate how the morphology of the ZSM-5-based materials synthesized according to this recipe, and without stirring, changes with increasing temperature, SEM micrographs of representative samples are shown in Figure 5.19 and Figure 5.20. Figure 5.19(a) shows an amorphous crust-like structure for the sample synthesized at 90°C, where a percentage crystallinity of 0% was determined. This amorphous material looks different from those obtained previously with the Aerosil 200 recipe (see Figure 5.13(a)), which could possibly account for the shift of the hump, bearing in mind that different amorphous materials can give the hump at different degrees 2θ (Chung and Scott, 1973). Although Figure 5.19(b), which is the SEM micrograph of the sample synthesized at 100°C is also 0% XRD crystalline, the "crusts" so formed in this case has some protrusions on their surface. These protrusions increased in size with increasing synthesis temperature (see Figure 5.19(c) which is the sample synthesized at 110°C).

At 130°C these protrusions seem to have formed small spheres amongst the amorphous material, as illustrated in Figure 5.20(a). Solid spheres of the crystalline products are much more prevalent in the samples synthesized at higher temperatures (see Figure 5.20(b), which is the sample synthesized at 140°C). At 150°C the SEM micrograph of the sample having an 89% crystallinity showed spheres and a mixture of other morphologies ranging from rectangles to hexagons and octagons (see Figure 5.20(c) and Figure 5.20(d)). Crystals growing out of the spheres as protrusions can also be observed. This crystalline growth is different from that observed in our previous work with Aerosil 200 where it was more of an agglomerate of crystals growing out of the spheroids (Ramatsetse, 1998). In this case they are relatively large rectangular crystals growing as protrusions out of a smooth sphere (see Figure 5.20(e)). The average diameters of the spheres obtained in the synthesis without stirring with this method are

(a)
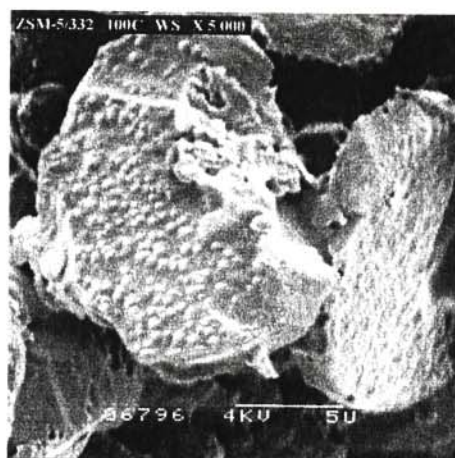
(b)
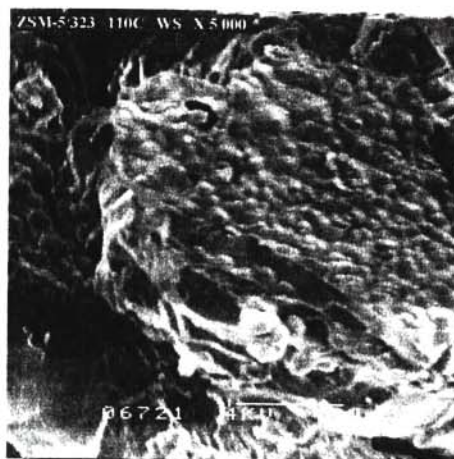
(c)

Figure 5.19 SEM micrographs of the ZSM-5-based samples synthesized without stirring using the water glass method at different temperatures: (a) 90°C, (b) 100°C and (c) 110°C.

(a)   (b)

(c)   (d)

(e)   (f)

Figure 5.20 SEM micrographs of the ZSM-5-based samples synthesized without stirring using the water glass method at different temperatures: (a) 130°C, (b) 140°C, (c) 150°C (X 2 000), (d) 150°C (X 5 000), (e) 150°C (another spot), and (f) 180°C.

shown in Table 5.11. It can be seen that the average diameters of the spheres increase with increasing synthesis temperature.

Table 5.11 Influence of synthesis temperature on the average diameters of the spheres formed in the ZSM-5-based samples synthesized without stirring using the water glass method

Batch no.	Synthesis temp. (°C)	%XRD crystallinity	Av. diameter (μm)	Standard deviation
307	130	9	2.4	0.3
302	140	36	5.1	0.9
264	150	89	12.7	1.1

At 180°C, crystals of elongated hexagonal and octagonal morphologies are observed (and the absence of spheres), as illustrated in Figure 5.20(f). This shows that that instead of the solid spheres, the products have the hexagonal and octagonal morphology at the higher synthesis temperature. We believe that such a transformation has not been reported previously for ZSM-5. Table 5.12 shows the sizes of the crystallites obtained using this method at 150°C and 180°C.

Table 5.12 Morphology and dimensions of the largest crystals formed in the ZSM-5 samples synthesized at 150°C and 180°C without stirring using the water glass method

Batch no.	Synthesis temp. (°C)	%XRD crystallinity	Crystallite morphology	Length (μm)	Breadth (μm)	Thickness (μm)
264	150	89	Rectangular	5.4	4.9	3.3
			Rectangular	5.5	4.4	2.2
			Hexagonal	---- [a]	7.7	3.8
			Octagonal	4.6	2.4	1.1
			Octagonal	6.5	3.1	3.9
311	180	86	Hexagonal	10.1	3.3	2.2
			Octagonal	6.2	4.8	3.9

[a]Could not be determined from the SEM micrograph.

5.3.1.2 *Synthesis with stirring*

XRD analysis

The X-ray diffractograms of some of the ZSM-5-based materials (and of other phases) prepared with stirring are shown in Figure 5.21. For the sample prepared at 120°C, again the characteristic hump previously observed for the amorphous material prepared with the Aerosil 200 ZSM-5 synthesis mixtures was not found at 23° 2θ, but instead at 38° 2θ (see Figure 5.21(a)). The characte-ristic peaks for the ZSM-5 zeolite are observed for the samples synthesized at 130°C (Figure 5.21(b)), indicating therefore that this sample has a higher XRD crystallinity. However, other peaks are also observed, e.g. at 9.7° 2θ, 25.6° 2θ and 26.0° 2θ, which indicate the presence of other crystalline phases which we have not identified. Although these impurity peaks are also evident in the samples synthesized at higher temperatures, their intensities decrease with increasing temperatures (see Figure 5.21(c)). The same was obtained for the synthesis without stirring using this recipe, but only, however, at 210°C.

From 150°C to 180°C, there is a significant increase in peak intensities of the ZSM-5 peaks, as is evident by Figure 5.21(d). At higher temperatures there is a minor decrease in peak intensities as shown in Figure 5.21(e), which is the X-ray diffractogram of the sample synthesized at 190°C.

The percentage XRD crystallinities of the ZSM-5-based samples from this recipe and the reaction temperatures employed are tabulated in Table 5.13. The results show that there is no ZSM-5 formed at temperatures lower than 120°C. From 130°C up to 180°C, there is a gradual increase in percentage XRD crystallinity of ZSM-5 with increasing synthesis tempe-rature. This is followed by a decline in percentage crystallinity with increasing synthesis temperature up to
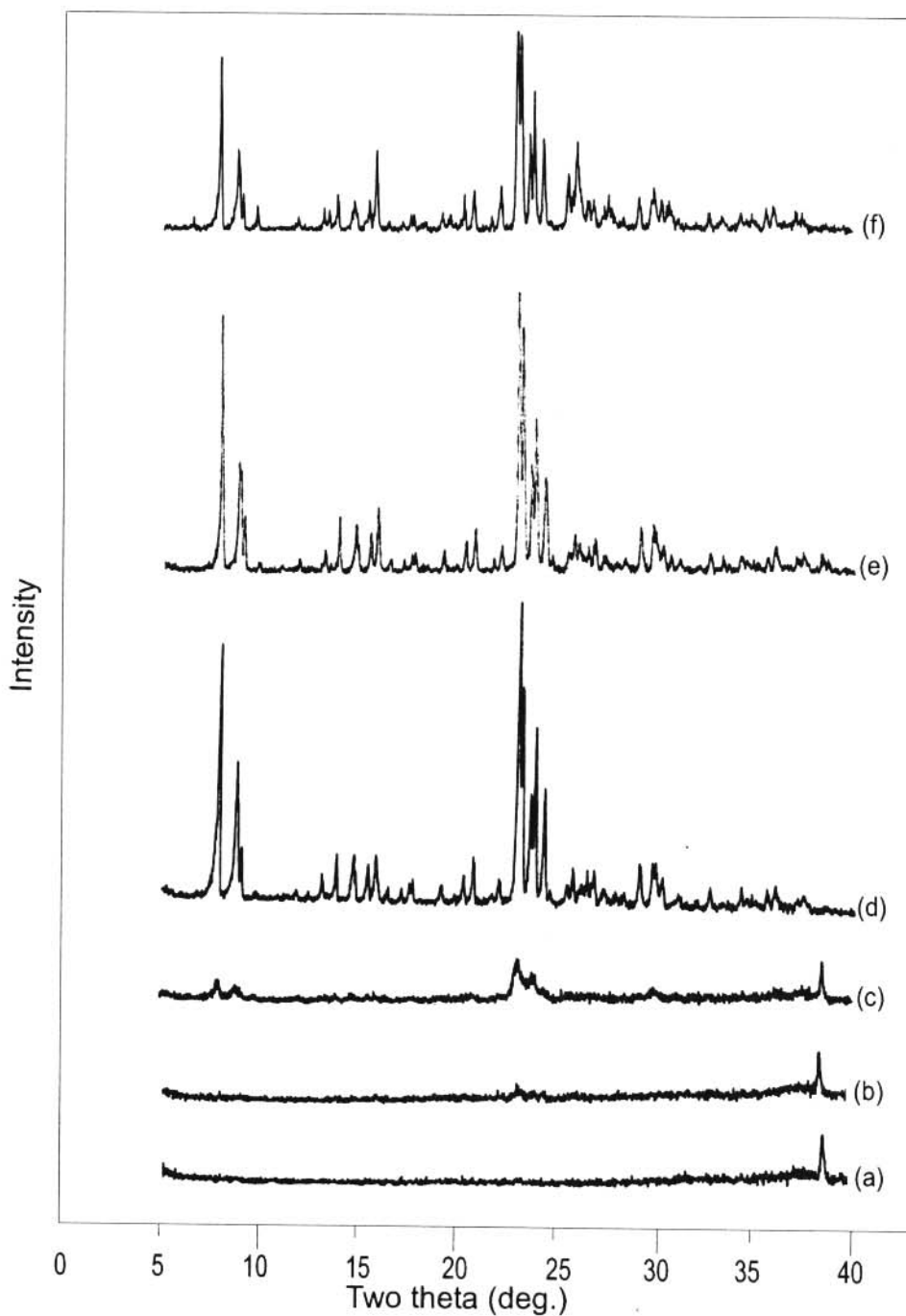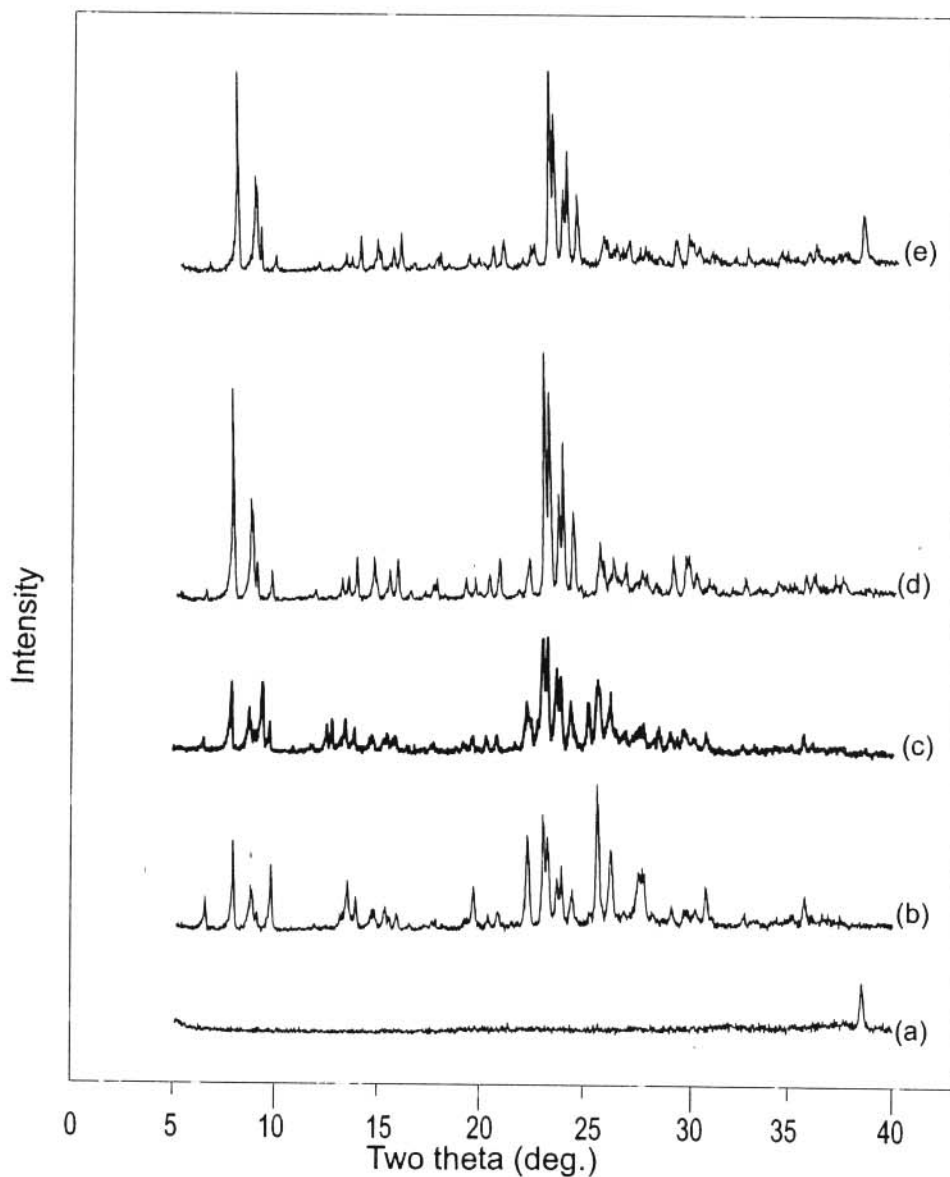
Figure 5.21 X-ray diffractograms of the ZSM-5-based samples, and of other phases, synthesized with stirring using the water glass method at different temperatures: (a) 120°C (batch no. 446), (b) 130°C (batch no. 457), (c) 150°C (batch no. 394), (d) 180°C (batch no. 407), and (e) 190°C (batch no. 410).

ratures up to 210°C. The latter could be attributed to amorphotization, e.g. see Figure 5.21(e), where the peak at 38.4° 2θ has again appeared in the diffractogram.

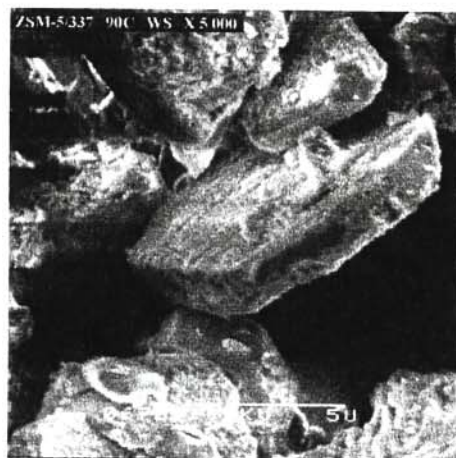**Table 5.13** Percentage XRD crystallinities of the ZSM-5 phase in the samples synthesized with stirring using the water glass method at different temperatures

Batch no.	Synthesis temperature ($^{\circ}$C)	%XRD crystallinity
449	90	0
447	100	0
448	110	0
446	120	0
457	130	32
482	135	21
415	140	49
483	145	35
394	150	48
398	160	·56
401	170	64
407	180	81
410	190	64
456	200	71
469	210	69

SEM analysis

Figure 5.22 shows the SEM micrographs of some of the ZSM-5-based samples, and of other phases, synthesized with stirring. As in the case of the samples synthesized without stirring, at 90°C crust-like amorphous materials are observed (not shown). At higher temperatures, crusts with protrusions are observed in the samples synthesized at temperatures up to 120°C (e.g. Figure 5.22(a)). At 135°C, the formation of distorted spheroids are observed (see Figure 5.22(b)). At 145°C, spheroids consisting of crystallites are observed, and these are evident in Figure 5.22(c).

At higher temperatures, crystals of definite morphology are formed as shown in Figure 5.22(d) through to Figure 5.22(f), which are the micrographs of the zeolite samples synthesized in the range 160°C to 200°C. As shown in Figure 5.22(d), at 160°C rectangular crystallites are formed, also rectangular and elongated octagonal and hexagonal crystallites are observed in the micro-

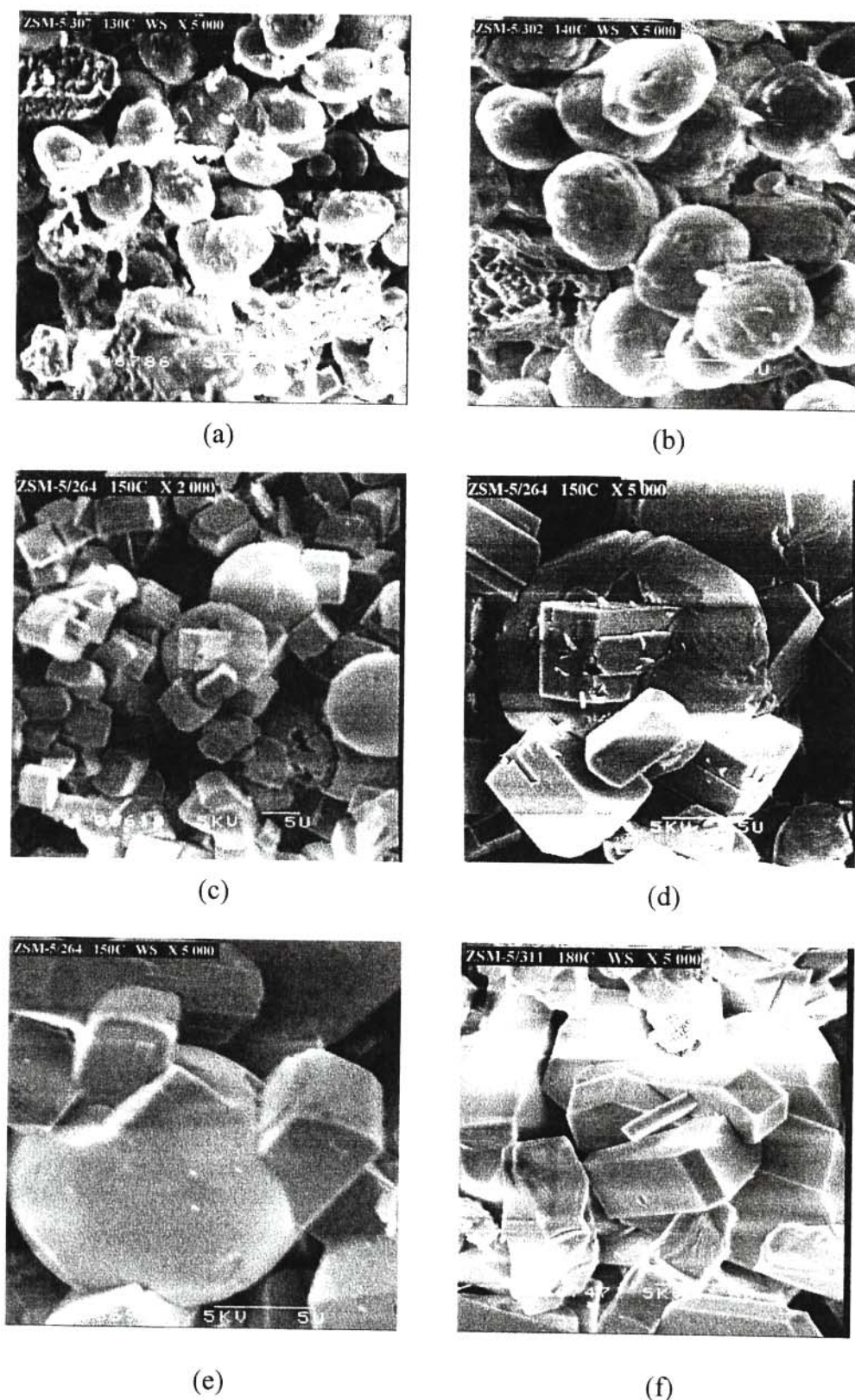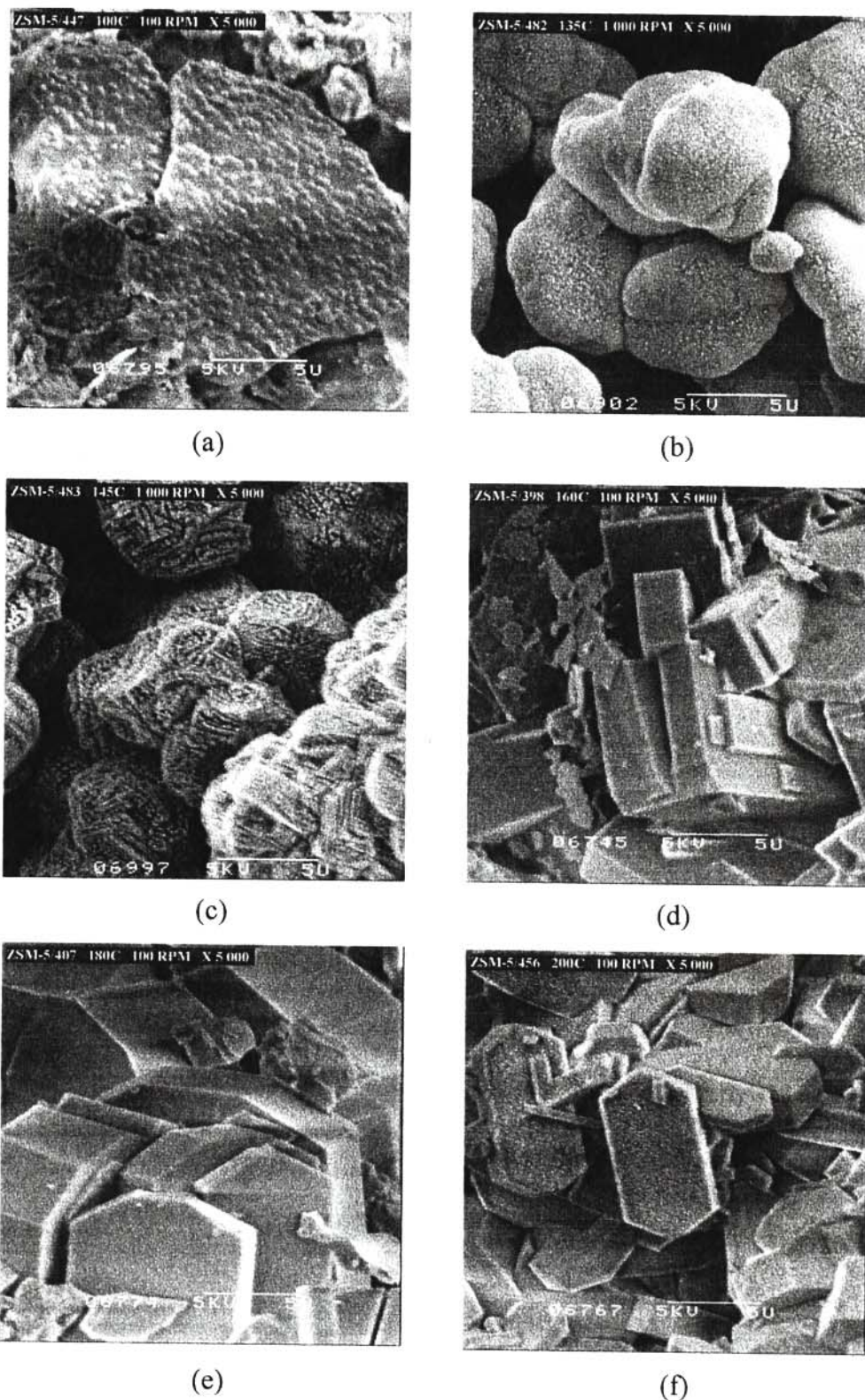**Figure 5.22** SEM micrographs of the ZSM-5-based samples, and of other phases, synthesized with stirring using the water glass method at different temperatures: (a) 100°C, (b) 135°C, (c) 145°C, (d) 160°C, (e) 180°C and (f) 200°C.

graphs of the samples synthesized at 180°C (Figure 5.22(e)). At 200°C hexagonal crystallites with "rough" surfaces are observed (Figure 5.22(f)). This could be due to the dissolution of the crystalline phase to give the amorphous phase (see also X-ray diffractogram in Figure 5.21(e)). The sizes of these crystals are shown in Table 5.14. A comparison of the sizes of the crystallites is a difficult process since different shapes are obtained at different tempe-ratures. However, it can be stated that the largest dimensions are observed at 180°C.

Table 5.14 Morphology and dimensions of some of the largest crystals of ZSM-5-based materials, and of other phases, synthesized with stirring using the water glass method

Batch no.	Synthesis temp.(°C)	%XRD crystallinity of ZSM-5 phase	Crystallite morphology	Length (μm)	Breadth (μm)	Thickness (μm)
398	160	56	Rectangular	----[a]	3.7	2.6
			Rectangular	4.7	4.2	2.4
			Rectangular	10.1	3.0	1.8
407	180	81	Rectangular	----[a]	6.0	3.8
			Hexagonal	----[a]	4.5	3.5
			Hexagonal	----[a]	6.8	4.3
			Octagonal	----[a]	8.0	0.8
			Octagonal	----[a]	11.5	1.8
			Octagonal	19.0	4.0	5.5
			Octagonal	15+	7.5	4.5
			Octagonal	9.4	4.0	1.6
456	200	71	Hexagonal	9.0	4.7	0.3
			Hexagonal	9.0	4.3	0.8
			Hexagonal	6.2	2.1	0.5
			Octagonal	11	8.5	2.5

[a]Could not be determined from the SEM micrograph.

5.3.1.3 *Comparison of results*

The percentage XRD crystallinity versus the synthesis temperature of the zeolite ZSM-5-based materials prepared with water glass as the silica source, either under static or stirred reaction conditions, are graphically compared in Figure 5.23. The plots give S-shaped curves for the percentage XRD crystallinity as a function of hydrothermal synthesis temperature. The samples synthesized with stirring give on average lower percentage XRD crystallinities than the unstirred samples. This is caused by the transformation of ZSM-5 into another phase as observed by the development of additional peaks in the diffractograms of these samples. Furthermore, it appears that with this recipe we were able to obtain samples of intermediate percentage crystallinities, i.e. 30% to 60%, which were not obtained with the Aerosil 200 method for both autoclaves and
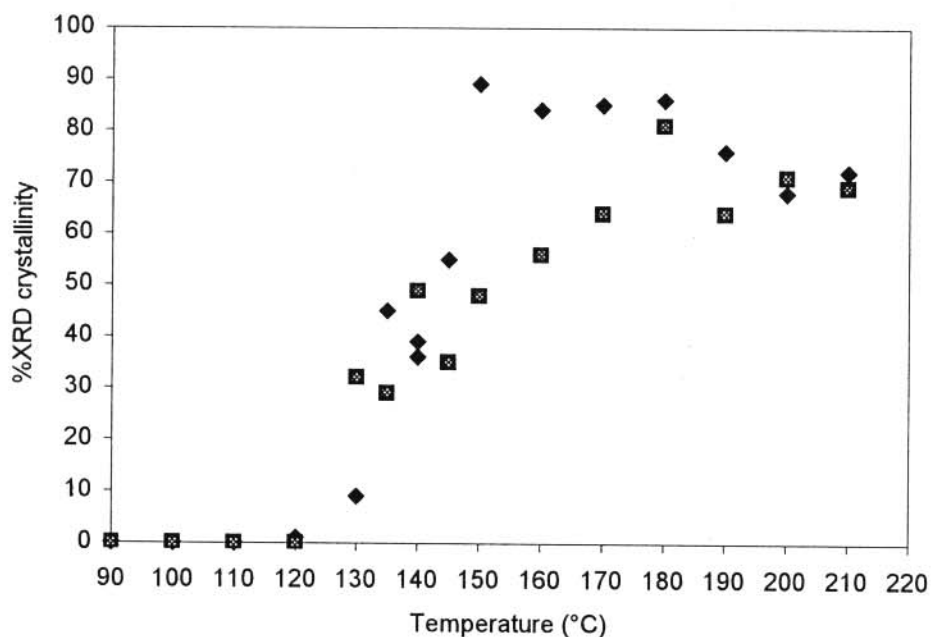
Figure 5.23 Plot of percentage XRD crystallinity of the ZSM-5 phase versus the synthesis temperature for the samples synthesized with stirring (∎) and without stirring (♦) using the water glass method.

modes of synthesis. The crystal sizes also seem to be bigger, especially for the synthesis with stirring. However, with this recipe, preparation with stirring is not preferred since impurities were obtained under this mode of synthesis.

The SEM micrographs of both with and without stirring samples show the formation of spheroids at low temperatures (130°C through to 150°C) and crystals of definite morphology at higher temperatures. Most significant is the transformation of the spheres at higher temperatures into hexagons and octagons. This suggests that the protrusions formed on the spheres grow continuously until the sphere becomes an integral part of the hexagons or octagons.

5.3.2 Silicic acid

ZSM-5-based materials were synthesized with silicic acid as a silica source according to the method by Copperthwaite *et al.* (1986) and Whittingham (1995) (see Section 4.3.2.3).

5.3.2.1 *Synthesis without stirring*

XRD analysis

Examples of the X-ray diffractograms of some of the ZSM-5-based samples synthesized without stirring are shown in Figure 5.24. Figure 5.24(a) is the diffractogram of the ZSM-5-based sample which was hydrothermally synthesized at 80°C. A hump around 23° 2θ, characteristic of amorphous materials, is once again observed which indicates, as previously indicated, that the product is X-ray amorphous.

Figure 5.24 X-ray diffractograms of the ZSM-5-based samples synthesized without stirring using the silicic acid method at different temperatures: (a) 80°C (batch no. 503), (b) 90°C (batch no. 366), (c) 100°C (batch no. 375), (d) 120°C (batch no. 507), and (e) 210°C (batch no. 384).

The 90°C sample shows a peak at 23.2° 2θ (see Figure 5.24(b)) which indicates that the product is substantially amorphous, or having only a very low degree of crystallinity. From 100°C to 120°C, there is a gradual increase in intensities of the characteristic peaks of ZSM-5 zeolite, as is evident from a comparison between Figure 5.24(c) and Figure 5.24(d). A further gradual increase in peak intensities is observed with increasing synthesis temperature up to 210°C (see Figure 5.24(e)). However, it is very significant to note that this increase in peak intensities at temperatures up to 210°C observed with this method (and under this mode of synthesis) was not found with any of the other methods investigated in this thesis.

The percentage XRD crystallinity for these synthesis conditions are listed in Table 5.15. The values in this table indicate an increase in percentage XRD crystallinity with increasing synthesis temperature up to 210°C, which was the highest temperature investigated. This method therefore gave the ZSM-5 sample with the highest percentage XRD crystallinity, higher than that of our previous reference sample (Ramatsetse, 1998). As a consequence, this sample was therefore used as the reference material in this thesis for the XRD analysis.

Table 5.15 Percentage XRD crystallinity for the ZSM-5-based samples synthesized without stirring using the silicic acid method at different temperatures

Batch no.	Synthesis temperature (°C)	%XRD crystallinity
503	80	0
366	90	4
375	100	9
378	110	38
507	120	47
286	130	28
282	140	39
279	150	47
272	160	55
274	160	63
276	170	70
278	180	80
281	190	81
284	200	89
384	210	100

It is also noteworthy, that whereas the other two recipes gave lower percentage XRD crystallinities at these high temperatures, with the silicic acid method we were able to obtain the most crystalline sample to be used as our XRD reference.

SEM analysis

To illustrate the effect of temperature on the morphology of the ZSM-5-based samples synthesized according to this recipe and without stirring, SEM micrographs of certain representative samples are shown in Figure 5.25. Figure 5.25(a) and Figure 5.25(b) show the SEM micrographs of the 55% and 100% XRD crystalline samples synthesized at 160°C and 210°C respectively. Both these samples show the formation of crystallites in the spheroidal structures. The spheroidal structures formed at 210°C are larger than those of the sample prepared at 160°C. Both, however, appear to be composed of more well formed crystallites.

(a)   (b)
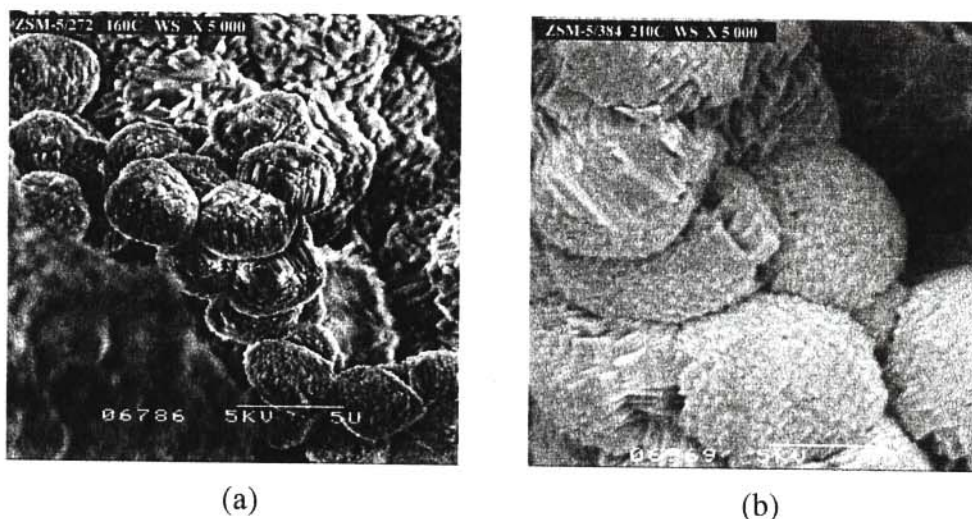
Figure 5.25 SEM micrographs of the ZSM-5 zeolite samples synthesized without stirring at different temperatures using the silicic acid method: (a) 160°C and (b) 210°C.

5.3.2.2 Synthesis with stirring

XRD analysis

The X-ray diffractograms of some of the ZSM-5 zeolite-based samples prepared with stirring are shown in Figure 5.26. For the sample synthesized at 90°C, no peaks are observed on the hump around 23° 2θ (Figure 5.26(a)), indicating that crystallization starts at a higher temperature for
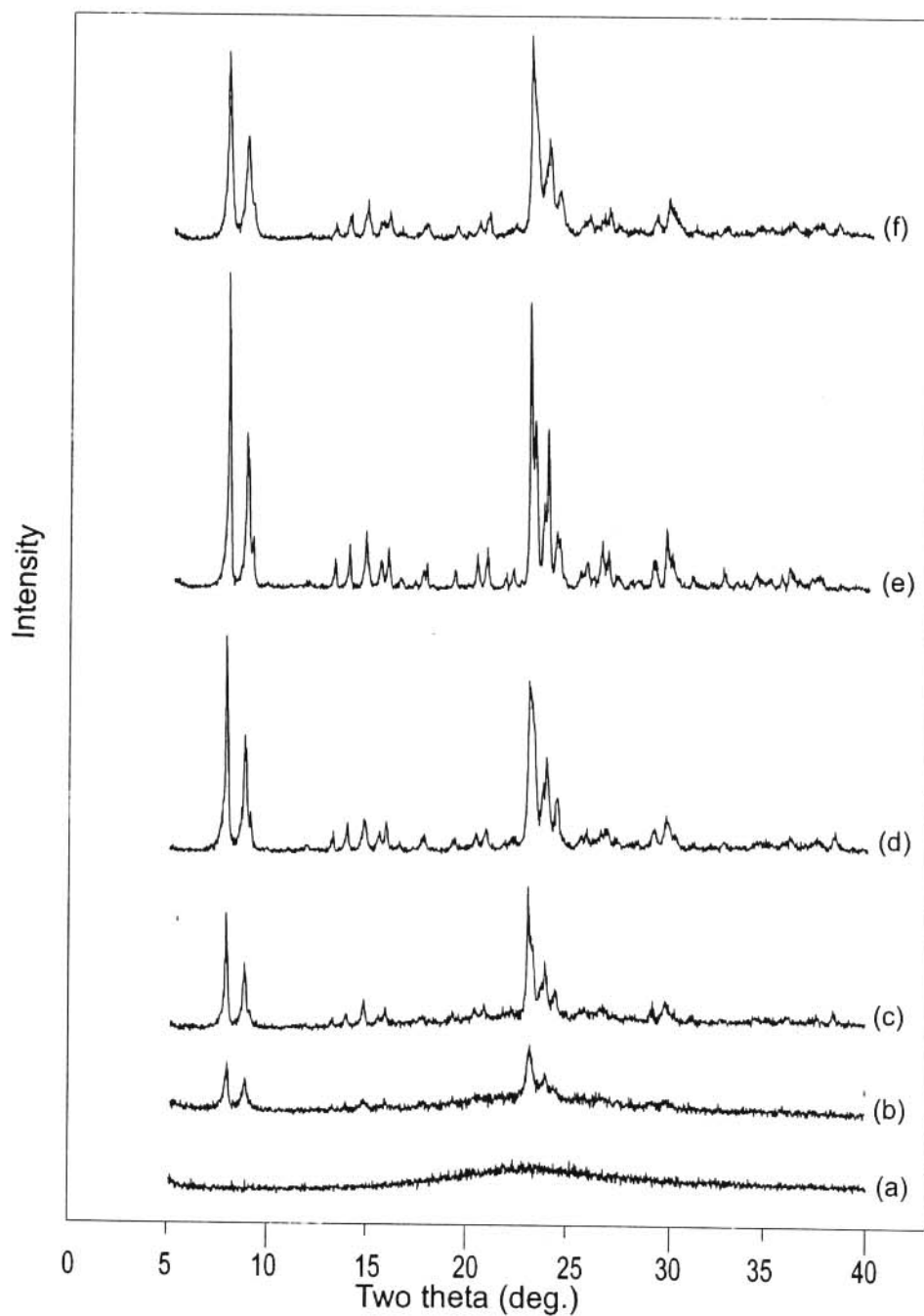
Figure 5.26 X-ray diffractograms of the ZSM-5-based samples synthesized with stirring in the in-house built autoclave using the silicic acid method at different temperatures: (a) 90°C (batch no. 470), (b) 100°C (batch no. 472), (c) 110°C (batch no. 505), (d) 140°C (batch no. 500), (e) 160°C (batch no. 490), and (f) 200°C (batch no. 495).

this reaction mode than for the synthesis without stirring. This is followed by a gradual increase in intensities of the characteristic peaks of ZSM-5 with increase in synthesis temperature as seen in Figure 5.26(b) through to Figure 5.26(e), which are diffractograms of the samples synthesized at 100°C to 160°C. At higher temperatures than these, there is on average a minor decline in peak intensities but with no development of obvious impurity peaks, as can be observed in Figure 5.26(f), which is the diffractogram of the sample synthesized at 200°C.

The percentage XRD crystallinities for this mode of synthesis are listed in Table 5.16. Although the trend followed by the values in this case is not as clear-cut as it was with those of the samples

Table 5.16 Percentage XRD crystallinity of the ZSM-5-based samples synthesized with stirring using the silicic acid method at different temperatures

Batch no.	Synthesis temperature (°C)	%XRD crystallinty
504	80	0
470	90	0
472	100	16
474	110	46
505	110	40
473	120	42
506	120	43
489	130	58
502	130	72
491	140	79
500	140	52
492	150	63
501	150	59
490	160	90
496	160	58
498	170	61
499	180	73
497	190	86
495	200	56
494	210	77

synthesized without stirring, within experimental error and the deviations observed, there is on average an increase in percentage XRD crystallinity with increasing synthesis temperature up to 160°C and a gradual decrease thereafter.

SEM analysis

Figure 5.27 shows the SEM micrographs of some of the ZSM-5-based samples synthesized using this methodology. The amorphous structure of the sample synthesized at 80°C is shown in Figure 5.27(a), while Figure 5.27(b) is the SEM micrograph of the sample synthesized at 100°C. In this sample, the formation of some spheroids among the amorphous phase is evident. The spheroids are much more prevalent in the sample synthesized at 120°C (Figure 5.27(c)) where the diameters of the spheroids are also larger. This increase in spheroid sizes with increasing temperature was observed throughout for the batches synthesized at temperatures up to 210°C (see Figure 5.27(d) to Figure 5.27(f) and Table 5.17). Some distortions of the spheroidal structures are observed on the sample synthesized at 190°C (Figure 5.27(e)).

Most interestingly, the largest spheroid of the sample synthesized at 210°C (Figure 5.27(f)) appears to have burst open and exposed many other smaller spheroids (see top and bottom cracked crust layers) which is an unusual observation not previously reported. The diameters of these smaller spheroids are around 1.6 μm. The results suggest that this method of ZSM-5 synthesis proceeds via a continuous spheroid growth up to a particular critical size and then it burst open hatching smaller spheres. This is in contrast to the water glass method where the spheres were "consumed" by the growing rectangular protrusions to become part of the hexagons and octagons. Therefore, it is obvious that the different recipes produce different final morphologies which have proceeded via different intermediate morphologies.
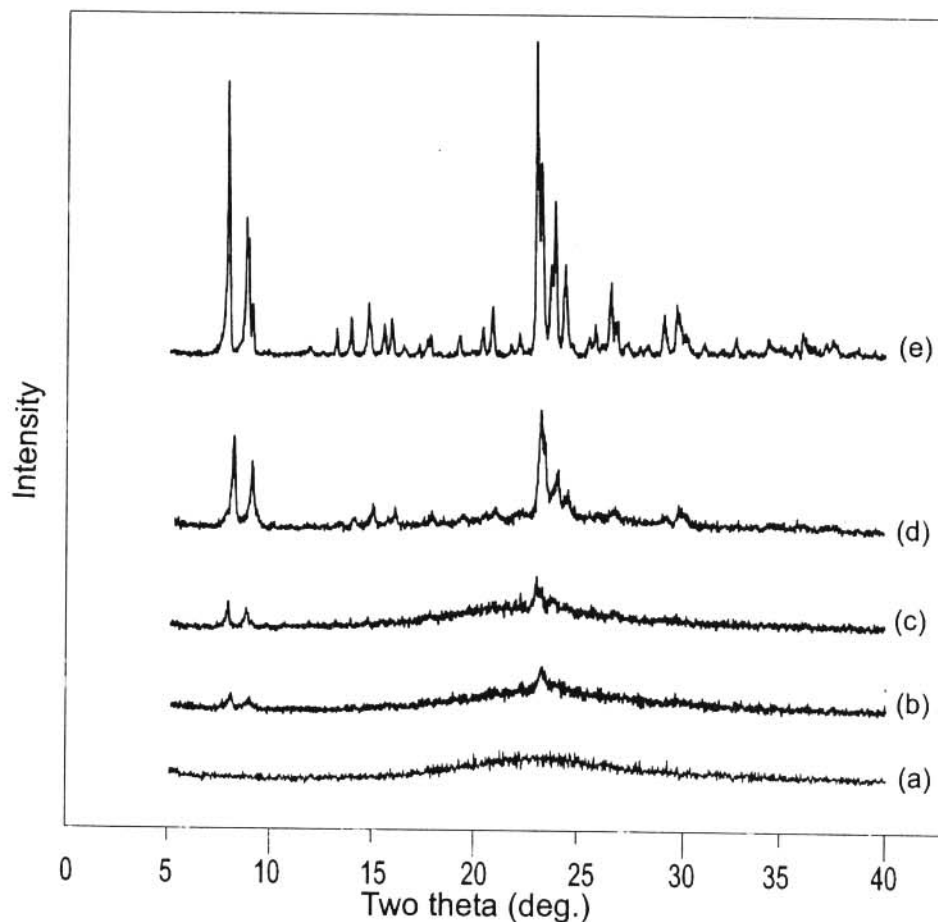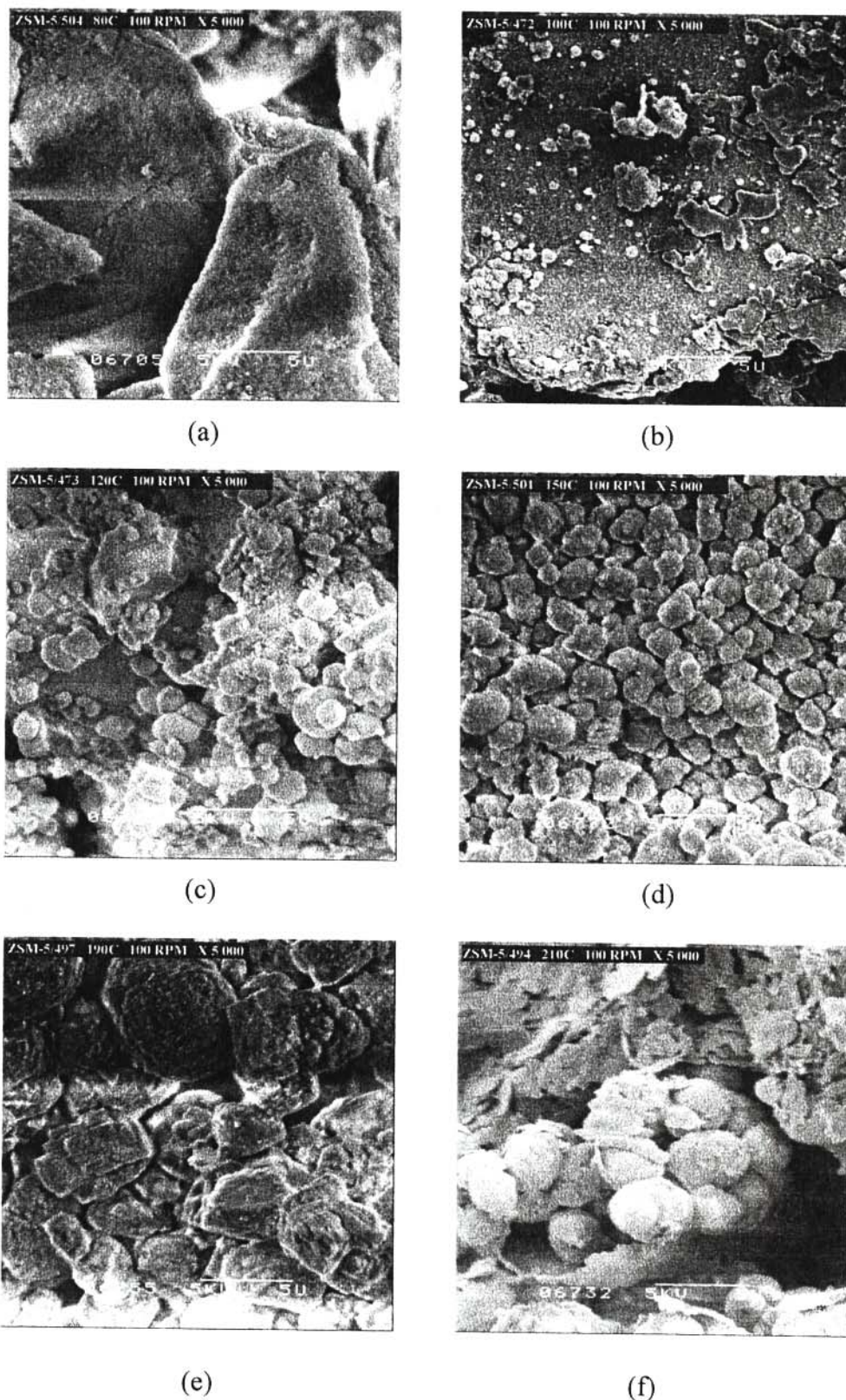
Figure 5.27 SEM micrographs of the ZSM-5 zeolite-based samples synthesized with stirring using the silicic acid method and at different temperatures: (a) 80°C, (b) 100°C, (c) 120°C, (d) 120°C, (e) 190°C and (f) 210°C.

Table 5.17 Influence of synthesis temperature on the average diameters of the spheroids formed in the zeolite ZSM-5-based samples synthesized with stirring using the silicic acid method

Batch no.	Synthesis temperature (°C)	%XRD crystallinity	Av. diameter (μm)	Standard deviation
472	100	16	0.8	0.5
473	120	42	2.0	1.6
501	150	63	2.1	0.8
490	160	90	3.4	1.4
497	190	86	4.0	1.2
494	210	77	5.9	2.3

5.3.2.3 Comparison of results

The percentage XRD crystallinity versus the synthesis temperature for the ZSM-5 zeolite-based samples prepared either under static or stirred reaction conditions are shown in Figure 5.28. The
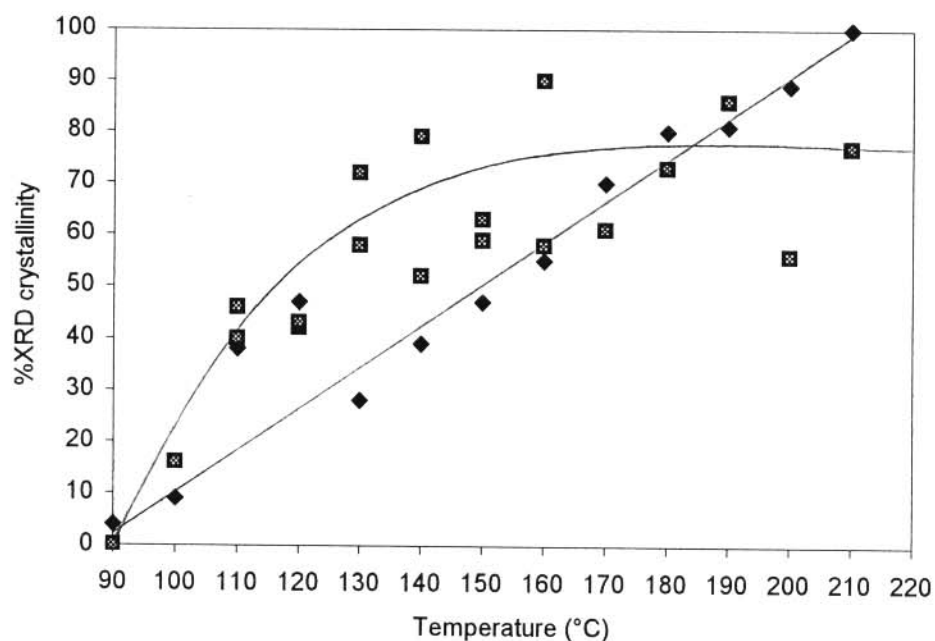
Figure 5.28 Plot of percentage XRD crystallinity of the ZSM-5 phase versus the synthesis temperature for the samples synthesized with stirring (■) and without stirring (♦) at different temperatures using the silicic acid method.

plot obtained for the samples synthesized without stirring, gives an approximately straight line of percentage XRD crystallinity versus temperature for synthesis temperatures up to 210°C, with some deviations for the samples prepared at 110°C and 120°C. A possible experimental error in these two preparations could be the reason for the deviation. The linear increase in XRD crystallinity is nevertheless a most surprising result, not observed with the other recipes, nor reported in the literature.

For the samples prepared with stirring an S-shaped curve for the percentage XRD crystallinity as a function of hydrothermal synthesis temperature was obtained, but a lot of scatter can be observed.

The smooth line obtained for the percentage XRD crystallinity of the samples prepared without stirring, shows that this is possibly the preferred mode of synthesis for this recipe and is therefore the most appropriate method in providing samples over the whole crystallinity range in a controlled and reproducible manner.

In terms of the morphology of the products, there were no crystals of definite morphology for both the with and without-stirring mode of synthesis at all the synthesis temperatures investigated using this recipe. Only spheroidal structures were observed with the largest spheroid being formed under the stirring mode of synthesis, and as shown by SEM, it burst open and released smaller spheroids, which is an unusual crystallization process for ZSM-5, as far as we could ascertain from our review of the literature.

5.3.3 **Aerosil 200 and glycerol**

The recipe investigated in this section is from a published method by Jacobs and Martens (1987). Although this method uses Aerosil 200 as the silica source, this recipe differs from the previously indicated "Aerosil 200" one in that glycerol and a solution of 25% ammonia were used as additional reagents, and aluminium nitrate nona-hydrate was used instead of aluminium hydroxide (see Chapter 4, Section 4.3.2.1 and Section 4.3.2.4). As in the previous sections, the zeolite-based samples were synthesized under both static and stirred conditions in the in-house built autoclave and the synthesis time was again 72 hours.

5.3.3.1 *Synthesis without stirring*

XRD analysis

Figure 5.29 shows the diffractograms of some of the ZSM-5 zeolite-based samples synthesized without stirring. The diffractogram of the sample which was hydrothermally synthesized at 90°C is shown in Figure 5.29(a) and again the hump around 23° 2θ was observed, as was the case with most of the other recipes at this temperature, and is of course indicative of the fact that an amorphous material was obtained. From 100°C up to 170°C there is a significant increase in the intensities of the characteristic peaks of ZSM-5 and gradual disappearance of the hump (see Figure 5.29(b) to Figure 5.29(e)).

At higher temperatures (e.g. 200°C, see Figure 5.29(f)), a decline in the intensities of the peaks are observed. The hump at around 23° 2θ, which is associated with amorphous materials, also

Figure 5.29 X-ray diffractograms of the ZSM-5 zeolite-based samples synthesized without stirring using the Aerosil 200 and glycerol recipe at different temperatures: (a) 90°C (batch no. 321), (b) 100°C (batch no. 477), (c) 150°C (batch no. 325), (d) 160°C (batch no. 334), (e) 170°C (batch no. 391), and (f) 200°C (batch no. 374).

surprisingly re-appears in this diffractogram. No development of impurity peaks could be observed and this could be ascribed to a gradual dissolution or amorphotization of the zeolite struc-ture under these reaction conditions and employing this particular recipe, and such decline in crystallinity is similar to that observed in Sections 5.3.1.2 and 5.3.2.2 with the water glass and silicic acid methods respectively, both with stirring.

The percentage XRD crystallinities as a function of synthesis temperature are listed in Table 5.18. The values indicate that although there is no clear-cut trend of percentage XRD crystallinity as a function of synthesis temperature at temperatures up to 110°C, there is a gradual increase in percentage XRD crystallinity with increasing synthesis temperature up to 170°C. From 175°C and higher, there is on average, a steady decrease in percentage XRD crystallinity with increasing temperature.

Table 5.18 Percentage XRD crystallinity for the ZSM-5-based samples synthesized without stirring at different temperatures using the Aerosil 200 and glycerol method

Batch no.	Synthesis temperature (°C)	%XRD crystallinity
321	90	0
477	100	20
479	110	0
478	120	18
338	130	11
329	140	37
325	150	49
334	160	62
391	170	90
438	175	53
359	180	44
369	190	27
374	200	14
485	210	26

SEM analysis

To illustrate the effect of temperature on the morphology of the ZSM-5-based samples synthesized according to this recipe and without stirring, SEM micrographs of certain representative samples at different synthesis temperatures are shown in Figure 5.30. Figure 5.30(a) shows the SEM micrograph of the XRD amorphous sample synthesized at 90°C. At higher temperatures, up to 160°C, twinned cubic crystallite structures with rounded off edges and surrounded by amorphous material are observed, of which Figure 5.30(b) and Figure 5.30(c) are examples. Figure 5.30(d) is the micrograph of the 90% XRD crystalline sample synthesized at 170°C where the twinned structure is no longer observed, and instead the morphology of the crystals is now rectangular and octagonal, with no amorphous material being evident. The twinned structures among the amorphous materials are again observed for preparation above 180°C, examples of which are Figure 5.30(e) and Figure 5.30(f). However, the twinned structures at these higher temperatures are hexagonal and not cubic as was observed for the synthesis in the lower temperature region. Furthermore, this increase in the amount of amorphous material present correlates with the decline in percentage XRD crystallinity at higher synthesis temperatures as shown in Table 5.18.

The spheroidal structures which were observed with the other synthesis recipes for ZSM-5 presented above were therefore not observed with this particular recipe. The sizes of the largest crystallites obtained are listed in Table 5.19. There is a fluctuation in crystallite sizes with increasing synthesis temperature, which is different from the results obtained with other ZSM-5 synthesis recipes studied used in this project, where an increase in crystallite size was observed at higher synthesis temperature. In this case smaller crystallites together with amorphous materials are formed at high temperatures where low percentage crystallinity was also measured.

Figure 5.30 SEM micrographs of ZSM-5 zeolite samples synthesized without stirring using the Aerosil and glycerol method at different temperature (a) 90°C, (b) 140°C, (c) 150°C and (d) 170°C, (e) 200°C and (f) 210°C.

Table 5.19 Morphology and dimensions of the largest crystals of the ZSM-5-based materials synthesized at different temperatures without stirring using the Aerosil 200 and glycerol method

Batch no.	Synthesis temp. (°C)	%XRD crystallinity	Crystallite morphology	Length (μm)	Breadth (μm)	Thickness (μm)
329	140	37	Twinned cubic	13.4	10.7	2.5
325	150	49	Twinned cubic	11.6	10.7	2.3
334	160	62	Twinned cubic	14.1	11.9	1.2
391	170	90	Octagonal	12.1	6.8	1.9
374	200	14	Twinned hexagonal	8.3	3.3	1.8
485	210	26	Twinned hexagonal	7.7	3.2	1.5

5.3.3.2 Synthesis with stirring

XRD analysis

The diffractograms of some of the ZSM-5-based samples prepared with stirring are shown in Figure 5.31. The 90°C sample shows only the hump at about 23° 2θ (see Figure 5.31 (a)) along with a peak at 38.4° 2θ. This indicates that no ZSM-5 has formed at this temperature, and similarly at 100°C. In Figure 5.31(b), which is the X-ray diffractogram of the sample prepared at 110°C, the appearance of small peaks on top of the hump can be observed. It can further be observed from the other diffractograms shown in Figure 5.31 that the intensities of the characteristic peaks for ZSM-5 zeolite increase with increasing reaction temperature up to 175°C, as illustrated by Figure 5.30(c) and Figure 5.31(d). This is then followed by a decline in peak intensities, as shown in Figure 5.31(e) and Figure 5.30(f) which are the diffractograms of the samples synthesized at 180°C and 210°C respectively. These observations are in agreement with the SEM results which are shown below.
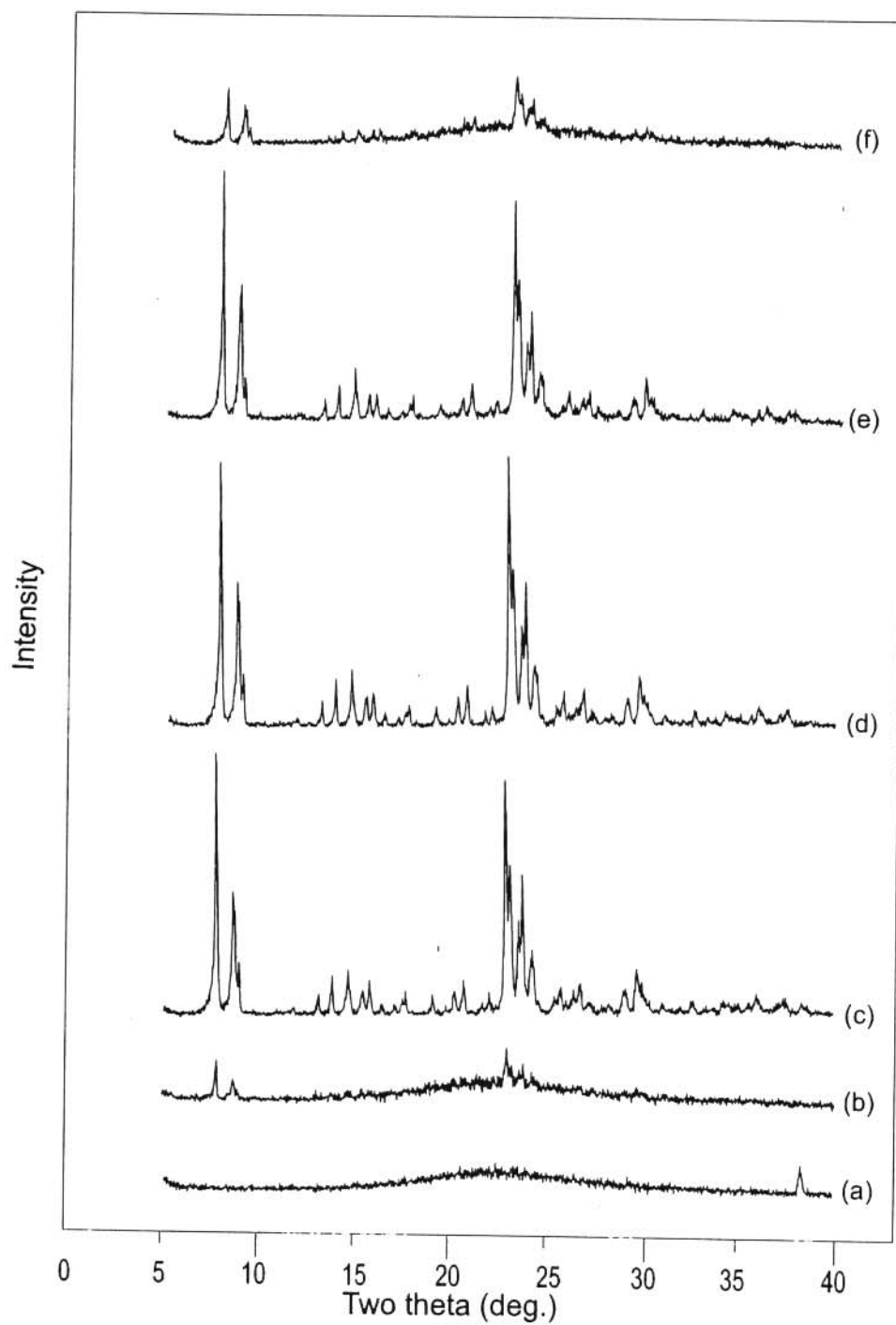
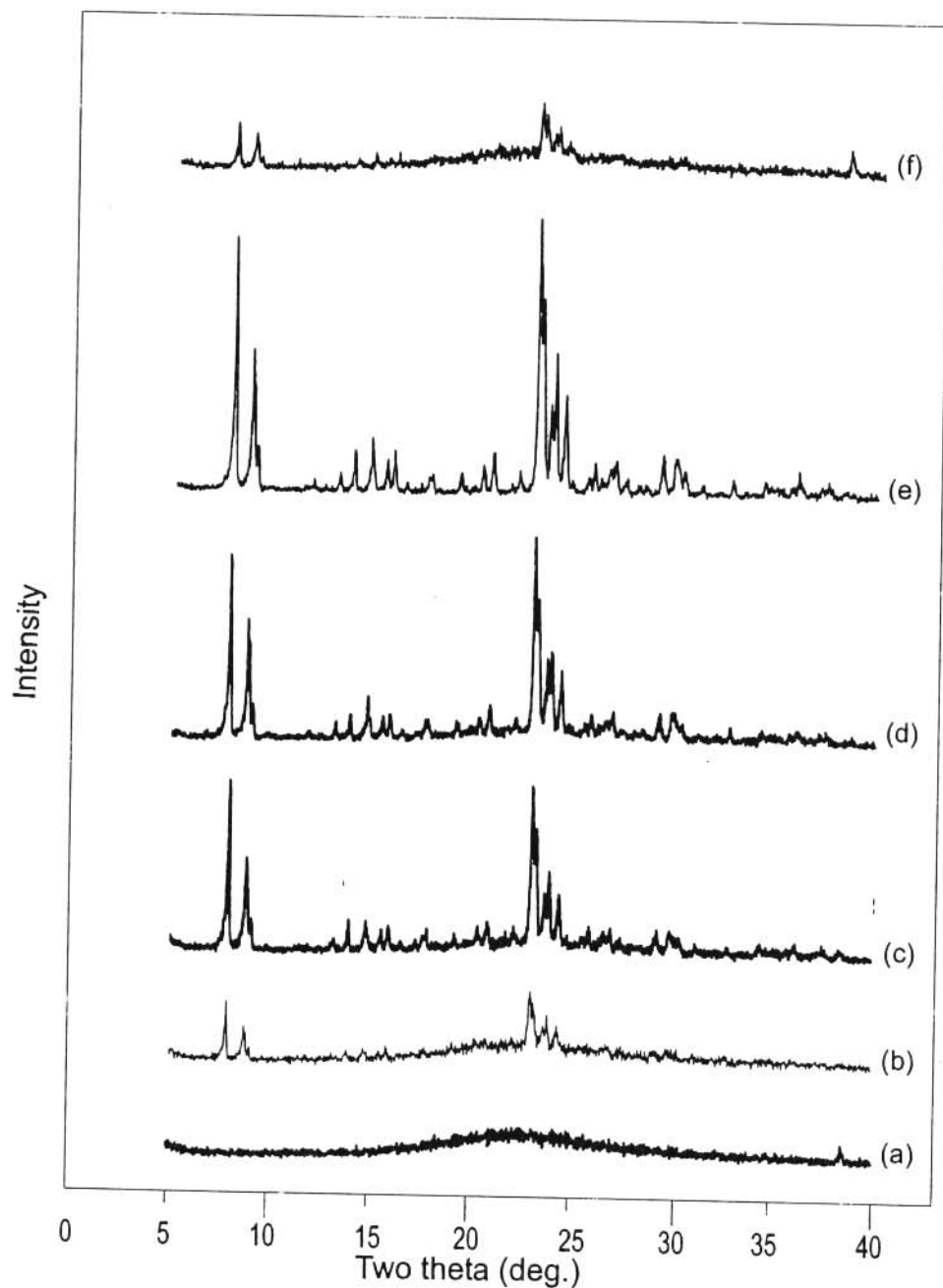**Figure 5.31** X-ray diffractograms of the ZSM-5-based samples synthesized with stirring using the Aerosil 200 and glycerol method at different temperatures: (a) 90°C (batch no. 455), (b) 110°C (batch no. 462), (c) 150°C (batch no. 405), (d) 160°C (batch no. 416), (e) 180°C (batch no. 464), and (f) 210°C (batch no. 458).

The percentage XRD crystallinities obtained under these synthesis conditions are summarized in Table 5.20. The data indicates that although substantially amorphous ZSM-5-based materials were formed at temperatures between 110°C and 140°C, there was no clear trend of either an increase or decrease in XRD crystallinity with increasing synthesis temperatures up to 140°C. These results indicate therefore that reproducibility is a problem with this recipe (with stirring) at low percentage XRD crystallinities. A tremendous increase in crystallinity was detected between 140°C and 150°C which remained constant up to 175°C, after which a constant decrease was again obtained.

Table 5.20 Percentage XRD crystallinity for the ZSM-5 zeolite-based samples synthesized with stirring at different temperatures using the Aerosil 200 and glycerol method

Batch no.	Synthesis temperature (°C)	%XRD crystallinity
455	90	0
460	100	0
462	110	9
461	120	1
459	130	14
409	140	8
405	150	79
416	160	83
420	170	80
465	170	57
420	170	80
487	175	82
464	180	64
467	190	60
466	200	36
458	210	17

SEM analysis

Figure 5.32 shows the SEM micrographs of some of the ZSM-5-based samples synthesized with stirring. Figure 5.32(a) shows the amorphous structure of the sample synthesized at 90°C. Figure 5.32(b) is the SEM micrograph of the sample synthesized at 130°C. In this sample, formation of twinned cubic crystals with rounded off edges are evident, which are almost similar to the ones previously obtained for synthesis without stirring using this recipe (Figure 5.30). Such formations are also prevalent in the samples synthesized at 180°C and 190°C (Figure 5.32(c) and Figure 5.32(d)). At the synthesis temperatures of 200°C and 210°C (see Figure 5.32(e) and Figure 5.32(f)), the crystal structures are clearly twinned hexagons. Once again, the morphology of the crystallites undergoes a change with increasing synthesis temperatures between 130°C and 190°C, that is from cubic to hexagonal.

The sizes of the crystals are shown in Table 5.21. On average, one could conclude that the twinned structures increase in sizes as the synthesis temperature increases up to 200°C after which a decline was observed and goes hand in hand with amorphotization of the ZSM-5-based material. An increase in the amount of amorphous materials can be observed with increasing temperature above 190°C (see Figure 5.32(e) and Figure 5.32(f)) and this correlates with the XRD analysis of these samples. Lastly, it can be stated that from all the recipes described above, formation of the twinned cubic or hexagonal crystallites was only observed with the Aerosil 200 and glycerol method.
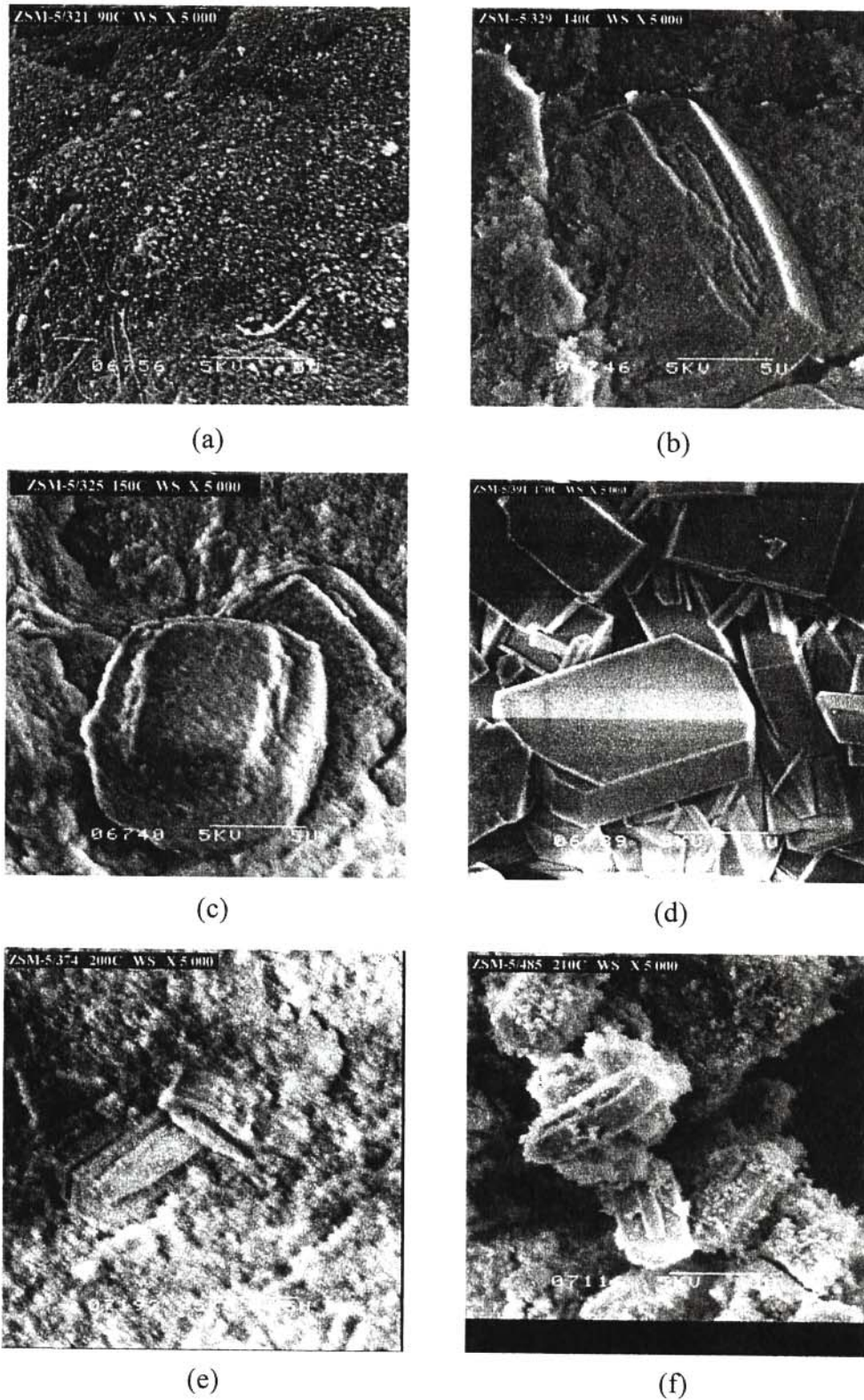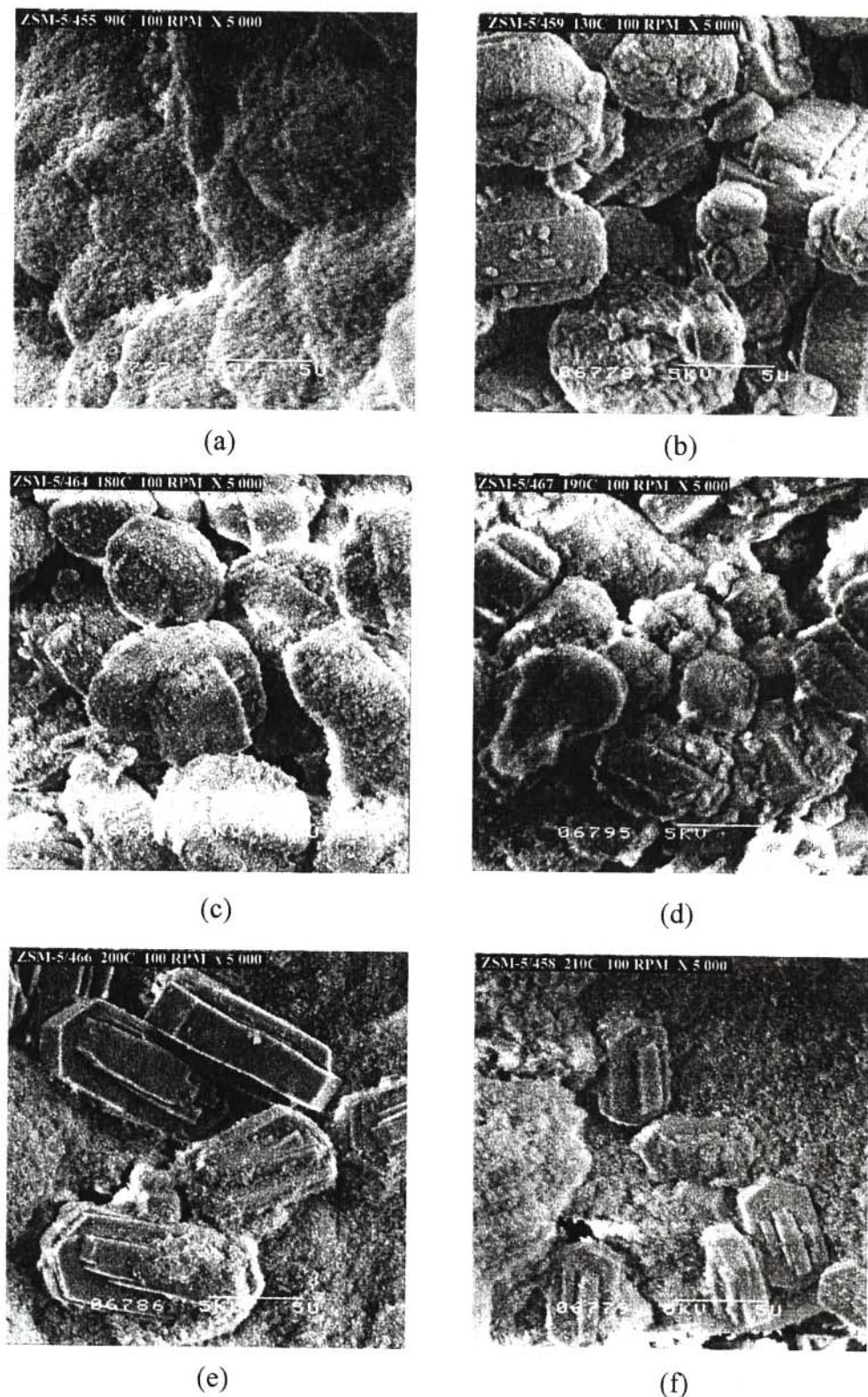
Figure 5.32 SEM micrographs of the ZSM-5-based samples synthesized with stirring using the Aerosil 200 and glycerol method at different temperatures: (a) 90°C, (b) 130°C, (c) 180°C, (d) 190°C, (e) 200°C and (f) 210°C.

Table 5.21 Influence of synthesis temperature on the morphology and average dimensions of the crystallites of the ZSM-5-based samples synthesized with stirring using the Aerosil 200 and glycerol method

Batch no.	Synthesis temp. (°C)	%XRD crystallinity	Crystallite morphology	Length (μm)	Breadth (μm)	Thickness (μm)
459	130	14	Twinned cubic	5.9	4.6	3.1
416	160	85	Twinned cubic	5.8	4.6	3.2
464	180	64	Twinned cubic	7.1	6.3	2.4
467	190	60	Twinned cubic	9.8	4.0	2.1
466	200	36	Twinned hexagonal	10.7	4.9	1.3
458	210	17	Twinned hexagonal	6.0	2.8	0.7

5.3.3.3 Comparison of results

The percentage XRD crystallinity versus the synthesis temperature for the zeolite-based samples prepared according to the Aerosil 200 and glycerol method are presented in Figure 5.33. The plots obtained for both sets of samples are essentially S-shaped curves. A gradual increase can be observed in percentage crystallinity with increasing temperature up to the synthesis temperature of 170°C (from 0% to 90%) for the samples prepared without stirring. This is then followed by a decrease in percentage XRD crystallinity up to the synthesis temperature of 210°C (from 90% to 14%). For the samples prepared with stirring, the curve shows an increase in percentage XRD crystallinity with increasing synthesis temperature up to 160°C, where the percentage crystallinity is 83%, and thereafter the crystallinity decreases to 17% at 210°C.

The SEM micrographs of the samples synthesized according to this recipe, show the formation of twinned cubic crystallites with rounded off edges in the lower temperature region (hydrothermal treatment up to 160°C for the preparation without stirring, and up to 190°C for the
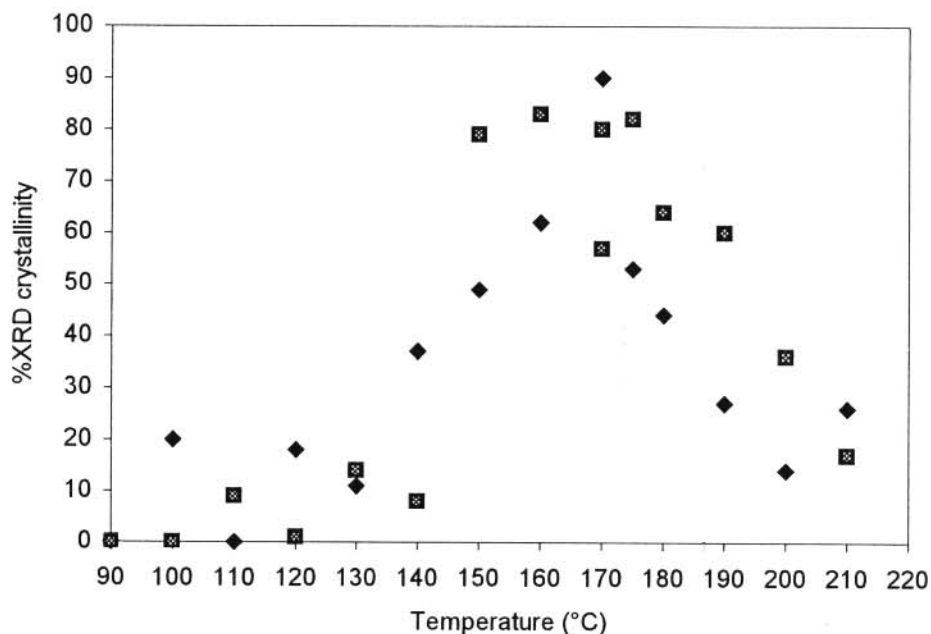
Figure 5.32 Plot of percentage XRD crystallinity of the ZSM-5 phase versus the synthesis temperature for the samples synthesized with stirring (■) and without stirring (♦) at different temperatures using the Aerosil 200 and glycerol method.

synthesis with stirring) and without the formation of spheroids as was observed with the other recipes. At 170°C and 180°C non-twinned octagonal and rectangular crystallites were observed for the synthesis without stirring. From 190°C to 210°C, twinned hexagons were obtained for the synthesis without stirring while the same structures were also identified above 190°C for preparation with stirring. Such morphologies were also obtained by Beschmann *et al.* (1994) (at 185°C) and Kim *et al.* (1998) (at 100°C) who used Ludox AS-40 as a silica source, and Suzuki *et al.* (1986) for their preparation using water glass as a silica source (at 150°C). Those obtained by Beschmann *et al.* (1994) were also twinned hexagonal structures (see Figure 2.9(b)), while those obtained by Suzuki *et al.* (1986) (see Figure 2.1) and by Kim *et al.* (1998) (see Figure 2.3(b)) are similar to the twinned cubic structures with rounded off edges, which they indicated in their publications as "cross-twinned discs" and "euhedrals", respectively.

5.3.4 **Conclusions**

From the four recipes used for ZSM-5 synthesis, the method in which silicic acid was used as a silica source, seems to have some outstanding features. Although some of the reagents used in this method are expensive, under the unstirred mode of synthesis, this method gave the highest percentage XRD crystallinity for all synthesis methods and reaction conditions investigated and within the shortest synthesis time, namely 44 hours. This is also the only method that gave a linear plot of percentage XRD crystallinity versus synthesis temperature and it shows that the reproducible synthesis of ZSM-5-based materials at different levels of percentage XRD crystallinity can be easily obtained under the unstirred mode of synthesis using this recipe.

As was shown above, the different recipes (with different silica sources) of ZSM-5 zeolite syntheses may produce samples with the same percentage XRD crystallinities but of different morphologies. The trends followed by these percentage XRD crystallinities as a function of temperature differ from one method to the other. These range from the linear plot (see Figure 5.28) for the silicic acid method (unstirred) to the sigmoidal plot (Figure 5.2) for the Aerosil 200 method (unstirred) respectively. Examples of the changes in morphology observed in the Aerosil 200 method (Section 5.2) and the Aerosil 200 and glycerol method (Section 5.3.3) have been described. In both cases tetrapropylammonium bromide was used as a template, but their morphologies differ totally as is evident by the SEM results shown in Figure 5.3 and Figure 5.30 respectively. In this section, therefore, we have shown the effect of the different recipes, with and without stirring at different temperatures, on the resultant morphology (see Table 5.22) by our detailed synthesis, XRD and SEM studies.

Table 5.22 Transformation of the morphology of ZSM-5-based materials prepared in the temperature range between 80°C and 210°C with different synthesis methods

Synthesis temperature (°C): 210, 200, 190, 180, 170, 160, 150, 140, 130, 120, 110, 100, 90, 80

Aerosil 200 method

With stirring:
(Formation of α-quartz) Rectangular and hexagonal ← Crystallites in spheroids ← Spheroids ← Amorphous

Without stirring:
Cubic and hexagonal ← Crystallites in spheroids ← Spheroids ← Amorphous

Water glass method

With stirring:
Rectangular, hexagonal and octagonal ← Crystallites in the form of spheroids ← Distorted spheroids (ZSM-5 and additional phase) ← Crust-like amorphous with circular protrusions

Without stirring:
(Formation of additional phase) Rectangular, hexagonal and octagonal ← Rectangular protrusions on spheres ← Spheres ← Crust-like amorphous with circular protrusions

Silicic acid method

With stirring:
Spheroids open and "hatch" more spheres ← Spheroids ← Amorphous

Without stirring:
Spheroids with crystallites ← Spheroids ← Amorphous

Aerosil 200 and glycerol method

With stirring:
(Amorphotization sets in) Twinned hexagonal ← Twinned cubic with rounded off edges ← Amorphous

Without stirring:
(Amorphotization sets in) Twinned hexagonal ← Rectangular and octogonal ← Twinned cubic with rounded off edges ← Amorphous

5.4 CATALYTIC TEST REACTIONS

5.4.1 Introduction

The catalytic activity of some of the samples was evaluated using probe reactions in order to investigate whether samples of almost the same percentage XRD crystallinity but synthesized in different ways will exhibit similar or dissimilar catalytic behaviour. Some of the H-ZSM-5-based materials synthesized with stirring both in the in-house built and the Parr autoclave and those prepared without stirring in the Parr autoclave using the Aerosil 200 method were ion-exchanged into the H⁺-form and *n*-hexane cracking and/or propane cracking were used as catalytic test reactions. The hypothesis to be tested therefore was the catalytic properties of the samples synthesized with and without stirring and having almost the same percentage XRD crystallinity, as well as to examine the catalytic activity of the samples synthesized in the same way (with stirring) but in different autoclaves.

Both the Parr and in-house built autoclaves behaved alike in producing samples of similar XRD crystallinities when the samples were synthesized without stirring as a function of reaction temperature (see Figure 5.14), but this was not the case with the samples which were prepared with stirring (see Figure 5.15). The percentage XRD crystallinities of the samples synthesized with stirring in the Parr autoclave were similar to those synthesized without stirring in both the Parr and the in-house built autoclaves (Figure 5.14 and Figure 5.16). It is therefore suspected that this was due to the fact that the stirring rate of 100 rpm used in the Parr autoclave was apparently too low to produce any differences in the crystallinities of the stirred and the unstirred samples prepared at the same temperatures.

As already indicated above, catalytic test reactions were chosen as the third technique to supplement the XRD and SEM analyses carried out in order to characterize the samples. Selected samples of different percentage XRD crystallinities ranging from 2% to 80% were chosen from the samples synthesized with and without stirring in the Parr autoclave (see Table 4.2) for testing using both propane cracking and n-hexane cracking as CTR's. The third group of samples was chosen from the ZSM-5-based samples synthesized with stirring in the in-house built autoclave. With this third set of samples, only n-hexane cracking was used as CTR because of the low amount of each sample that was available.

The percentage conversion and activity versus percentage XRD crystallinity, and the product selectivities and molar ratios of the products, that could be anticipated from monomolecular cracking (see Section 3.11, and Haag and Dessau, 1984; Bandiera and Taarit, 1990) of the alkane reactants over H-ZSM-5 catalysts are presented and discussed in the following two sections.

5.4.2 Propane cracking

As mentioned above, because of the small amounts of each sample available and the fact that propane cracking needed more sample (0.5 g per run) than n-hexane cracking (0.1 g per run), propane cracking was carried out only over the H-ZSM-5-based materials synthesized with and without stirring in the Parr autoclave.

5.4.2.1 *H-ZSM-5-based materials synthesized with stirring at 100 rpm in the Parr autoclave*

Appendix A shows the chromatograms from the cracking of propane at 500°C over the H-ZSM-5-based materials synthesized with stirring at 100 rpm in the Parr autoclave. The crystallinities

of the samples ranged from 2% to 78% and were synthesized at temperatures between 90°C to 180°C.

As indicated in Section 4.4.3.3 the propane source contained (in mass percentage) 94.154% propane, 2.204% ethane and 3.642% butanes, and as a result it was difficult to obtain the percentage conversion of propane directly, and was therefore calculated from the feed components that had reacted (propane and butanes). The changes in mass percentage of reactants and products formed are given in Table 5.23. Considering that the hydrogen formed could not be detected by our GC set-up, there is a good correlation between the amounts of feed components reacted and products formed. As can be seen in Table 5.24, there is a gradual increase in the percentage conversion (calculated from the feed components reacted, both propane and butanes) and activity with increasing percentage crystallinity of these samples. These results are also shown in Figure 5.33 and Figure 5.34 as percentage conversion and activity respectively as

Table 5.23 Changes (in mass%) of reactants and products formed during the cracking of propane (which contains ethane and butanes as impurities) at 500°C over H-ZSM-5-based materials of different levels of crystallinity synthesized with stirring in the Parr autoclave

%XRD crystallinity	C_1	$C_2^=$	C_2^-	$C_3^=$	C_3^-	C_4's	C_5's	C_{6+}	Products formed	Feed components reacted
2	0.01	0.01	0.06	----[a]	0.32 [a]	-0.39	0.00	0.00	0.39	0.39
18	0.10	0.19	0.06	----[a]	0.18 [a]	-0.53	0.00	0.00	0.53	0.53
27	0.15	0.26	0.23	----[a]	0.31 [a]	-0.95	0.00	0.00	0.95	0.95
51	0.69	1.07	0.15	----[a]	-0.94 [a]	-1.00	0.04	0.00	1.94	1.95
63	1.22	1.51	0.48	0.83	-3.55	-1.45	0.16	0.79	5.00	4.99
78	2.13	2.02	1.21	1.35	-8.67	0.38	0.37	1.21	8.67	8.67

[a]$C_3^=$ could not be separated from the C_3^- peak.

Table 5.24 Percentage conversion and catalytic activity for propane cracking (in the presence of ethane and butanes as impurities) at 500°C over H-ZSM-5-based materials of different levels of crystallinity synthesized with stirring in the Parr autoclave

%XRD crystallinity	Particle sizes (μm)	%Conversion	Activity
2	0	0.40	0.004
18	----[a]	0.54	0.005
27	----[a]	0.97	0.010
51	1.5	1.99	0.020
63	1.2	5.11	0.052
78	2.1	8.86	0.093

[a]SEM micrograph not available.
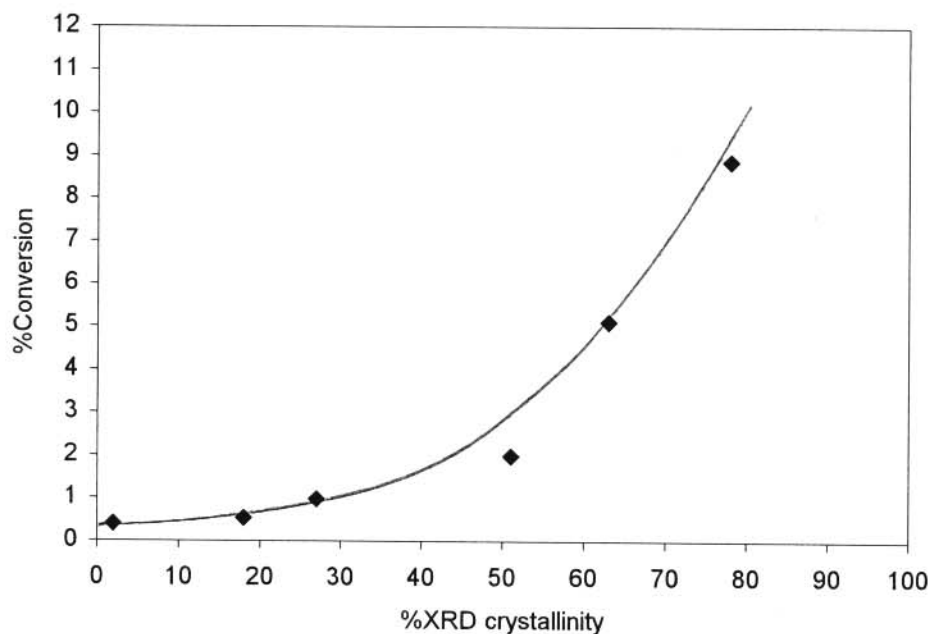
Figure 5.33 Plot of percentage conversion versus percentage XRD crystallinity for propane cracking (in the presence of the impurities ethane and butanes) at 500°C over H-ZSM-5-based catalysts synthesized with stirring in the Parr autoclave.
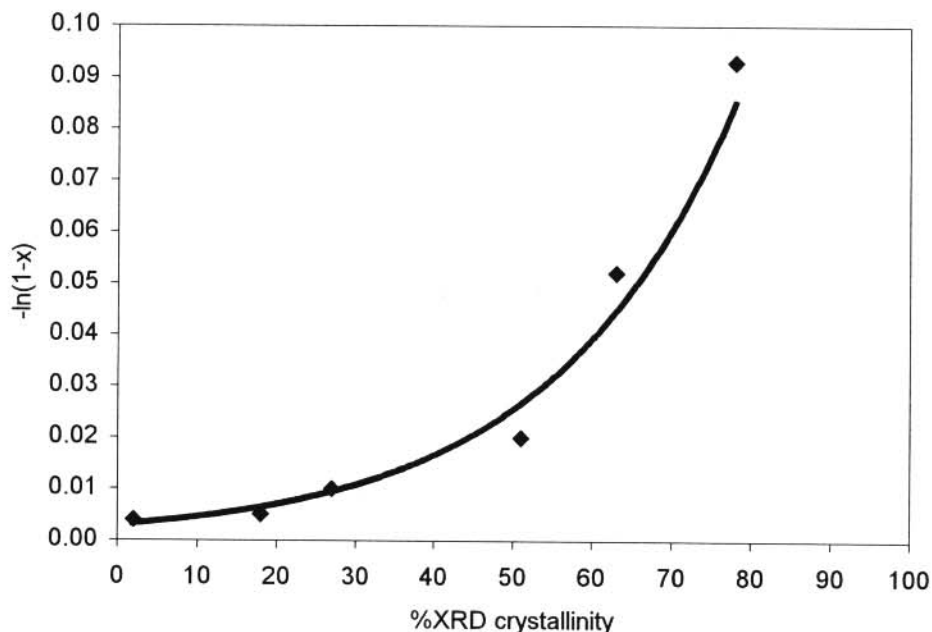
Figure 5.34 Plot of catalytic activity versus percentage XRD crystallinity for propane cracking (in the presence of the impurities ethane and butanes) at 500°C over H-ZSM-5-based materials synthesized with stirring in the Parr autoclave.

as function of percentage XRD cystallinity of the H-ZSM-5-based catalytic materials. There is an exponential increase in percentage conversion with increasing percentage XRD crystallinity from about 0.4% to 8.9% over the crystallinity range of 2% to 78% of the catalytic material. However, except for the value at the highest percentage conversion, i.e. 8.9%, the others could be excepted to be slightly higher since in those cases separation of the product propene from the propane peak was not achievable. To illustrate this, if the changes in mass% was combined for $C_3^=$ and C_3^- for the cracking over the 78% H-ZSM-5 (see Table 5.23), a conversion of 7.5% would be obtained instead of the 8.9%.

The analysis of the selectivities of the products formed is complex due to the fact that both the paraffins propane and *n*-butane present in the feed undergo catalytic conversion. The primary

products expected from propane cracking are equimolar amounts of methane and ethene as well as propene (see Section 3.11) as a result of protolytic monomolecular cracking according to Figure 3.35.

$$C_3H_8 \begin{cases} \text{(a)} \longrightarrow CH_4 + C_2H_4 \\ \\ \text{(b)} \longrightarrow H_2 + C_3H_6 \end{cases}$$
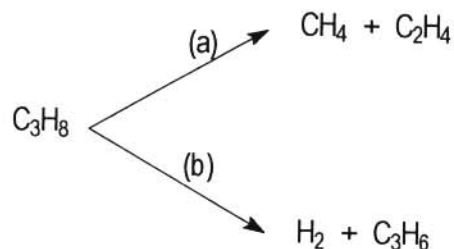
Figure 3.35 Monomolecular cracking of propane and products of the reaction.

Kwak *et al.* (1994) observed that in the catalytic cracking of propane at 530°C over H-ZSM-5 catalysts, at different contact times, and by extrapolation of the selectivities to zero conversion, the cracking of the propane occurs 63% by path (a) and 37% by path (b) in Figure 3.35. The selectivity towards methane increased at higher conversions relative to those of ethene and propene. Ethane, butene and aromatics were detected as minor secondary products at higher conversions.

On the other hand, monomolecular *n*-butane cracking is expected to occur as is indicated in Figure 3.36 (Krannilla *et al.* 1992; Kotrel *et al.*, 2000).

$$n\text{-}C_4H_{10} \begin{cases} \text{(a)} \longrightarrow CH_4 + C_3H_6 \\ \text{(b)} \longrightarrow C_2H_6 + C_2H_4 \\ \text{(c)} \longrightarrow H_2 + C_4H_8 \end{cases}$$
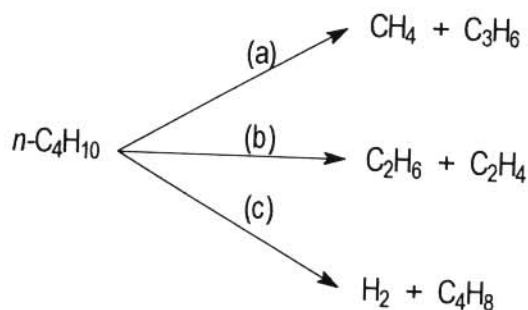
Figure 3.36 Monomolecular cracking of *n*-butane and products of the reaction.

Krannilla *et al.* (1992) reported product selectivities at zero conversion of 36% by path (a), 34% by path (b) and 30% by path (c) in Figure 3.36 for conversion over H-ZSM-5 at 496°C. The main secondary product obtained was propane.

Based on the results given in the above two reports by Krannilla *et al.* (1992) and Kwak *et al.* (1994), one should therefore expect as products from the cracking of the feed at low conversions, in addition to hydrogen, almost equimolar amounts of methane and ethene, and a smaller amount of propene, due to the conversion of both propane and *n*-butane, and minor amounts of ethane and butene which result from *n*-butane cracking. However, from these products, the formation of only the species up to ethane could be definitely quantified from our GC results and their mole percentages are given in Table 5.25, together with the $C_1/C_2^=$ ratios. The relative mole percentages of these products are plotted as a function of percentage conversion in Figure 5.37.

Table 5.25 Product spectrum (in mole%, up to ethane only) and the $C_1/C_2^=$ molar ratios obtained from the cracking of propane (which contains ethane and butanes as impurities) at 500°C as function of XRD crystallinity over H-ZSM-5-based materials synthesized with stirring in the Parr autoclave

%XRD crystallinity	%Conversion	C_1	$C_2^=$	C_2^-	$C_1/C_2^=$
2	0.40	12.02	17.88	70.10	0.67
18	0.54	41.96	43.95	14.09	0.95
27	1.02	36.01	35.49	28.50	1.01
51	1.99	50.17	44.22	5.62	1.13
63	5.11	51.05	36.27	10.80	1.41
78	8.86	54.35	29.36	16.28	1.85
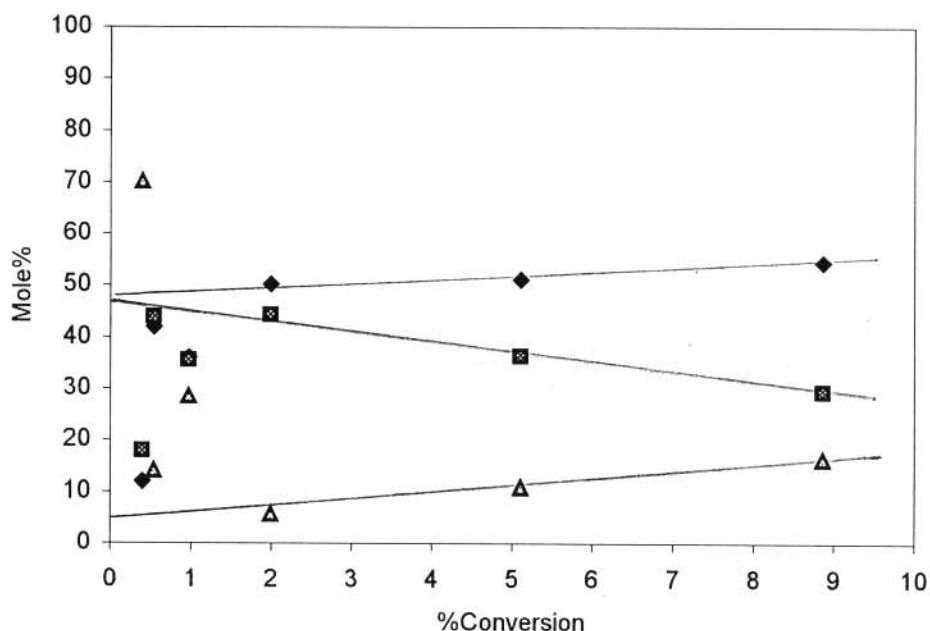
Figure 5.37 Plot of mole% of C_1 ($\blacklozenge$), $C_2^=$ ($\blacksquare$) and C_2^- ($\triangle$) versus percentage conversion for propane cracking (in the presence of the impurities ethane and butanes) at 500°C over H-ZSM-5-based materials synthesized with stirring in the Parr autoclave.

The product spectrum for cracking over the 2% H-ZSM-5 catalytic material seems not to be inline with the rest of the results, and the mole% of C_2^- formed at low conversions (up to 1%) is unrealistic high. These deviations are probably due to accuracy problems with the determination of the change in C_2^- concentrations within the experimental work. Ethane at a mass% of 2.204 is present in the feed and the uncertainty is magnified when small changes in this concentration are reported. Nevertheless, these results seem to be in accordance to what is expected. The formation of methane and ethane increased with an increase in conversion while that of ethene decreased. Extrapolation to zero conversion (see Figure 5.37), where only the formation of the primary products are expected (Krannilla *et al.*, 1992), give mole% values of 48.38 for C_1, 47.58 for $C_2^=$ and 5.65 for C_2^-. This results in a $C_1/C_2^=$ ratio of 1.02 as expected for monomolecular cracking and remains about constant for conversions up to 2% and the hydrogen transfer to

produce ethane from ethene at higher conversions, which is in accordance with the Haag-Dessau mechanism of protolytic cracking of alkanes (Kotrel *et al.*, 2000). The small amount of ethane at zero conversion, originates from the monomolecular cracking of *n*-butane.

At higher conversion and hence higher alkene partial pressure, the alkene interconversion reaction produces increasing equilibrium quantities of higher alkenes which can undergo acid-catalyzed cyclization and hydride transfer reactions to form aromatics (Kwak *et al.*, 1994). Hence the formation of C_5's and C_{6+} at higher conversions (see Table 5.23).

5.4.2.2 *H-ZSM-5-based materials synthesized without stirring in the Parr autoclave*

Appendix B contains the chromatograms for propane cracking at 500°C over H-ZSM-5-based catalytic materials synthesized without stirring in the Parr autoclave. The XRD crystallinities of these samples range from 5% to 80% and were synthesized at temperatures ranged from 100°C to 160°C. The changes in mass percent of reactants and products formed are given in Table 5.26. Again there is an exponential increase in the percentage conversion and activity with increasing percentage crystallinity of these samples (see Table 5.27). These results are also shown in Figure 5.38 and Figure 5.39 as percentage conversion and activity respectively as function of percentage XRD cystallinity of the H-ZSM-5-based catalytic materials investigated. There is an increase in percentage conversion with increasing percentage XRD crystallinity from 0.4% to 5.3% over the crystallinity range of catalytic materials investigated. The results also show that for synthesis without stirring, these H-ZSM-5 zeolitic materials give lower conversions than the samples prepared with stirring, especially at higher crystallinities. This is caused by the bigger crystallite sizes of the samples prepared without stirring (compare the activities in Table 5.24 and Table 5.27).

Table 5.26 Changes (in mass%) of reactants and products formed during the cracking of propane (which contains ethane and butanes as impurities) at 500°C over H-ZSM-5-based materials of different levels of crystallinity synthesized without stirring in the Parr autoclave

%XRD crystallinity	C_1	$C_2^=$	C_2^-	C_3's[a]	C_4's	C_5's	C_{6+}	Products formed	Feed components reacted
5	0.03	0.06	0.06	0.23	-0.38	0.00	0.00	0.38	0.38
13	0.13	0.24	0.00	0.10	-0.47	0.00	0.00	0.47	0.47
39	0.44	0.68	0.11	-0.07	-1.17	0.00	0.00	1.24	1.24
63	1.14	1.48	0.44	-2.74	-0.75	0.18	0.25	3.48	3.48
80	0.96	1.37	0.46	-3.91	-1.29	0.14	2.26	5.19	5.19

[a]$C_3^=$ could not be separated from C_3^- peaks.

Table 5.27 Percentage conversion and catalytic activity for propane cracking (with impurities) at 500°C over H-ZSM-5-based materials of different levels of crystallinity synthesized without stirring in the Parr autoclave

%XRD crystallinity	Particle sizes (μm)	%Conversion	Activity
5	---[a]	0.39	0.004
13	3.5	0.48	0.005
39	4.0	1.26	0.013
63	---[a]	3.56	0.036
80	4.0	5.31	0.055

[a]SEM micrograph not available.
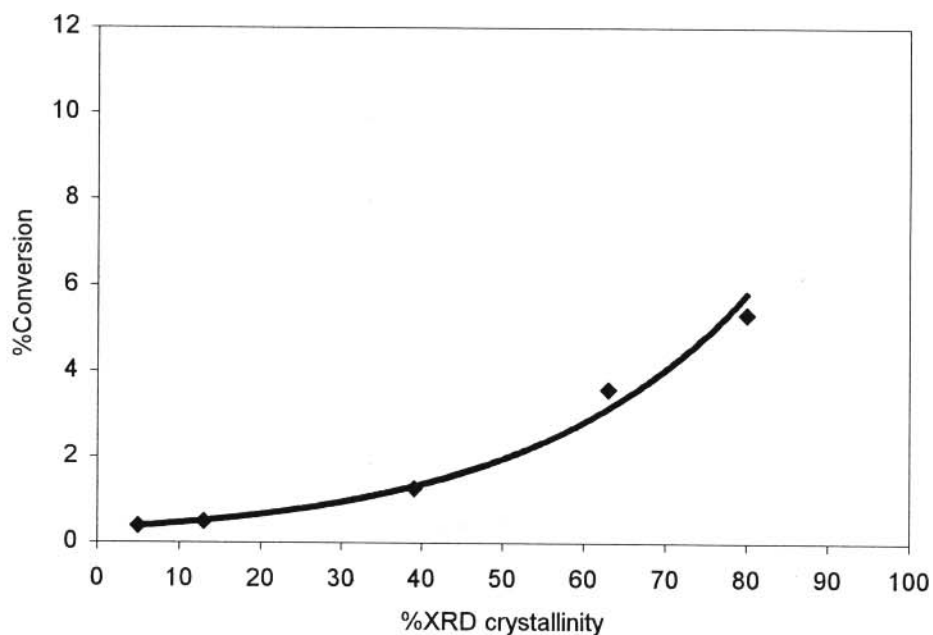
Figure 5.38 Plot of percentage conversion versus percentage XRD crystallinity for propane cracking (in the presence of the impurities ethane and butanes) at 500°C over H-ZSM-5-based materials synthesized without stirring in the Parr autoclave.
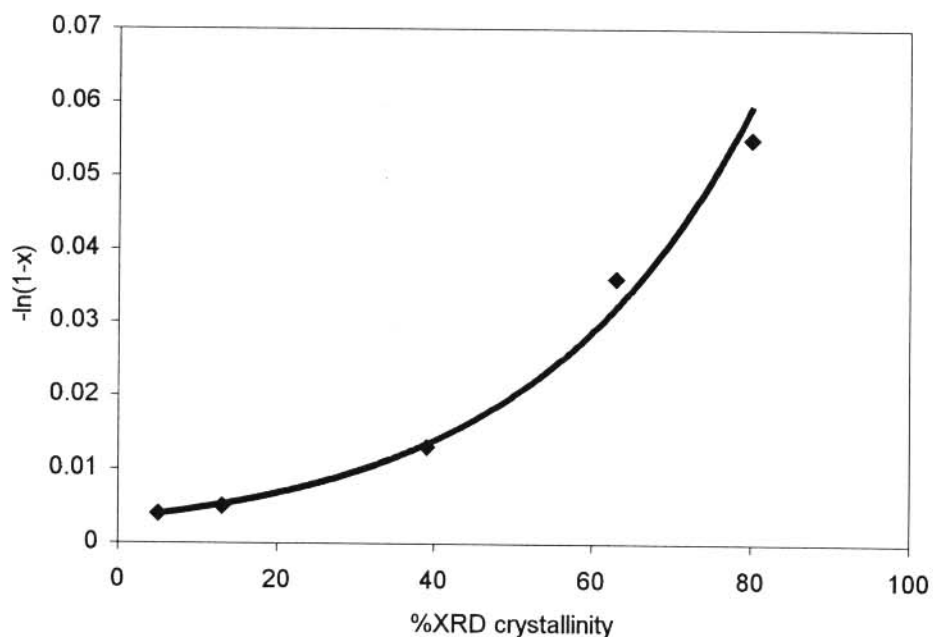
Figure 5.39 Plot of catalytic activity versus percentage XRD crystallinity for propane cracking (which contains the impurities ethane and butanes) at 500°C over H-ZSM-5-based materials synthesized without stirring in the Parr autoclave.

Table 5.28 gives the product spectrum up to ethane and the $C_1/C_2^=$ product ratio. The selectivities to these products are graphically presented as function of percentage conversion in Figure 5.40. Extrapolation to zero conversion of these plots results in mole% values of 48.00, for C_1, 47.20 for $C_2^=$ and 4.40 for C_2^- for monomolecular cracking. For the cracking of propane over the samples synthesized with stirring, the $C_1/C_2^=$ ratio calculated for zero conversion is 1.02, which is supported by the protolytic monomolecular cracking mechanism. In this case, for the ZSM-5-based materials synthesized without stirring, monomolecular cracking was only obtained for conversions up to 1.3% (see Table 5.28). A maximum of 1.35 in the $C_1/C_2^=$ ratio was obtained for the 63% crystalline sample after which a decline in this ratio was evident for the 80% crystallinity sample.

Table 5.28 Product spectrum (in mole%, up to ethane only) and the $C_1/C_2^=$ molar ratios obtained from the cracking of propane (in the presence of the impurities ethane and butanes) at 500°C as function of XRD crystallinity over H-ZSM-5-based materials synthesized without stirring in the Parr autoclave

%XRD crystallinity	%Conversion	C_1	$C_2^=$	C_2^-	$C_1/C_2^=$
5	0.39	32.10	33.66	34.24	0.95
13	0.48	48.63	51.37	0.00	0.95
39	1.26	49.25	43.91	6.84	1.12
63	3.56	51.33	38.10	10.57	1.35
80	5.31	48.28	39.33	12.38	1.23
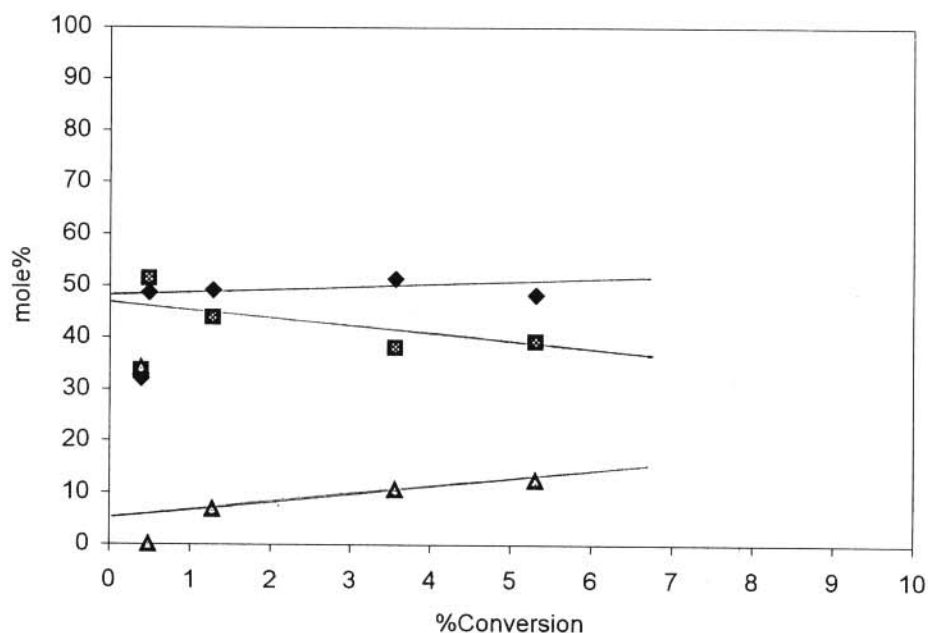
Figure 5.40 Plot of mole% of C_1 (♦), $C_2^=$ (▣) and C_2^- (▲) versus percentage conversion for propane cracking (with impurities) at 500°C over H-ZSM-5-based materials synthesized without stirring in the Parr autoclave.

5.4.2.3 *Comparison of results*

Figure 5.41 gives the plots of catalytic activity for propane cracking (in the presence of the impurities ethane and butanes) versus percentage XRD crystallinity for the samples synthesized with and without stirring in the Parr autoclave. At lower percentage XRD crystallinity (up to about 20%), their activities are almost the same. Above this percentage XRD crystallinity, the activity of the samples prepared without stirring is lower. It can be stated that samples of almost similar percentage XRD crystallinities synthesized in different ways do not necessarily have the same catalytic activities, due to differences in the crystallite sizes (and/or differences in the incorporation of Al in the MFI lattice)
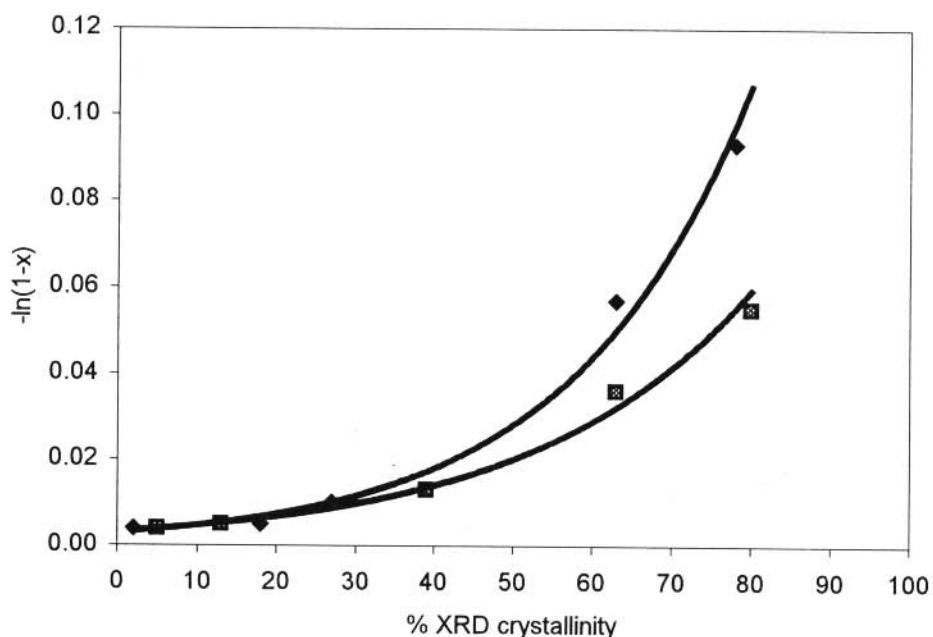
Figure 5.41 Plot of catalytic activity versus percentage XRD crystallinity for propane cracking (with ethane and butanes as impurities) at 500°C over H-ZSM-5-based materials synthesized with stirring (♦) and without stirring (▣) in the Parr autoclave.

5.4.3 *n*-Hexane cracking

In this investigation, all the H-ZSM-5-based materials shown in Table 4.2 were tested as catalysts for *n*-hexane cracking. For the catalytic reactions, 0.1 g of a catalyst was diluted with 3.7 g of quartz and the reaction temperature was 500°C.

5.4.3.1 *H-ZSM-5-based materials synthesized with stirring at 100 rpm in the Parr autoclave*

The gas chromatograms of the product stream obtained from *n*-hexane cracking over H-ZSM-5-based materials of different percentage XRD crystallinities synthesized with stirring at 100 rpm in the Parr autoclave are shown in Appendix C. The catalytic reaction was carried out over the 2% to 78% crystallinity ZSM-5-based samples synthesized from 90°C to 180°C.

Some of the data obtained in this set of experiments are shown in Table 5.29, Figure 5.42 and Figure 5.43. It can be observed that the percentage conversion and catalytic activity increase exponentially with increasing percentage XRD crystallinity for this set of samples. As expected, these percentage conversions are higher than those for the cracking of the shorter chain propane over the same series of catalytic materials (see Section 5.4.2.1). Furthermore, one has to keep in mind that the conversion is calculated from the decrease in mass% (i.e. area%) of the n-hexane chromatographic peak (see Section 4.4.3.3), and due to its relative excess in comparison to the other C_6 products, like the hexenes (see Section 3.11), separation could not be achieved. Due to this, the real conversion and activity could even be expected to be slightly higher than the values calculated. The relatively lower catalytic activity of the H-ZSM-5-based samples with XRD crystallinities of up to 30% is in agreement with the results obtained by Nicolaides et al. (2002a), who showed that the number of strong acid sites for the NAS samples (novel aluminosilicates) at these lower levels of crystallinities is comparatively low, which is consistent with a low framework aluminium content in such samples (Jacobs and Martens, 1987).

Table 5.29 Percentage conversion and catalytic activity for the cracking of n-hexane at 500°C over H-ZSM-5-based materials of different percentage XRD crystallinities synthesized with stirring in the Parr autoclave

Batch no.	Synthesis temp.(°C)	%XRD crystallinity	Particle size of spheroids (μm)	%Conversion	Activity
493	90	2	0	0.21	0.002
510	110	18	----[a]	4.44	0.05
511	120	27	----[a]	9.17	0.10
513	140	51	1.5	25.25	0.29
519	160	63	1.2	66.04	1.08
520	180	78	2.1	82.47	1.74

[a]SEM micrograph not available.
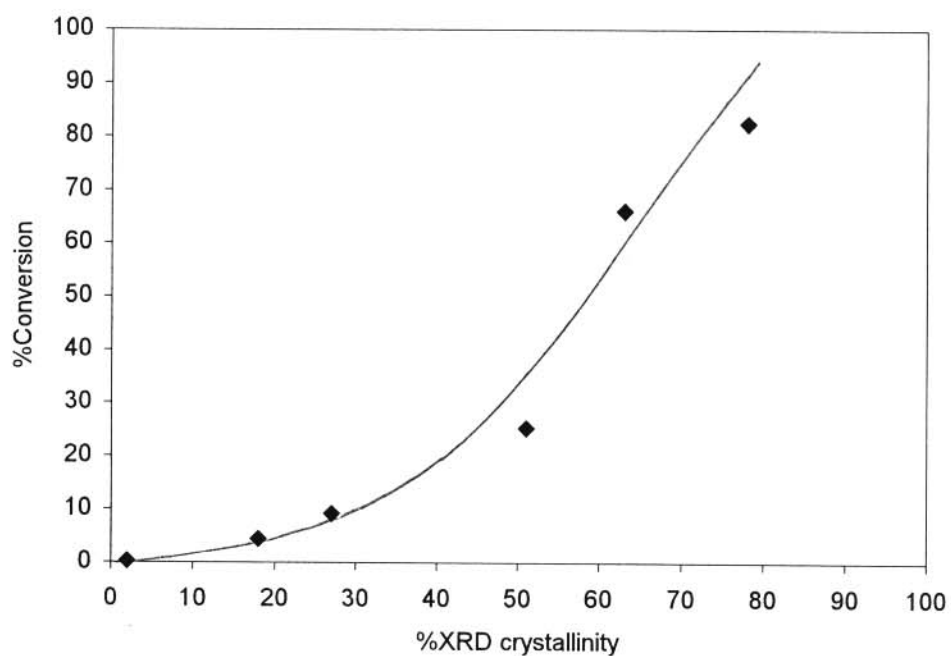
Figure 5.42 Plot of percentage *n*-hexane cracking at 500°C versus percentage XRD crystallinity for the H-ZSM-5-based catalysts synthesized with stirring in the Parr autoclave.
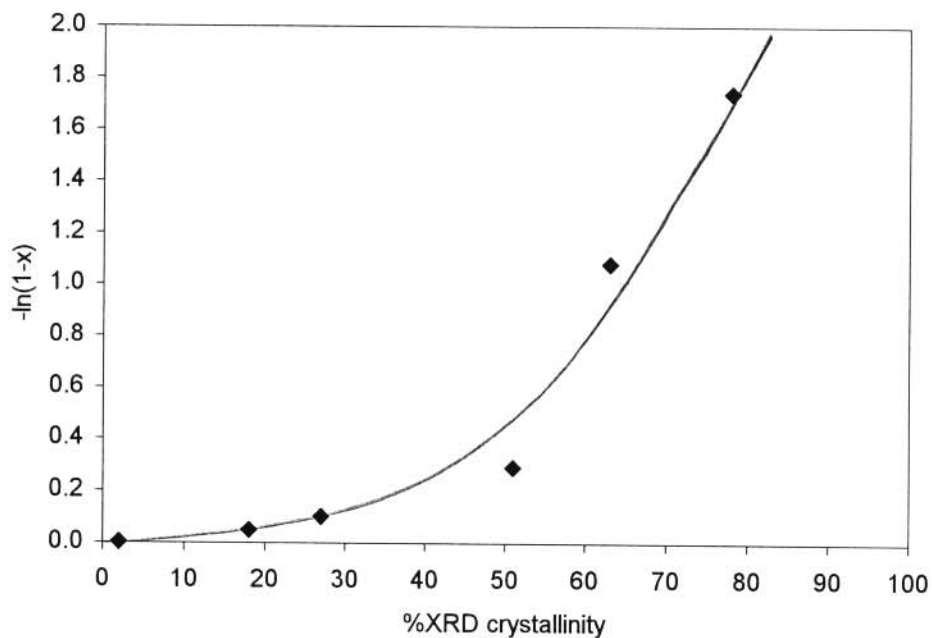
Figure 5.43 Plot of catalytic activity for *n*-hexane conversion at 500°C versus percentage XRD crystallinity for the H-ZSM-5-based catalysts synthesized with stirring in the Parr autoclave.

The percentage selectivities (in mass%) to the different products (including aromatization products, C_{6+}) arising from n-hexane cracking using these catalysts are given in Table 5.30. In Table 5.31, the product spectrum in moles/100 moles of n-hexane converted (up to C_5's), and the C_2^-/C_1 and C_3^-/C_1 ratios, are given. To calculate the moles of C_4's and C_5's formed, the average molar mass of the alkanes and alkenes were used. The formation of the alkanes that could be separated by the GC column (up to C_3^-), and ethene, are plotted as a function of percentage conversion in Figure 5.44.

Table 5.30 Percentage selectivity (in mass%) to products obtained from n-hexane cracking over the different H-ZSM-5-based catalysts synthesized with stirring in the Parr autoclave

%Crystallinity	%Conversion	C_1	$C_2^=$	C_2^-	$C_3^=$	C_3^-	C_4's	C_5's	C_{6+}
18	4.44	1.72	6.02	6.09	29.48	7.77	38.28	2.60	8.04
27	9.17	1.19	6.77	7.34	36.11	8.69	28.08	2.79	8.97
51	25.25	1.32	9.41	8.63	29.87	17.36	25.71	3.08	4.41
63	66.04	1.08	10.93	6.53	16.77	22.76	23.69	5.02	13.23
78	82.47	1.23	11.48	6.69	14.40	20.79	20.55	5.51	20.35

Table 5.31 Product spectrum (in moles/100 moles converted, up to the C_5's), and C_2^-/C_1 and C_3^-/C_1 molar ratios obtained from the cracking of n-hexane at 500°C over H-ZSM-5-based materials of different percentage XRD crystallinities synthesized with stirring in the Parr autoclave

%Crystalinity	%Conversion	C_1	$C_2^=$	C_2^-	$C_3^=$	C_3^-	C_4's	C_5's	C_2^-/C_1	C_3^-/C_1
18	4.44	9.24	18.49	17.45	60.37	15.18	57.76	3.15	1.88	1.64
27	9.17	6.39	20.80	21.04	73.95	16.98	42.37	3.38	3.29	2.66
51	25.25	7.09	28.91	24.73	61.17	33.93	38.79	3.73	3.49	4.79
63	66.04	5.80	33.58	18.71	34.34	44.48	35.74	6.08	3.23	7.67
78	82.47	6.61	35.26	19.13	29.49	40.63	31.01	6.67	2.90	6.15
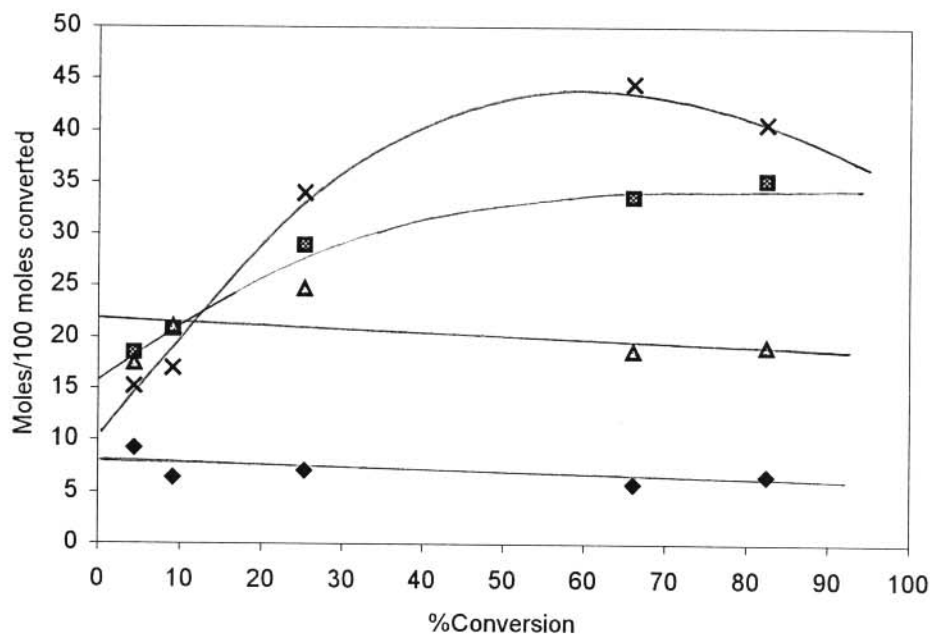
Figure 5.44 Product selectivities (moles/100 moles converted) of C_1 (♦), $C_2^=$ (▣), C_2^- (▲) and C_3^- (✗) obtained from *n*-hexane cracking over H-ZSM-5-based samples synthesized with stirring in the Parr autoclave .

The formation of methane and ethane decreases slightly with an increase in conversion due to the higher crystallinity of the zeolite-based catalysts. Both are products formed by the monomolecular cracking mechanism (see Section 3.11), while ethene and propane are, amongst others, formed by both the monomolecular and bimolecular (β-scission) cracking mechanisms. The increase of the latter products at higher conversions reflects an increase in the continuation by β-scission to the product spectrum.

In an investigation on the cracking of alkanes, Haag and Dessau (1984) showed that high temperatures, low partial pressures of the alkanes and low conversion favour monomolecular cracking above bimolecular cracking. Their results on 3-methylpentane and *n*-hexane, and the

work by Krannilla *et al.* (1992) on the cracking of *n*-butane, showed that in the limit approaching zero conversion, only the primary products of the monomolecular mechanism, proceeding through the pentacoordinated carbonium ion, were formed. The extrapolated results to zero conversion in this work (see Figure 5.44) give moles/100 moles *n*-hexane converted values of 8.17 for C_1, 14.94 for $C_2^=$, 22.31 for C_2^- and 8.76 for C_5^-. This results in a C_2^-/C_1 ratio of 2.73 for monomolecular cracking of *n*-hexane over H-ZSM-5 catalysts which correlates well with the ratio of 2.75 obtained by Haag and Dessau (1984) under their experimental conditions. Protonation of *n*-hexane occurs at either the two position or the three position (see Figure 3.8), of which the latter will be the more stable due to the inductive effect. The C_2^-/C_1 ratio of ~2.7 reflects this higher stability in that more ethane than methane were formed. This ratio remains almost constant at higher conversions while the C_3^-/C_1 ratio increases with increase in conversion due to the additional propane formed through β-scission.

Furthermore, for monomolecular cracking, one should have expected that the amount of C_2^- for-med should be almost the same as $C_4^=$ formed and that of the moles of $C_2^=$ formed be equal to the moles of C_4^- formed. Therefore, the C_4's formed should be almost equal to the sum of C_2^- and $C_2^=$. Considering the possibility of large experimental errors at low conversions (e.g. at 4.44%), these values compare well and at 9.17% conversion (see Table 5.31) they could be considered as equal, i.e. 41.84 and 42.37 moles formed per 100 moles of *n*-hexane converted. At higher con-versions the differences increase due to the contribution of the classical bimolecular mechanism.

5.4.3.2 *H-ZSM-5-based materials synthesized without stirring in the Parr autoclave*

The chromatograms of the product stream obtained for *n*-hexane cracking over the samples synthesized without stirring in the Parr autoclave are shown in Appendix D for *n*-hexane

cracking over 5% to 80% crystallinity ZSM-5-based samples synthesized at 100°C to 160°C. There is an increase in percentage conversion with increasing percentage XRD crystallinity up to 63%. However, the percentage conversion and activity of the 80% crystallinity H-ZSM-5 zeolite is considerably lower (see Table 5.32, Figure 5.45 and Figure 5.46). The analysis and interpretation of the data are given below.

Table 5.32 *n*-Hexane cracking at 500°C over H-ZSM-5 zeolite-based samples of different levels of percentage XRD crystallinity synthesized without stirring in the Parr autoclave

Batch no.	Synthesis temp.(°C)	%XRD crystallinity	Particle size of the spheroids (μm)	%Conversion	Activity
242	100	5	---[a]	1.80	0.02
244	110	13	3.5	4.50	0.05
71	120	39	4.0	25.50	0.29
250	140	63	---[a]	55.60	0.81
258	160	80	4.0	34.70	0.43

[a]SEM micrograph not available.
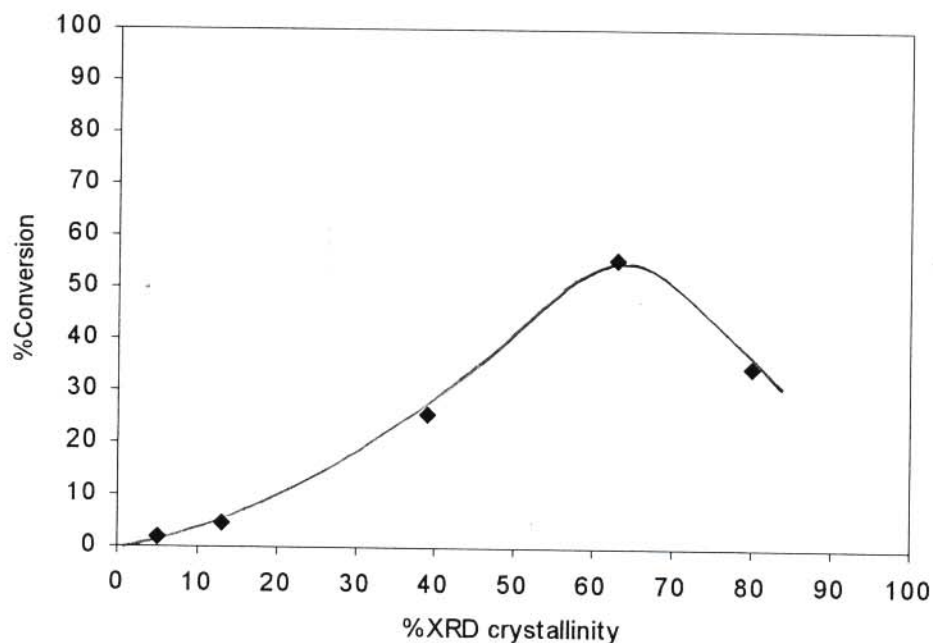
Figure 5.45 Plot of percentage *n*-hexane conversion at 500°C versus percentage XRD crystallinity for the H-ZSM-5-based catalysts synthesized without stirring in the Parr autoclave.
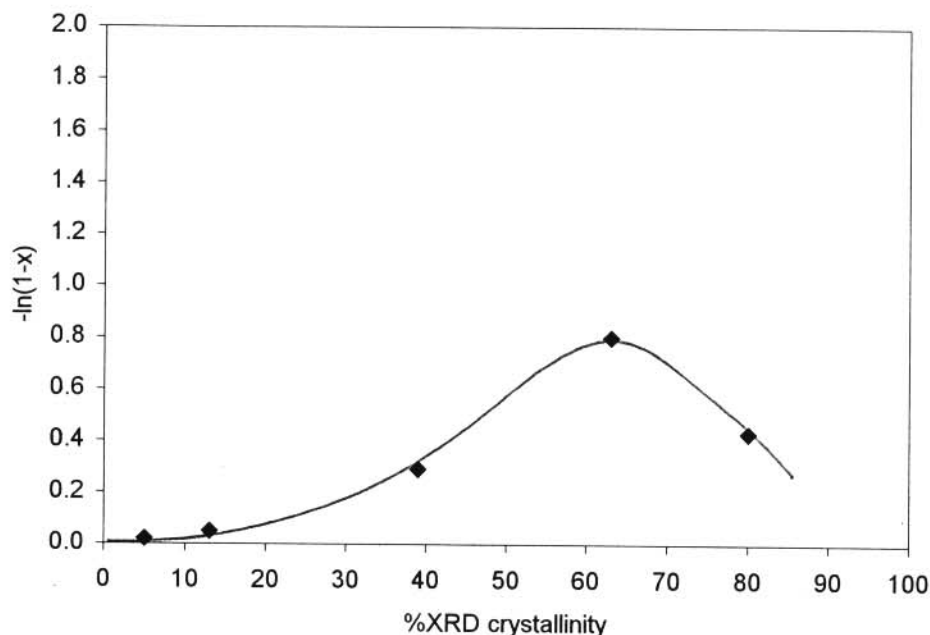
Figure 5.46 Plot of catalytic activity for *n*-hexane cracking at 500°C versus percentage XRD crystallinity for the H-ZSM-5-based catalysts synthesized without stirring in the Parr autoclave.

This decrease in percentage conversion and catalytic activity at high percentage XRD crystallinity correlates with the formation of larger crystallites at the higher temperatures, hence longer pore lengths. SEM micrographs of the H-ZSM-5-based materials prepared according to the different recipes investigated in this project indicated that the crystallite sizes increase with synthesis at higher temperatures, and that larger crystallites are formed at lower temperatures (and lower percentage XRD crystallinity) for synthesis without stirring than for synthesis with stirring. Using the Aerosil 200 method, individual crystallites within spheroids were observed in the samples synthesized at 160°C without stirring, while for synthesis with stirring, crystallites could only be identified at 180°C (see Section 5.2). On average the sizes of the spheroids formed also increase with increasing temperature and are bigger for the synthesis without stirring than for synthesis with stirring. For example, comparing the spheroid sizes of the sample synthesized at 160°C without stirring, and those prepared with stirring, the former are bigger (~4.0 μm) than

those synthesized with stirring (1.2 µm) (compare Table 5.2 and Table 5.8). The samples with larger crystallite sizes (especially crystals in the spheroids), result in lower activities than with samples of smaller crystallites due to higher diffusional limitations occurring within the larger crystallites.

Figure 5.47 shows the plots of catalytic activity versus percentage XRD crystallinity for both the samples synthesized with and without stirring in the Parr autoclave. These show that at low percentage XRD crystallinities, up to about 50%, the samples prepared without stirring are slightly more active than those prepared with stirring. At higher percentage crystallinity, however, the samples synthesized with stirring are more active than the ones prepared without stirring. Thus the spheroidal ZSM-5 samples results in higher conversion rates than the crystallite forms of ZSM-5.

Figure 5.47 Plots of catalytic activity of *n*-hexane cracking versus percentage XRD crystallinity for the H-ZSM-5-based catalyst samples synthesized with stirring (♦) and without stirring (▣) in the Parr autoclave.

These results again emphasize that not only percentage XRD crystallinity is important in determining the catalytic activity of a zeolite, but as an extension of that parameter, it is also strongly dependent on the crystallite size.

Table 5.33 shows the percentage selectivities of n-hexane cracking products over this series of catalytic materials. In Table 5.34, the product spectrum in moles/100 moles n-hexane converted (up to C_5's) and the C_2^-/C_1 and C_3^-/C_1 ratios are tabulated. The alkanes that could be separated by the GC column used (up to C_3^-), and ethene, are also plotted as a function of percentage conversion for this series of catalysts as seen in Figure 5.48. As it was observed with the materials synthesized with stirring, the formation of the smaller alkanes, methane and ethane, decreases slightly with an increase of conversion over the higher crystallinity zeolite-based catalysts while the production of ethene and propane increases. This again emphasizes that at low conversion of n-hexane over H-ZSM-5-based catalysts, mainly the protolytic mono-molecular cracking mechanism occurs with an increase in the classical bimolecular hydride transfer mechanism at higher conversions as was found by Haag and Dessau (1984).

Table 5.33 Percentage selectivity (in mass%) of n-hexane cracking products over the different H-ZSM-5 zeolite-based catalysts synthesized without stirring in the Parr autoclave

%Crystallinity	% Conversion	C_1	$C_2^=$	C_2^-	$C_3^=$	C_3^-	C_4's	C_5's	C_{6+}
5	1.80	1.83	5.33	9.11	33.56	11.83	33.72	4.67	0.00
13	4.50	1.35	5.33	8.82	31.02	12.57	32.89	2.95	5.06
39	25.46	1.22	9.28	8.30	29.67	17.54	25.46	3.35	5.17
63	55.60	1.21	12.12	7.13	20.99	20.50	21.81	3.37	12.47
80	34.70	1.10	10.06	7.41	24.89	19.62	24.66	4.15	8.11

Table 5.34 Product spectrum (in moles/100 moles n-hexane converted, up to C_5's) and C_2^-/C_1 and C_3^-/C_1 molar ratios obtained from the cracking of n-hexane at $500^{\circ}C$ over H-ZSM-5-based materials of different levels of percentage XRD crystallinity synthesized without stirring in the Parr autoclave

%Crystallinity	% Conversion	C_1	$C_2^=$	C_2^-	$C_3^=$	C_3^-	C_4's	C_5's	C_2^-/C_1	C_3^-/C_1
5	1.80	9.83	16.37	26.11	68.73	23.12	50.89	5.66	2.66	2.35
13	4.50	7.25	16.37	25.28	63.53	24.57	49.62	3.57	3.49	3.38
39	25.46	6.55	28.51	23.79	60.76	34.28	38.41	4.06	3.63	5.23
65	55.60	6.50	37.23	20.43	42.99	40.06	32.90	4.08	3.14	6.16
80	34.70	5.91	30.87	21.24	50.97	38.34	37.21	5.02	3.59	6.49
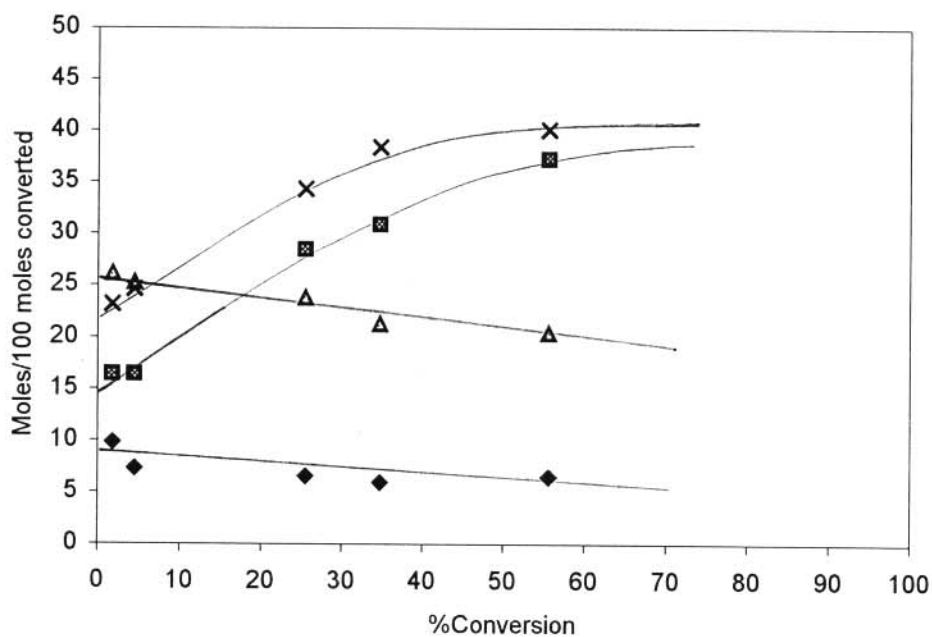
Figure 5.48 Product selectivities (moles/100 moles converted) of C_1 (♦), $C_2^=$ (◪), C_2^- (△) and C_3^- (✗) obtained from n-hexane cracking over H-ZSM-5-based samples synthesized without stirring in the Parr autoclave.

From Figure 5.48 the values extrapolated to zero conversion in moles/100 moles n-hexane converted are 8.76 for C_1, 14.34 for $C_2^=$, 26.10 for C_2^- and 21.91 for C_3^-. The ratio of C_2^-/C_1 at zero conversion is 2.98 which again correlate well with the ratio of 2.75 obtained by Haag and Dessau (1984) for monomolecular cracking of n-hexane with H-ZSM-5. The C_2^-/C_1 ratio remains almost constant at higher conversions while that of C_3^-/C_1 increases with increase in conversion due to the additional propane formed through β-scission.

5.4.3.3 *H-ZSM-5-based materials synthesized with stirring at 1 000 rpm in the in-house built autoclave*

The chromatograms for the cracking of n-hexane over H-ZSM-5-based samples earlier synthesized (Ramatsetse, 1998) with stirring at 1 000 rpm in the in-house built autoclave and having crystallinities of 5% to 65% are shown in Appendix E, i.e. using as catalysts H-ZSM-5-based samples synthesized at 100°C to 140°C. Again, the percentage conversion obtained and catalytic activity increase with increasing percentage XRD crystallinity (Table 5.35). However, most significantly, with this set of samples a linear correlation was observed with increasing percentage XRD crystallinity up to 65% (see Figure 5.49 and Figure 5.50). The linear correlation was not observed with either of the Parr results. This can be ascribed to the smaller crystallites and sizes involved.

Table 5.35 n-Hexane cracking at 500°C over H-ZSM-5-based materials of different percentage XRD crystallinities synthesized with stirring in the in-house built autoclave

Batch no.	Synthesis temp.(°C)	%XRD crystallinity	Particle size (μm)	%Conversion	Activity
11	100	5	1.7	5.37	0.06
43	105	33	2.0	22.26	0.25
29	120	54	2.9	37.65	0.47
18	140	65	2.3	40.46	0.52

Figure 5.49 Plot of percentage *n*-hexane cracking at 500°C versus percentage XRD crystallinity for the H-ZSM-5-based catalysts synthesized with stirring in the in-house built autoclave.
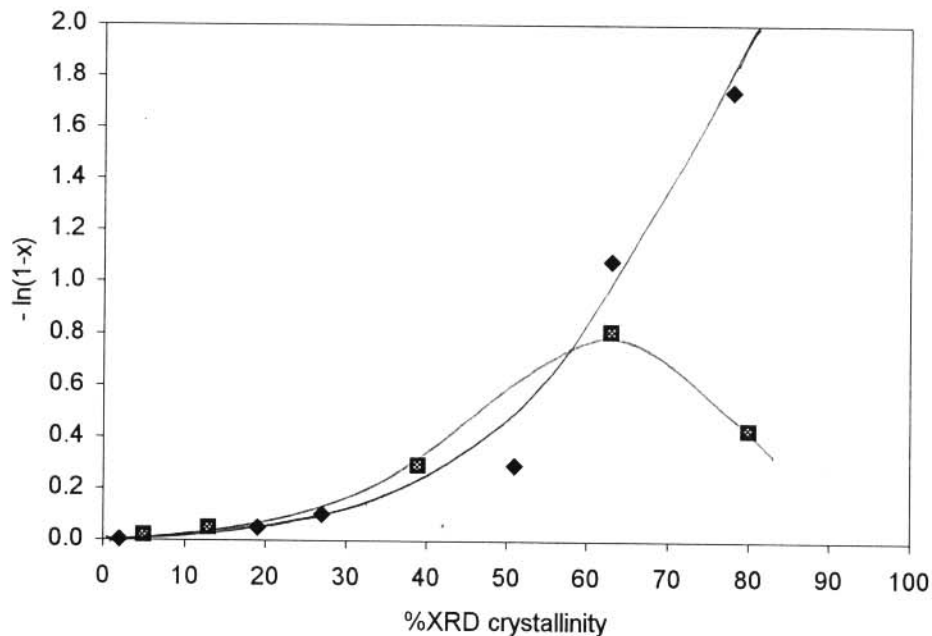

Figure 5.50 Plot of catalytic activity of *n*-hexane cracking at 500°C versus percentage XRD crystallinity for the H-ZSM-5-based catalysts synthesized with stirring in the in-house built autoclave.

The product selectivity of these samples are shown in Table 5.36. It can be noted that the amounts of C_6^+-compounds formed by the samples prepared without stirring (and hence higher crystallite sizes) is on average higher than with the samples synthesized with stirring in the Parr and in the in-house built autoclave. Thus, the larger the crystallite size, the higher the probability of the occurrence of the sequential reactions to give higher molecular weight products, apart from the primary cracking products.

Table 5.36 Percentage selectivity (mass%) of n-hexane cracking products formed over different H-ZSM-5-based catalysts synthesized with stirring in the in-house built autoclave

%Crysallinity	%Conversion	C_1	$C_2^=$	C_2^-	$C_3^=$	C_3^-	C_4's	C_5's	C_{6+}
5	5.37	1.95	5.97	11.41	34.67	14.16	30.00	1.54	0.00
33	22.26	1.71	8.28	10.25	36.05	16.47	23.31	1.99	1.93
54	37.65	1.59	11.40	8.56	35.59	15.77	18.38	0.98	7.74
65	40.46	1.46	11.07	9.35	31.94	18.87	19.87	4.79	4.66

In Table 5.37, the product spectrum in moles/100 moles converted (up to C_5's) and the C_2^-/C_1 and C_3^-/C_1 ratios are given. The paraffins that could be separated by the GC column (up to C_3^-), and ethene, are again plotted as a function of percentage conversion in Figure 5.51.

As was the case with the other two series of H-ZSM-5-based materials used as catalysts, the formation of methane and ethane decrease slightly while those of ethene and propane increase with an increase of conversion over the higher crystalline samples. Since the highest conversion obtained with this series of catalysts was around 40%, the flattening of the increase of the latter products observed above 40% conversion for the series of samples prepared in the Parr autoclave (see Figure 5.43 and Figure 5.48) was not detected.

Table 5.37 Product spectrum (in moles/100 moles converted, up to C_5's) and C_2^-/C_1 and C_3^-/C_1 molar ratios obtained from the cracking of *n*-hexane at 500°C over H-ZSM-5-based materials of different percentage XRD crystallinity synthesized with stirring in the in-house built autoclave

%Crystal-linity	%Con-version	C_1	$C_2^=$	C_2^-	$C_3^=$	C_3^-	C_4's	C_5's	C_2^-/C_1	C_3^-/C_1
5	5.37	10.47	18.34	32.70	71.00	27.67	45.26	1.87	3.12	2.64
33	22.26	9.18	25.43	29.38	73.83	32.19	35.17	2.41	3.20	3.50
54	37.65	8.54	35.02	24.53	73.88	30.82	27.73	1.19	2.87	3.61
65	40.46	7.84	34.00	26.80	65.41	32.88	29.98	5.80	3.42	4.70
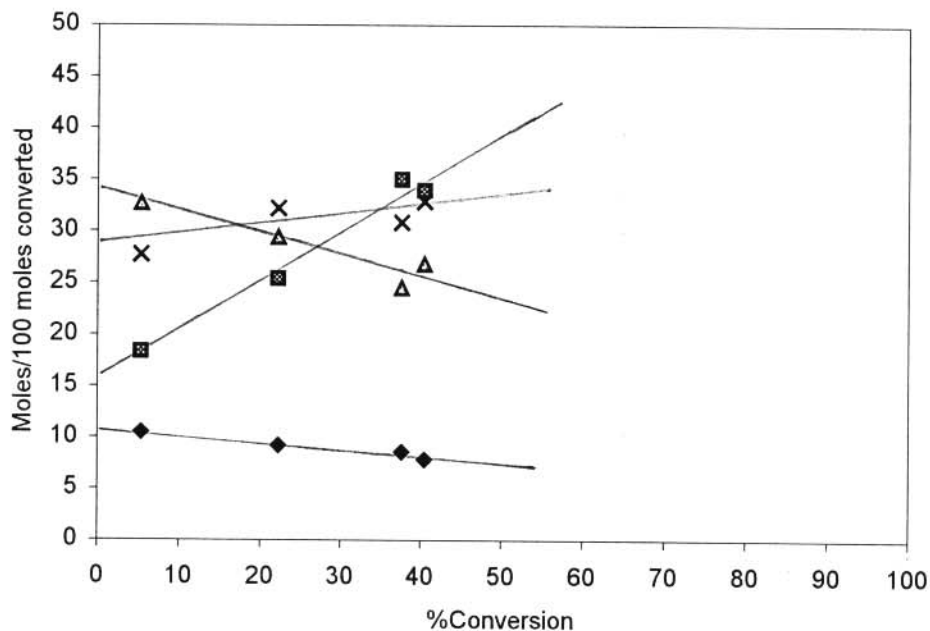
Figure 5.51 Product selectivities (moles/100 moles converted) of C_1 (♦), $C_2^=$ (▧), C_2^- (▲) and C_3^- (✕) for *n*-hexane cracking over ZSM-5-based samples synthesized with stirring in the in-house built autoclave.

As obtained from Figure 5.51, the conversion to C_1 was 16.76, to $C_2^=$ 15.49, to C_2^- 33.86 and to C_3^- 28.09 moles of each 100 moles of *n*-hexane converted, at the extrapolation to zero conversion in order to determine the formation of the primary products. The ratio of C_2^-/C_1

calculated from these values gives 3.15, which is slightly higher than the value of 2.75 obtained by Haag and Dessau (1984). Within experimental error, the C_2^-/C_1 ratio remains constant throughout, while those of C_3^-/C_1 increases from 2.67 at zero conversion to 4.70 at 40.46% conversion

5.4.3.4 *Comparison of results*

Figure 5.52 gives the plots of catalytic activity versus percentage XRD crystallinity for the samples synthesized with and without stirring in the Parr autoclave and with stirring in the in-house built autoclave. Comparing the activities of the samples synthesized with stirring in the Parr autoclave and the samples synthesized with stirring in the in-house built autoclave, one may conclude that the samples from the in-house built autoclave at low percentage XRD crystal-
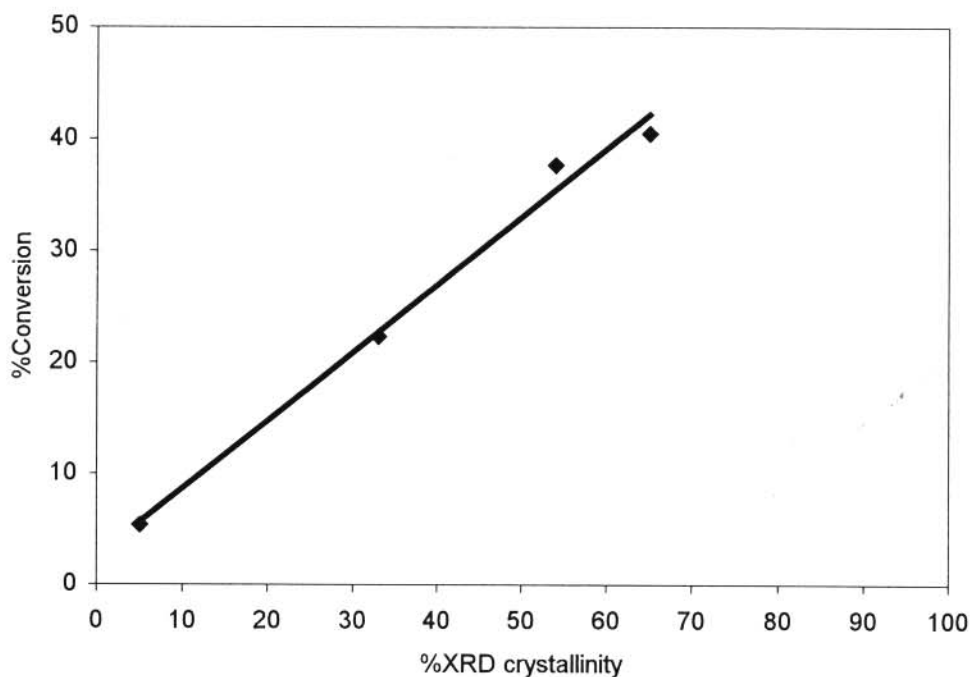

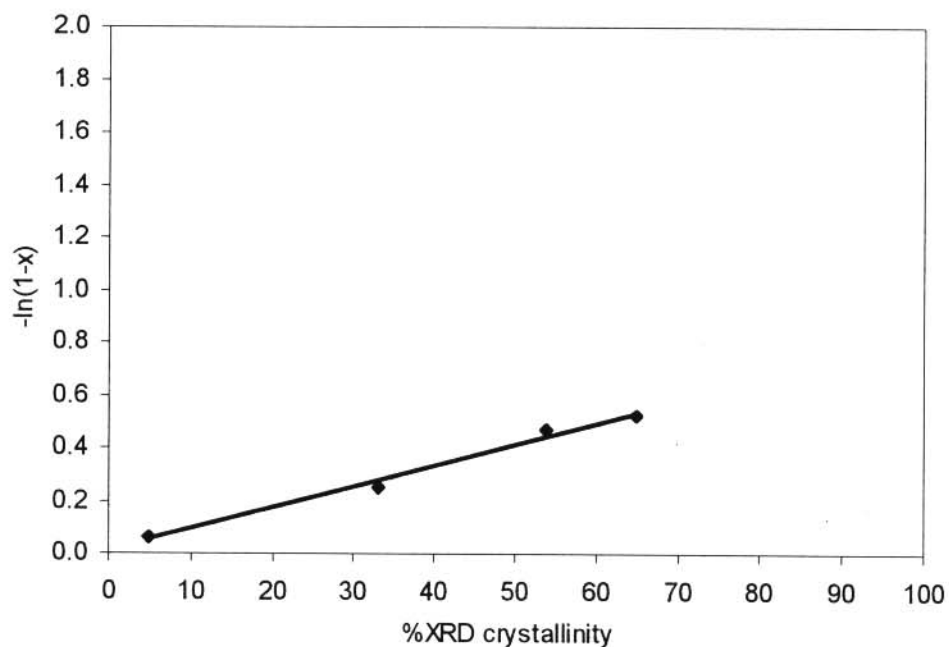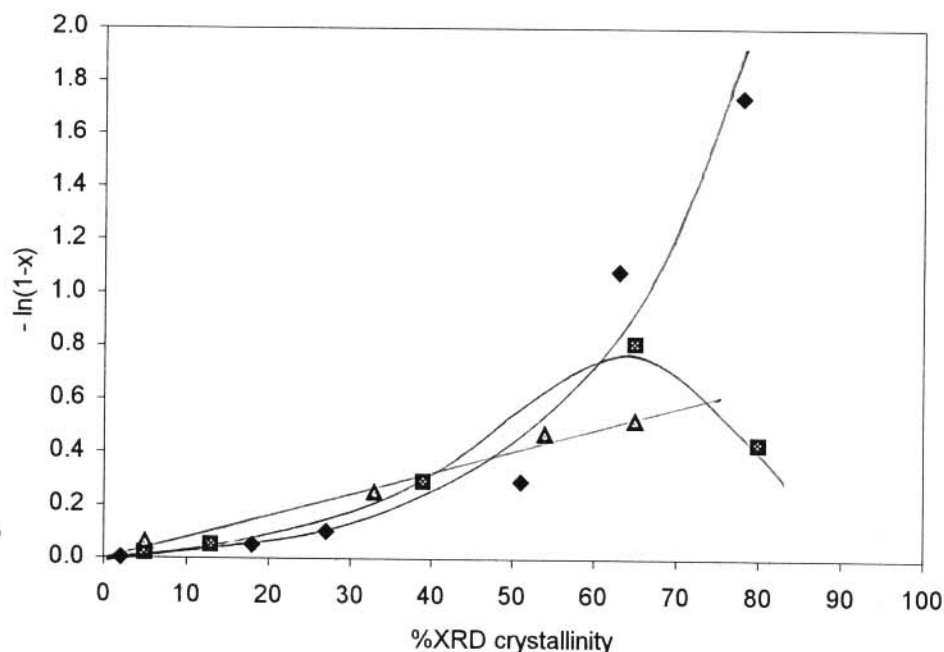**Figure 5.52** Plot of catalytic activity of *n*-hexane cracking versus percentage XRD crystallinity for the H-ZSM-5-based catalysts synthesized with stirring in the Parr autoclave (♦), without stirring in the Parr autoclave (▩) and with stirring in the in-house built autoclave (▲).

linities (up to 55%) are slightly more active than the samples from the Parr autoclave. At higher percentage XRD crystallinities, this is the other way round. The direct proportionality observed for the activities with percentage crystallinity of the samples synthesized with stirring in the in-house built autoclave is not observed for the samples synthesized with and without stirring in the Parr autoclave. At low percentage XRD crystallinity, the activity is high for the samples synthesized with stirring in the in-house built autoclave, followed by the unstirred samples from the Parr autoclave (although these coincide at some points), then the stirred samples from the Parr autoclave. At higher percentages XRD crystallinity (above about 75%), the activities of the stirred samples from the Parr autoclave is higher than the samples prepared without stirring.

Figure 5.53 gives the $C_2^=/C_3^=$ ratios as function of the percentage conversion for the three series of samples tested. According to the monomolecular cracking of n-hexane through the intermediate pentacoordinated carbonium ions (see Figure 3.8), equimolar amounts of $C_2^=$ and C_4^-, as well as of $C_3^=$ and C_3^- are expected. Since it was shown by Haag and Dessau (1984) that the ratio of C_4^-/C_3^- formed at zero conversion is 0.23, a similar ratio for $C_2^=/C_3^=$ can be expected. Extrapolation of the $C_2^=/C_3^=$ ratios to zero conversion indeed gives a ratio of 0.22 for all three series of samples, which again supports other results previously reported that at low conversions cracking occurs according to the protolytic monomolecular mechanism. Furthemore, interestingly, both series of samples synthesized in the Parr autoclave, with and without stirring, followed the same linear relationship, despite the decrease in conversion at higher crystallinity observed over the H-ZSM-5 catalysts synthesized without stirring (see Figure 5.53). These results indicate that the cracking mechanism correlates with the degree of conversion for these series of catalysts. Similarly, a linear relationship was also obtained for the samples obtained with stirring in the in-house built autoclave, although the gradient of this straight line is lower, indicating an increase the contribution from bimolecular conversion with these probably smaller crystallites.
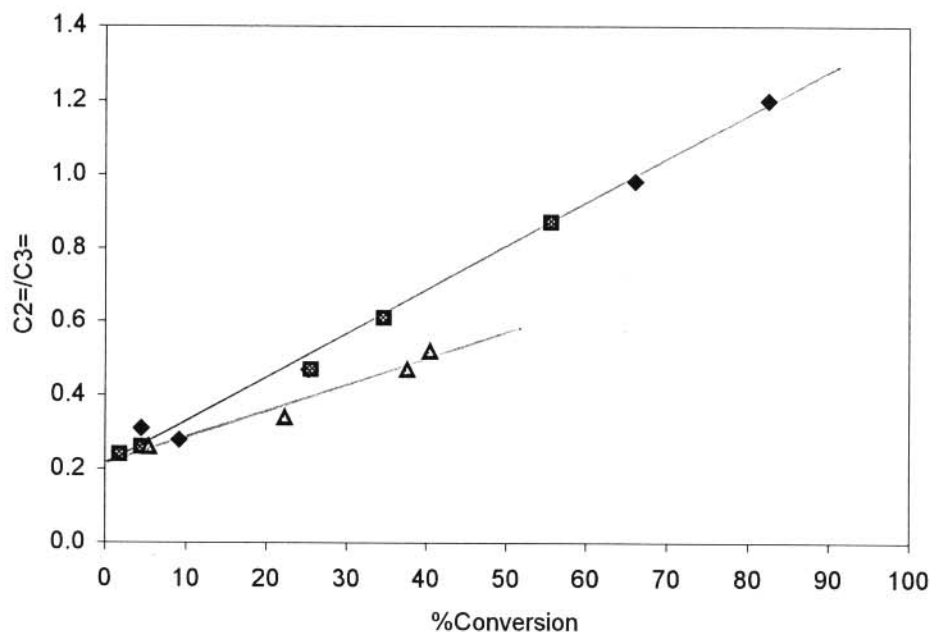
Figure 5.53 Plot of $C_2^=/C_3^=$ ratio of *n*-hexane cracking versus percentage conversion for the H-ZSM-5-based catalysts synthesized with stirring in the Parr autoclave ($\blacklozenge$), without stirring in the Parr autoclave ($\blacksquare$) and with stirring in the in-house built autoclave ($\triangle$).

5.5 CONCLUSIONS

It is observed that the percentage XRD crystallinities of the ZSM-5-based samples synthesized from the Parr and the in-house built autoclaves are the same if the unstirred mode of synthesis is used. When the stirred mode of synthesis is used, their percentage XRD crystallinities differ. Since the plot of the percentage XRD crystallinity as a function of synthesis temperature for the stirred samples synthesized from the Parr autoclave is the same as those of the unstirred samples from both autoclaves, it is suspected that the lower stirring rate (100 rpm) used in the Parr autoclave is the cause of this similarity.

We have also observed that although the percentage XRD crystallinities of the ZSM-5-based materials synthesized by using different methods may be the same, their morphologies differ. An example of this change in morphology is observed in the Aerosil 200 method (Section 5.2) and the Aerosil 200 and glycerol method (Section 5.3.3). In both cases tetrapropylammonium bromide was used as a template, but their morphologies differ totally as evident from Figure 5.3 and Figure 5.30, which are the micrographs of the samples synthesized without stirring in both recipes.

From the four methods used for ZSM-5 synthesis, the method in which silicic acid was used as a silica source, appear to give the most interesting results in terms of percentage XRD crystallinity. Under the unstirred mode of synthesis, this method gave the highest percentage XRD crystallinity in the shortest time (44 hours, even 20 hours could be used in this method). In addition, this is the only method that gave a linear plot of percentage XRD crystallinity versus synthesis temperature and is therefore the most controllable in terms of producing samples having different percentage XRD crystallinities.

Catalytic test reactions such as *n*-hexane cracking is one of the techniques used to supplement the XRD and SEM analyses of the samples. The catalytic test reaction indicated that the zeolite samples of almost the same percentage XRD crystallinities synthesized in different ways do not necessarily have the same catalytic properties. More importantly, this CTR indicated that the stirred samples, containing spheroids, are more active for *n*-hexane cracking than the highly crystalline samples obtained without stirring. Similar observations were made with propane as feed. With this lower alkane, however, the highly crystalline samples (80%) gave similar percentage conversion as their lower crystallinity analogues (65%) while for *n*-hexane cracking for samples prepared without stirring a lower percentage conversion was obtained for the 80%

crystalline sample than for the 63% sample. This could be ascribed to the lower diffusional limitation with propane due to its smaller chain length. This suggests, therefore, that n-hexane cracking is a more discriminating catalytic test reaction in detecting differences in ZSM-5 samples such as crystallite size and form.

A comparison of the morphology of the samples prepared with stirring in the Parr and the in-house built autoclaves according to the Aerosil 200 recipe emphasizes that stirring at a rate of 100 rpm in the Parr was not as effective than stirring with the magnetic stirrer bar at a setting of 1 000 rpm in the in-house built autoclave. For the samples synthesized with stirring in the Parr autoclave individual crystallites within the spheroidal structures were observed at hydrothemal treatment as low as 180°C while for the samples previously synthesized with stirring in the in-house build autoclave (Ramatsetse, 1998) no individual crystallites were observed up to the synthesis temperature of 190°C, which is the maximum temperature previously employed with this autoclave. Therefore, considering that the results indicated that stirring results in the formation of smaller crystallites at a specific temperature, and that crystals in the spheroids were observed at 160°C for synthesis without stirring in the Parr autoclave (see Figure 5.3(b)), the effect of stirring at 100 rpm in the Parr lies somewhere between that of without stirring and with stirring at a setting of 1 000 rpm with the in-house built autoclave.

CHAPTER SIX

RESULTS AND DISCUSSION ON THE SYNTHESIS OF THE FERRIERITE-BASED MATERIALS

6.1 INTRODUCTION

As in the case of ZSM-5, the aim here is also to investigate further whether the conclusions reached earlier (Ramatsetse, 1998) on the synthesis of ferrierite could be generalized and/or extended in terms of other synthetic procedures and recipes. A summary of our previous conclusions was given in Section 2.3.5 on how the hydrothermal synthesis temperature for synthesis with and without stirring in the in-house built autoclave affected the ferrierite-based material formed, in terms of the percentage crystallinity and the morphology of the crystallites. These investigations are repeated in this thesis using the recipe of Grandvallet *et al.* (1992) (see Section 4.3.3.1), except that the synthesis was conducted in a commercial one litre Parr autoclave using overhead stirring. This synthetic method makes use of silica gel (Grace S432) as the silica source, and the influence of the silica gel particle size was also investigated. Our previous study also indicated that ferrierite crystallite formation was observed on the silica gel particles that were cracked during the synthesis (Ramatsetse, 1998). The formation and possible effects of these cracks are also dealt with in the present thesis. In addition, results are also presented on how different literature recipes (using different silica sources) are affected by the synthesis temperature and stirring conditions in terms of the percentage crystallinity, its controllability and

reproducibility of the samples obtained, over the whole crystallinity range, and the morphology of the crystallites formed.

The samples prepared at different temperatures and stirring conditions reported in this chapter were hydrothermally synthesized for a period of 75 hours, 80 hours or 113 hours depending on the method used (see Section 4.3.3). These syntheses were carried out at temperatures ranging from just before crystallization commenced, and up to 200°C in steps of 10°C, or for certain investigations at one specific temperature but changing the conditions such as the stirring rate. In each case the calculation of the percentage XRD crystallinity of the ferrierite zeolite-based samples was performed according to the method used earlier (see Section 3.7 and Ramatsetse, 1998).

As was the case for the ZSM-5-based materials, the zeolites synthesized were given batch numbers in a consecutive way according to the duration of the preparation. These batch numbers are also indicated on the SEM micrographs together with the synthesis temperature and the stirring rate, in order to allow for easy sample identification and for facilitating comparisons. Once again, the acronym "WS" refers to synthesis without stirring.

6.2 THE EFFECT OF TYPE OF AUTOCLAVE

In this investigation, the method previously used for the preparation of ferrierite with silica gel (S432) as silica source in the in-house built autoclave was repeated in a commercial Parr autoclave (see Section 4.3.1). The main difference between these autoclaves is that the Parr autoclave has a top stirrer made up of impellers, whereas in the in-house built autoclave, use is

made of a magnetic stirrer bar which is situated at the bottom of the autoclave. Furthermore, the Parr autoclave has a volume of 1 000 ml in comparison with the 350 ml of the in-house built autoclave. Various batches were synthesized with and without stirring at different temperatures. The effect of the stirring rate which had to be used in the Parr autoclave was also investigated.

6.2.1 Synthesis in the Parr autoclave

6.2.1.1 Synthesis without stirring

XRD analysis

Examples of the X-ray diffractograms of some of the ferrierite-based materials synthesized without stirring are shown in Figure 6.1. Figure 6.1(a) is the diffractogram of a ferrierite-based sample which was hydrothermally synthesized at 120°C. The hump in the diffractogram, which is characteristic of amorphous material, is observed at around 22° 2θ. At higher temperatures, as the crystallinity increases, the hump diminishes and it is not seen in the diffractograms of the samples synthesized at temperatures of 150°C and higher.

At 130°C we obtained the first appearance of the characteristic peaks of ferrierite as shown in Figure 6.1(b). The positions of these peaks, as is clearly evident in Figure 6.1(c), are at the same degrees 2θ as the major peaks for ferrierite (Von Ballmoos and Higgings, 1990). It can further be observed from the other diffractograms shown in Figure 6.1 that the peak intensities increase with increasing reaction temperature up to 150°C (see Figure 6.1(d)). This is followed by a decrease in peak intensities of the characteristic peaks of ferrierite at higher synthesis tempera-
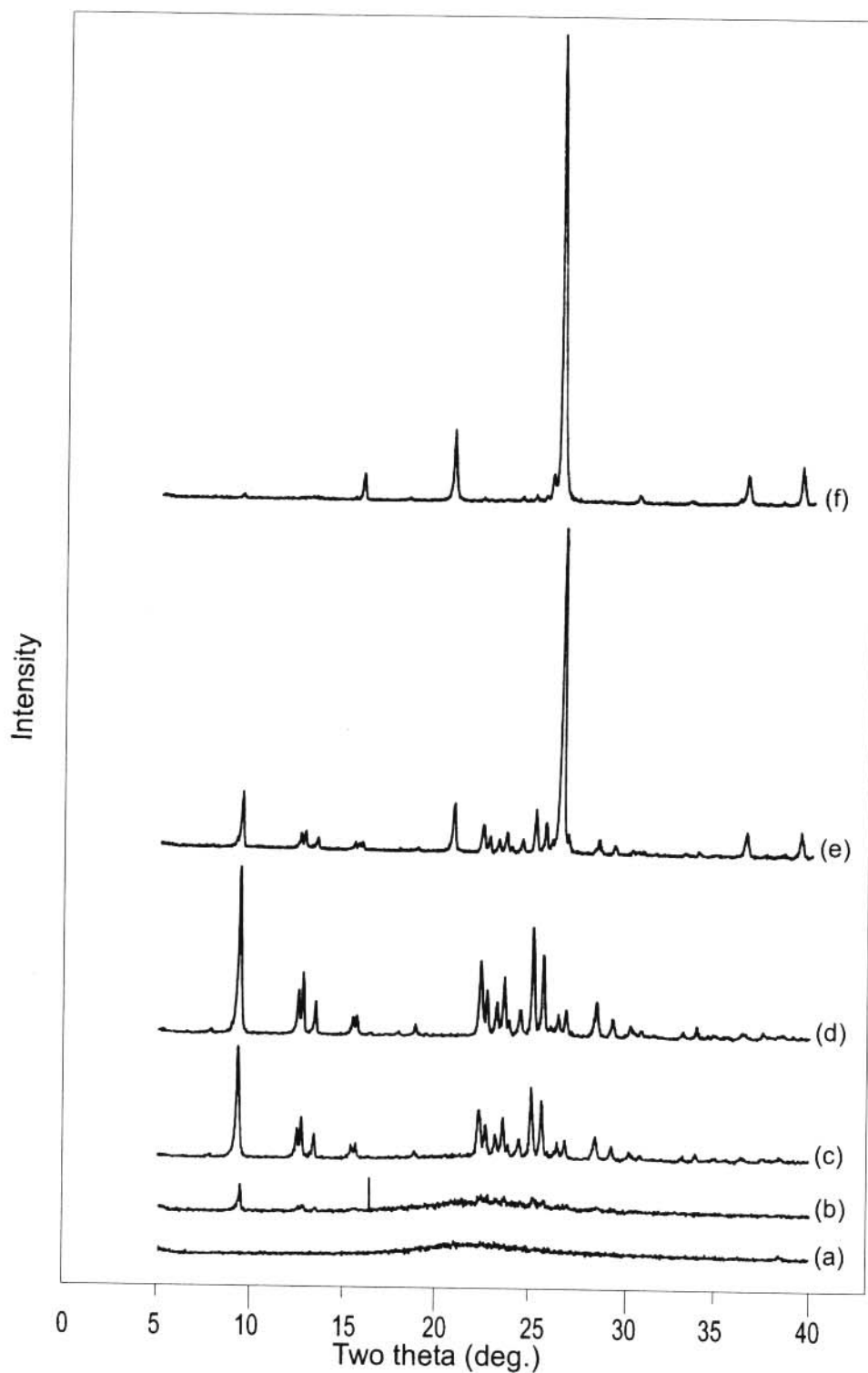
Figure 6.1 X-ray diffractograms of the ferrierite-based samples, and of other phases, synthesized without stirring in the Parr autoclave at different temperatures: (a) 120°C (batch no. 238), (b) 130°C (batch no. 236), (c) 140°C (batch no. 234), (d) 150°C (batch no. 200), (e) 190°C (batch no. 200), and (f) 200°C (batch no. 205).

tures. However, this decrease is concomitant with the appearance of additional peaks (see Figure 6.1(e) and Figure 6.1(f) which are samples synthesized at 190°C and 200°C respectively), indicating the transformation of ferrierite into mainly α-quartz (e.g. peaks at 20.78° 2θ, 26.55° 2θ, 36.46° 2θ and 39.36° 2θ) and some analcime (e.g. peaks at 15.88° 2θ, 26.04° 2θ and 30.67° 2θ) crystalline phases. The identification of these new phases is dealt with in Section 6.2.1.2. (see Figure 6.11).

The percentage XRD crystallinities for the samples synthesized without stirring at the various temperatures are tabulated in Table 6.1 and graphically shown in Figure 6.2. These data confirm

Table 6.1 Percentage XRD crystallinities of the ferrierite phase in the samples synthesized without stirring in the Parr autoclave at different temperatures using the silica gel (S432) method

Batch no.	Synthesis temperature (°C)	%XRD crystallinity	Mean	Standard deviation
238	120	0		
239	120	0	0.0	0.0
236	130	5		
235	130	26	15.5	14.9
233	140	52		
234	140	58	55.0	6.0
200	150	79		
202	150	31	58.3	24.7
232	150	65		
195	160	47		
197	160	64	55.5	12.0
219	170	47		
221	170	52	49.5	3.5
196	180	40		
198	180	50	45.0	7.1
220	190	33		
237	190	26	29.5	5.0
199	200	21		
205	200	3	12.0	12.7
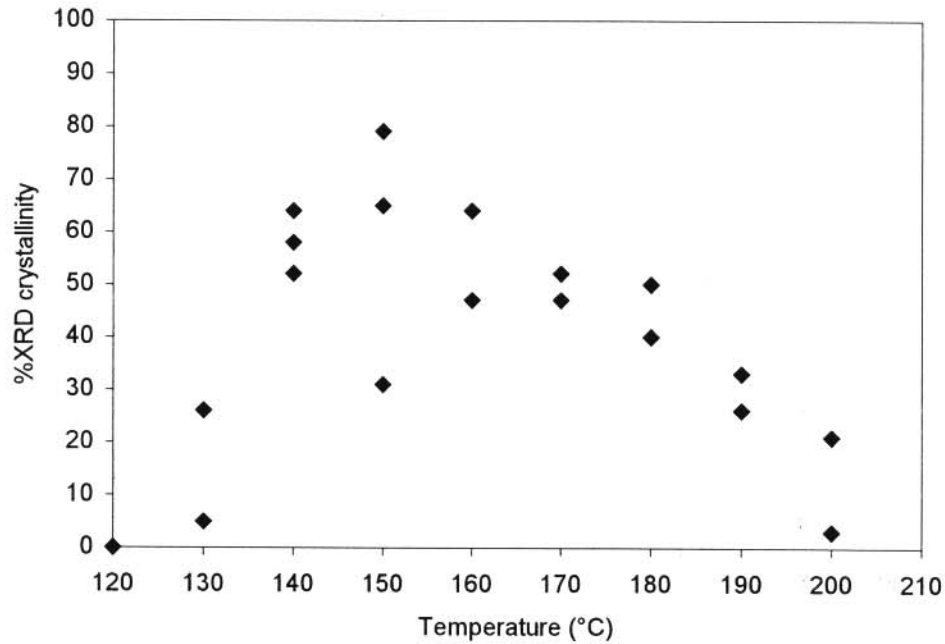
Figure 6.2 Plot of percentage XRD crystallinity of the ferrierite phase versus the synthesis temperature for the samples synthesized without stirring in the Parr autoclave at different temperatures.

that with this recipe and this mode of synthesis the highest crystallinity (79%) is obtained at 150°C, although the standard deviation is also the highest at this temperature. At 130°C, where crystallization starts, it was possible to synthesize substantially amorphous (< 30% XRD crystalline) ferrierite-based materials, although controllability seems to be a problem.

SEM analysis

To illustrate the morphology of the ferrierite-based samples synthesized according to this recipe and without stirring at different temperatures, SEM micrographs of certain representative samples are shown in Figure 6.3 and Figure 6.4. In addition to these, the micrograph of the untreated silica gel (S432) is included in Figure 6.3(a). If one compares this micrograph with that of the sample synthesized at 120°C, where 0% crystallinity was determined (Figure 6.3(b)),

(a)

(b)
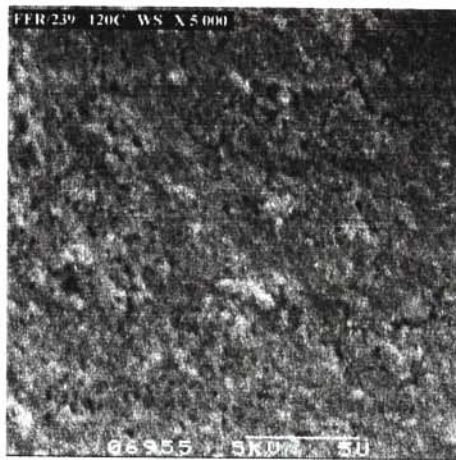
(c)

Figure 6.3 SEM micrographs of (a) the untreated silica gel (S432) particles (X 50), and the ferrierite-based sample prepared without stirring at 120°C using the silica gel (S432) method: (b) 120°C (X 50) and (c) 120°C (X 5 000).
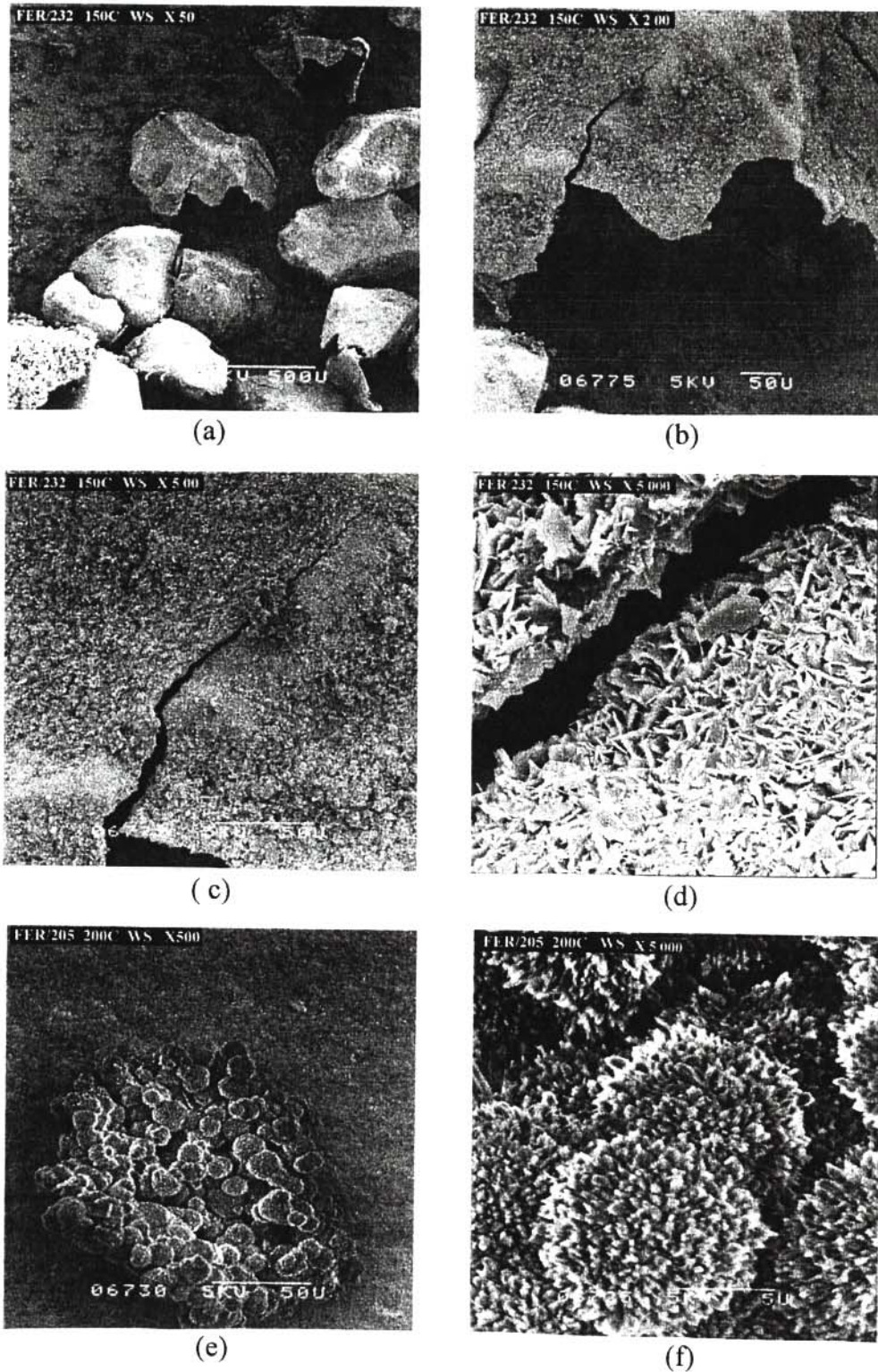
Figure 6.4 SEM micrographs of ferrierite-based samples, and of other phases, synthesized without stirring at different temperatures using the silica gel (S432) method: (a) 150°C (X 50), (b) 150°C (X 200), (c) 150°C (X 500), (d) 150°C (X 5 000), (e) 200°C (X 500) and (f) 200°C (X 5 000).

both of which are at a magnification of X 50, it can be concluded that the particles of the silica gel hydrothermally treated at 120°C were still of the same size, but had cracked in the process. With further magnification to X 5 000 of this sample it can be observed that zeolitization did not take place at this temperature and the amorphous morphology is readily observed.

Figure 6.4(a) through to Figure 6.4(d) are the SEM micrographs at different magnifications of the 65% XRD crystallinity sample synthesized at 150°C. The X 50 magnification shows undissolved silica particles as well as the presence of the crusts of cracked particles which remained undissolved, with dissolution, however, of the inner part of the particles having taken place. Figure 6.4(b), Figure 6.4(c) and Figure 6.4(d) are micrographs of one of these cracked outer crusts (the one almost in the middle of Figure 6.4(a)) magnified X 200, X 500 and X 5 000 respectively, to show the formation of crystallites on the crust. Such crystallites were also obtained on the other particles. The intergrown crystallites observed at higher magnification are similar to those reported by Xu *et al.* (1995a) (see Section 2.3, Figure 2.2(b)). It seems as if crystallization occurred on the outside of the particles as soon as dissolution of the silica gel took place and that is probably the reason why the crusts do not completely dissolve since it is covered by insoluble ferrierite.

Figure 6.4(e) and Figure 6.4(f) illustrate the morphology of the sample synthesized at 200°C at different magnifications (X 500 and X 5 000 respectively). This different morphology which is observed, is probably representative of α-quartz since the sample consists mainly of α-quartz with only small amounts of analcime and ferrierite (see Figure 6.1(e)).

From the results in Table 6.1 and Figure 6.2 it can be concluded that maximum crystallinity is

obtained at 150°C when performing the synthesis without stirring. Higher synthesis tempe-ratures result in the formation of α-quartz and analcime.

6.2.1.2 *Synthesis with stirring*

Zeolite ferrierite-based samples were synthesized at different stirring rates to determine the optimum stirring rate in terms of obtaining the maximum percentage crystallinity of the zeolite samples produced in the Parr autoclave at the constant synthesis temperature of 150°C.

Determination of the effect of the stirring rate

The ferrierite-based materials were synthesized in the Parr autoclave at different stirring rates ranging from 0 rpm to 800 rpm in order to determine the stirring rate that gives the highest percentage XRD crystallinity. This series of experiments was conducted at 150°C, which is the temperature at which the highest percentage XRD crystallinity was obtained in a previous study (see Section 2.3.5 and Ramatsetse, 1998).

The X-ray diffractograms of the samples synthesized in the course of this investigation show that pure ferrierite samples with little observable differences in peak intensities are obtained at 0 rpm, 100 rpm, 300 rpm and 800 rpm (Figure 6.5(a) through to Figure 6.5(d)). The characteristic peaks of ferrierite are evident in these diffractograms.
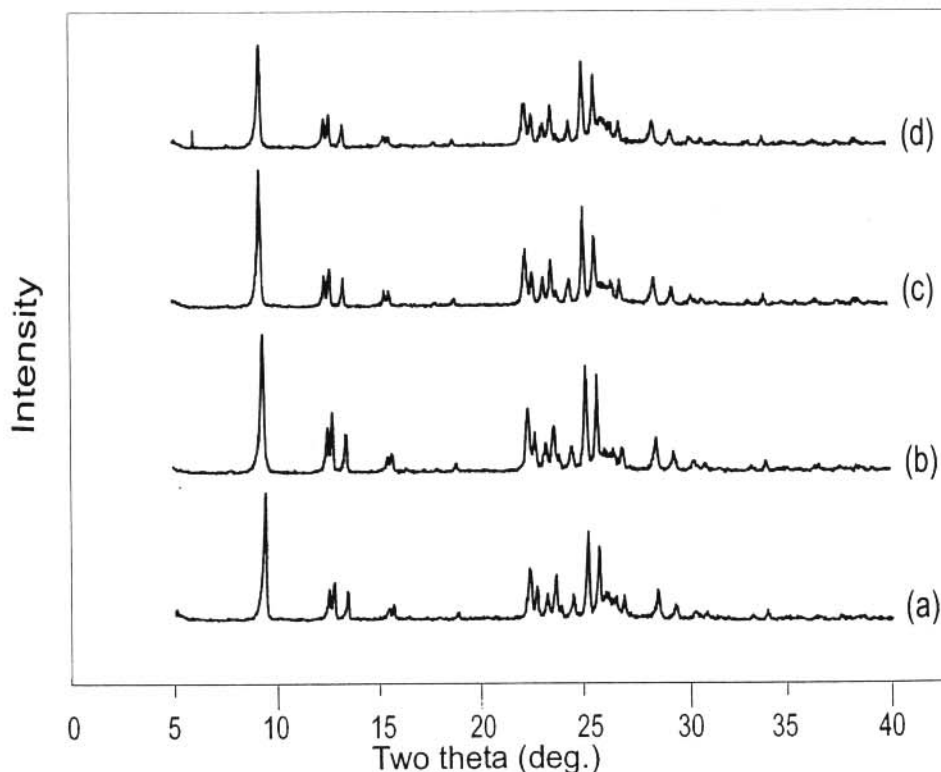
Figure 6.5 X-ray diffractograms of the ferrierite-based samples synthesized in the Parr autoclave at 150°C and at different stirring rates: (a) 0 rpm (batch no. 232), (b) 100 rpm (batch no. 203), (c) 300 rpm (batch no. 218), and (d) 800 rpm (batch no. 215).

The results for the syntheses under these conditions are listed in Table 6.2 and the percentage XRD crystallinity of the zeolite-based materials prepared versus the stirring rate are graphically presented in Figure 6.6. Although there is a variation in the average percentage XRD crystallinities at the different stirring rates, the standard deviations are smaller than for without stirring (24.7) at this temperature. The computer generated plot gives a straight line which slightly declines with increasing stirring rate. This emphasizes the fact that better reproducibility in terms of percentage crystallinity is attained for each batch prepared at stirring rates from 25 rpm to 800 rpm at this temperature, and that there is almost no significant effect of stirring on the percentage XRD crystallinity of the ferrierite samples prepared (see Table 6.2).

Table 6.2 Percentage XRD crystallinity of ferrierite-based samples synthesized at different stirring rates at 150°C

Batch no.	Stirrng rate (rpm)	%XRD crystallinity	Mean	Standard deviation
200	0	79		
202	0	31	58.3	24.7
232	0	65		
227	25	59		
228	25	55	57.0	2.8
226	50	58		
231	50	54	56.0	2.8
225	75	59		
230	75	56	57.5	2.1
201	100	76		
203	100	68	72.0	5.7
224	125	60		
229	125	64	62.0	2.8
204	200	53		
207	200	54	53.5	0.7
186	300	62		
218	300	64	63.0	1.4
206	400	53		
208	400	48	50.5	3.5
209	500	41		
210	500	51	46.0	7.1
211	600	57		
213	600	53	55.0	2.8
214	700	62		
216	700	66	64.0	2.8
215	800	65		
217	800	52	58.5	9.2

However, the SEM analyses show that the crystallites have been broken and less prominent rectangular platelets occur, which is the morphology of ferrierite-based materials as previously obtained (Ramatsetse, 1998). Their morphology is more of a "snowflake"-type as shown in Figure 6.7(a) and Figure 6.7(b), which are the micrographs of the 76% crystalline sample synthesized at a stirring rate of 100 rpm. This shows that the crystals so formed are broken. Figure 6.7(c) and Figure 6.7(d), micrographs of a sample synthesized at 800 rpm, also suggest
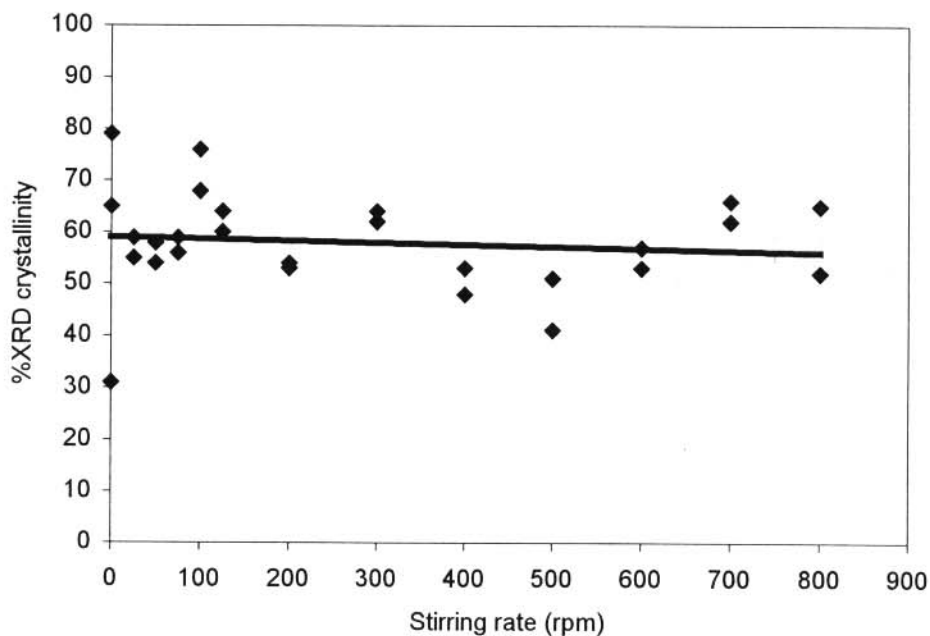
Figure 6.6 Plot of percentage XRD crystallinity versus synthesis stirring rate of the ferrierite-based samples prepared by using the silica gel (S432) method.

that the crystallites are broken at the high rpm's.

Since from these experiments conducted at different stirring rates, the optimum stirring rate is not clear, it was decided to investigate the influence of temperature on the preparation of ferrierite-based materials at two different stirring rates, i.e. at 100 rpm and 300 rpm. At 100 rpm, the average percentage XRD crystallinity obtained was 72%, while an average of 63% was obtained with stirring at 300 rpm (see Table 6.2).

(a)

(b)

(c)

(d)
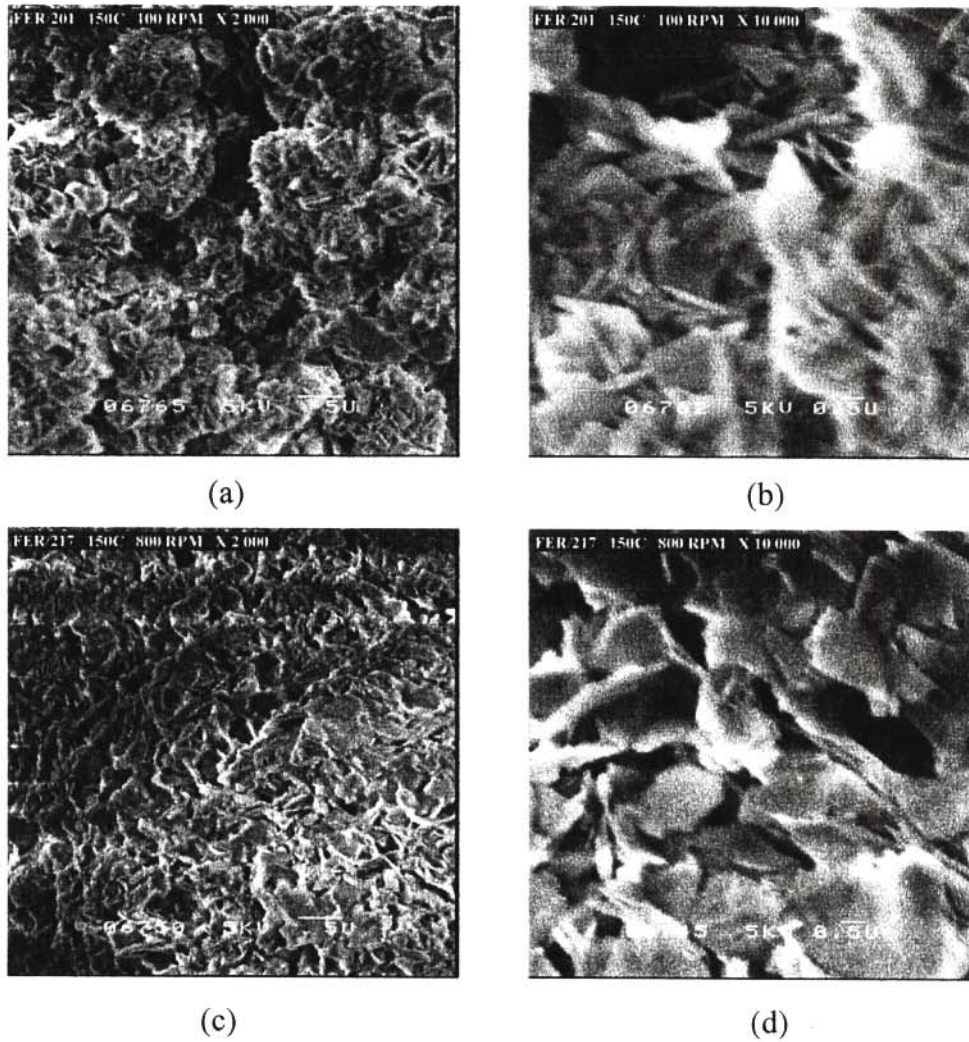
Figure 6.7 SEM micrographs of ferrierite-based samples synthesized at 150°C and at different stirring rates: (a) 100 rpm (X 2 000), (b) 100 rpm (X 10 000), (c) 800 rpm (X 2 000) and (d) 800 rpm (X 10 000).

Synthesis at 100 rpm

XRD analysis

The X-ray diffractograms of some of the ferrierite-based samples prepared with stirring at 100 rpm are shown in Figure 6.8. No diffraction peaks are observed on the hump for the sample

Figure 6.8 X-ray diffractograms of the ferrierite-based samples, and of other phases, synthesized with stirring at 100 rpm and at different temperatures: (a) 120°C (batch no. 299), (b) 150°C (batch no. 201), (c) 170°C (batch no. 322), (d) 180°C (batch no. 314), and (e) 200°C (batch no. 326).

synthesized at 120°C (Figure 6.8(a)), indicating therefore that the sample is X-ray amorphous. This lack of diffraction peaks is also observed in the samples synthesized at 130°C and 140°C. At 150°C the characteristic peaks of ferrierite are observed which are of relatively high intensity as is evident in Figure 6.8(b). As shown in Figure 6.8(c) to Figure 6.8(e), there is a decrease in peak intensities of ferrierite with increasing synthesis temperature (from 170°C to 200°C), and the development of the α-quartz and the analcime peaks (e.g. an α-quartz peak at 26.55° 2θ and an analcime peak at 15.88° 2θ). These results clearly show the gradual transformation of ferrierite into α-quartz and analcime phases with increasing temperatures higher than 170°C. Thus, once again, one is limited to a hydrothermal synthesis temperature of 150°C for the synthesis of relatively pure, and of medium crystallinity, ferrierite samples using this recipe.

The percentage XRD crystallinities for the samples synthesized at 100 rpm are listed in Table 6.3. It can be observed from this table that, unlike with the without stirring mode of synthesis,

Table 6.3 Percentage XRD crystallinities of the ferrierite phase in the samples synthesized with stirring at 100 rpm and at different temperatures using the silica gel (S432) method

Batch no.	Synthesis temperature (°C)	%XRD crystallinity
299	120	0
341	130	0
336	140	0
304	150	54
201	150	76
330	160	62
322	170	51
314	180	49
318	190	31
326	200	1

crystallization starts only at 150°C, at which temperature, however, the highest percentage XRD crystallinity (76%) was also obtained. A gradual decline in the percentage crystallinity is observed at higher temperatures up to 180°C, after which a steep decline due to the transformation into α-quartz and analcime is encountered.

SEM analysis

In addition to the micrographs given in Figure 6.7(a) and Figure 6.7(b), which illustrate the morphology of the most crystalline ferrierite-based material prepared at the stirring rate of 100 rpm and at 150°C, SEM micrographs at different magnifications of the sample synthesized at 190°C are also shown in Figure 6.9 to show the morphology of the mixed crystalline phases obtained at this temperature. Both broken ferrierite crystallites and probably α-quartz, as was seen in Figure 6.4(f), are observed. Figure 6.9(a), which is magnified to X 5 000, shows mainly the α-quartz morphology with some amount of the typical ferrierite crystallites, while at the X

(a)   (b)
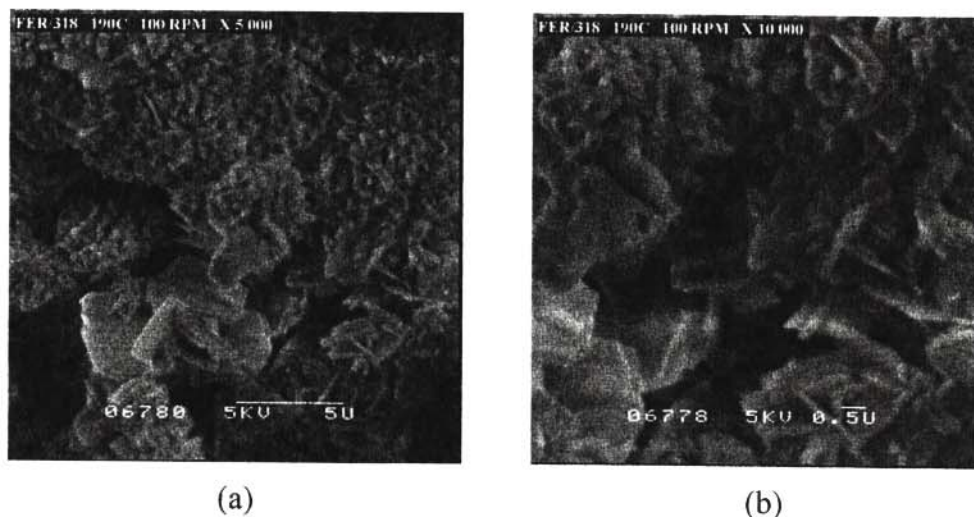
Figure 6.9 SEM micrographs of the sample synthesized with stirring at 100 rpm and 190°C using the silica gel (S432) method showing different magnifications: (a) X 5 000 and (b) X 10 000.

10 000 magnification (Figure 6.9(b)), mainly the broken crystallites are observed.

Synthesis at 300 rpm

XRD analysis

Figure 6.10 shows some of the X-ray diffractograms of the ferrierite zeolite-based samples prepared with stirring at 300 rpm. As in the case of the stirred batches at 100 rpm, no characteristic peaks are observed on the hump for the samples synthesized at 120°C (Figure 6.10(a)), indicating therefore that the sample is X-ray amorphous. Unlike in the case of the samples stirred at 100 rpm, where the ferrierite peaks appeared only at 150°C, in this case, the appearance of the characteristic peaks of ferrierite occurred at the synthesis temperature of 130°C (see Figure 6.10(b)). It can further be observed from the other X-ray diffractograms shown in Figure 6.10 that on average, the peak intensities increase with increasing reaction temperature up to 140°C (see Figure 6.10(c)). From 150°C to 170°C, there is a significant decrease in peak intensities of ferrierite, as is evident by Figure 6.10(d) which is the sample synthesized at 160°C. In this diffractogram the formation of α-quartz and analcime is evident as can be seen by the formation of peaks at 26.55° 2θ and 26.04° 2θ respectively. A further decrease in peak intensities of the characteristic peaks of ferrierite and an increase in the α-quartz and analcime peaks are observed with an increase in synthesis temperature from 180°C to 200°C as shown in Figure 6.10(e) and Figure 6.10(f).

Detailed XRD analysis of the material synthesized at 190°C with stirring at 300 rpm were repeated using a Siemens D500 X-ray diffractometer operating with CoK$_\alpha$ radiation, which was
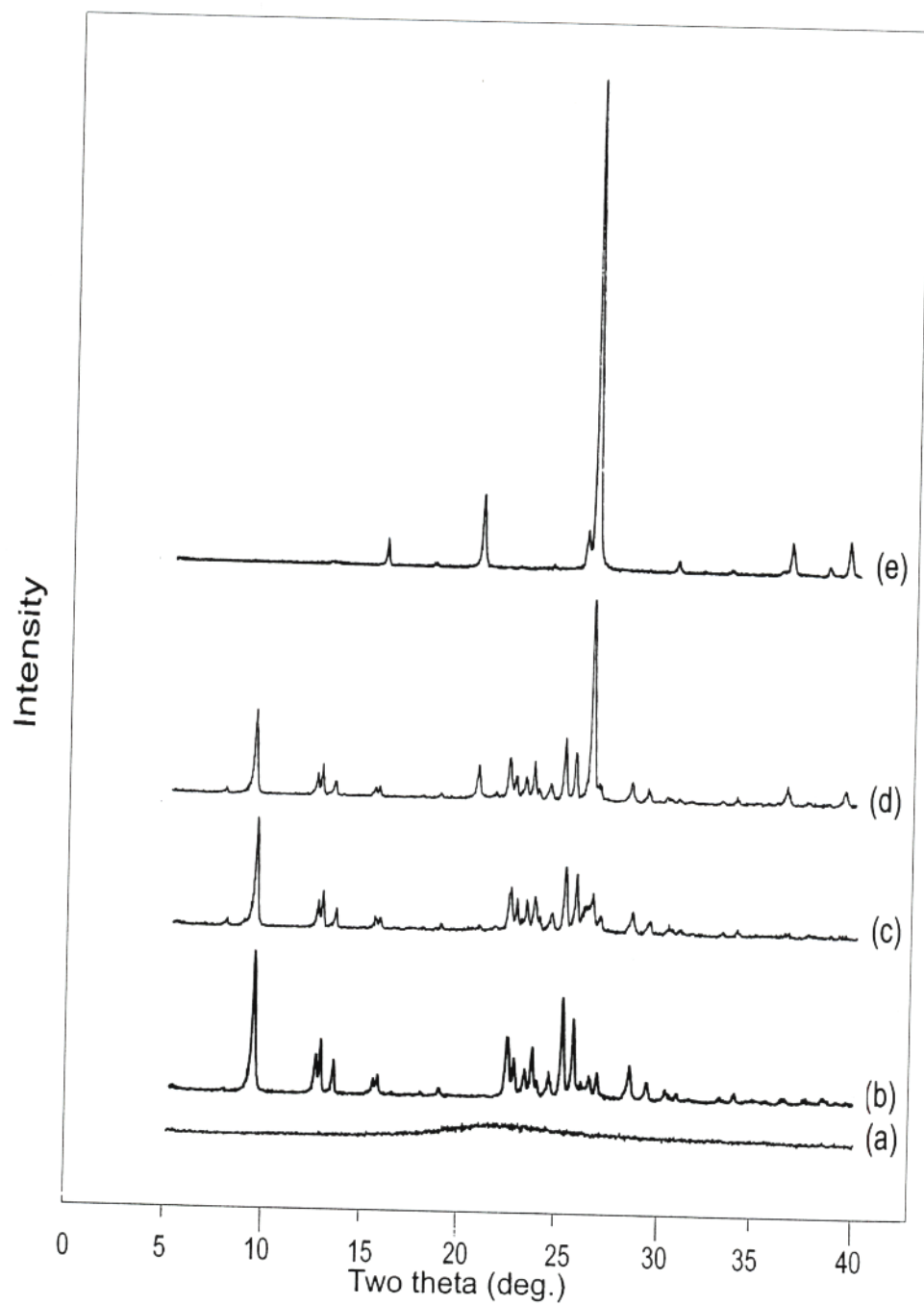
Figure 6.10 X-ray diffractograms of the ferrierite zeolite-based samples, and of other phases, synthesized with stirring at 300 rpm and at different temperatures using the silica gel (S432) method: (a) 120°C (batch no. 192), (b) 130°C (batch no. 191), (c) 140°C (batch no. 162), (d) 160°C (batch no. 165), (e) 180°C (batch no. 172), and (f) 200°C (batch no. 176).

230

able to identify the crystalline phases present (see Figure 6.11(b)). It revealed that these

additional peaks were mainly due to α-quartz (e.g. peaks at 20.78° 2θ, 26.55° 2θ, 36.46° 2θ and
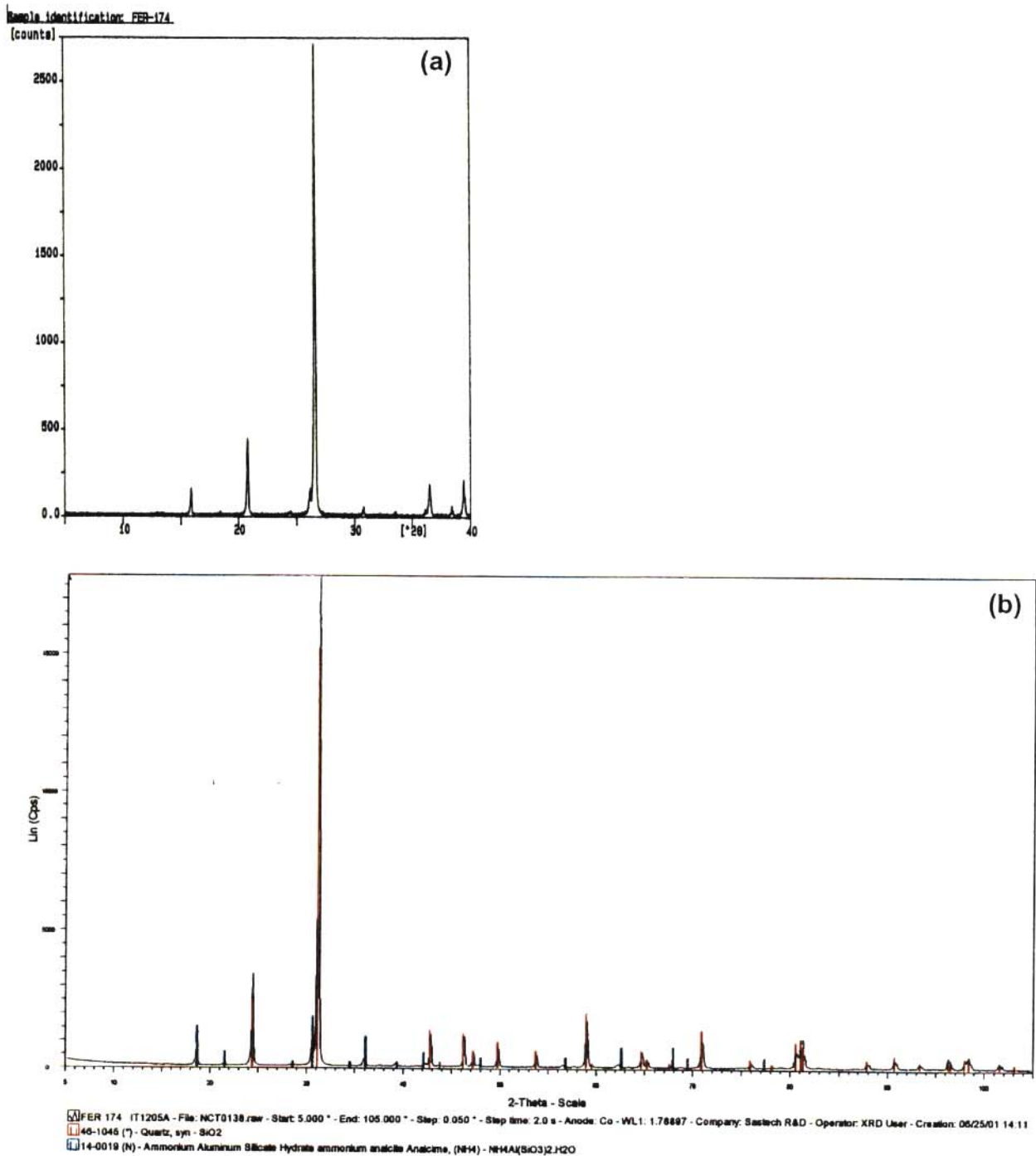
Figure 6.11 X-ray diffractograms of the materials synthesized at 190°C with stirring at 300 rpm

(batch no. 174) in the Parr autoclave: (a) CuK$_\alpha$ radiation and (b) CoK$_\alpha$ radiation, α-quartz (red

line) and analcime (blue line).

$39.36°$ 2θ) and traces of analcime (e.g. peaks at $15.88°$ 2θ, $26.04°$ 2θ and $30.67°$ 2θ) (see Figure 6.11(a), and Figure 6.11(b)). The diffraction degrees 2θ mentioned above are according to the data obtained with the Siemens PW17 based diffractometer which used CuK_α radiation (Figure 6.11(b)) and by which all other X-ray diffractograms were done.

The percentage XRD crystallinity for the samples synthesized with stirring at 300 rpm are listed in Table 6.4. As it was observed with the without stirring mode of synthesis, in this case crystal-

Table 6.4 Percentage XRD crystallinities of the ferrierite phase in the samples synthesized with stirring at 300 rpm and at different temperatures using the silica gel (S432) method

Batch no.	Synthesis temperature (°C)	%XRD crystallinty	Mean	Standard deviation
192	120	0		
194	120	0	0.0	0.0
189	130	41		
191	130	25	33.0	11.3
182	140	63		
187	140	57	60.0	4.2
162	150	52		
186	150	62	53.7	7.6
218	150	47		
164	160	39		
165	160	38	38.5	0.7
168	170	30		
170	170	28	29	1.4
171	180	32		
172	180	22	27	7.1
173	190	0.7		
174	190	0.4	0.6	0.2
175	200	0.4		
176	200	0.4	0.4	0.0

lization starts at 130°C and the larger standard deviation is obtained at this temperature. However, in this case maximum crystallinity (63%) is obtained at 140°C and the decline in crystallinity occurs at lower temperatures, which shows that stirring facilitates the formation of the additional phases, analcime and α-quartz. On the other hand, as is evident from the standard deviation values, this mode of synthesis gives better reproducibility for the preparation of a specific percentage XRD crystallinity, chosen according to synthesis temperature, than synthesis without stirring.

SEM analysis

Figure 6.12 shows the SEM micrographs of some ferrierite-based samples synthesized with stirring at 300 rpm. The crystals of pure ferrierite so formed are also broken (see Figure 6.12(a), which is a sample synthesized at 160°C) as was the case for the synthesis with stirring at 100 rpm (see Figure 6.7 and Figure 6.9). At higher temperatures, in addition to these broken "snowflake"-type ferrierite crystals, crystallites of a morphology different from those previously seen for α-quartz (see Figure 6.4(f) and Figure 6.9) are observed. Figure 6.12(b) and Figure 6.12(c) are examples of such a sample synthesized at 180°C at different magnifications. This morphology could be due to the crystallites of analcime which is the minor component. The sizes of these probable analcime crystallites are also smaller than those observed for ferrierite. The latter two micrographs were obtained using a Joel JSM-6 100 scanning electron microscope.

(a)
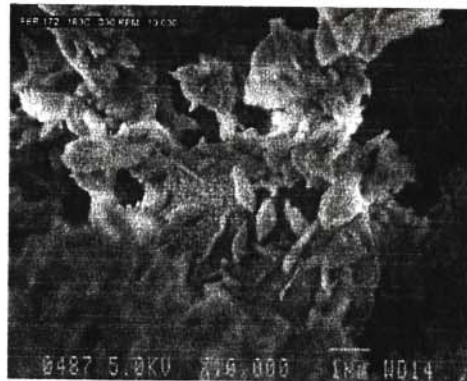
(b)

(c)

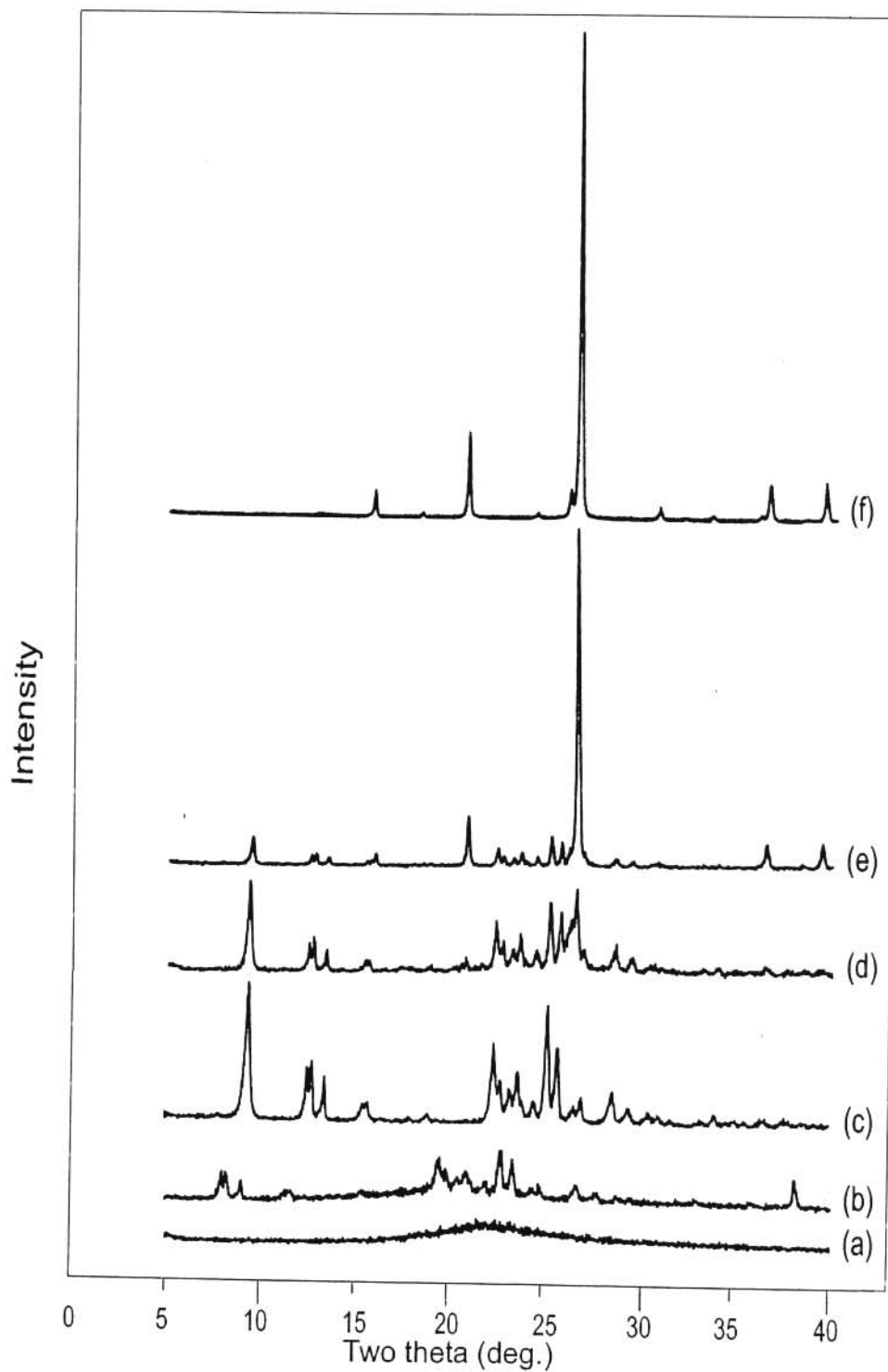**Figure 6.12** SEM micrographs of ferrierite-based samples, and of other phases, synthesized with stirring at 300 rpm and at different temperatures using the silica gel (S432) method: (a) 160°C (X 10 000), (b) 180°C (X 10 000) and (c) 180°C (X 25 000).

6.2.1.3 *Comparison of results*

The percentage XRD crystallinity as a function of synthesis temperature for the samples synthesized without stirring as compared to those obtained with stirring at 100 rpm is given in Figure 6.13.

The results in Figure 6.13 show that higher percentage XRD crystallinities are obtained without stirring than with stirring at 100 rpm and at temperatures up to 150°C, but that above this temperature, the percentage XRD crystallinity of the two sets of samples decreases in almost the same way. Furthermore, these results clearly demonstrate that using the unstirred mode of syn-
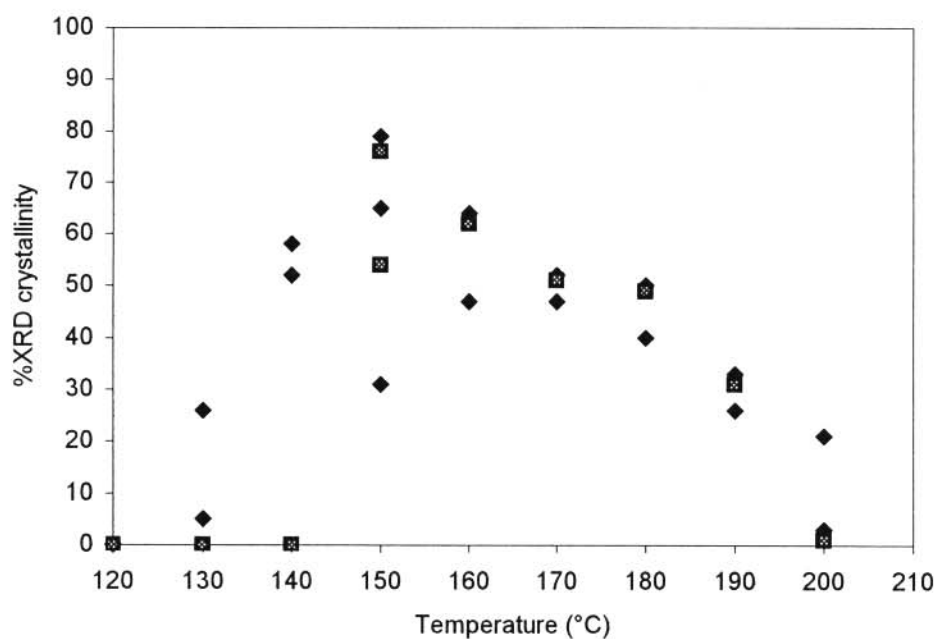
Figure 6.13 Plot of percentage XRD crystallinity of the ferrierite phase versus synthesis temperature of the samples synthesized with stirring at 100 rpm (■) and without stirring (♦) using the silica gel (S432) method.

thesis is preferred in obtaining the ferrierite phase at lower temperatures than using the stirred mode of synthesis.

Figure 6.14 depicts the curves for the percentage XRD crystallinity as a function of hydrothermal synthesis temperature for the samples synthesized without stirring and the samples synthesized with stirring at 300 rpm. Unlike with the first plots, the results in this figure show that at lower temperatures (below 150°C), the percentage XRD crystallinities increase in almost the same way for the two modes of synthesis, but higher percentage XRD crystallinities or higher yield of the ferrierite phase are obtained without stirring than with stirring at 300 rpm at higher temperatures from 150°C. This emphasizes further the fact that the higher stirring rates have a positive effect
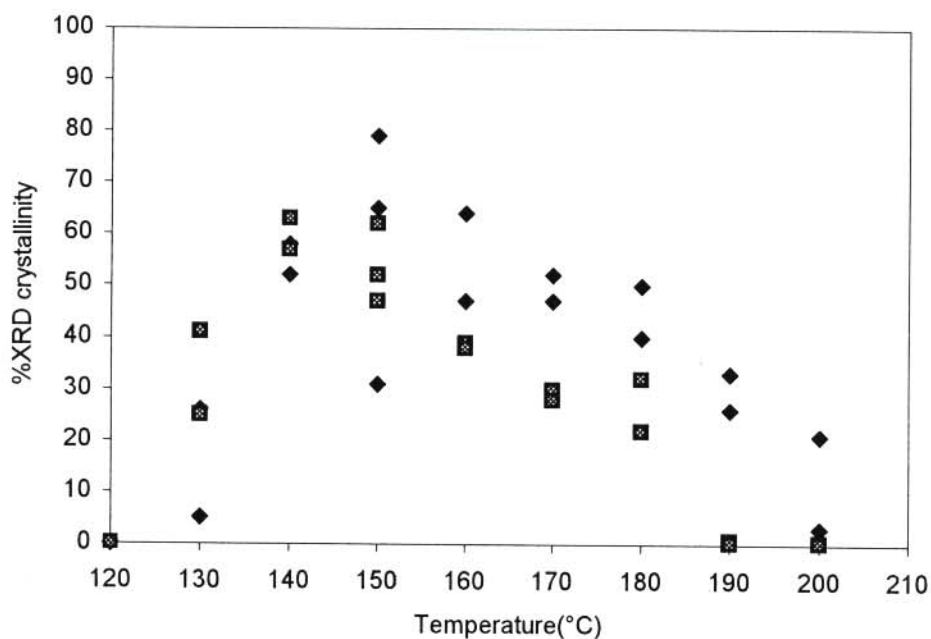
Figure 6.14 Plot of percentage XRD crystallinity of the ferrierite phase versus synthesis temperature for the samples synthesized with stirring at 300 rpm (■) and without stirring (♦) using the silica gel (S432) method.

on the formation of the additional phases of α-quartz and analcime, especially at higher temperatures.

6.2.2 **Synthesis with seeding**

Since the internal parts, i.e. the stirring and sampling systems of the Parr autoclave are of a complex design, the possibility cannot be excluded that in this autoclave small amounts of the zeolitic product from a previous batch was not totally removed at the end of each run, even after washing in caustic soda solution at 150°C (followed by thorough washing with water). These small amounts of zeolitic product therefore might then act as seeds for the subsequent hydrothermal synthesis. To investigate this issue further, a highly crystalline ferrierite batch was synthesized (see Section 6.2.2.1) and the same procedures as the ones followed above (i.e. with and without stirring) were repeated, except that the reaction mixtures were seeded in order to investigate the effect of seeding on the percentage crystallinity and morphology of the ferrierite-based zeolites, and that they were prepared in the in-house built autoclave. Experiments were conducted in which different amounts of the ferrierite seed were used.

6.2.2.1 *Synthesis of the seed ferrierite*

To determine the effect of seeding as indicated above, a highly crystalline ferrierite was synthesized using the patented method by Nanne *et al.* (1980), where water glass was used as the silica source (see Section 4.3.3.2). This preparation was conducted with stirring in the Parr autoclave with its bigger volume in order to obtain a sufficient amount of seed. The X-ray diffractogram and the SEM micrographs of one of the batches synthesized using this method are shown in Figure 6.15 and Figure 6.16 respectively.
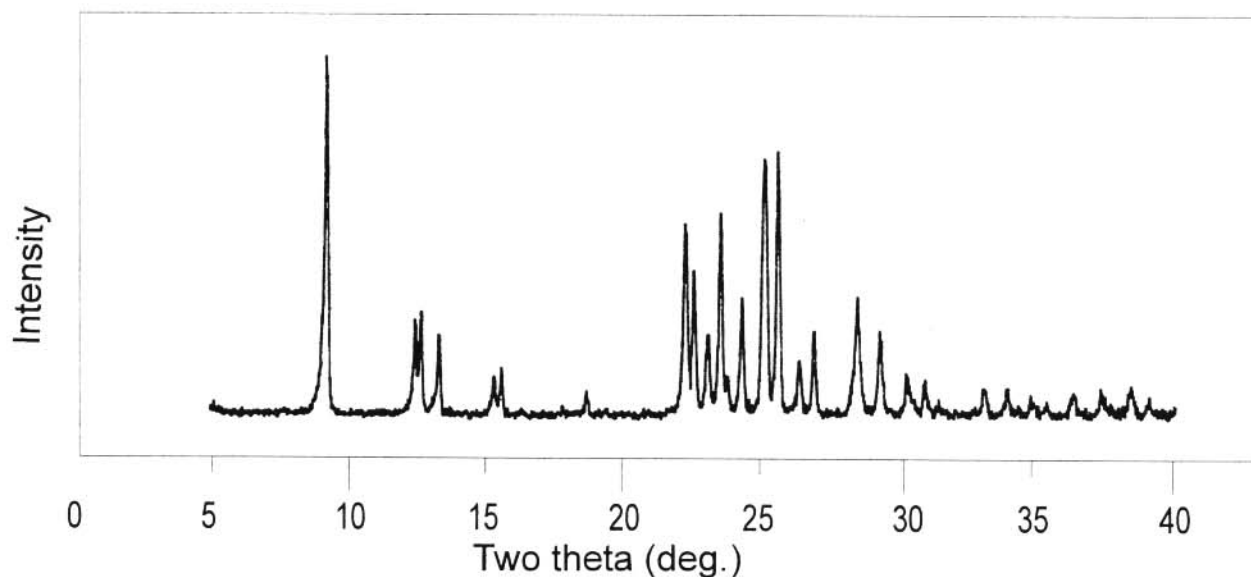
Figure 6.15 X-ray diffractogram of the ferrierite zeolite sample synthesized with stirring at 500 rpm and at 150°C (batch no. 222) using the Nanne *et al.* (1980) method.

The higher intensities of the peaks in this diffractogram and the flat base line (and absence of the hump), as well as the SEM micrographs which show mainly well-defined crystallites and only few patches of amorphous materials, allow us to conclude that this synthetic method produces highly crystalline samples (88%).

As can be seen in Figure 6.16, the morphology of the ferrierite crystallites can be described as being of layered platelets. Interesting with this method is that the shape of the crystals is not affected by stirring, i.e. although this sample was synthesized with stirring, the morphology of the crystals so formed is still well-defined. The silica source (water glass) used in this case may be the main cause of this, because the reaction mixture does not form a gel at the beginning and the end of zeolitization. Also see the morphology of the crystallites of the samples of ZSM-5 synthesized with stirring using water glass method (Section 5.3.1.2).

(a)

(b)
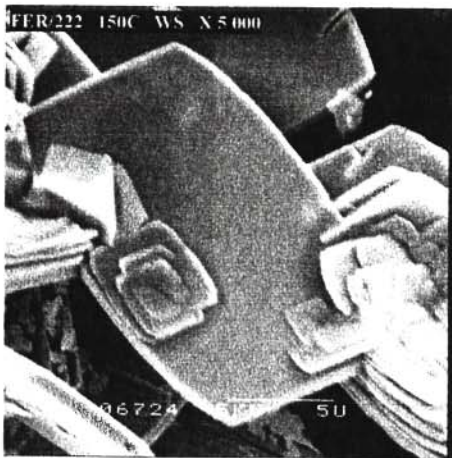
(c)

Figure 6.16 SEM micrographs showing different spots at X 1 000, (a) and (b), of a ferrierite zeolite sample synthesized with stirring at 500 rpm at 150°C using the Nanne *et al.* (1980) method and (c) zooming in on crystallites in centre of (a) (X 5 000).

6.2.2.2 *Synthesis without stirring and with seeding*

Synthesis with 0.5 g of the seed

The samples synthesized in this series of experiments using 0.5 g of the 88% crystalline ferrierite as seed were prepared without stirring in the in-house built autoclave.

XRD analysis

The X-ray diffractograms of some of the ferrierite-based samples prepared with seeding and without stirring are shown in Figure 6.17. Figure 6.17(a) is the diffractogram of the amorphous, or less than 1% XRD crystalline sample, as evident by the hump with small spikes on it, which was synthesized at 120°C. For the samples prepared at 130°C, the characteristic peaks of ferrierite are observed superimposed on the hump (see Figure 6.17(b)). This is followed by an increase in the intensities of the characteristic peaks of ferrierite with increasing synthesis temperature up to 170°C (Figure 6.17(d)). From 180°C to 200°C, there is a decrease in the peak intensities of the ferrierite peaks and the concomitant development of the α-quartz and analcime peaks with an increase in synthesis temperature (see Figure 6.17(e) and Figure 6.17(f)). This shows that although seeding delays the formation of the new phase, it does not totally eliminate its formation.

The percentage XRD crystallinities of the samples from this investigation are listed in Table 6.5. A comparison of these results, i.e. the unstirred preparation with seeding and in the in-house built autoclave, with those previously obtained (Ramatsetse, 1998) for the unseeded synthesis without stirring in the same autoclave, are given in Section 6.2.2.4 below.
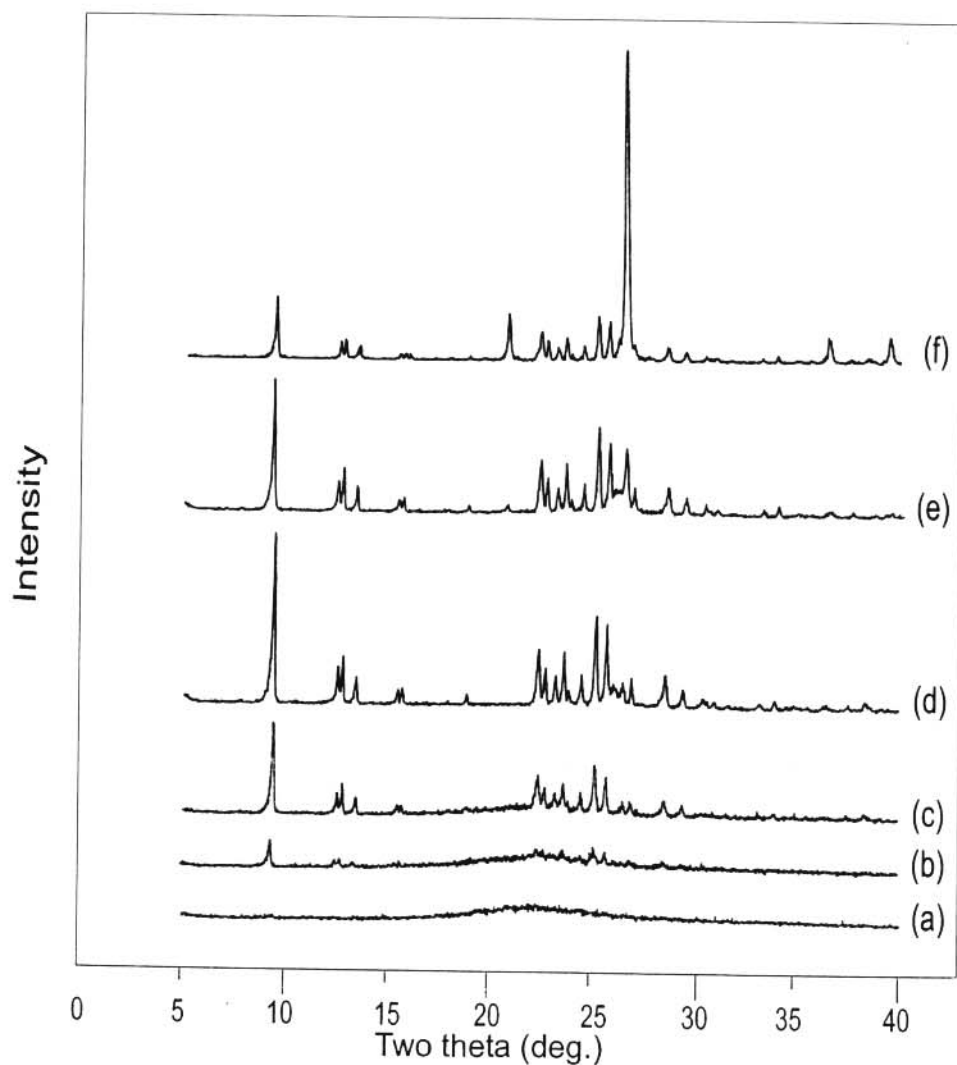
Figure 6.17 X-ray diffractograms of the ferrierite-based samples, and of other phases, synthesized in the in-house built autoclave without stirring at different temperatures using 0.5 g of the ferrierite seed: (a) 120°C (batch no. 331), (b) 130°C (batch no. 313), (c) 150°C (batch no. 310), (d) 170°C (batch no. 306), (e) 180°C (batch no. 335), and (f) 200°C (batch no. 355).

Table 6.5 Percentage XRD crystallinities of the ferrierite phase in the samples synthesized at different temperatures without stirring using 0.5 g of ferrierite seed

Batch no.	Synthesis temperature (°C)	%XRD crystallinity
331	120	0
313	130	9
443	140	45
310	150	36
444	160	66
306	170	72
335	180	51
370	190	58
355	200	26

SEM analysis

To illustrate the morphology of the ferrierite-based samples synthesized according to this recipe, i.e. with seeding, SEM micrographs of certain representative samples obtained at different synthesis temperatures are shown in Figure 6.18. Figure 6.18(a) and Figure 6.18(b) show one of the spots, magnified X 1 000 and X 5 000 respectively, of the amorphous material of a sample synthesized at 120°C where 0% (or less than 1%) XRD crystallinity was determined. Except for the amorphous phase, however, some "bud-like" structures are observed at lower magnification, but when magnified, crystallites are observed with a morphology such as those of the seed crystallites. These are rectangular platelet crystals lying on top of each other. Since the reaction mixture was not stirred, it is suspected that some crystals of the seed were just deposited on the surface of the silica gel (S432) particles.

Figure 6.18(c) and Figure 6.18(d) are the SEM micrographs of the 9% XRD crystallinity sample synthesized at 130°C at X 1 000 and X 5 000 magnifications respectively. Figure 6.18(c) shows different spots where nucleation and crystal-growth occurred on the crust of a silica gel particle
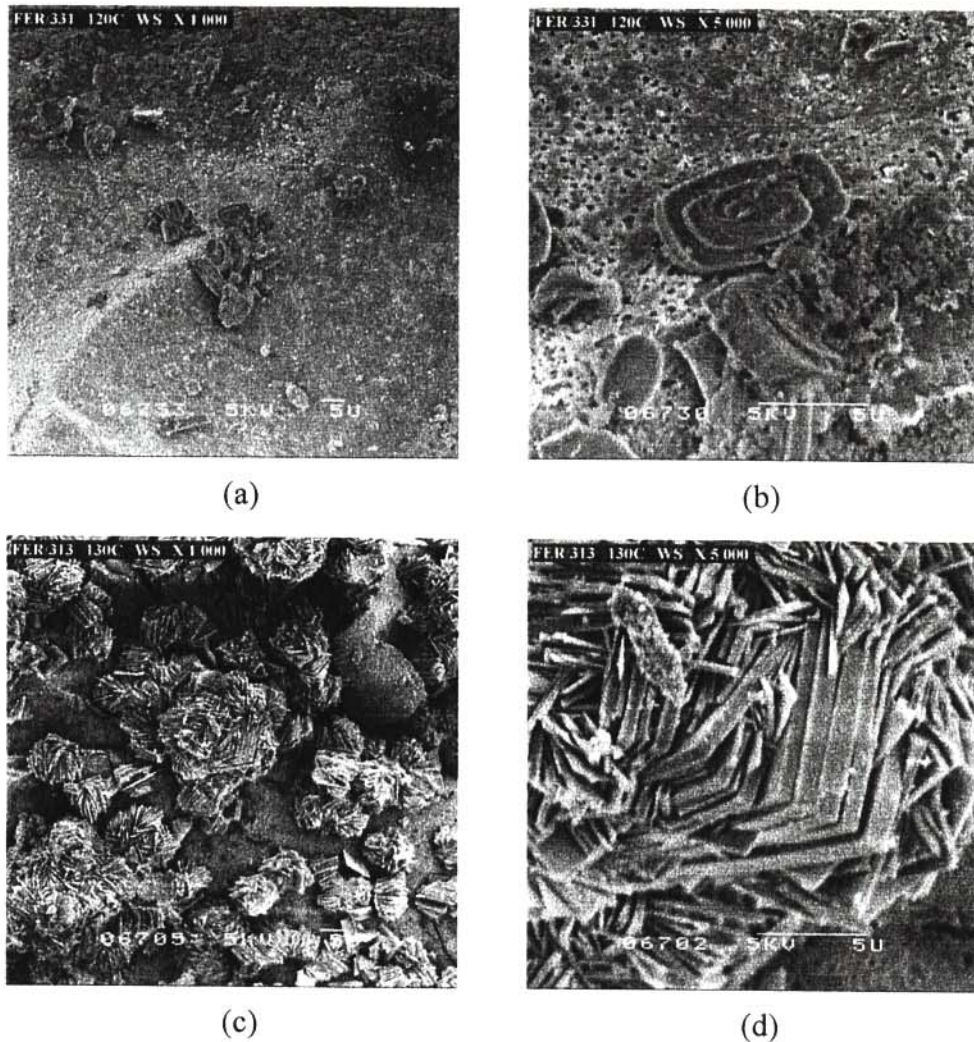
Figure 6.18 SEM micrographs of ferrierite zeolite-based samples synthesized without stirring using 0.5 g of the ferrierite seed using the silica gel (S432) method at different temperatures: (a) 120°C (X 1 000), (b) 120°C (X 5 000), (c) 130°C (X 1 000) and (d) 130°C (X 5 000).

while Figure 6.18(d) shows the formation of well-defined intergrown platelets.

Seeding with 1.0 g of the ferrierite seed

The above-mentioned investigation was repeated, but the mass of the seed was increased to 1.0g.

XRD analysis

Examples of the diffractograms of the ferrierite-based samples synthesized under this condition

at synthesis temperatures ranging from 120°C to 200°C are shown in Figure 6.19. Figure 6.19(a)

Figure 6.19 X-ray diffractograms of the ferrierite-based samples, and of other phases, synthesized without stirring in the in-house built autoclave with the 1.0 g of seed using the silica gel (S432) method at different temperatures: (a) 120°C (batch no. 427), (b) 140°C (batch no. 406), (c) 150°C (batch no. 317), and (d) 200°C (batch no. 421).

is the diffractogram of the sample which was hydrothermally synthesized at 120°C. Some spikes are observed on the hump and the sample is less than 1% crystalline (0.4% in this case), and is thus predominantly amorphous. There is a gradual increase in peak intensities with increasing synthesis temperature up to 150°C. These are evident by Figure 6.19(b) and Figure 6.19(c), which are the samples synthesized at 140°C and 150°C respectively. Above this temperature, there is a decline in peak intensities once again with increasing synthesis temperatures, as was previously observed.

As in the unseeded runs, at higher temperatures, the decrease of these characteristic peaks is concomitant with the development of α-quartz and analcime peaks which shows the transformation of ferrierite phase into other phases. This is evident by Figure 6.19(d) which is a sample synthesized at 200°C. Thus the preferred temperature for the synthesis of ferrierite is up to 150°C under this synthesis condition, whereas in the case of the 0.5 g of seed, maximum crystallinity (72%) was obtained at 170°C. It appears that with the silica gel method once the ±80% crystallinity range is attained, the ferrierite phase transforms into α-quartz and analcime.

Table 6.6 shows the percentage XRD crystallinity of the samples synthesized without stirring under these conditions. With this methodology we were able to obtain the highest crystallinity, 85%, for a ferrierite sample using the silica gel (S432) method. Crystallization starts also at 120°C, while with the other modes of synthesis discussed so far it started either at 130°C or 150°C.

Table 6.6 Percentage XRD crystallinities of the ferrierite phase in the samples synthesized without stirring at different temperatures using 1.0 g of the seed

Batch no.	Synthesis temperature (°C)	%XRD crystallinity
427	120	0.4
424	130	34
406	140	64
317	150	85
396	160	58
400	170	59
411	180	50
412	190	49
421	200	16

SEM analysis

Figure 6.20 shows the SEM micrographs of some of the ferrierite-based samples synthesized without stirring and seeded with 1.0 g of the ground seed. Figure 6.20(a) and Figure 6.20(b) is the SEM micrographs of the 85% crystallinity sample synthesized at 150°C. In this sample the formation of thick rectangular plates of crystals is evident, without any indication of an amorphous phase. This shows the positive influence of seeding in obtaining highly crystalline materials.

Figure 6.20(c) and Figure 6.20(d) show the SEM micrographs of the sample synthesized at 170°C. A rectangular platelet morphology is observed in this case. The transformation from thick plates at 150°C to thin plates at 170°C could be attributed to the dissolution and transformation of the ferrierite into α-quartz and analcime, as supported by the XRD analysis. At higher temperatures, a totally different morphology is observed (see Figure 6.20(e) and Figure 6.20(f) which are SEM micrographs of a sample synthesized at 200°C). This most probably represents the morphology of α-quartz which according to XRD is the main phase present in

(a) (b)

(c) (d)

(e) (f)
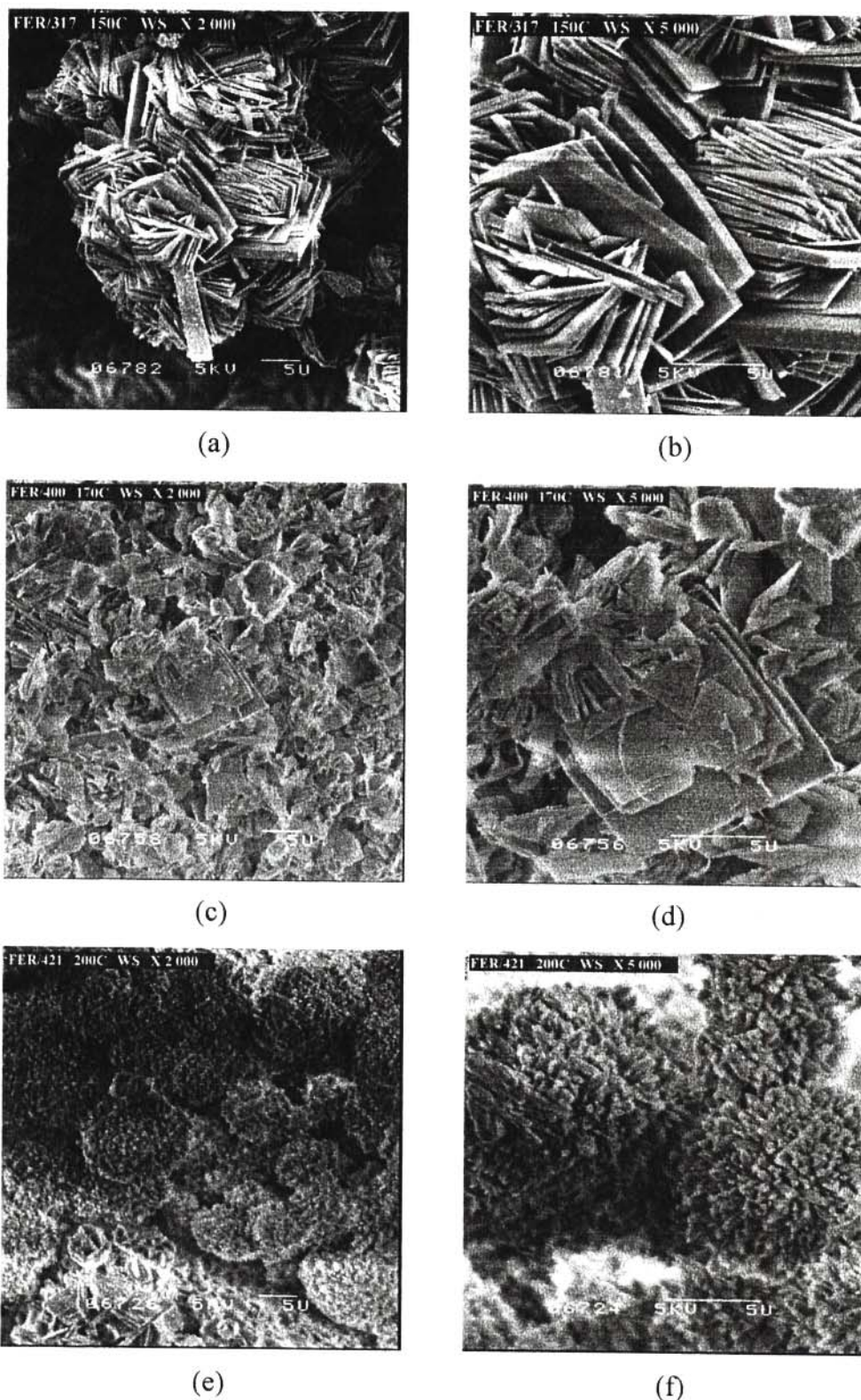
Figure 6.20 SEM micrographs of ferrierite-based samples, and of other phases, synthesized without stirring and seeded with 1.0 g of seed using the silica gel (S432) method at different temperatures: (a) 150°C (X 2 000), (b) 150°C (X 5 000), (c) 170°C (X 2 000), (d) 170°C (X 5 000), (e) 200°C (X 2 000), and (f) 200°C (X 5 000).

this sample, and is similar to the morphology obtained for other samples synthesized with mainly α-quartz (e.g. Figure 6.4(f) and Figure 6.20(f)).

6.2.2.3 *Synthesis with stirring and with seeding*

To investigate if stirring will have a further advantage on zeolitization at the lower temperatures of these seeded reaction mixtures, samples were also synthesized with stirring at 1 250 rpm using the magnetic stirrer bar in the in-house built autoclave using the silica gel (S432) method and seeded with 1.0 g of the 88% ferrierite seed.

XRD analysis

The diffractograms of some of the ferrierite-based samples prepared with seeding and with stirring are shown in Figure 6.21. Figure 6.21(a) is the diffractogram of the sample synthesized at 120°C. Unexpectedly, this diffractogram shows intense peaks for ferrierite which indicate high crystallinity. These intense peaks were observed up to 160°C, although a fluctuation of these intensities on average was observed (see Figure 6.21(b) and Figure 6 21(c), which are samples synthesized at 140°C and 160°C respectively). There is then a decrease in peak intensities with increasing synthesis temperature concomitant with the development of the α-quartz and analcime peaks. This is evident from Figure 6.21(d), which is the sample synthesized at 200°C showing the major peak of α-quartz at 26.55° 2θ and analcime at 30.67° 2θ. Thus, maximum crystallinity (71%) was obtained at 140°C and at higher temperatures we see the transformation of the ferrierite phase.
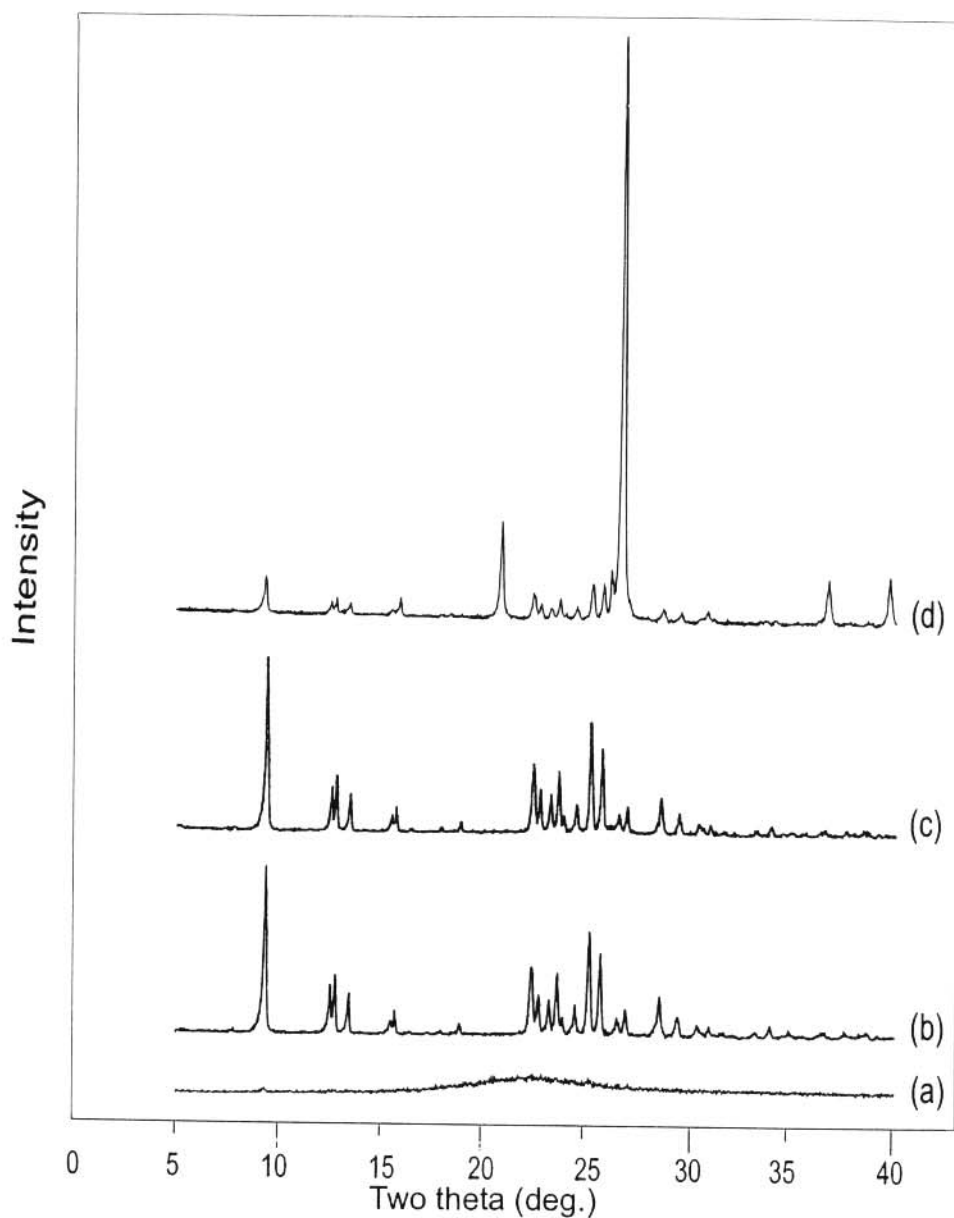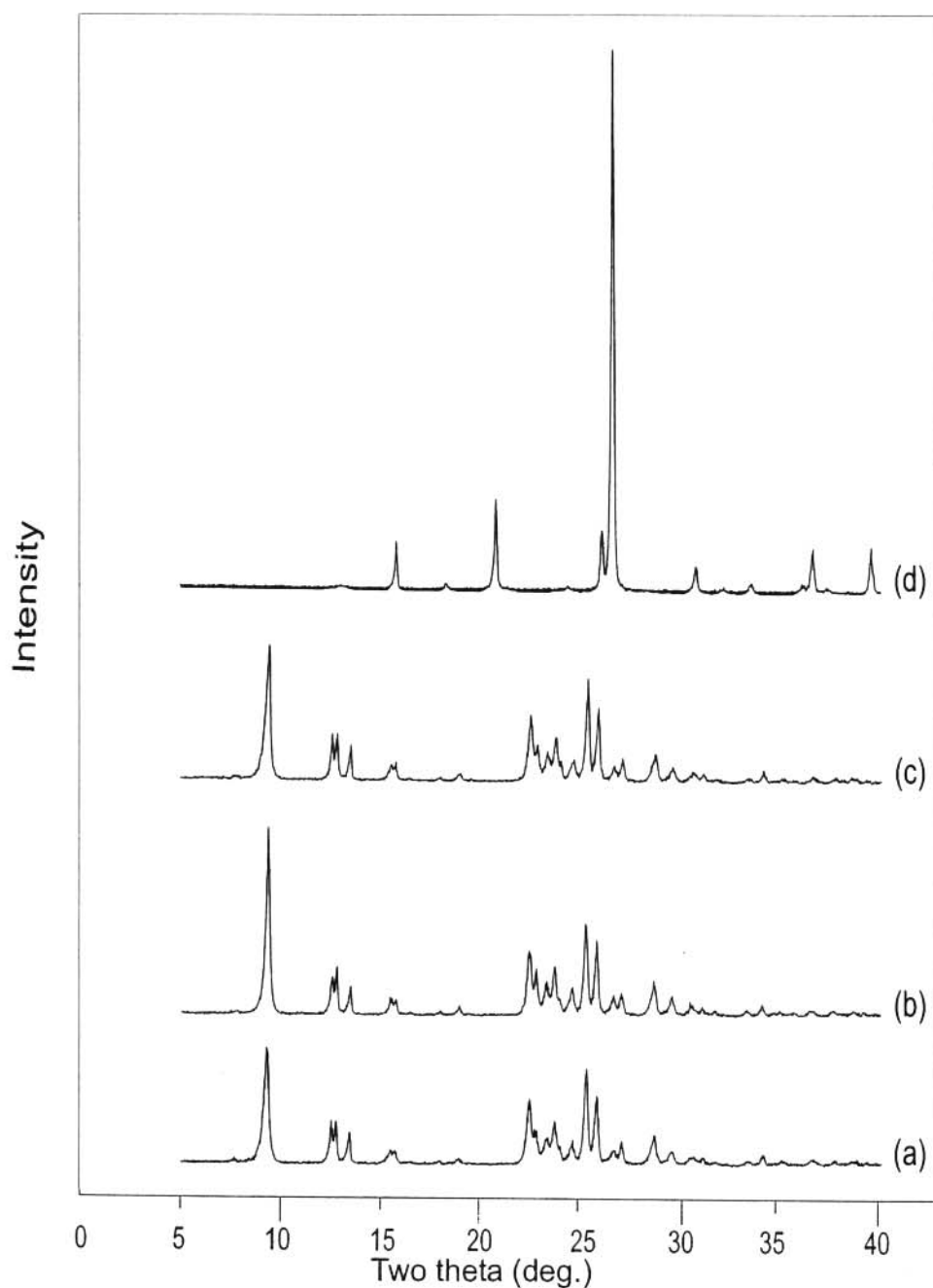
Figure 6.21 X-ray diffractograms of the ferrierite-based samples, and of other phases, synthesized with stirring with the 1.0 g seeded reaction mixture using the silica gel (S432) method at different temperatures: (a) and 120°C (batch no. 430), (b) 140°C (batch no. 435), (c) 160°C (batch no. 440), and (d) 200°C (batch no. 431).

Table 6.7 shows the percentage XRD crystallinity of the samples synthesized with stirring under these reaction conditions. From this table it can be seen that at 120°C a highly crystalline sample

Table 6.7 Percentage XRD crystallinities of the ferrierite phase in the samples synthesized with stirring, by seeding the reaction mixture with 1.0 g of the seed, using the silica gel (S432) method at different temperatures

Batch no.	Synthesis temperature ($^{\circ}$C)	%XRD crystallinity
430	120	57
429	130	48
435	140	71
434	150	54
440	160	63
441	170	31
442	180	39
437	190	0
431	200	1

(57%) was already obtained and the maximum crystallinity was obtained at 140°C, and there is a decrease in percentage crystallinity at higher temperatures.

SEM analysis

Figure 6.22 shows the SEM micrographs of some ferrierite-based samples synthesized with stirring and seeded with 1.0 g of the ground seed. Figure 6.22(a) is the SEM micrograph of the 57% crystallinity sample synthesized at 120°C. In this sample, pieces of broken crystals among the amorphous material are observed. This indicates that stirring breaks the crystals formed, as it was earlier observed (see Section 6.2.1.2 and Ramatsetse, 1998).

Figure 6.22(b) shows the SEM micrograph of the sample synthesized at 200°C. As was found with the sample synthesized without stirring at higher temperatures, a different morphology is observed which is consistent with the formation of α-quartz or analcime.

(a)   (b)
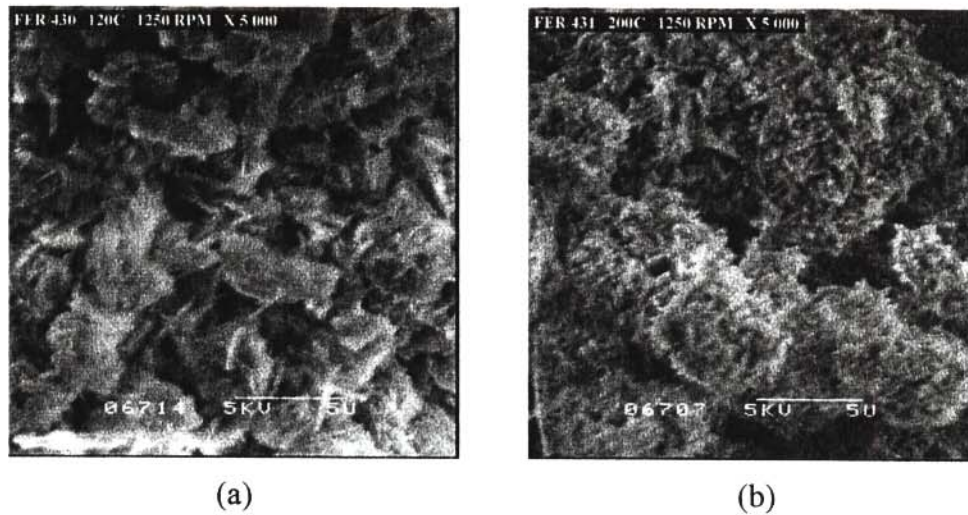
Figure 6.22 SEM micrographs of ferrierite-based samples, and of other phases, synthesized with stirring and seeded with 1.0 g of seed using the silica gel (S432) method and different temperatures: (a) 120°C and (b) 200°C.

6.2.2.4 *Comparison of results*

Figure 6.23 indicates the plots of percentage XRD crystallinities of the ferrierite phase as a function of synthesis temperatures for the ferrierite-based samples synthesized without stirring using either 0.5 g or 1.0 g of seed, and without seeding. The latter results are from the previous investigation (Ramatsetse, 1998). These plots show that the crystallization of the seeded reaction mixtures starts at lower temperatures and on average give higher crystallinities than that of the unseeded reaction mixtures. Without seeding crystallization starts only at 150°C, while with seeding a fair amount of crystallites were already formed at 130°C. Furthermore, the larger amount of seed, i.e. 1.0 g, gave higher percentage crystallinities at lower temperatures (up to 150°C) than the synthesis only with 0.5 g of seed.
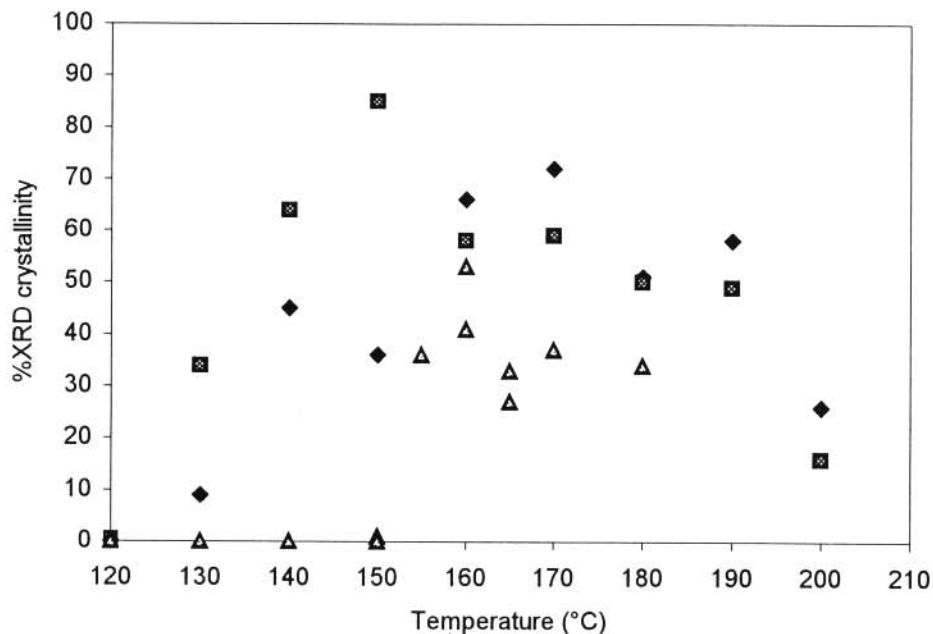
Figure 6.23 Plot of percentage XRD crystallinity of the ferrierite phase versus the synthesis temperature for ferrierite-based samples synthesized without stirring in the in-house built autoclave and with seeding using 0.5 g of seed (♦), 1.0 g of seed (▣), and without seeding (Ramatsetse, 1998) (▲).

The plots of percentage XRD crystallinities as a function of synthesis temperature for the samples synthesized with and without stirring using 1.0 g of seed are shown in Figure 6.24. The results indicate an increase in crystallinity up to 85% with an increase in synthesis temperature up to 150°C, after which a decrease in crystallinity was observed. Furthermore, on average higher percentage XRD crystallinities are obtained with stirring than without stirring at temperatures up to 140°C. Above this temperature, the plot for the samples prepared without stirring show higher percentage XRD crystallinity than those prepared with stirring. Since the "without-stirring" plot shows a smooth curve one may conclude that seeding has a positive effect on reproducibility when using the unstirred mode of synthesis.
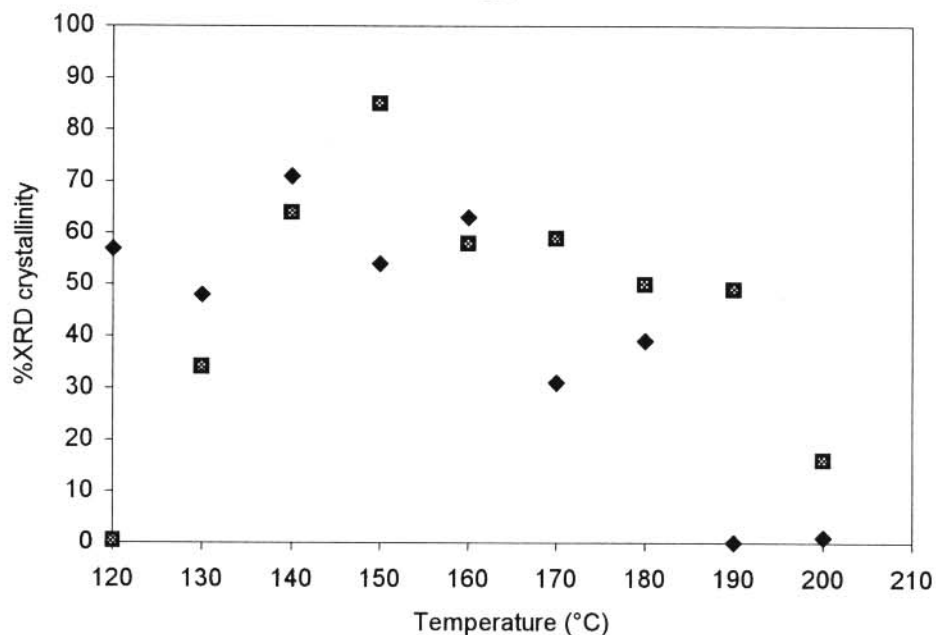
Figure 6.24 Plot of percentage XRD crystallinity of the ferrierite phase versus the synthesis temperature for samples synthesized with 1.0 g of ferrierite seed with stirring (♦) and without stirring (▣).

6.2.3 **Conclusions**

A comparison of the percentage XRD crystallinities of the samples synthesized at different temperatures without stirring in the Parr autoclave and the in-house built autoclave is given in Figure 6.25. This shows that the Parr autoclave gives higher percentage XRD crystallinity samples than the in-house built autoclave. Zeolitization also starts at lower temperatures in the Parr autoclave than in the in-house built autoclave. The possibility of some seeding occurring in the Parr autoclave, due to its complex internal stirring system, cannot be totally excluded as a reason for these differences.

SEM micrographs of these samples show the formation of intergrown rectangular platelets for the in-house built autoclave and a similar morphology for the Parr autoclave without stirring.
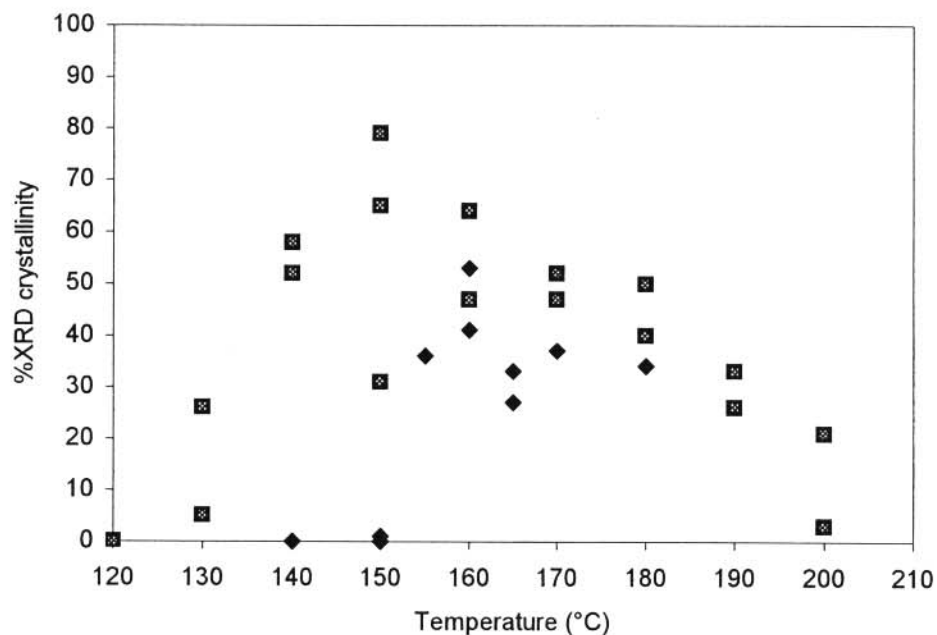
Figure 6.25 Plot of percentage XRD crystallinity of the ferrierite phase versus synthesis temperature for samples synthesized without stirring in the in-house built autoclave (Ramatsetse, 1998) (♦) and in the Parr autoclave (▣).

Cracks are obtained on the silica gel (S432) particles of the samples synthesized from both autoclaves. The only difference is that more crystals are evident on the surface of the cracked silica in the samples synthesized in the Parr autoclave at the same temperature (see Figure 6.26) and this is reflected in the higher percentage XRD crystallinity of the sample.

Figure 6.27 and Figure 6.28 give comparisons of the percentage XRD crystallinities of the samples synthesized with stirring at different temperatures using the in-house built and Parr autoclaves (at 100 rpm and 300 rpm for the Parr autoclave respectively, and at 1 250 rpm for the in-house built autoclave). Although crystallization starts at slightly higher temperatures for the syntheses with stirring at 100 rpm in the Parr autoclave, these figures indicate that the effect of temperature on the crystallinity of the ferrierite-based materials is similar for the synthesis in

(a)   (b)
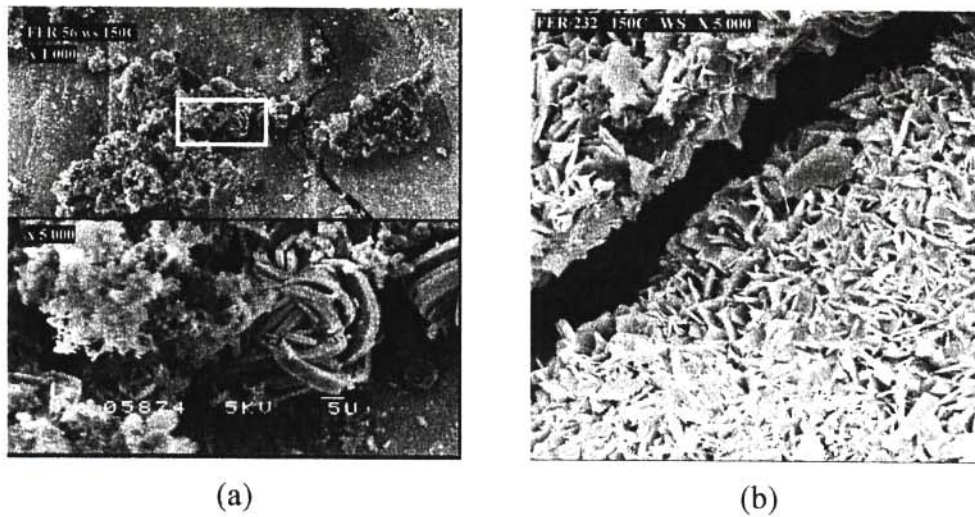
Figure 6.26 SEM micrographs of ferrierite-based samples synthesized without stirring at 150°C in different autoclaves using the silica gel (S432) method: (a) in-house built autoclave and (b) Parr autoclave.
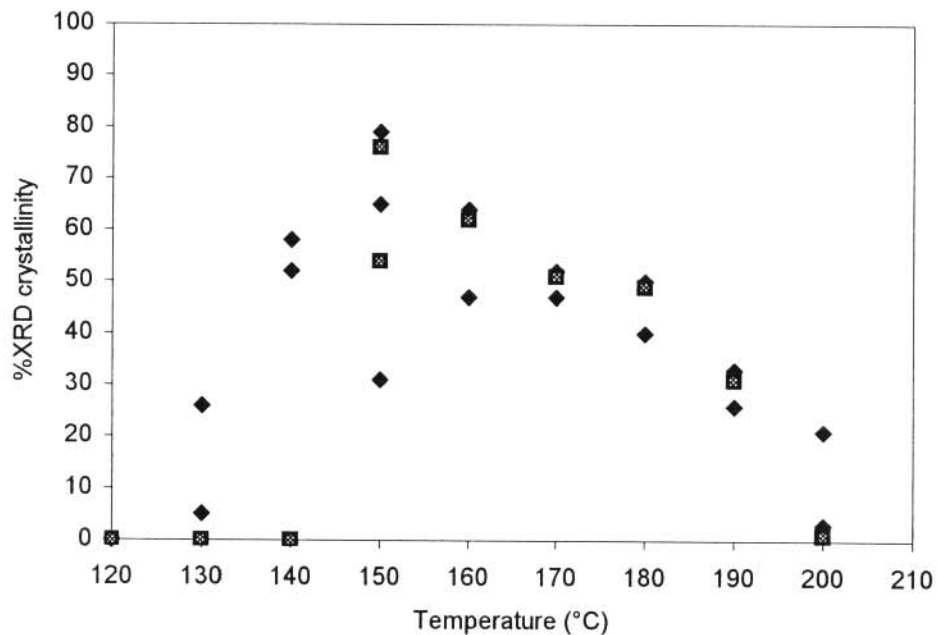
Figure 6.27 Plot of percentage XRD crystallinity of the ferrierite phase versus synthesis temperature for ferrierite-based samples synthesized with stirring in the in-house built autoclave (Ramatsetse, 1998) (♦) and in the Parr autoclave (at 100 rpm) (▣).
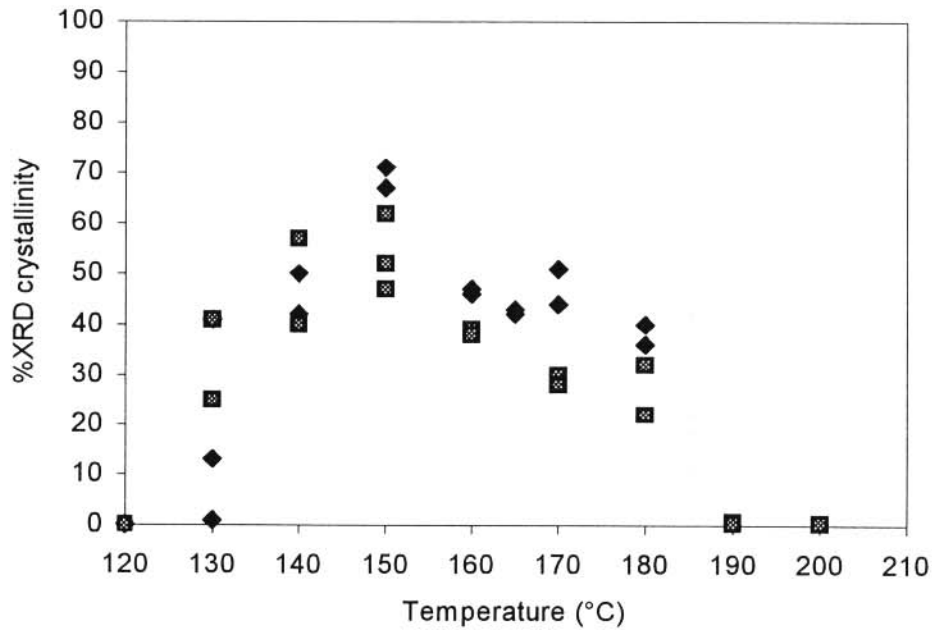
Figure 6.28 Plot of percentage XRD crystallinity of the ferrierite phase versus synthesis temperature for ferrierite-based samples synthesized with stirring in the in-house built autoclave (Ramatsetse, 1998) (♦) and in the Parr autoclave (at 300 rpm) (■).

both autoclaves. The differences observed at the lower temperatures in Figure 6.27 probably indicates that 100 rpm does not give effective agitation in the Parr autoclave.

The SEM micrographs of the samples synthesized with stirring in both autoclaves show "snow-flake" morphology, which indicates that the crystals are broken due to the agitation.

From the results at hand, it can be stated that the samples synthesized from the Parr are more crystalline than the samples synthesized from the in-house built autoclave. The complicated internal structure of the Parr autoclave might have play a role in seeding the crystallization process, since somewhere in the Parr autoclave's tubing system a certain amount of seed could have been trapped. Thus, our procedures for cleaning the Parr autoclave (see Section 4.3.1),

were probably not as sufficient as we thought.

At a later stage it was observed that there was some white material in the pipe leading to the sampling valve of the Parr autoclave. This materials could have seeded the reaction mixture of the next batch. This also showed that the Parr autoclave was not thoroughly cleaned at the end of each run and the next batch was seeded by the seed of the previous batch. It shows that in order to clean the Parr autoclave and to change the mode of synthesis in the Parr autoclave, the impellers of the stirring system and the pipe leading to the sampling valve of the Parr autoclave, should have been removed after each run. Hence the choice of the type of autoclave for zeolite synthesis is crucial, in avoiding especially the presence of any material from the previous batch to remain in the system.

6.3 INVESTIGATION OF THE CRACKS OBSERVED

In this study as well as in a previous project (Ramatsetse, 1998), it was observed that the crystallization of ferrierite appeared to start on cracked particles of the silica gel (S432) when using the recipe described in Section 6.2 (see Figure 6.4). Surprisingly, these cracked particles were mainly observed for the syntheses without stirring.

It was suspected that possibly the hydrothermal treatment and/or due to dissolution by the sodium hydroxide were the causes of the formation of these cracks on the particles of the silica gel (S432). To investigate this phenomenon, batches of silica gel and water ($SiO_2 + H_2O$) were placed in the Parr autoclave and subjected to the hydrothermal conditions with and without stirring at two different temperatures, namely 120°C and 150°C. Similarly, samples of silica gel, water and sodium hydroxide ($SiO_2 + H_2O + NaOH$) and silica gel, water, sodium hydroxide and

pyridine (SiO_2 + H_2O + NaOH + py) were also treated under the same reaction conditions.

The SEM micrographs of samples treated at 150°C are shown in Figure 6.29. If one compares the micrograph of the (SiO_2 + H_2O) sample treated under the unstirred conditions (Figure 6.29(a)) with the micrograph of the untreated silica gel (S432) (Figure 6.3(a)), it can be concluded that the particles of silica gel did not undergo any physical change, as can be observed from the similar structures and sizes of the particles, although one particle does show some small

(a)   (b)

(c)   (d)
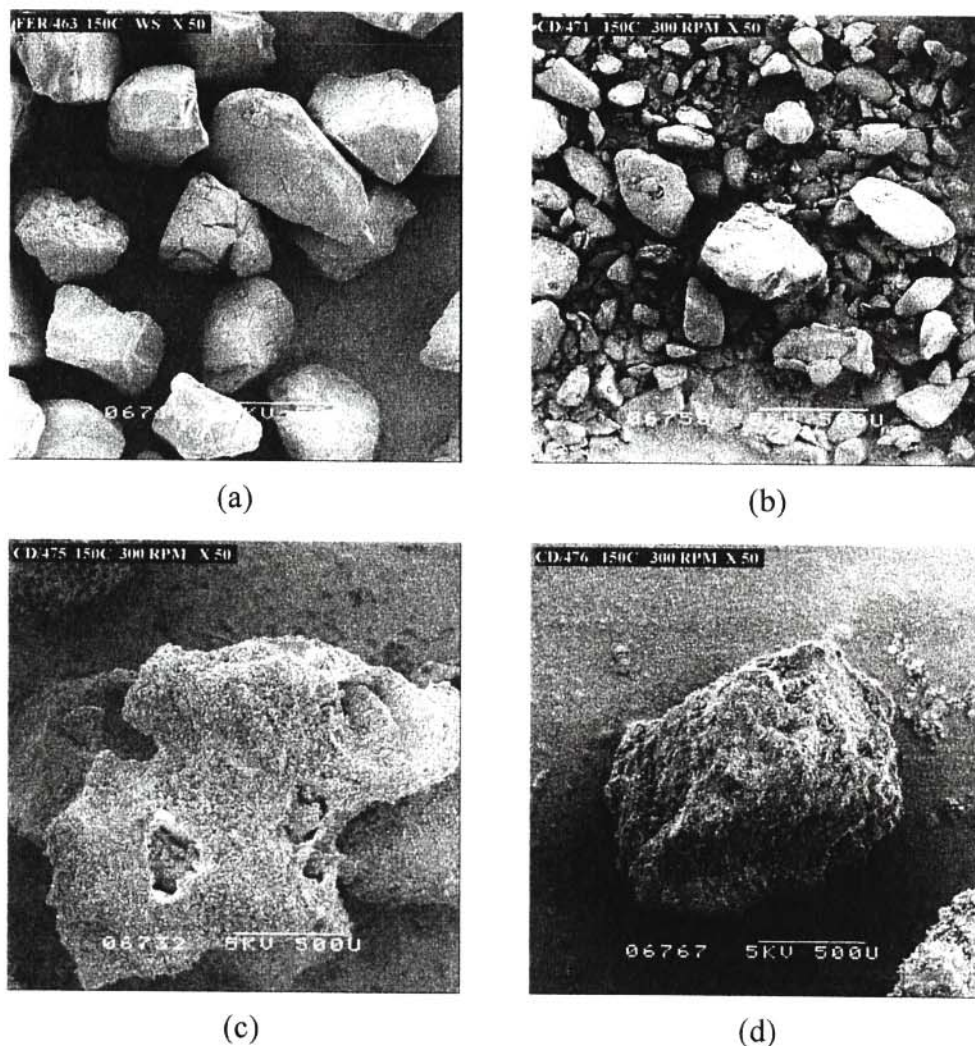
Figure 6.29 SEM micrographs of the samples hydrothermally treated with and without stirring at 150°C using different reagents: (a) (SiO_2 + H_2O) (unstirred), (b) (SiO_2 + H_2O) (stirred), (c) (SiO_2 + H_2O + NaOH) (stirred), and (d) (SiO_2 + H_2O + NaOH + py) (stirred).

cracks. However, when comparing the morphology of the (SiO_2 + H_2O) system treated without stirring, Figure 6.29(a), with the one with stirring, Figure 6.29(b), one readily observes that those of the latter are considerably smaller in size, indicating breakage during the treatment.

Figure 6.29(c) and Figure 6.29(d) are the micrographs of the samples treated hydrothermally at 150°C with stirring by using (SiO_2 + H_2O + NaOH) and (SiO_2 + H_2O + NaOH + py) respectively. In both cases bigger lumps with a rougher surface are observed, indicating that dissolution and precipitation have taken place due to the presence of sodium hydroxide. However, the above results do not clarify the issue of the formation of ferrierite crystallites on the cracked particles (e.g. Figure 6.26). Cracked particles were mainly observed at lower reaction temperatures. For this reason the above investigation was also repeated at the lower reaction temperature of 120°C.

The SEM micrographs of the samples synthesized with and without stirring at 120°C are shown in Figure 6.30. As was observed at the higher temperature (150°C), at 120°C the particles shown in the micrograph of the (SiO_2 + H_2O) unstirred sample (Figure 6.30(a)) are physically unchanged, whereas with the (SiO_2 + H_2O) stirred sample (Figure 6.30(b)) again shows the breakage of the silica particles.

The SEM results from the experiments where sodium hydroxide and sodium hydroxide and pyridine were added to the (SiO_2 + H_2O) system and hydrothermally treated without stirring are shown in Figure 6.30(c) and Figure 6.30(d). These micrographs show that most of the particles are cracked and no extensive dissolution is observed. It can thus be concluded that the formation of the cracks in the particles of the silica gel is due to the addition of sodium hydroxide to the reaction mixture.

(a)

(b)

(c)

(d)
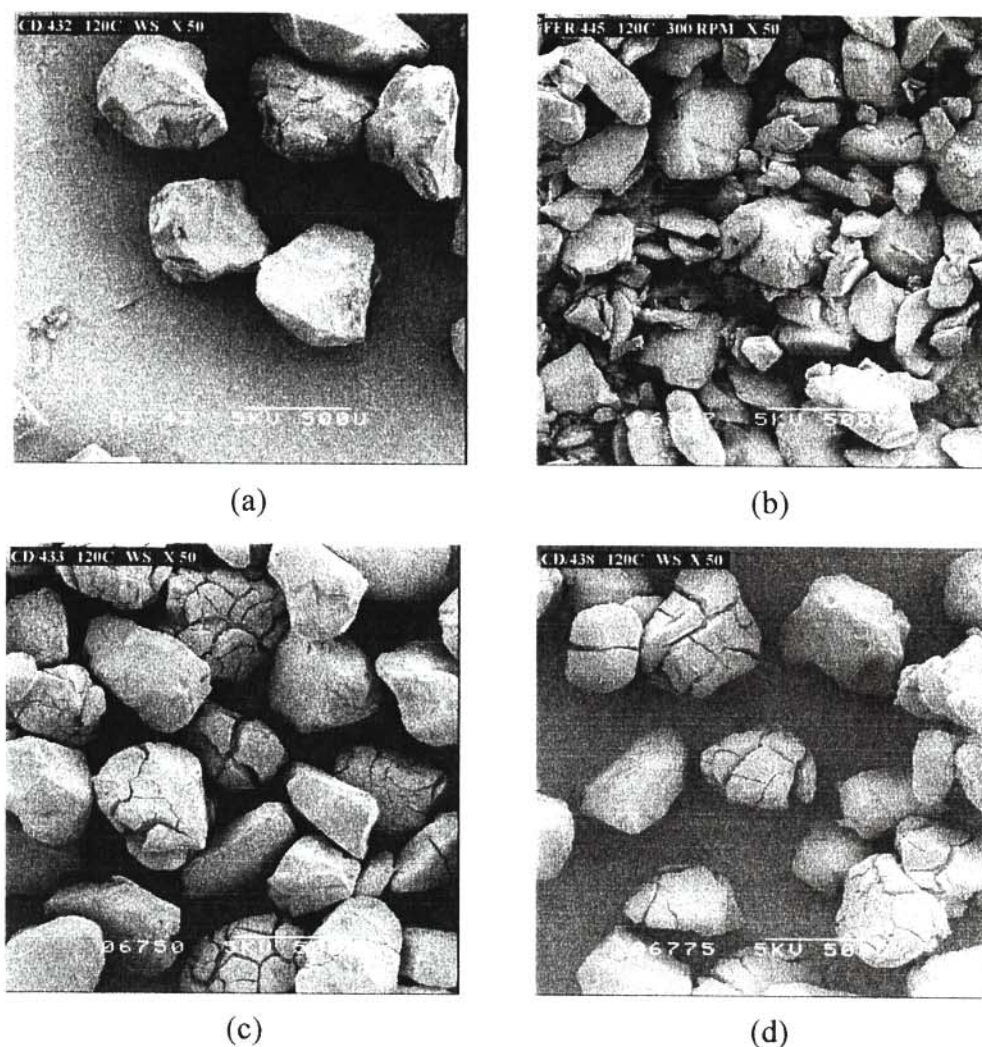
Figure 6.30 SEM micrographs of the samples hydrothermally treated with and without stirring at 120°C using different reagents: (a) (SiO_2 + H_2O) (unstirred), (b) (SiO_2 + H_2O)) (stirred) (c) (SiO_2 + H_2O + NaOH) (unstirred), and (d) (SiO_2 + H_2O + NaOH + py) (unstirred).

Since limited cracks are formed from the autoclaved suspension of silica gel in water at both temperatures, this indicates that perhaps thermal expansion may cause some crack formation. The presence of sodium hydroxide, however, appears to facilitate considerably the formation of these cracks. Furthermore, the results show that the sodium hydroxide leads to the dissolution of the silica gel particles at the higher temperatures, and therefore more cracks are evident at the lower temperatures than at higher temperatures, and that only limited dissolution occurs at the

lower temperatures. Crystallization therefore probably occurs from the dissolved silica gel in the reaction mixture on to the silica gel particles. In some of the ferrierite zeolite-based samples, silica gel particle crusts with crystallites on them were observed at temperatures up to 150°C (see Section 6.2 and Figure 6.4), while the inner sections of the particles were dissolved. An explanation might be that as soon as crystallization occurs (in the presence of an aluminium source) on the outer surface of the particle, dissolution is inhibited on that area. It is therefore to be expected that, since the cracked silica gel particles were broken under the stirring condition (see Figure 6.29(b) or Figure 6.30(b)), only crystals on cracked particles are observed with synthesis without stirring.

6.4 THE EFFECT OF PARTICLE SIZE

The effect of the particle sizes of the silica gel (S432) on the percentage XRD crystallinity and the morphology of the zeolite ferrierite synthesized using this particular synthesis method (Grandvallet et al., 1992) was also investigated. This investigation was conducted at a stirring rate of 100 rpm in the Parr autoclave (see Section 4.3.3.1). Grace (S432) silica gel particles of 2 mm diameter were ground and screened to smaller particle size fractions in the diameter ranges of 50 μm < d < 150 μm, 150 μm < d < 300 μm, 300 μm < d < 500 μm, 500 μm < d < 800 μm and 800 μm < d < 2 000 μm.

XRD analysis

The X-ray diffractograms of some of the samples synthesized using the different ranges of sieved particle sizes of silica gel are shown in Figure 6.31. Figure 6.31(a) is the diffractogram of the ferrierite-based material synthesized using particles with diameters between 50 μm < d < 150 μm. This shows all the characteristic peaks, which are indicative of a pure ferrierite. This is
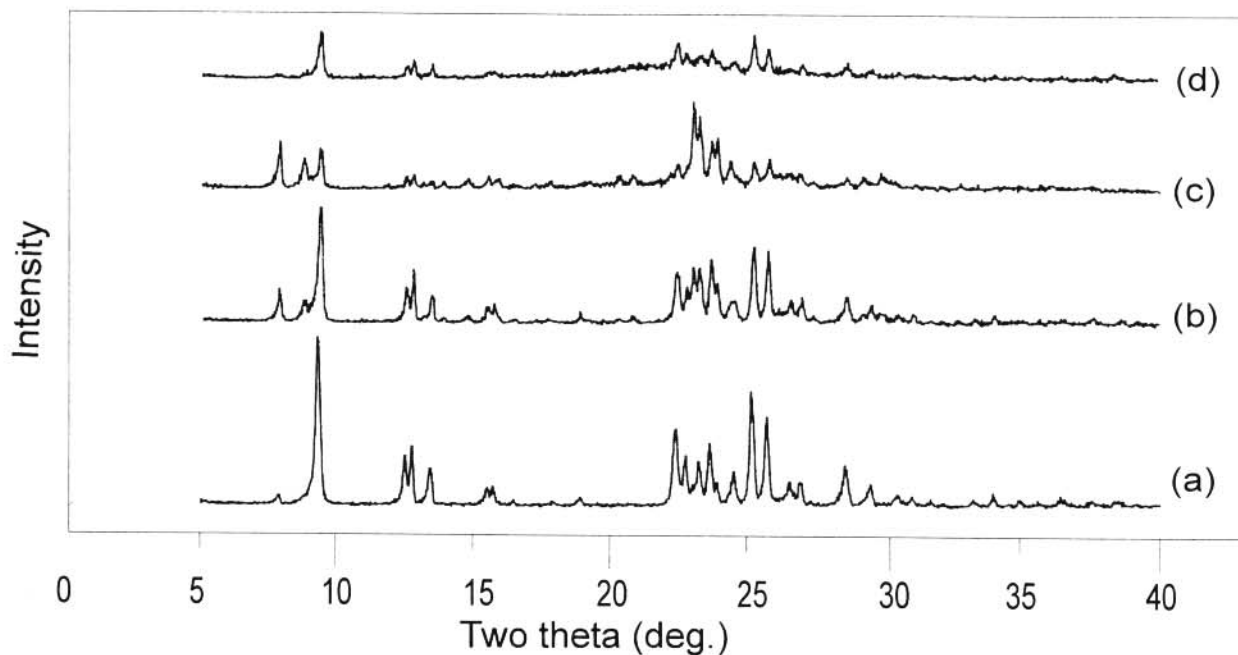
Figure 6.31 X-ray diffractograms of the ferrierite zeolite-based samples synthesized without stirring at 150°C with different particle sizes of the silica gel (S432): (a) 50 μm < d < 150 μm (batch no. 389), (b) 150 μm < d < 300 μm (batch no. 388), (c) 300 μm < d < 500 μm (batch no. 386), and (d) 800 μm < d < 2 000 μm (batch no. 346).

followed by a decrease in peak intensities with increasing particle sizes up to 800 μm < d < 2 000 μm, as shown in Figure 6.31(b) through to Figure 6.31(d). This indicates that with increasing particle size and without stirring, the rate of dissolution of the silica gel to produce a dissolved silica species is decreasing and becomes a limiting reagent resulting in lower percentage XRD crystallinities.

The percentage XRD crystallinities of the samples synthesized with the silica gel of different particle sizes are shown in Table 6.8. The results clearly show that the smaller the particle size, the higher the percentage XRD crystallinity of ferrierite-based samples produced, and this can

Table 6.8 Percentage XRD crystallinity of ferrierite-based samples synthesized without stirring by using different particle sizes of silica gel (S432)

Batch no.	Particle sizes (μm)	%XRD crystallinity
389	50 < d < 150	68
388	150 < d < 300	65
386	300 < d < 500	46
484	500 < d < 800	45
346	800 < d < 2 000	15

readily be observed in the bar diagram of percentage crystallinity as a function of particle sizes shown in Figure 6.32. The smaller particle sizes of the silica gel (S432) produce ferrierite-based materials of higher percentage XRD crystallinity for synthesis at a constant time and without stirring. This is therefore probably due to the better dissolution of the silica gel sample in the case of the smaller particle sizes.
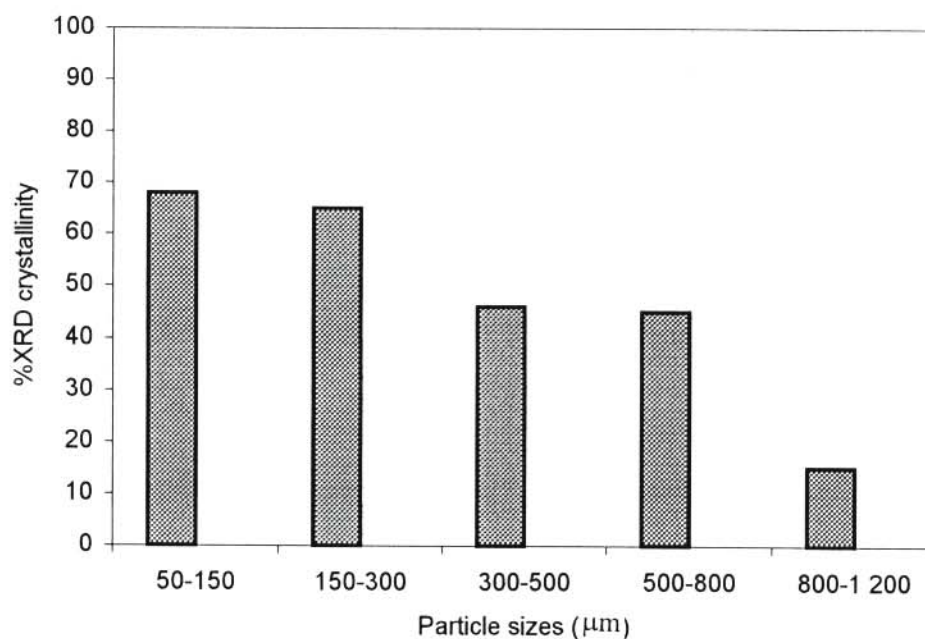
Figure 6.32 Bar diagram of percentage XRD crystallinity versus particle size of the silica gel for ferrierite-based materials synthesized without stirring at 150°C.

SEM analysis

The SEM results indicate that the morphology of these samples is similar to that of the ferrierite zeolite-based samples obtained in Section 6.2. SEM micrographs of the samples synthesized from two different particle size ranges are shown in Figure 6.33. At lower magnification (X 50) mainly clusters of crystallites (Figure 6.33(a)) are observed for samples synthesized with the smaller silica gel size range, while for the samples synthesized with the larger particles (Figure

(a)   (b)

(c)   (d)
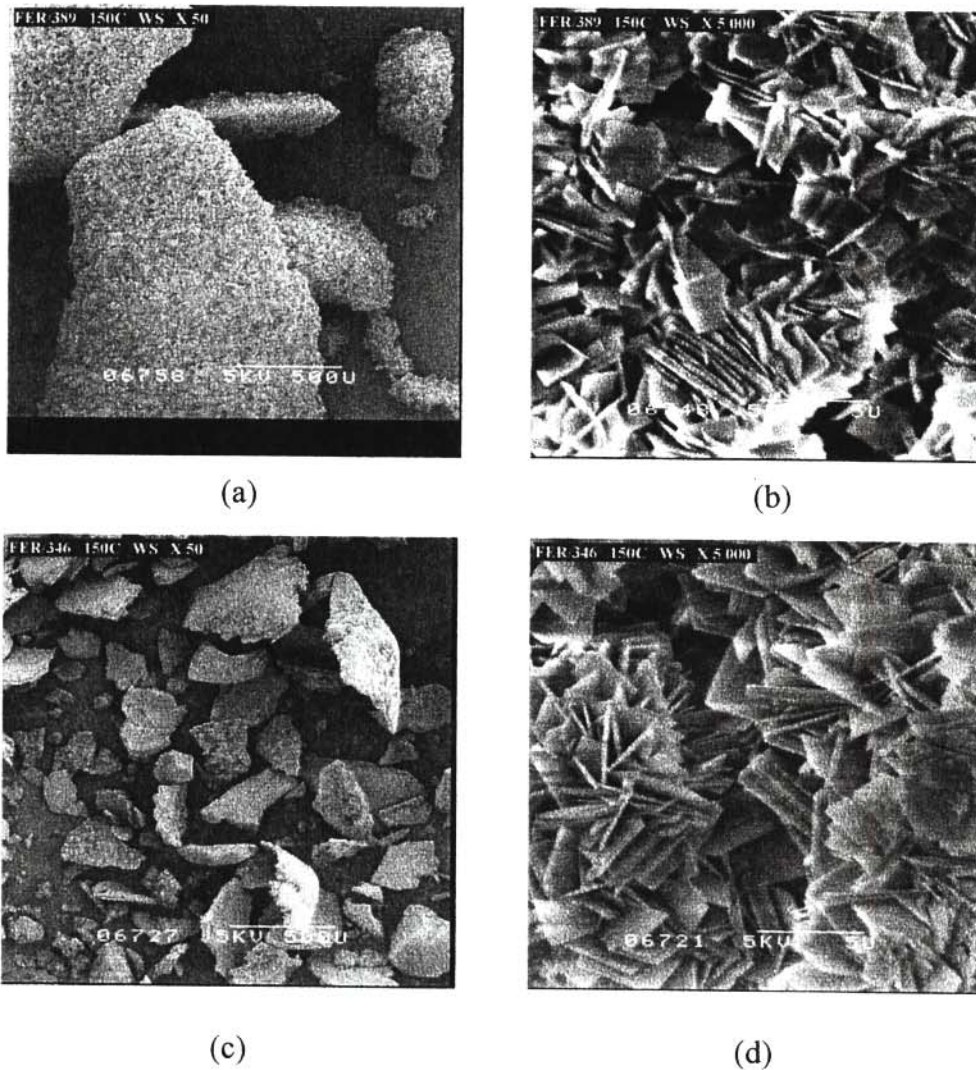
Figure 6.33 SEM micrographs of the ferrierite-based samples synthesized with different particle sizes of the silica gel: (a) 50 μm < d < 150 μm (X 50), (b) 50 μm < d < 150 μm (X 5 000), (c) 500 μm < d < 800 μm (X 50), and (d) 500 μm < d < 800 μm (5 000).

6.33(c)), where a lower overall crystallinity was determined, in addition to the typical crystalline material, also undissolved crusts and the inner parts of the particles are evident. The crystalline material at higher magnification for both samples show similar morphology, i.e. rectangular platelets.

6.5 LUDOX HS-30 METHOD

In this method ferrierite zeolite-based materials were synthesized for 80 hours according to the recipe of Xu *et al.* (1995a), using Ludox HS-30 as the silica source. This was done in the in-house built autoclave without stirring and with stirring at 1 250 rpm using a 52 mm X 8 mm magnetic stirrer bar (see Section 4.3.3.3).

6.5.1 Synthesis without stirring

Examples of the X-ray diffractograms of some of the ferrierite-based materials synthesized without stirring are shown in Figure 6.34. Figure 6.34(a) is the diffractogram of the ferrierite-based sample which was hydrothermally synthesized at 155°C. Only the hump, characteristic of amorphous material, is observed. Thus, for the syntheses using temperatures between 125°C and 155°C, only amorphous materials were obtained.

From 165°C and above, peaks are observed on the hump as is evident in Figure 6.34(b). In the diffractograms of the samples synthesized at 175°C to 205°C the characteristic peaks of ferrierite are clearly evident as shown in Figure 6.34(c) through to Figure 6.34(f). In addition to the ferrie-

Figure 6.34 X-ray diffractograms of ferrierite-based samples, and of other phases, synthesized without stirring at different temperatures using the Ludox-HS-30 method: (a) 155°C (batch no. 324), (b) 165°C (batch no. 360), (c) 175°C (batch no. 333), (d) 185°C (batch no. 238), (e) 195°C (batch no. 376), and (f) 205°C (batch no. 365).

rite peaks, there are peaks at 15.88° 2θ, 26.04° 2θ and 30.67° 2θ, which show the presence of analcime in the required ferrierite phase.

It was also observed that the hump appearing in the diffractogram of the substantially amorphous material diminishes at the higher temperatures as the crystallinity increases. No α-quartz peaks are observed in the samples using this synthesis method, as was the case when using silica gel (S432) as the source of silica (see Section 6.2).

The percentage XRD crystallinities of the ferrierite-based samples synthesized without stirring

Table 6.9 Percentage XRD crystallinities of the ferrierite phase in the samples synthesized without stirring at different temperatures using the Ludox HS-30 method

Batch no.	Synthesis temperature (°C)	%XRD crystallinity
339	125	0
316	135	0
320	145	0
324	155	0
360	165	1
333	175	13
328	185	37
376	195	28
365	205	32

using the Ludox HS-30 method are listed in Table 6.9. On average, the percentage XRD crystallinity of ferrierite increases with increasing temperatures up to 185°C after which a slight decrease occurs. Lower percentage XRD crystallinities are therefore obtained using the Ludox HS-30 method than when using the solid silica gel method.

SEM analysis

To illustrate how the morphology of the ferrierite-based samples synthesized according to this recipe and without stirring and at different temperatures differ, SEM micrographs of certain representative samples are shown in Figure 6.35. Figure 6.35(a) shows the SEM micrograph of the 0% amorphous materials "synthesized" at 155°C. In this sample the formation of "sponge-like" spheroids among the finer amorphous materials is observed. These spheroids could possibly be the solid phase present at the initial stage before crystallization starts. Figure 6.35(b) shows some of the above-mentioned spheroids magnified to X 5 000 to show the sponge-like morphology of the spheroids.
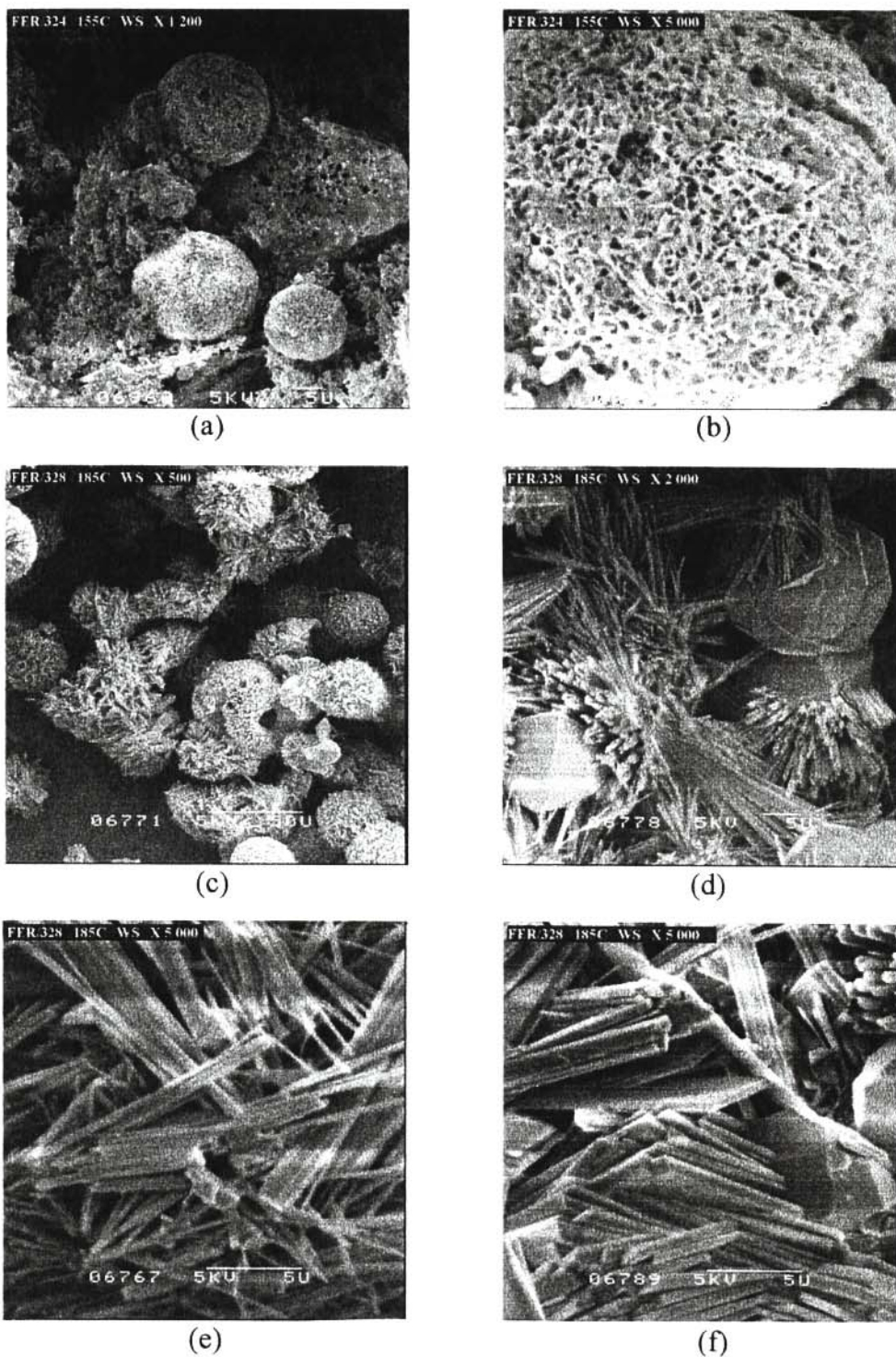
Figure 6.35 SEM micrographs of the ferrierite-based samples, and of other phases, synthesized without stirring at different temperatures using the Ludox HS-30 method: (a) 155°C (X 1 200), (b) 155°C (X 5 000), (c) 185°C (X 500), (d) 185°C (X 2 000), (e) 185°C (X 5 000) and (f) 185°C (X 5 000, another spot).

Figure 6.35(c) to Figure 6.35(f) show the structure of a sample synthesized at 185°C where 37% crystallinity was determined. In addition to the sponge-like spheroids, spheroids which look like pincushions covered with needles are also observed in this sample as shown in Figure 6.35(c) which is a spot magnified to X 500. Limited amounts of spheroidal crystallites are also observed in this sample. At the magnification of X 2 000 (Figure 6.35(d)), needle-like crystallites as well as the spheroidal crystallites could be observed. It is possible that these spheroidal crystallites are analcime which is present in a limited amount in this sample. Two spots which are further magnified to X 5 000 are also shown. In Figure 6.35(e) the needle-like morphology is evident, which is also the morphology reported by Xu *et al.* (1995a) for ferrierite using the Ludox HS-30 recipe. Figure 6.35(f) shows that in addition to the needle-like structures there are a few rectangular plates of ferrierite crystals and again some spheroidal crystallites.

6.5.2 Synthesis with stirring

XRD analysis

The X-ray diffractograms of some of the ferrierite-based samples prepared with stirring are shown in Figure 6.36. Figure 6.36(a) is a diffractogram of a ferrierite-based sample synthesized at 125°C. A hump is again observed. Unlike in the case of the samples synthesized without stirring, where no peak was observed up to the synthesis temperature of 165°C, in this case the characteristic peaks are already observed on the hump in the diffractogams of the samples synthesized at 135°C (Figure 6.36(b)) and higher. These peak intensities increase with an increase in synthesis temperature up to 205°C (see Figure 6.36(c) and Figure 6.36(d)). The peaks obtained with these samples synthesized using this method are broader than the peaks obtained with the unstirred mode of synthesis and other methods. This suggests the formation of extreme-
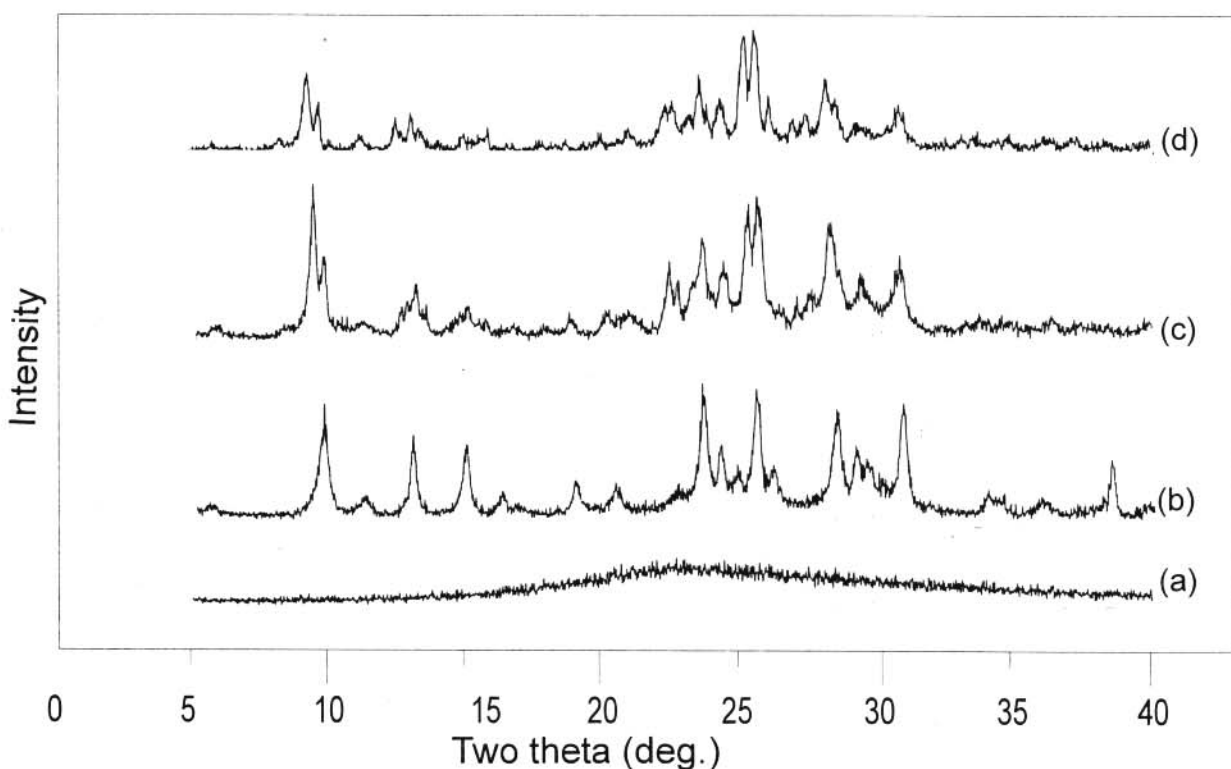
Figure 6.36 X-ray diffractograms of ferrierite-based samples, and of other phases, synthesized with stirring at different temperatures using the Ludox HS-30 method: (a) 125°C (batch no. 428), (b) 135°C (batch no. 390), (c) 175°C (batch no. 402), and (d) 205°C (batch no. 419).

ly small particle sizes (see SEM results below). In addition to the characteristic peaks of ferrierite, there are analcime peaks present at 15.88° 2θ, 26.04° 2θ and 30.67° 2θ for the samples synthesized at higher temperatures (from 185°C), which were also observed in the un-stirred mode of synthesis, but in that case they are also observed at lower temperatures (165°C).

The percentage XRD crystallinities for the ferrierite zeolite samples synthesized with stirring using the Ludox HS-30 method are shown in Table 6.10. On average an increase in percentage XRD crystallinity is observed with increasing reaction temperature, but the crystallinities are lower than those ones obtained with the silica gel method.

Table 6.10 Percentage XRD crystallinities of the ferrierite phase in the samples synthesized with stirring at different temperatures using the Ludox HS-30 method

Batch no.	Synthesis temperature ($^{\circ}$C)	%XRD crystallinity
428	125	0
390	135	13
397	145	18
425	155	6
413	165	19
402	175	20
377	185	17
404	195	24
419	205	32

SEM analysis

To illustrate the morphology of the zeolite synthesized with stirring using the Ludox HS-30 method, the SEM micrographs of some of the samples synthesized under these conditions are shown in Figure 6.37. Figure 6.37(a) is the SEM micrograph of the 0% crystallinity sample synthesized at 125°C. The amorphous phase is readily evident. Figure 6.37(b) is the micrograph of the sample synthesized at 145°C, which is 18% XRD crystalline. A mixture of very small crystallites and amorphous materials are observed in this figure. This shows that the crystallites so formed are small and mixed up with the amorphous material. Small broken needle-like crystalites of ferrierite are observed in Figure 6.37(c), which is the sample synthesized at 175°C. Figure 6.37(d) shows the micrograph of the sample synthesized at 205°C and which consists of a mixture of ferrierite and analcime. Although the crystals observed here are also broken, they appear to possess a different morphology, a feature probably due to the mixture of zeolitic phases.
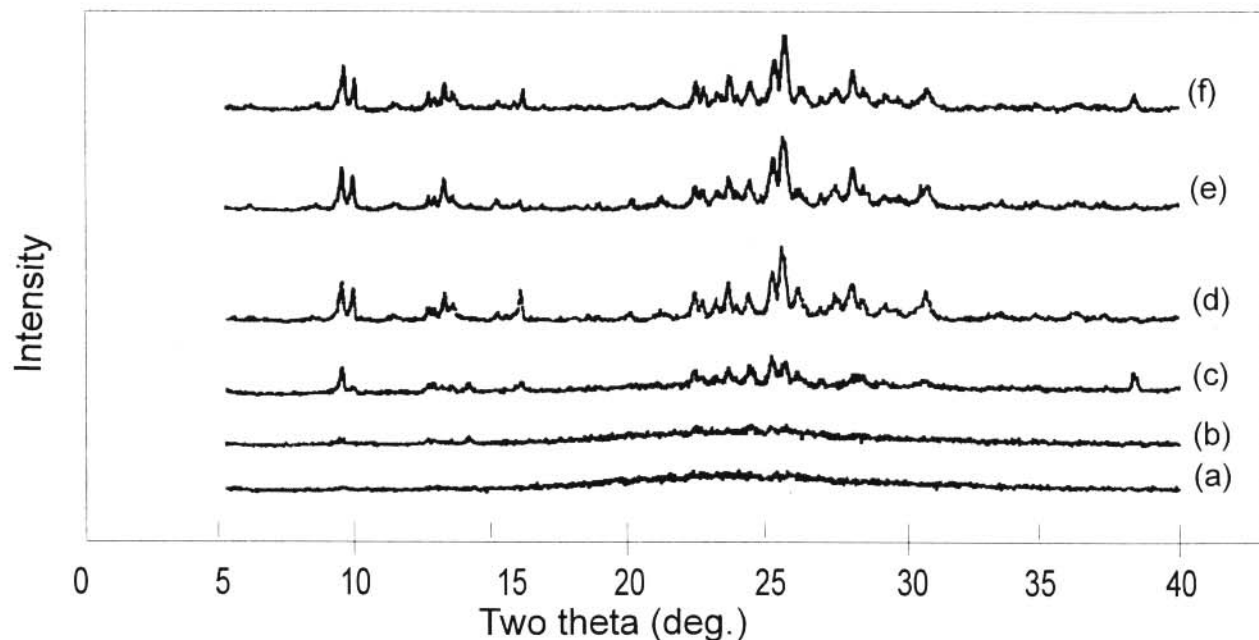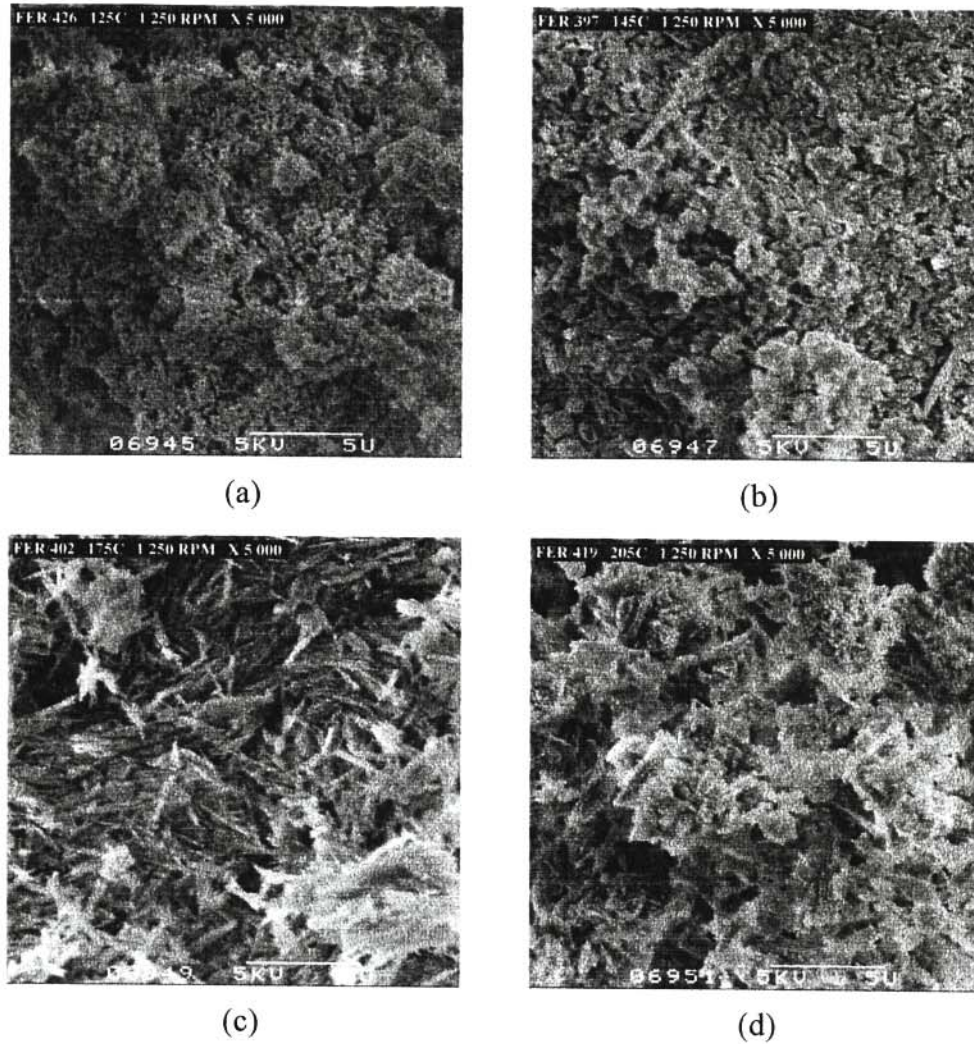
Figure 6.37 SEM micrographs of the ferrierite-based samples, and other phases, synthesized with stirring at different temperatures using the Ludox HS-30 method: (a) 125°C, (b) 145°C, (c) 175°C and (d) 205°C.

6.5.3 Comparison of results

The percentage XRD crystallinity as a function of synthesis temperature for the samples synthesized with and without stirring are shown in Figure 6.38. It can be observed that the crystallization of the samples prepared without stirring starts at a higher temperature than for the

samples synthesized with stirring. The percentage crystallinity for the with-stirring samples increases almost linearly with the maximum of 32%, while those prepared without stirring increase with increasing synthesis temperature, above 165°C, up to 37% XRD crystallinity at the synthesis temperature of 185°C. This is followed by a decrease in percentage crystallinity with increasing temperature up to 205°C. In addition to the formation of the zeolite ferrierite, the zeolite analcime also crystallized, but no α-quartz phase was observed as was the case in the silica gel (S432) method. Furthermore, unlike in the silica gel S432 method, the relative amounts of the impure crystalline phase (analcime) decreases with an increase in synthesis temperature. The ferrierite prepared according to this method has mainly a needle-like structure, while the crystallites formed with the silica gel (S432) method showed a platelet morphology.
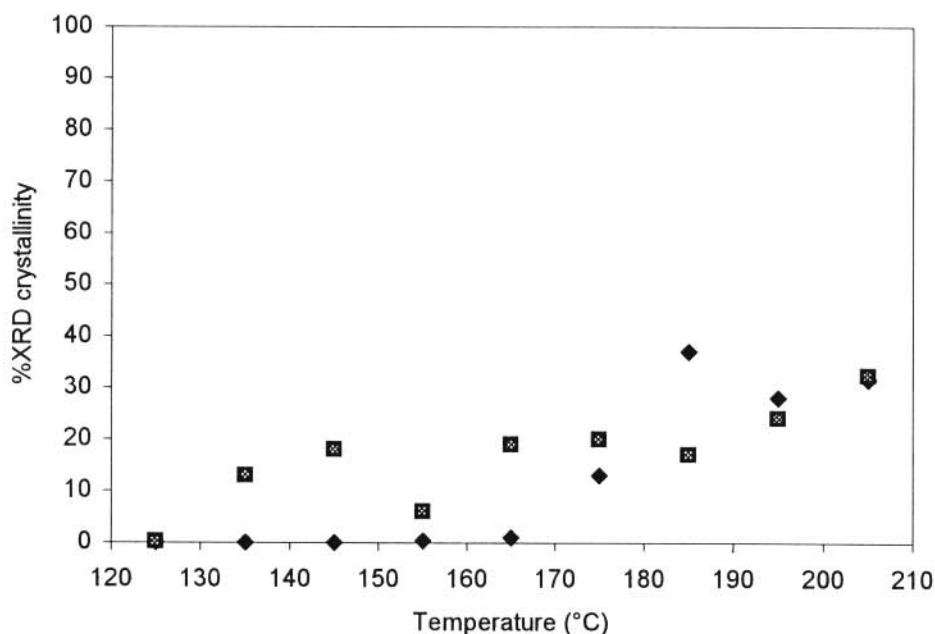
Figure 6.38 Plot of percentage XRD crystallinity of the ferrierite phase versus synthesis temperature for ferrierite-based samples synthesized with stirring (■) and without stirring (♦) using the Ludox HS-30 method.

6.6 CONCLUSIONS

The percentage XRD crystallinity of the ferrierite zeolite-based samples obtained by hydrothermal synthesis at different temperatures and using different methods of synthesis show that there is an increase in percentage XRD crystallinity with increasing synthesis temperature up to a certain temperature (e.g. 150°C in the silica gel method), then a decrease in percentage XRD crystallinity with increasing synthesis temperature thereafter. The decrease in percentage XRD crystallinity is concomitant with the formation of the analcime and/or of the α-quartz phase in the required phase depending on which synthesis method is used.

We also showed that the samples synthesized in the Parr autoclave are more crystalline than the samples synthesized in the in-house built autoclave. It is possible that the complicated internal structure of the Parr autoclave contributed in seeding the crystallization process by trapping some ferrierite product from a previous run in the autoclave's tubing system, which could then act as seed for the subsequent run. Thus, our methodology for cleaning the Parr autoclave (see Section 4.3.1) were probably not as efficient as it was thought.

It is therefore clearly shown from this study that the choice of the autoclave for the zeolite synthesis is one of the crucial parameters in zeolite preparation. When making a choice, the construction of the autoclave to be used should be given high consideration.

The cracks observed on the particles of silica gel (S432) are probably formed by thermal expansion and the presence of sodium hydroxide. It was also observed that the particle sizes of the silica gel (at a constant hydrothermal synthesis time, e.g. 75 hours) have a significant

influence on the XRD crystallinity of the product. The smaller particle sizes produced ferrierite-based materials of higher crystalliniy than the larger particles.

The choice of the synthesis method used (using different silica sources) is also a crucial parameter to be considered in ferrierite synthesis. This affects both the percentage XRD crystallinity and the morphology of the zeolite so formed. It also influences the transformation of ferrierite into other crystalline phases.

The percentage XRD crystallinities for the ferrierite zeolite samples obtained by hydrothermal synthesis at different temperatures, both with and without stirring under the different stirring conditions investigated, are generally and reasonably reproducible. This conclusion is made from the relatively smooth plots of the experimental values in all the figures, except for Figure 6.23 which was for seeding with stirring. These results compare favourable with those obtained for the synthesis of ZSM-5 zeolite which was discussed in Section 5.5. However, for the synthesis of ferrierite zeolite at 130°C, with and without stirring in the Parr autoclave, and with stirring in the in-house built autoclave, there was a large deviation in the percentage XRD crystallinities obtained. Irreproducibility was also observed for the samples synthesized at 0 rpm and 150°C where the effect of different stirring rates was investigated (see Figure 6.6).

CHAPTER SEVEN

CONCLUSIONS

Although conclusions were made in all the previous sections, a recapitulation of our general conclusions is given in this chapter. It should be borne in mind that the results reported in this thesis were obtained by using several recipes (methods) for the synthesis of each type of zeolite and using two types of autoclaves.

It was observed that there is a change in percentage XRD crystallinity with a change in synthesis temperature for both ZSM-5 and ferrierite zeolite-based materials with all the methods/recipes used in this project. The smooth curves obtained emphasize the reproducibility of the results obtained, which are in agreement with earlier studies (Ramatsetse, 1998). Although a change in stirring rate did not show a dramatic effect on the percentage XRD crystallinity and morphology of the zeolites ZSM-5 and ferrierite, the unstirred and the stirred samples did, however, show a difference in both percentage XRD crystallinity and morphology for these two zeolites, when all the other synthesis parameters were maintained. In addition, the morphology of both the ZSM-5-based and the ferrierite-based materials changed completely once the recipe was changed. Therefore, by manipulating the investigated synthesis parameters, it is possible to prepare zeolite-based materials at different levels of percentage XRD crystallinity, from the substantially amorphous through to the partially crystalline and to the highly crystalline.

When two different autoclaves were used for the hydrothermal synthesis of the ZSM-5-based materials and using the same recipe, viz. the Aerosil 200 method, similar results (in terms of

percentage XRD crystallinity) were obtained for synthesis without stirring as can be observed in Figure 5.14. However, a difference was obtained when the same zeolite-based materials (using the same recipe) were synthesized with stirring (see Figure 5.15). This can be attributed to the fact that the two stirring rates were different (a setting of 1 000 rpm for the in-house built autoclave with a magnetic stirrer bar and 100 rpm for the Parr autoclave with mechanical stirring from the top).

For the ferrierite-based materials, the trend followed by the percentage XRD crystallinity differed when this zeolite was synthesized without stirring using the same recipe, viz. the silica gel (S432) method, but in the different two autoclaves (see Figure 6.25). Crystallization started at lower temperatures (about 130°C) for the samples synthesized both with and without stirring in the Parr autoclave (see Figure 6.14). This observation is in contrast to those made previously (see Figure 2.7) using the in-house built autoclave where the crystallization of the stirred samples started at 130°C, and that of the samples prepared without stirring at 150°C. It is believed that the Parr autoclave seeded the reaction mixture, since it was later found that a certain amount of solid seed materials, which could act as seed for the reaction, are trapped in the complicated structure of the stirring and sampling system of the Parr autoclave. Both the top and bottom stirred autoclaves break the crystals of the ferrierite-based materials and result in the formation of a snowflake-type morphology.

In most of the recipes used for the synthesis of ZSM-5 zeolite-based materials, the morphology changed with the change in synthesis temperature (see Table 5.22). An example of which is the formation of spheroids at lower temperatures and of crystallites of definite shapes at higher temperatures (see Figure 5.3 and Figure 5.20, which are micrographs obtained from the Aerosil and water glass methods respectively). Our work also showed that the different recipes for

zeolite syntheses may produce the same percentage XRD crystallinities but different morphologies. The change in morphology with the change in synthesis recipes is observed even if other parameters are kept constant (e.g the silica source, the template, etc.) and only one or more additional species is added, or using a different sequence of adding those reagents. An example of this change in morphology is observed in the Aerosil 200 method (Section 5.2) and the Aerosil 200 and glycerol method (Section 5.3.3). In both cases tetrapropylammonium bromide was used as the template, but the morphologies of the ZSM-5-based products so formed differed totally as evident from Figure 5.13 and Figure 5.32 respectively.

A comparison of our ZSM-5 results in terms of percentage XRD crystallinity versus synthesis temperature for the different ZSM-5 recipes are shown in Figure 7.1 and Figure 7.2 for without
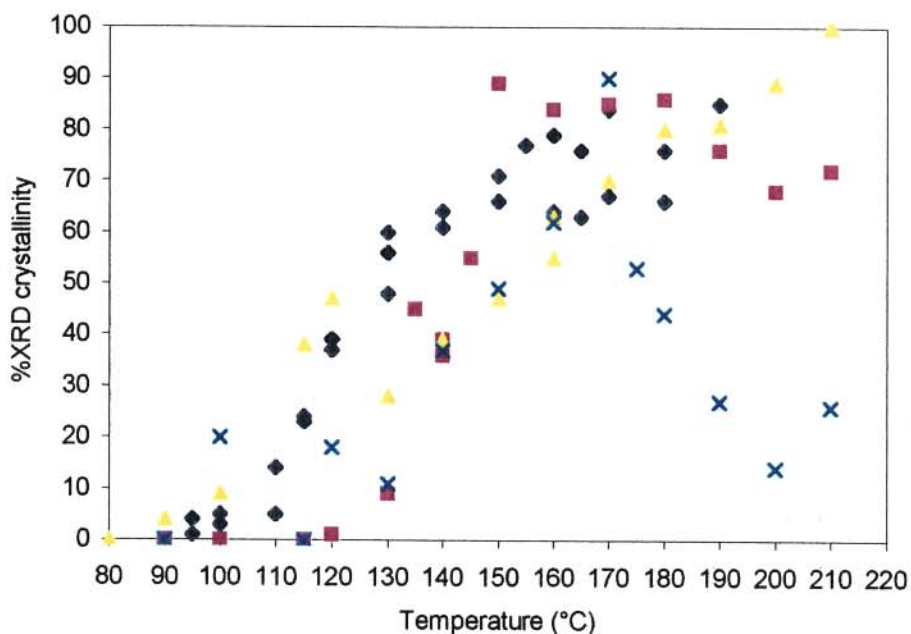
Figure 7.1 Plots of percentage XRD crystallinity of the ZSM-5 phase of the materials prepared without stirring at different hydrothermal synthesis temperatures using different methods: Aerosil 200 method (♦), water glass method (■), silicic acid method (▲), and Aerosil 200 and glycerol method (✕).
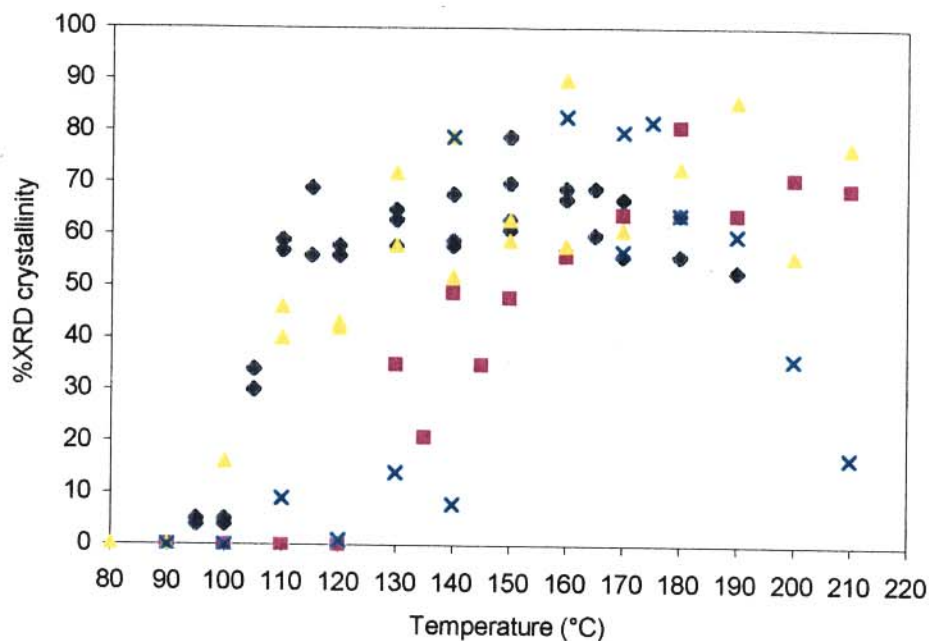
Figure 7.2 Plots of percentage XRD crystallinity of the ZSM-5 phase of the materials prepared with stirring at different hydrothermal synthesis temperatures using different methods: Aerosil 200 method (♦), water glass method (■), silicic acid method (▲) and Aerosil and glycerol method (✗).

stirring and for with stirring samples respectively synthesized in the in-house built autoclave. There is an increase in percentage XRD crystallinity with increasing synthesis temperature. The trends followed by these percentage XRD crystallinities as a function of temperature differ from one method to the other. These range from linear to sigmoidal plots for the synthesis of the ZSM-5-based materials. Thus, some recipes permit samples to be obtained at different percentage crystallinities (controllability) while others, due to the sharp increase in XRD crystal-linities at small temperature increments (S-shaped curves), do not allow this to be achieved.

From the four recipes used for ZSM-5 synthesis, the method in which silicic acid was used as a silica source, has some outstanding features. Although some of the reagents used in this method

are expensive, under the unstirred mode of synthesis, this method gave the highest percentage XRD crystallinity within the shortest time (44 hours and at 210°C). As a consequence, this sample was used as a standard in this project. This is also the only method that gave a linear plot of percentage XRD crystallinity versus synthesis temperature (hence a controllable method).

In addition to the controllable silicic acid method used without stirring, substantially amorphous ZSM-5-based materials (< 30% XRD crystallinity) could also be prepared controllably using the Aerosil 200 method, unstirred with hydrothermal treatment between 90°C and 120°C. It should be remembered that ZSM-5-based materials of low percentage XRD crystallinity are important for the skeletal isomerization of *n*-butene to iso-butene (Nicolaides, 1996) and possibly of other alkenes. Also, this recipe can be employed to synthesize the partially crystalline materials (30% < percentage XRD crystallinity < 70%), in the temperature range of 120°C and 150°C. Although the reaction time is longer (72 hours) for this method than for the silicic acid method (44 hours), the mass yield is higher.

Although it was possible to synthesize highly crystalline zeolites (> 70% XRD crystallinity) at temperatures usually above 150°C, with all methods under consideration, the only method investigated that gave pure ZSM-5 materials and controllable crystallinities in this range is the silicic acid method used without stirring.

A catalytic test reaction (CTR) such as *n*-hexane cracking is one of the techniques employed to supplement the XRD and SEM results for the characterization of the samples. The CTR technique clearly showed that there are some properties of zeolites which cannot be evaluated by either XRD or SEM. It was found that zeolite samples of almost the same percentage XRD crystallinities, but synthesized in different ways, did not necessarily have the same catalytic

properties, and that the percentage XRD crystallinity is not the only characteristic of the zeolites that can be used to predict the catalytic properties of these zeolite-based materials. The cracking of *n*-hexane over these ZSM-5-based materials showed that the highly crystalline samples synthesized with stirring are more active than the samples of similar crystallinity, but synthesized without stirring and which have formed bigger crystallites. Similar observations were made with propane as feed, although the effect of the morphology of zeolitic materials was not as conspicuous as for *n*-hexane cracking. This could be ascribed to the lower diffusional limitations with propane due to its smaller carbon chain length.

The summaries of the ferrierite results in terms of percentage XRD crystallinity versus synthesis temperature for the two different ferrierite recipes are shown in Figure 7.3 and Figure 7.4 for the
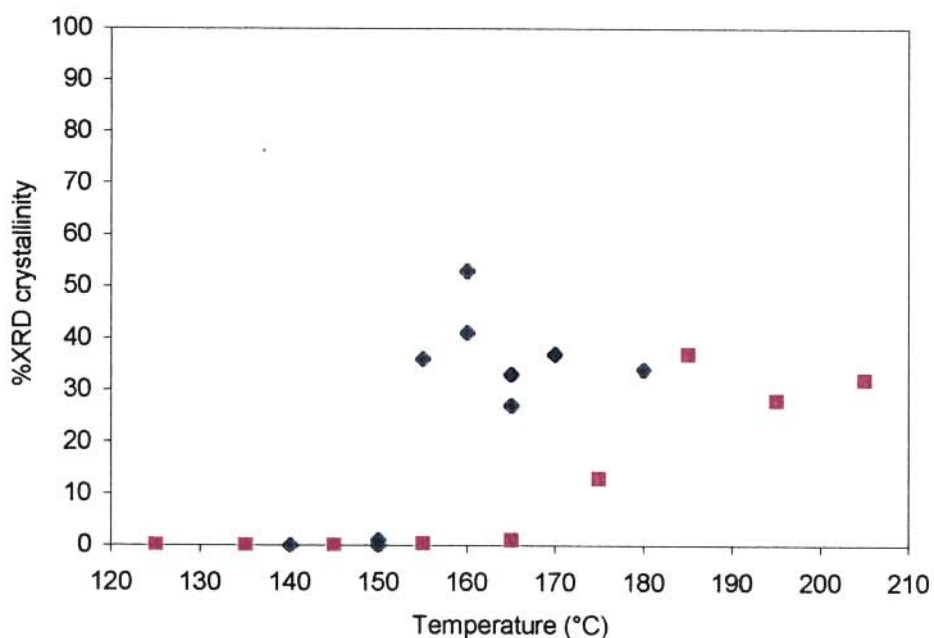
Figure 7.3 Plots of percentage XRD crystallinity of the ferrierite phase of the materials prepared without stirring at different hydrothermal synthesis temperatures using different methods: silica gel method (♦) and Ludox method (■).
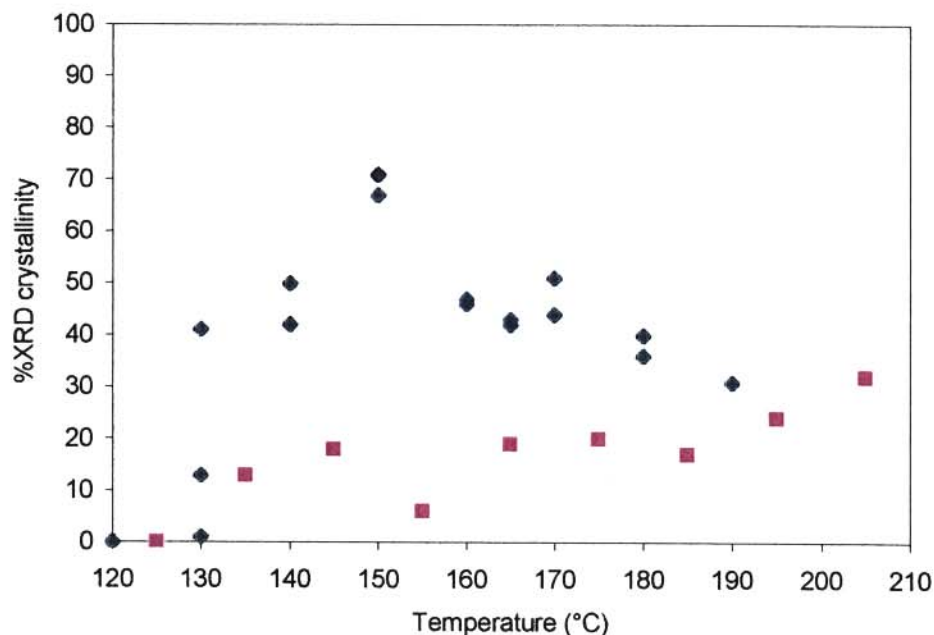
Figure 7.4 Plots of percentage XRD crystallinity of the ferrierite phase of the materials prepared with stirring at different hydrothermal synthesis temperatures using the silica gel method (♦) and Ludox method (■).

preparations without stirring and with stirring samples respectively. The in-house built autoclave was used for all these ferrierite syntheses. The results show that there is a general increase in percentage XRD crystallinities with increasing synthesis temperatures up to a certain temperature, except for the Ludox method synthesized with stirring where the crystallinity kept increasing up to the highest temperature investigated, viz. 210°C. Beyond this temperature (where maximum crystallinity was obtained), there is a decrease in percentage XRD crystallinity concomitant with the formation of totally different zeolitic phases, which were found by XRD to be α-quartz and/or analcime depending on the method used. Even for the preparation according to the Ludox HS-30 method with stirring, where no decline in percentage XRD crystallinity was obtained at higher temperatures, analcime was formed as an additional phase at synthesis temperatures above 185°C.

From the above figures it can further be observed that the without stirring mode gives lower percentages XRD crystallinity than synthesis with stirring for ferrierite with both recipes, especially at lower temperatures. Figure 7.4 shows that in order to obtain ferrierite-based materials with high percentage XRD crystallinities and without impurities (different phases), the silica gel (S432) method should be employed at temperatures from 130°C to 150°C, while the Ludox method can be used for the synthesis of samples of lower percentage crystallinities.

Also with ferrierite, a change in morphology with a change in synthesis method was obtained. The silica gel (S432) method produces inter-grown rectangular platelets with the unstirred samples (see Figure 6.4) and snowflake morphology with the stirred samples (see Figure 6.9), whereas the water glass recipe gave rectangular plates with flower-like structures on top in some cases (see Figure 6.16). In the case of the Ludox HS-30 method, needle-like crystals are observed for the preparations without stirring (Figure 6.35) and broken needle-like crystallites when the reaction mixture was stirred.

The studies showed that different particle sizes of the ground silica gel (S432) produce different crystallinities of zeolite ferrierite-based materials under the same reaction conditions. The larger the particle size, the lower the percentage XRD crystallinity (see Figure 6.33). This emphasizes the fact that silica gel of smaller particle sizes should be used for the synthesis of ferrierite samples of high percentage XRD crystallinities, if this is the desired product. For lower crystallinity ferrierite samples, therefore, large particle sizes of silica gel ought to be used. Our studies also showed that the cracks observed in the silica gel particles for the synthesis in both autoclaves appears to be caused by the presence of sodium hydroxide and the thermal expansion.

Future research

A project that may be developed from this work is one that involves the other ZSM-5-based samples which were prepared via the different recipes and having the same percentage XRD crystallinities and their characterization by CTR's such as *n*-hexane and propane cracking in order to obtain a fuller understanding of the effect of percentage XRD crystallinity, morphology and particle sizes on catalytic activity. Other CTR's, apart from the ones mentioned, may also be studied.

It would be interesting if the recipes were duplicated with all the reagents used except for the silica source which would be substituted by fly-ash in each case. This work would aim at investigating the effect of this cheap silica source (Park *et al.*, 2000) on the morphology and particle sizes in terms of the catalytic properties of the above-mentioned zeolites. Fly-ash was used in attempts to synthesize other zeolites such as cancrinite (Park *et al.*, 2000), but no work has been published on the synthesis of ZSM-5 and ferrierite using fly-ash as a silica source. It would be interesting if the effect of different methods (not recipes), for example hydrothermal, non-aqueous, kneading and molten-salt, on the percentage XRD crystallinity and morphology of these samples were investigated.

APPENDICES

APPENDIX A

Gas chromatograms of the products from propane cracking over H-ZSM-5-based samples of different percentage XRD crystallinities synthesized with stirring in the Parr autoclave


```
CHANNEL A      INJECT           01:05:22
          .59
0.18
                                    3.11

                                                        12.89

                                    16.50
        17.30
```

```
                              01:05:22    CH= "A"  PS=  1.
FILE  1.     METHOD  0.     RUN  22     INDEX  22
PEAK#      AREA%       RT        AREA BC

   1       0.005      0.59        251  01
   2       0.013      2.18        633  01
   3       2.259      3.11     114074  01
   4      94.471     12.89    4771131  01
   5       1.961     16.5       99017  02
   6       1.293     17.3       65279  03

TOTAL    100.                 5050385
```
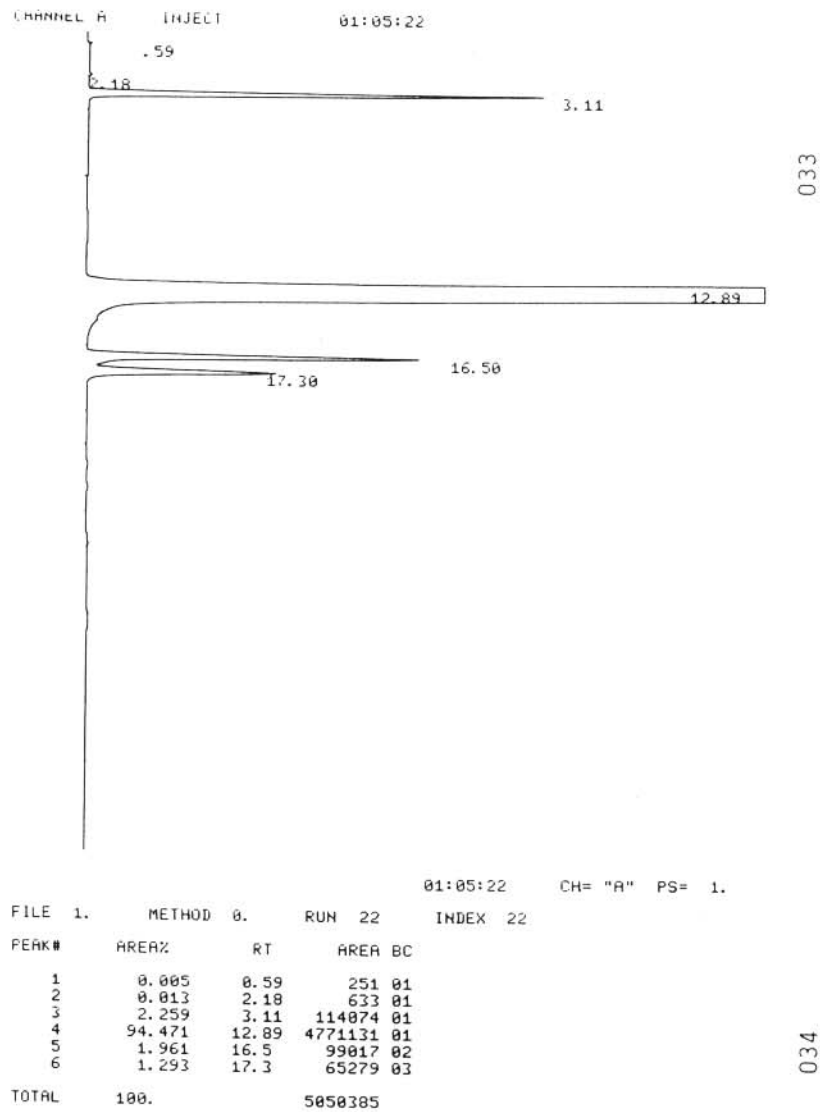
Chromatogram A.1 Propane cracking over the 2% XRD crystalline H-ZSM-5-based sample.

CHANNEL A   INJECT   22:07:23

.57

2.15

3.06

12.83

16.47

17.24

24.96

22:07:23   CH= "A"   PS= 1.

031
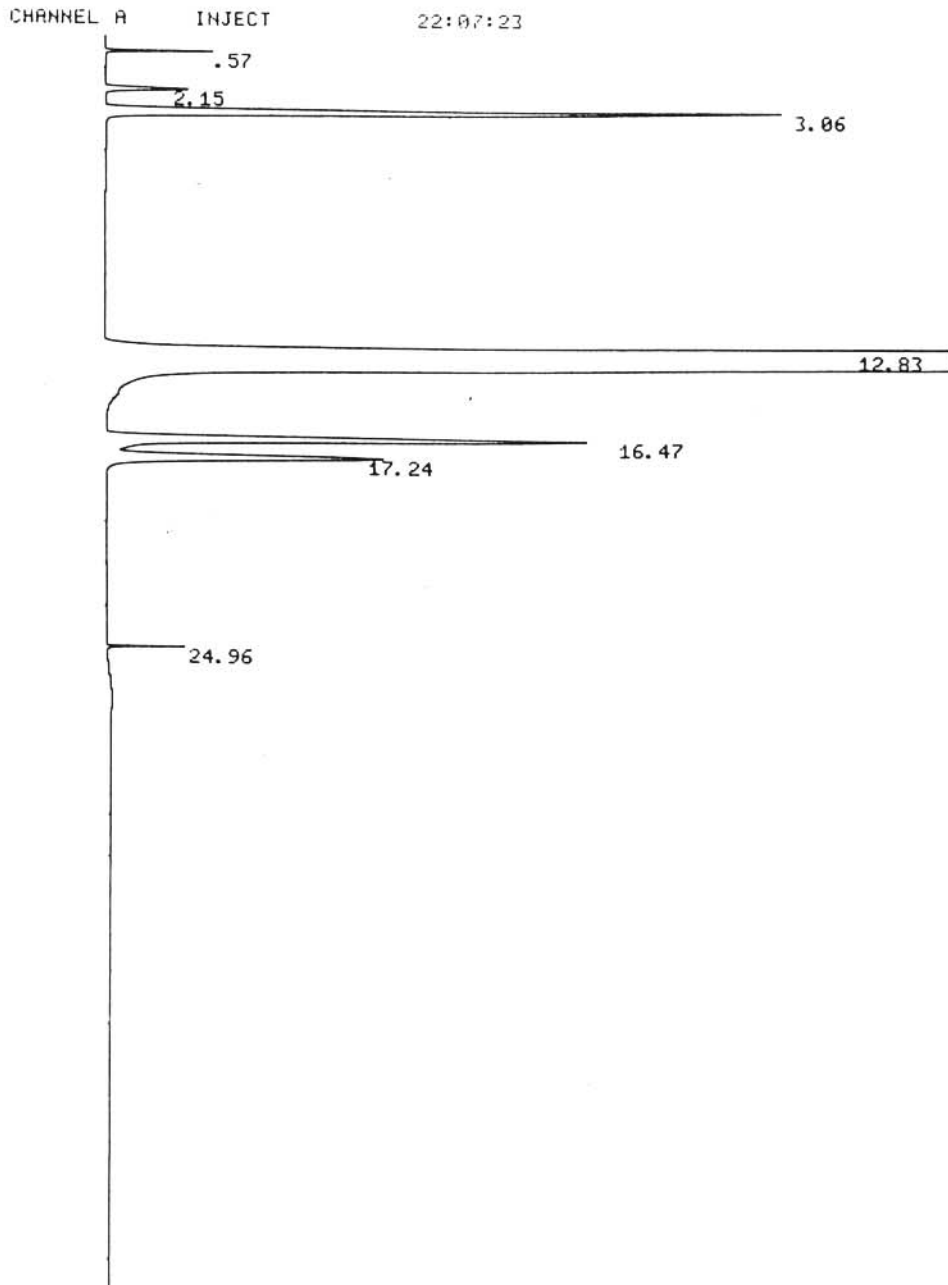
FILE 1.   METHOD 0.   RUN 20   INDEX 20

PEAK#	AREA%	RT	AREA	BC
1	0.101	0.57	5989	01
2	0.185	2.15	10985	01
3	2.267	3.06	134854	01
4	94.291	12.83	5609188	01
5	1.882	16.47	111959	02
6	1.234	17.24	73390	03
7	0.042	24.96	2471	01

TOTAL   100.   5948836

Chromatogram A.2 Propane cracking over the 18% XRD crystalline H-ZSM-5-based sample.

CHANNEL A   INJECT   05:46:43
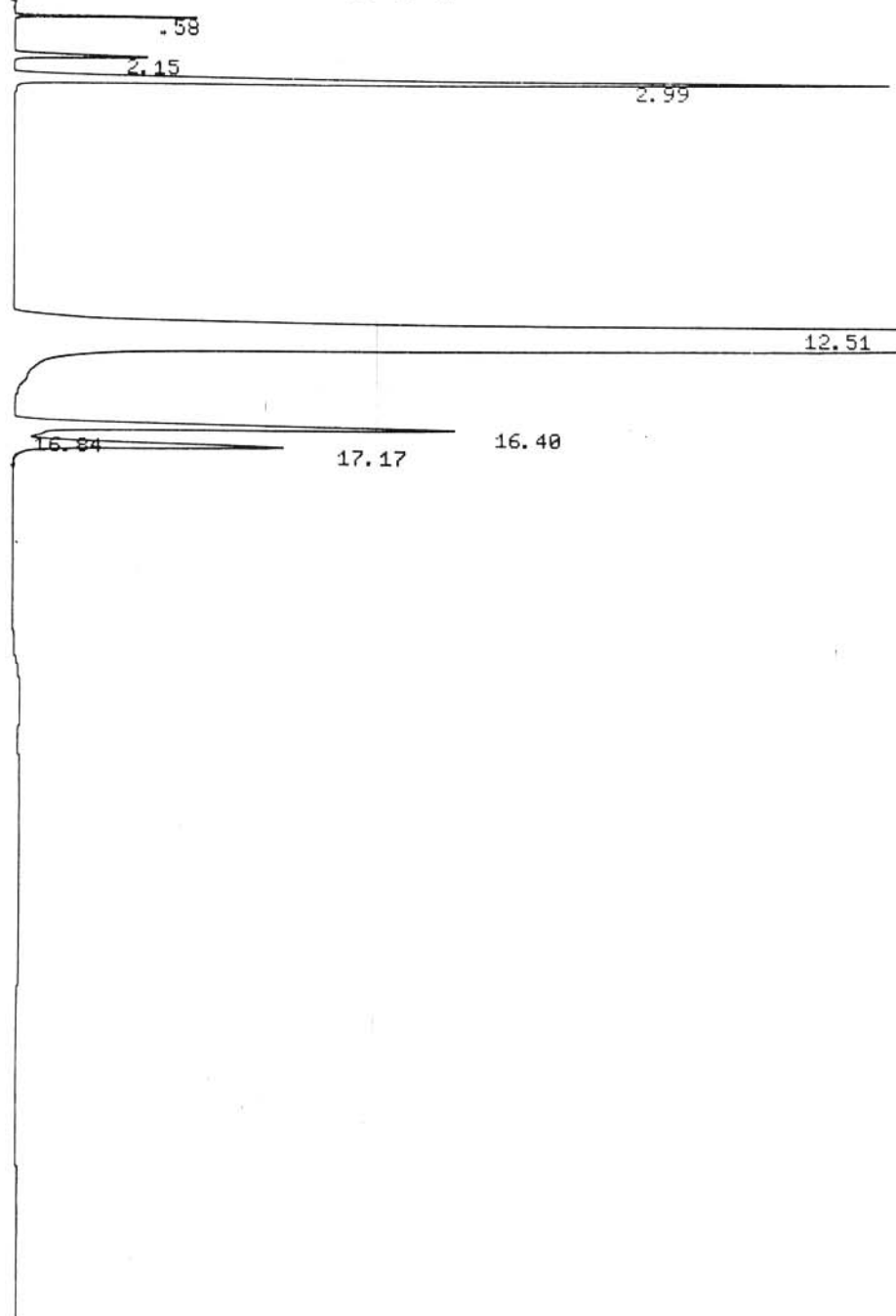

```
                                          05:46:43    CH= "A"  PS=  1.

FILE  1.      METHOD  0.     RUN  17    INDEX  17

PEAK#    AREA%        RT       AREA BC

    1     0.152      0.58      9647 01
    2     0.262      2.15     16639 01
    3     2.431      2.99    154387 01
    4    94.462     12.51   5998307 01
    5     1.589     16.4     100901 02
    6     0.026     16.84      1654 02
    7     1.077     17.17     68402 03

TOTAL   100.                6349937
```

Chromatogram A.3 Propane cracking over the 27% XRD crystalline H-ZSM-5-based sample.

CHANNEL A   INJECT   19:08:55

.56

2.21

3.18

12.95

16.45
16.80
17.20

23.13

25.77

39.78
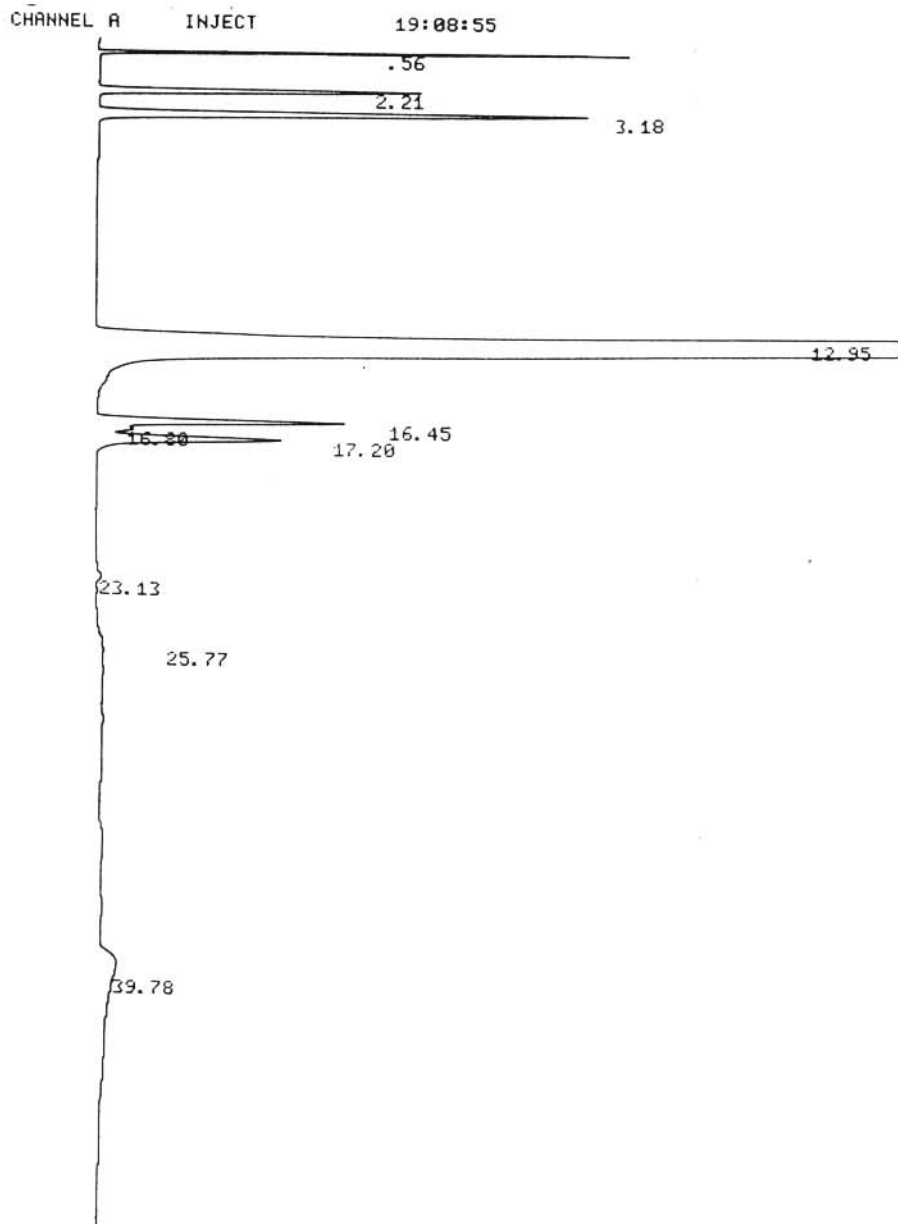
028

19:08:55   CH= "A"   PS= 1.

FILE   1.   METHOD   0.   RUN   18   INDEX   18

PEAK#	AREA%	RT	AREA	BC
1	0.678	0.56	31275	01
2	1.045	2.21	48236	01
3	2.306	3.18	106417	01
4	91.467	12.95	4221191	01
5	1.252	16.45	57765	02
6	0.165	16.8	7622	02
7	1.173	17.2	54153	03
8	0.041	23.13	1912	01
9	0.802	25.77	37029	02
10	1.07	39.78	49384	03
TOTAL	100.		4614984	

Chromatogram A.4 Propane cracking over the 51% XRD crystalline H-ZSM-5-based sample.

CHANNEL A ' INJECT)10/90/0' 13:16:34

185

3.87
4.61 4.99

9.27　　　　　　　9.62

19.11
19.63
20.17

26.09 25.78
26.63
27.32

30.28 29.70

34.23

40.74

42.31
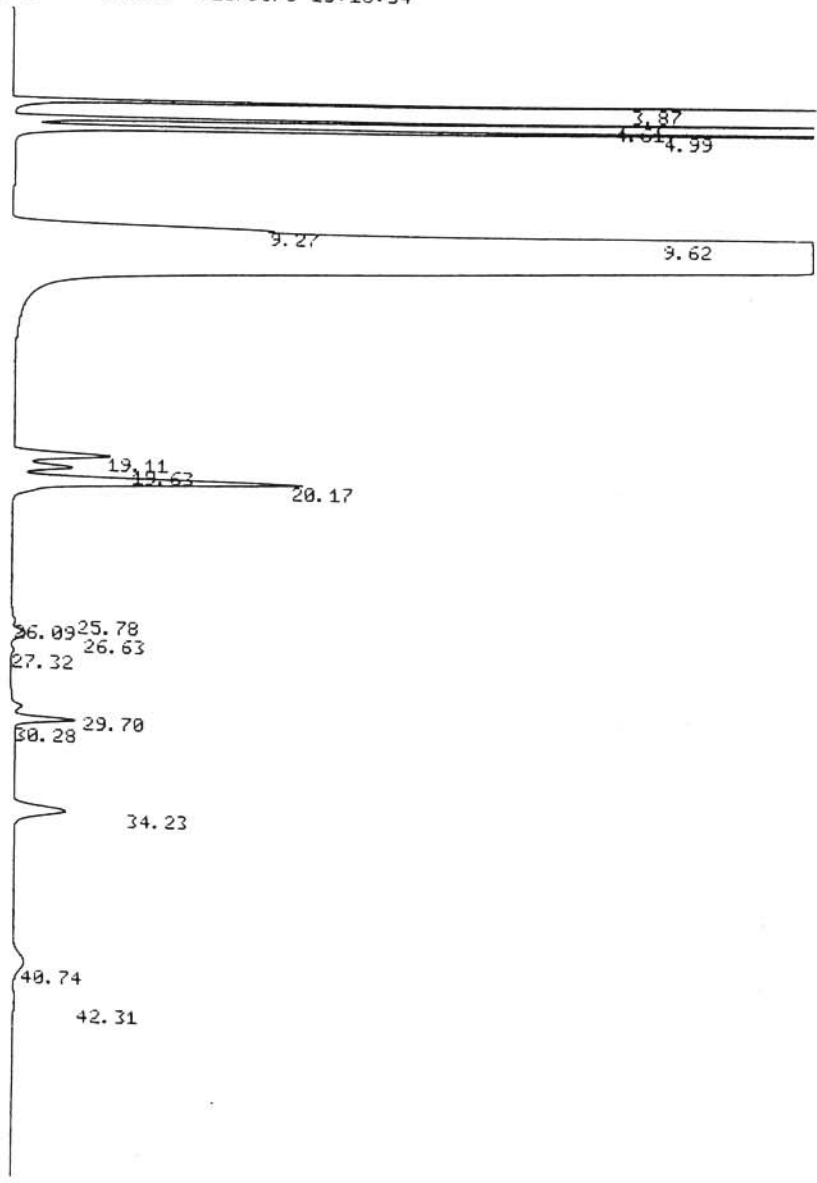
)10/90/0 13:16:34　　CH= "A"　PS=　1.

FILE　1.　　METHOD　0.　　RUN　35　　INDEX　35

PEAK#	AREA%	RT	AREA	BC
1	1.217	3.87	83118	01
2	1.512	4.61	103278	02
3	2.686	4.99	183456	03
4	0.834	9.27	56962	02
5	90.568	9.62	6186292	03
6	0.439	19.11	29957	02
7	0.259	19.63	17678	02
8	1.494	20.17	102037	03
9	0.018	25.78	1223	02
10	0.021	26.09	1420	02
11	0.1	26.63	6814	02
12	0.017	27.32	1176	03
13	0.049	29.7	3316	02
14	0.244	30.28	16677	03
15	0.341	34.23	23258	01
16	0.158	40.74	10816	02
17	0.045	42.31	3054	03

TOTAL　100.　　　　6830532

186

Chromatogram A.5 Propane cracking over the 63% XRD crystalline H-ZSM-5-based sample.

CHANNEL A   INJECT >10/90/0 15:07:41

```
                                                    .53
                                                   1.92 44
                                                   1.92

              7.59                          8.09


                        16.17
              16.68     17.24


                22.12
            22.95  23.49
          24.17
             25.89
          26.50  27.06

        28.84
              31.11


        37.85
          39.45
```
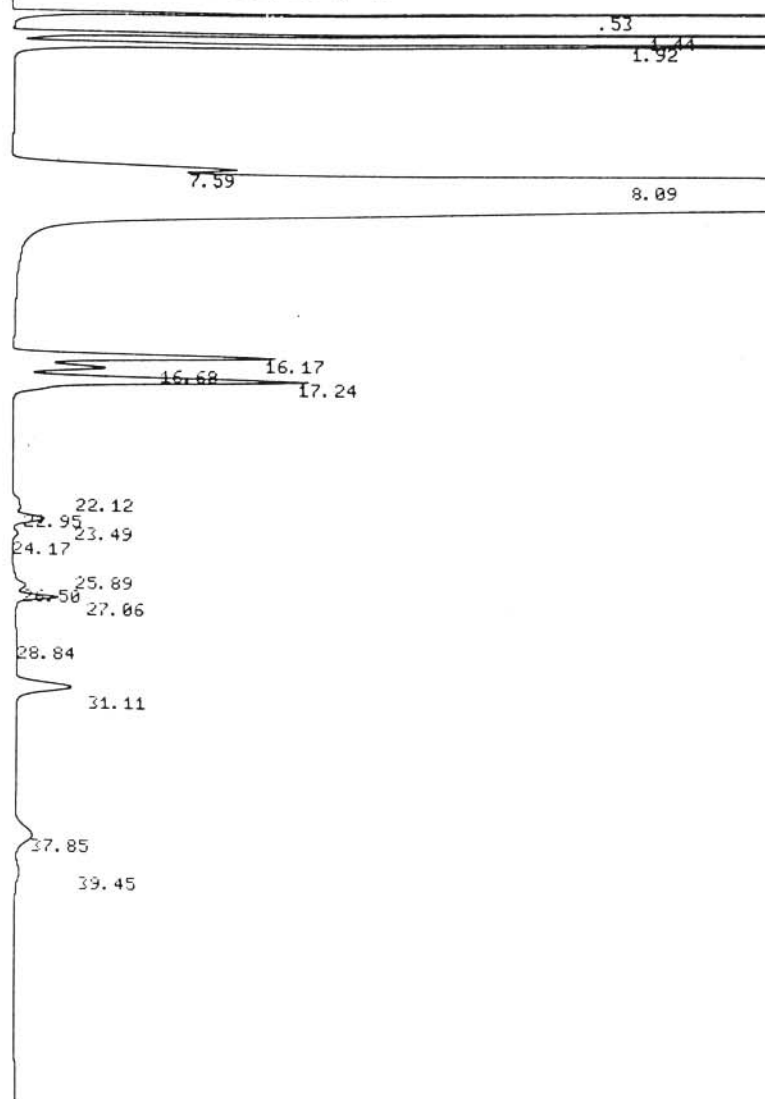
187

>10/90/0 15:07:41   CH= "A"   PS= 1.

FILE 1.   METHOD 0.   RUN 36   INDEX 36

PEAK#	AREA%	RT	AREA	BC
1	2.133	0.53	123621	01
2	2.015	1.44	116746	02
3	3.41	1.92	197619	03
4	1.349	7.59	78192	02
5	85.488	8.09	4954160	03
6	1.455	16.17	84341	02
7	0.532	16.68	30819	02
8	2.038	17.24	118078	03
9	0.008	22.12	445	02
10	0.095	22.95	5495	02
11	0.236	23.49	13686	02
12	0.032	24.17	1882	03
13	0.005	25.89	287	02
14	0.102	26.5	5902	02
15	0.216	27.06	12525	03
16	0.035	28.84	2030	02
17	0.489	31.11	28319	03
18	0.286	37.85	16563	02
19	0.077	39.45	4476	03

TOTAL   100.   5795186

Chromatogram A.6 Propane cracking over the 78% XRD crystalline H-ZSM-5-based sample.

APPENDIX B

Gas chromatograms of the products from propane cracking over H-ZSM-5-based samples of different percentage XRD crystallinities synthesized without stirring in the Parr autoclave
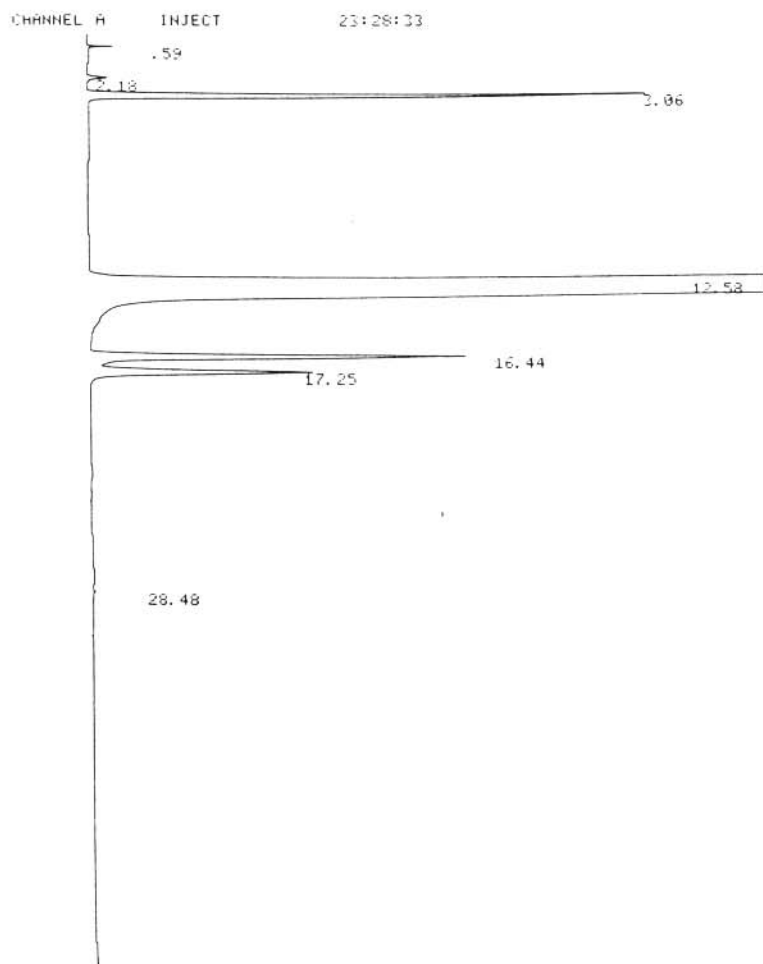

```
CHANNEL A    INJECT        23:28:33
              .59
  2.18
                                          3.06

                                                    12.58

                                16.44
              17.25


      28.48




                            23:28:33    CH= "A"  PS=  1.
FILE   1.      METHOD  0.     RUN  65     INDEX  65

PEAK#    AREA%        RT       AREA BC

  1      0.03        0.59      1732 01
  2      0.055       2.18      3211 01
  3      2.264       3.06    131544 01
  4     94.388      12.58   5483669 01
  5      1.956      16.44    113621 02
  6      1.306      17.25     75858 03
  7      0.001      28.48        82 01

TOTAL  100.                 5809717
```

Chromatogram B.1 Propane cracking over the 5% XRD crystalline H-ZSM-5-based sample.

CHANNEL A   INJECT   19:12:12

.57

2.22

3.19

12.91

16.45

17.21

062
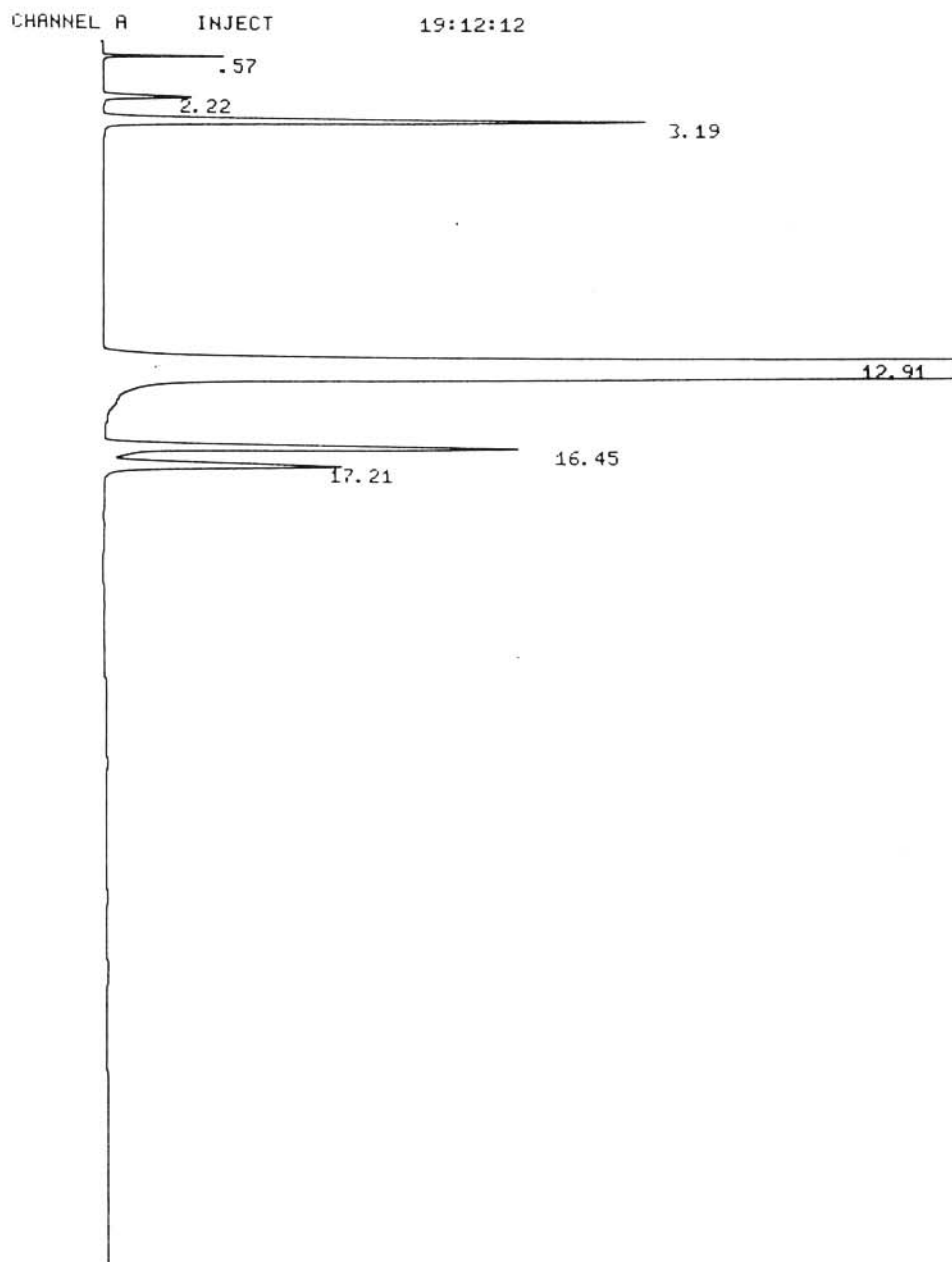
19:12:12   CH= "A"   PS= 1.

FILE 1.   METHOD 0.   RUN 57   INDEX 57

PEAK#	AREA%	RT	AREA	BC
1	0.131	0.57	6629	01
2	0.242	2.22	12235	01
3	2.204	3.19	111252	01
4	94.252	12.91	4757143	01
5	1.92	16.45	96886	02
6	1.25	17.21	63098	03
TOTAL	100.		5047243	

063

Chromatogram B.2 Propane cracking over the 13% XRD crystalline H-ZSM-5-based sample.

```
CHANNEL A      INJECT          04:55:42
```

```
              .57
```
```
             2.13
                                          2.97
```
```
                                          12.47
```
```
                                    16.44
           17.25
```

```
49.3749.17
  49.53
```
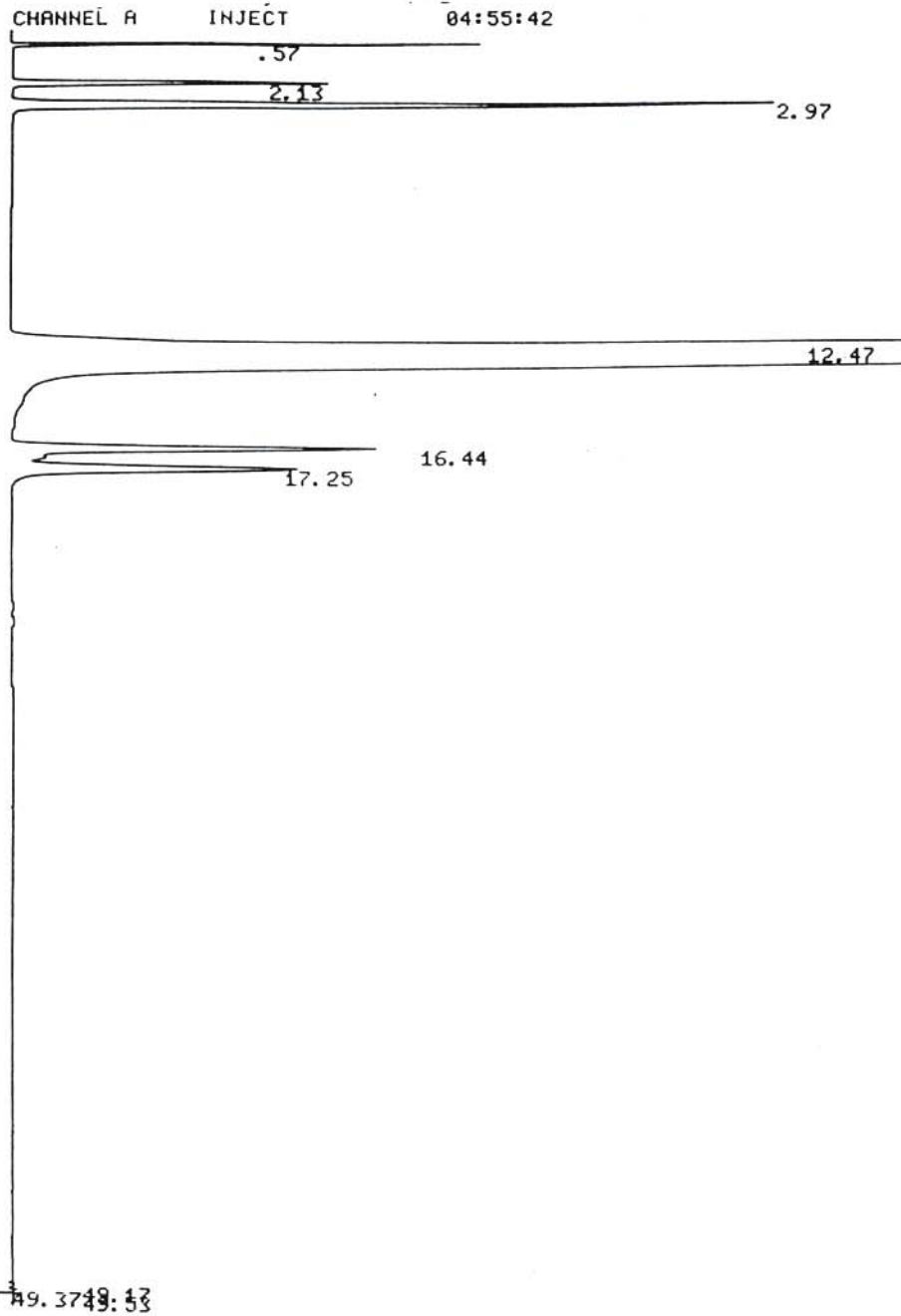
```
                          04:55:42    CH= "A"  PS=  1.

FILE  1.      METHOD  0.      RUN   41      INDEX  41

PEAK#     AREA%       RT      AREA  BC

   1      0.438      0.57     24908  01
   2      0.683      2.13     38801  01
   3      2.318      2.97    131782  01
   4     94.073     12.47   5348059  01
   5      1.288     16.44     73216  01
   6      1.185     17.25     67388  01
   7      0.003     49.17       143  01
   8      0.004     49.37       226  01
   9      0.008     49.53       464  01

TOTAL   100.              5684987
```

Chromatogram B.3 Propane cracking over the 39% XRD crystalline H-ZSM-5-based sample.

CHANNEL A   'INJECT   23:01:21

.94

2.44

3.26

12.75

16.82
17.23   17.64

22.95
23.62
24.23

26.76   26.34

30.15
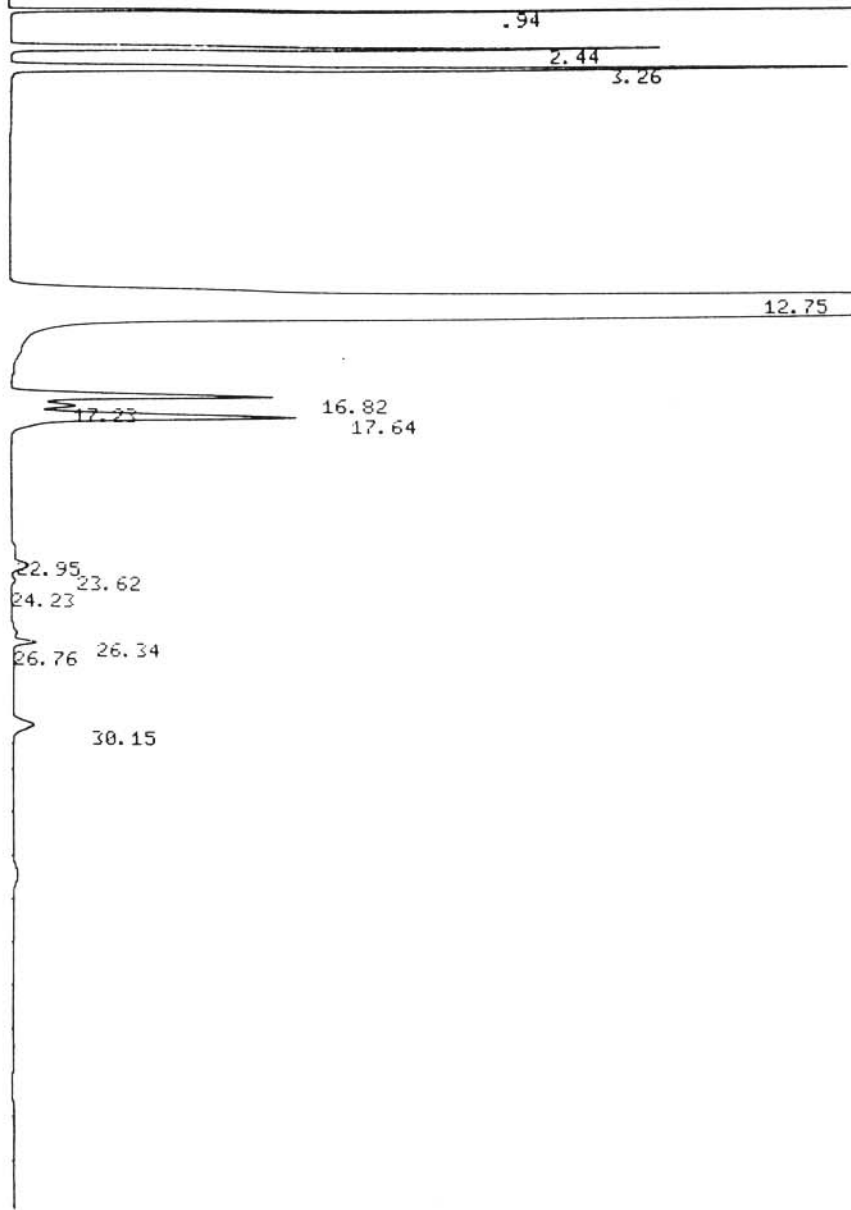
041

23:01:21   CH= "A"   PS= 1.

FILE 1.   METHOD 0.   RUN 29   INDEX 29

PEAK#	AREA%	RT	AREA	BC
1	1.137	0.94	64109	01
2	1.476	2.44	83239	01
3	2.643	3.26	149044	01
4	91.416	12.75	5155782	01
5	1.065	16.82	60079	02
6	0.276	17.23	15563	02
7	1.556	17.64	87747	03
8	0.048	22.95	2684	02
9	0.111	23.62	6279	02
10	0.02	24.23	1108	03
11	0.019	26.34	1081	02
12	0.082	26.76	4636	03
13	0.152	30.15	8561	01

TOTAL   100.   5639912

042

Chromatogram B.4 Propane cracking over the 63% XRD crystalline H-ZSM-5-based sample.

CHANNEL A   INJECT   20:05:28

.58

2.13

2.99

037

12.59

16.45
16.84
17.25

22.76 23.21

25.89 26.31

29.62

20:05:28   CH= "A" PS= 1.

038
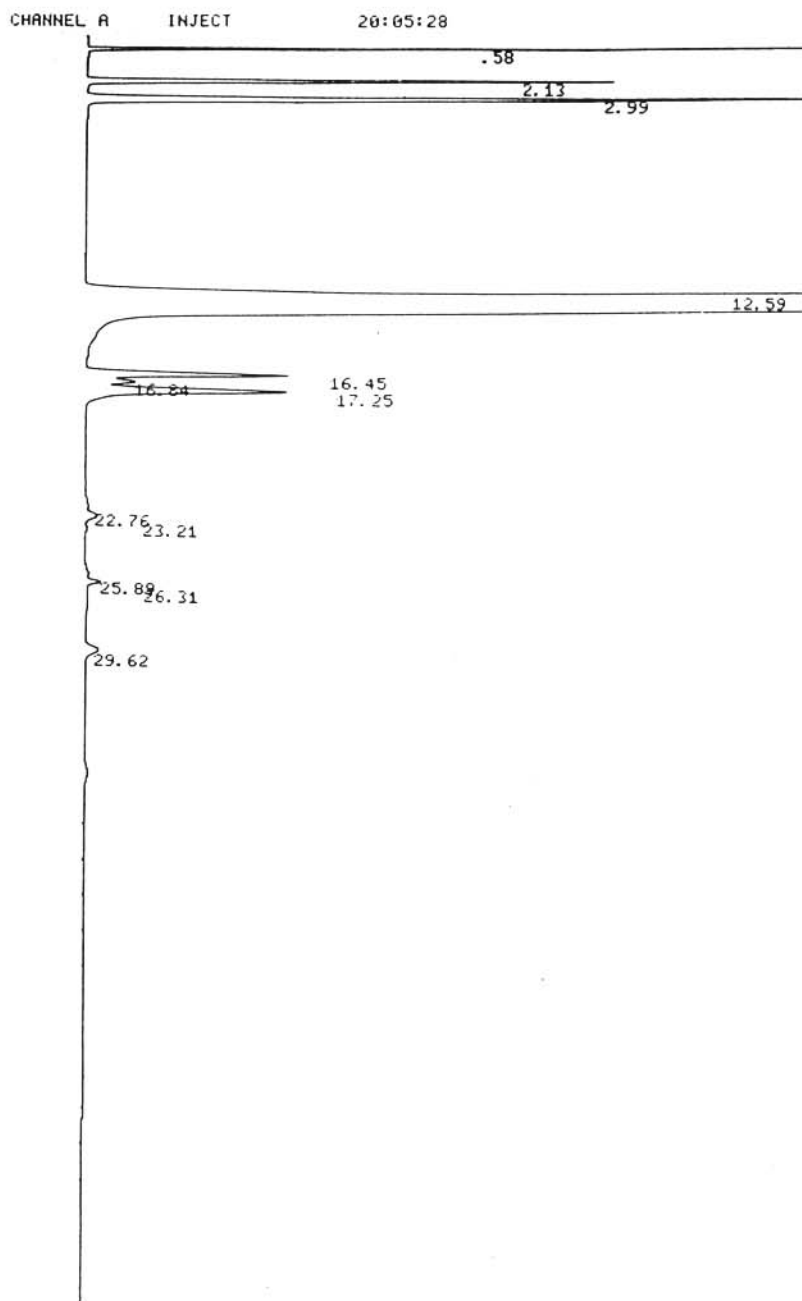
FILE 1.   METHOD 0.   RUN 25   INDEX 25

PEAK#	AREA%	RT	AREA	BC
1	0.961	0.58	56929	01
2	1.369	2.13	81156	01
3	2.666	2.99	158007	01
4	90.249	12.59	5348379	01
5	0.92	16.45	54519	02
6	0.227	16.84	13424	02
7	1.209	17.25	71627	03
8	0.034	22.76	1996	02
9	0.102	23.21	6067	03
10	0.016	25.89	944	02
11	0.057	26.31	3351	03
12	0.104	29.62	6190	01
13	2.086	62.04	123526	01

Chromatogram B.5 Propane cracking over the 80% XRD crystalline H-ZSM-5-based sample.

APPENDIX C

Gas chromatograms of the products from *n*-hexane cracking over H-ZSM-5-based samples of different percentage XRD crystallinities synthesized with stirring in the Parr autoclave

```
CHANNEL A     INJECT  )10/30/0 11:14:55

3.06 2.97
3.59 3.11

      7.76


11.30
12.85 12.28




      21.09



27.06 27.47



33.06


                              36.29
```
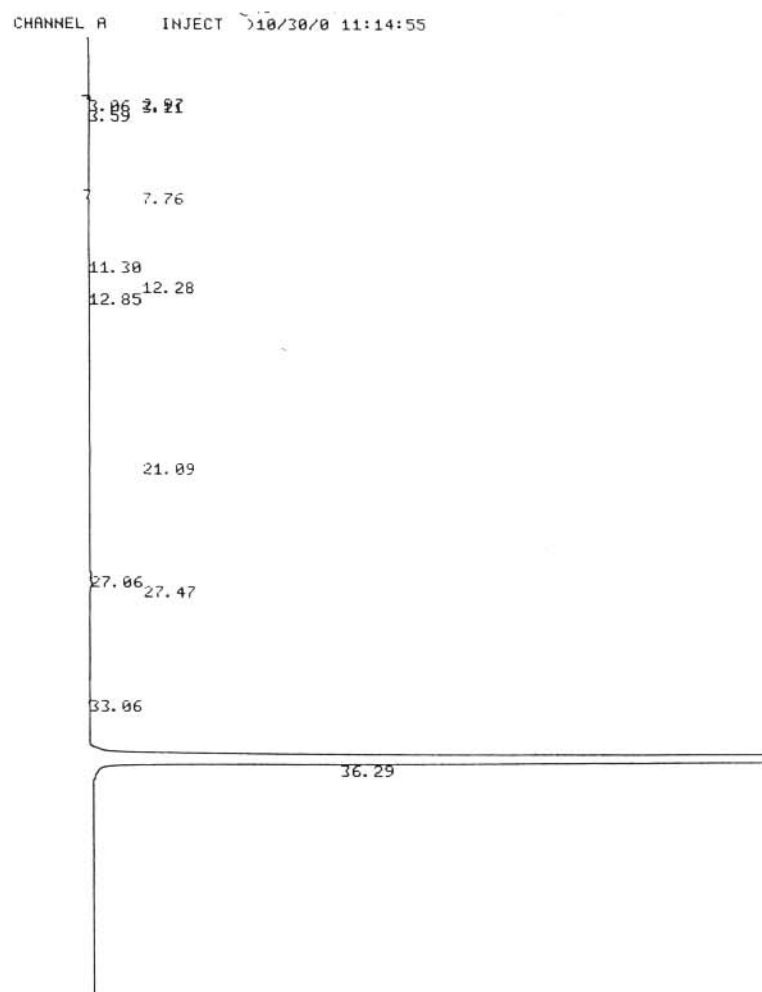
152

```
                   )10/30/0 11:14:55    CH= "A"  PS=  1.
FILE  1.    METHOD  0.    RUN   6    INDEX   6

PEAK#     AREA%       RT      AREA BC
   1      0.026      2.97      433 02
   2      0.008      3.06      136 02
   3      0.014      3.11      239 03
   4      0.003      3.59       49 01
   5      0.015      7.76      242 01
   6      0.006     11.3       106 01
   7      0.009     12.28      141 01
   8      0.008     12.85      130 01
   9      0.04      21.09      668 01
  10      0.024     27.06      398 02
  11      0.035     27.47      576 03
  12      0.023     33.06      376 01
  13     99.789     36.29  1650677 01

TOTAL    100.              1654171
```

153

Chromatogram C.1 *n*-Hexane cracking over the 2% XRD crystalline H-ZSM-5-based sample.

CHANNEL A   INJECT 10.23.00 11:30:14

.42
1.42
1.99

10.20
11.35

15.77 16.17
16.69

20.49
22.29

24.65
25.48

27.08
28.23
29.45

33.35
34.82

10.23.00 11:30:14   CH= "A" PS= 1.

FILE 1.   METHOD 0.   RUN 2   INDEX 2

PEAK#	AREA%	RT	AREA BC
1	0.075	0.42	771 01
2	0.262	1.42	2703 01
3	0.265	1.99	2732 01
4	1.283	10.2	13250 02
5	0.338	11.35	3495 03
6	0.013	15.77	138 02
7	0.824	16.17	8512 02
8	0.829	16.69	8566 03
9	0.636	20.49	6569 01
10	0.113	22.29	1168 01
11	0.082	24.65	851 02
12	93.717	25.48	967794 02
13	0.683	27.08	7056 02
14	0.374	28.23	3859 02
15	0.35	29.45	3617 03
16	0.155	34.82	1599 01

TOTAL   100.   1032680

Chromatogram C.2 *n*-Hexane cracking over the 18% XRD crystalline H-ZSM-5-based sample.

```
CHANNEL A      INJECT  10.24.00 09:06:56
                .42
              1.43
                   2.01




              10.02
           11.4311. 44.27


              71    16.13
              16.65

              20.57
           21.57
              22.28
           26.07                                    25.47

         29.45


           34.90


           40.80
```

```
                    10.24.00 09:06:56    CH= "A"  PS=  1.
FILE  1.    METHOD  0.    RUN   6    INDEX   6
PEAK#    AREA%      RT      AREA BC
  1     0.108     0.42     1123 01
  2     0.617     1.43     6404 01
  3     0.669     2.01     6951 01
  4     3.289    10.02    34151 02
  5     0.792    11.27     8228 02
  6     0.143    11.43     1489 02
  7     0.364    11.56     3782 03
  8     0.024    15.71      250 02
  9     1.21     16.13    12562 02
 10     1.324    16.65    13751 03
 11     0.094    20.57      974 01
 12     0.022    21.57      233 02
 13     0.138    22.28     1432 03
 14    90.233    25.47   936935 02
 15     0.54     26.07     5611 03
 16     0.277    29.45     2878 01
 17     0.153    34.9      1591 01
TOTAL  100.             1038345
```

Chromatogram C.3 *n*-Hexane cracking over the 27% XRD crystalline H-ZSM-5-based sample.

CHANNEL A   INJECT >10/20/0 16:14:40

1.55
2.43
2.94

10.73
12.18
14.93
16.88
17.29 17.76
22.15
22.77
23.48
24.15
26.63
27.21
29.70
30.63
36.07
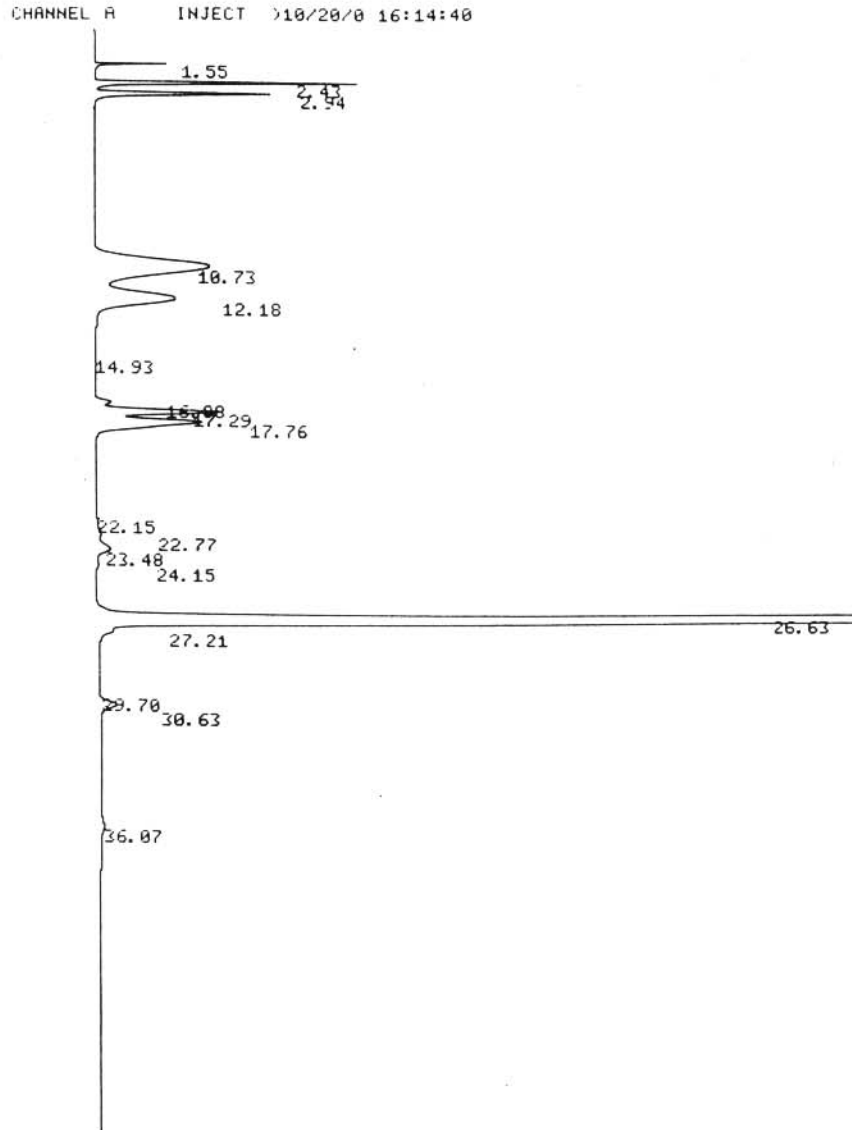
148

>10/20/0 16:14:40   CH= "A" PS= 1.

FILE 1.   METHOD 0.   RUN 2   INDEX 2

PEAK#	AREA%	RT	AREA	BC
1	0.333	1.55	4568	01
2	2.375	2.43	32583	02
3	2.178	2.94	29888	03
4	7.541	10.73	103462	02
5	4.43	12.18	60784	03
6	0.002	14.93	22	01
7	0.295	16.88	4044	02
8	2.613	17.29	35850	02
9	3.584	17.76	49176	03
10	0.006	22.15	83	01
11	0.164	22.77	2254	02
12	0.542	23.48	7431	02
13	0.072	24.15	992	03
14	74.751	26.63	1025577	02
15	0.3	27.21	4117	03
16	0.052	29.7	715	02
17	0.556	30.63	7633	03
18	0.205	36.07	2818	01
TOTAL	100.		1371997	

Chromatogram C.4 *n*-Hexane cracking over the 51% XRD crystalline H-ZSM-5-based sample.

CHANNEL A   INJECT 10.23.00 16:31:56

1.55

2.98   2.45

5.21

10.92

12.26

16.90
17.30   17.74

21.41
22.76
23.46
24.17

26.07
27.25   26.71

28.81
29.78
30.61

36.04
37.33

44.81

48.01

138

10.23.00 16:31:56   CH= "A"   PS= 1.

FILE 1.   METHOD 0.   RUN 5   INDEX 5

PEAK#	AREA%	RT	AREA BC
1	0.706	1.55	8819 01
2	7.155	2.45	89325 08
3	4.277	2.98	53403 05
4	0.037	5.21	458 01
5	10.987	10.92	137166 02
6	14.914	12.26	186195 03
7	2.661	16.9	33222 02
8	4.718	17.3	58906 02
9	8.141	17.74	101641 03
10	0.083	21.41	1041 02
11	1.002	22.76	12516 02
12	1.89	23.46	23601 02
13	0.397	24.17	4952 03
14	0.03	26.07	375 02
15	33.691	26.71	420629 02
16	1.135	27.25	14176 03
17	0.148	28.81	1845 01
18	0.073	29.78	913 02
19	3.706	30.61	46263 03
20	2.91	36.04	36330 02
21	0.698	37.33	8714 03
22	0.287	44.81	3583 01
23	0.354	48.01	4417 01

TOTAL   100.   1248490

Chromatogram C.5 *n*-Hexane cracking over the 63% XRD crystalline H-ZSM-5-based sample.

CHANNEL A   INJECT 10.19.20 10:40:02

1.54

2.77   2.32

9.29

10.64

16.76
17.18
17.53

22.73
23.46
24.17

26.73
27.24

28.82
29.81
30.61

36.09

37.35

44.93
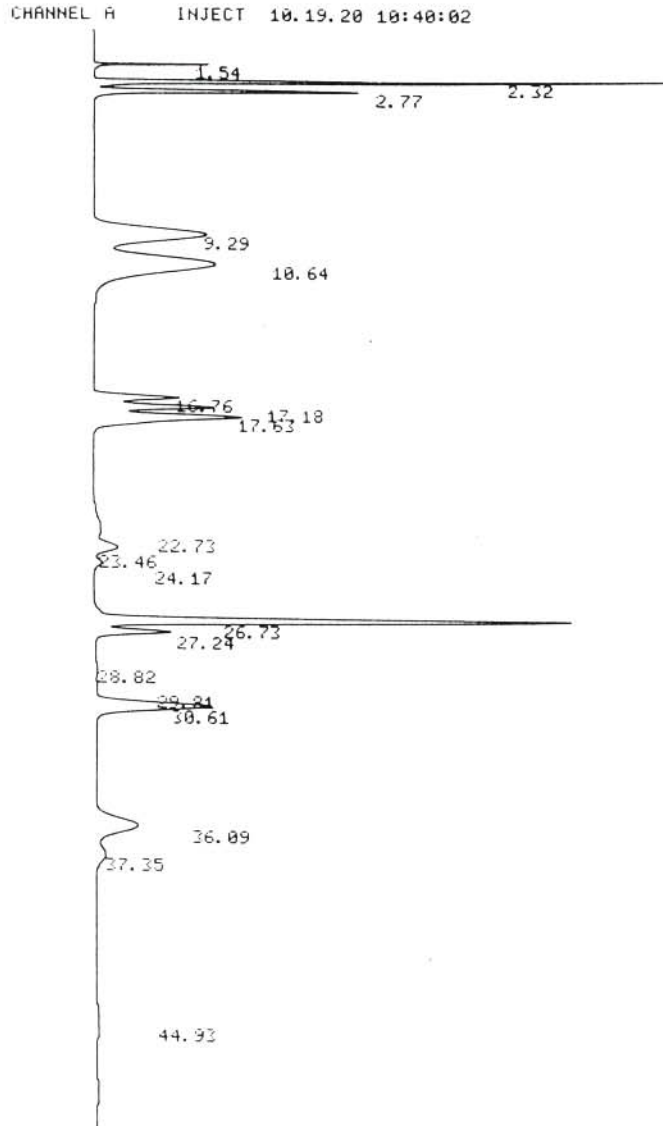
128

10.19.20 10:40:02   CH= "A" PS= 1.

FILE 1.   METHOD 0.   RUN   7   INDEX 7

PEAK#	AREA%	RT	AREA	BC
1	1.007	1.54	7347	01
2	9.404	2.32	68578	08
3	5.477	2.77	39940	05
4	11.798	9.29	86042	02
5	17.031	10.64	124200	03
6	3.41	16.76	24866	02
7	4.847	17.18	35350	02
8	8.578	17.63	62558	03
9	1.341	22.73	9782	02
10	1.865	23.46	13598	02
11	0.488	24.17	3559	03
12	17.417	26.73	127020	02
13	2.854	27.24	20811	03
14	0.187	28.82	1365	02
15	0.115	29.81	838	02
16	7.317	30.61	53360	03
17	4.993	36.09	36412	02
18	1.2	37.35	8754	03
19	0.671	44.93	4895	01

TOTAL   100.   729275

Chromatogram C.6 *n*-Hexane cracking over the 78% XRD crystalline H-ZSM-5-based sample.

APPENDIX D

Gas chromatograms of the products from *n*-hexane cracking over H-ZSM-5-based samples of different percentage XRD crystallinities synthesized without stirring in the Parr autoclave
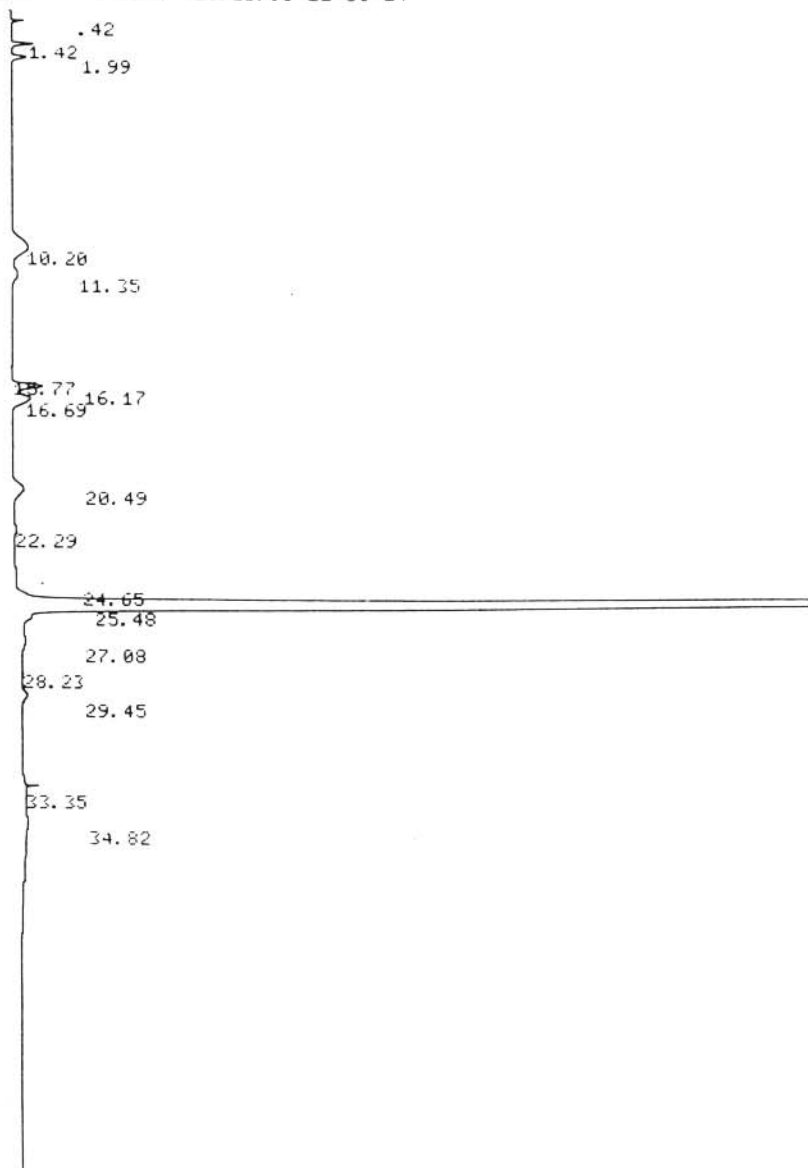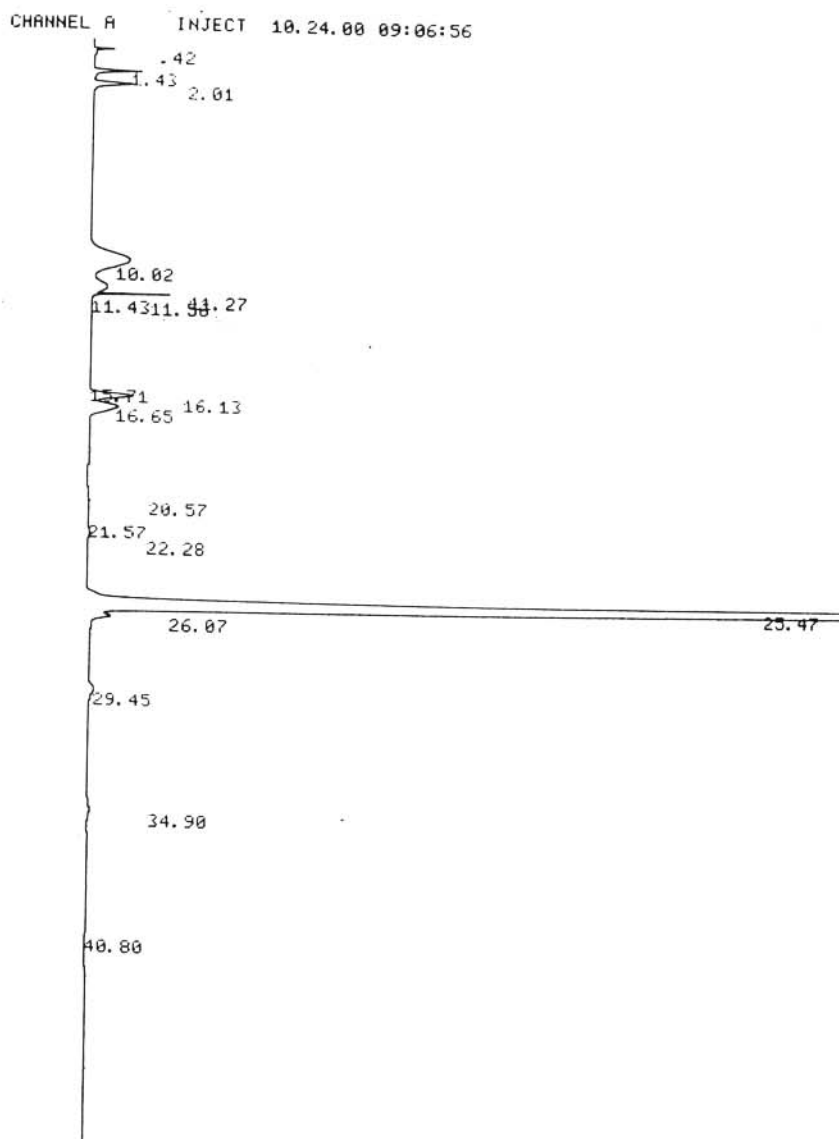


```
CHANNEL  A        INJECT   )10/80/0 14:01:15

         1.31
  2.24  2.77




  11.21
      12.34



  17.08 17.57



  22.44
      23.11

                                          26.28


      30.31



  35.56
```
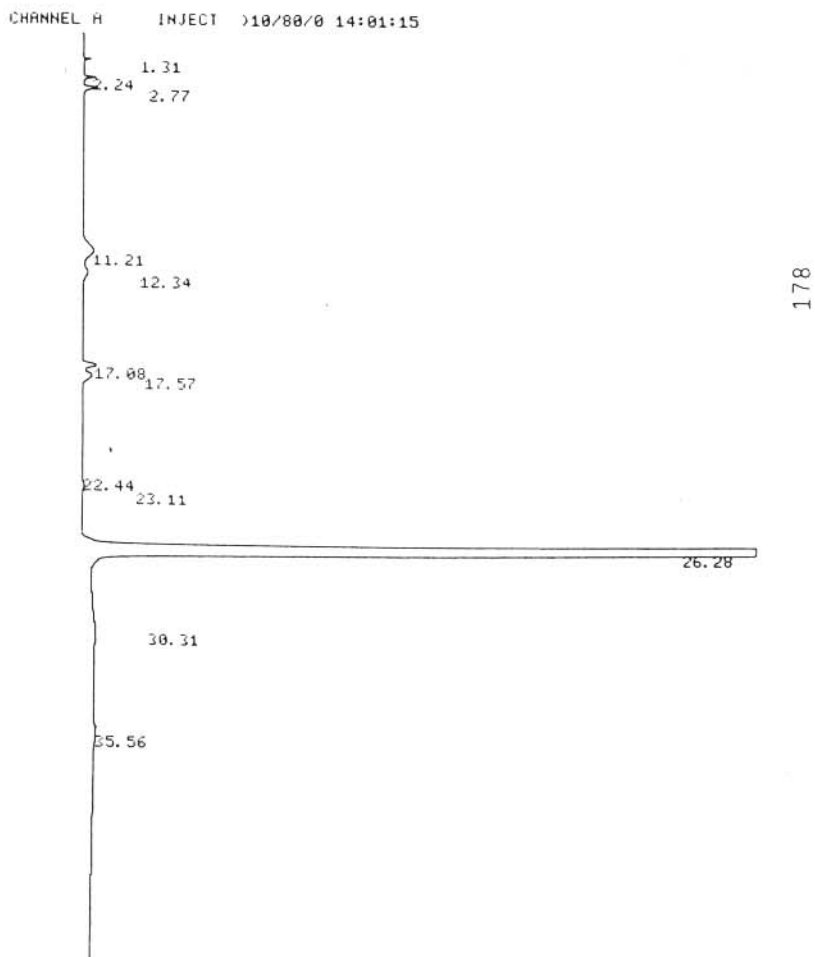
```
                        )10/80/0 14:01:15     CH= "A"  PS=  1.

FILE  1.      METHOD  8.     RUN  28     INDEX  28

PEAK#     AREA%       RT       AREA BC
   1      0.033      1.31        531 01
   2      0.096      2.24       1546 01
   3      0.164      2.77       2645 01
   4      0.604     11.21       9756 02
   5      0.213     12.34       3443 03
   6      0.283     17.08       4568 02
   7      0.324     17.57       5241 03
   8      0.019     22.44        302 02
   9      0.065     23.11       1046 03
  10     97.993     26.28    1583297 01
  11      0.165     30.31       2672 01
  12      0.042     35.56        671 01

TOTAL   100.                 1615718
```

Chromatogram D.1 *n*-Hexane cracking over the 5% XRD crystalline H-ZSM-5-based sample.

```
CHANNEL A    INJECT  )10/80/0 10:12:48
```

```
        1.44
        33   2.85


       10.82

          12.17



      76 17.16
    17.65


         23.29

              26.44


         30.47


    35.81
```
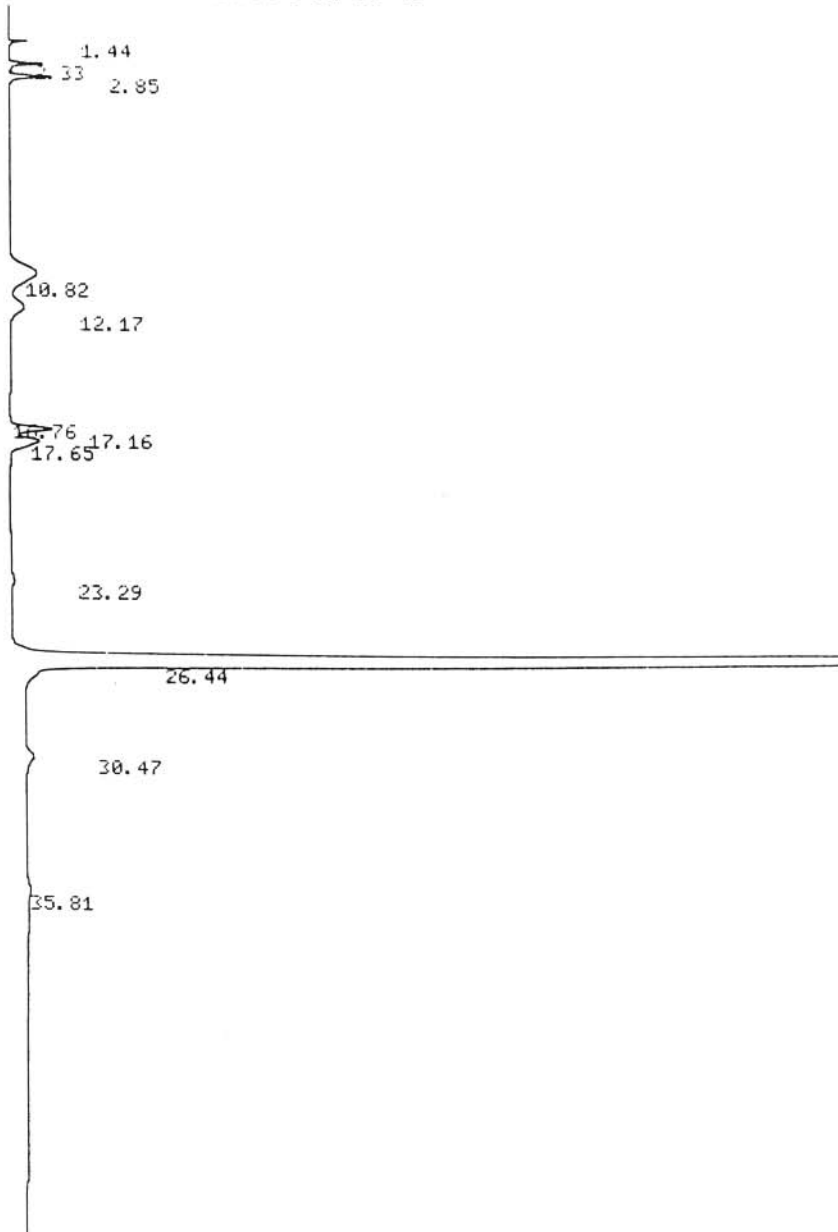
```
                  )10/80/0 10:12:48    CH= "A"  PS=  1.

FILE  1.     METHOD  0.     RUN  25    INDEX  25

PEAK#     AREA%       RT      AREA BC

   1      0.061      1.44      964 01
   2      0.24       2.33     3779 01
   3      0.397      2.85     6259 01
   4      1.395     10.82    22007 02
   5      0.565     12.17     8911 03
   6      0.011     16.76      167 02
   7      0.676     17.16    10665 02
   8      0.792     17.65    12497 03
   9      0.133     23.29     2091 01
  10     95.391     26.44  1505100 01
  11      0.228     30.47     3598 01
  12      0.113     35.81     1778 01

TOTAL   100.               1577816
```
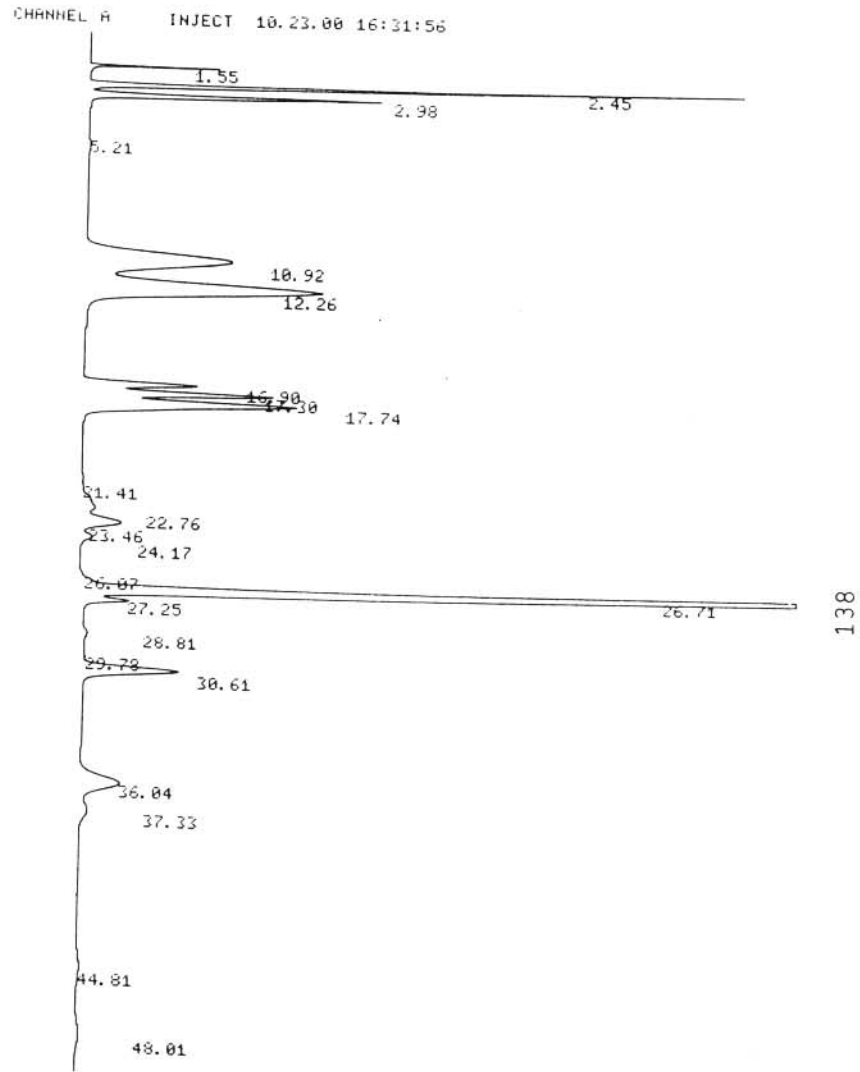
Chromatogram D.2 *n*-Hexane cracking over the 13% XRD crystalline H-ZSM-5-based sample.

CHANNEL A   INJECT >10/30/0 16:43:41

2.68

3.55
4.05

11.53

13.08

159

12.99
18.87 18.40

23.91
24.58
25.29

28.36   27.75

29.89

31.76

37.17
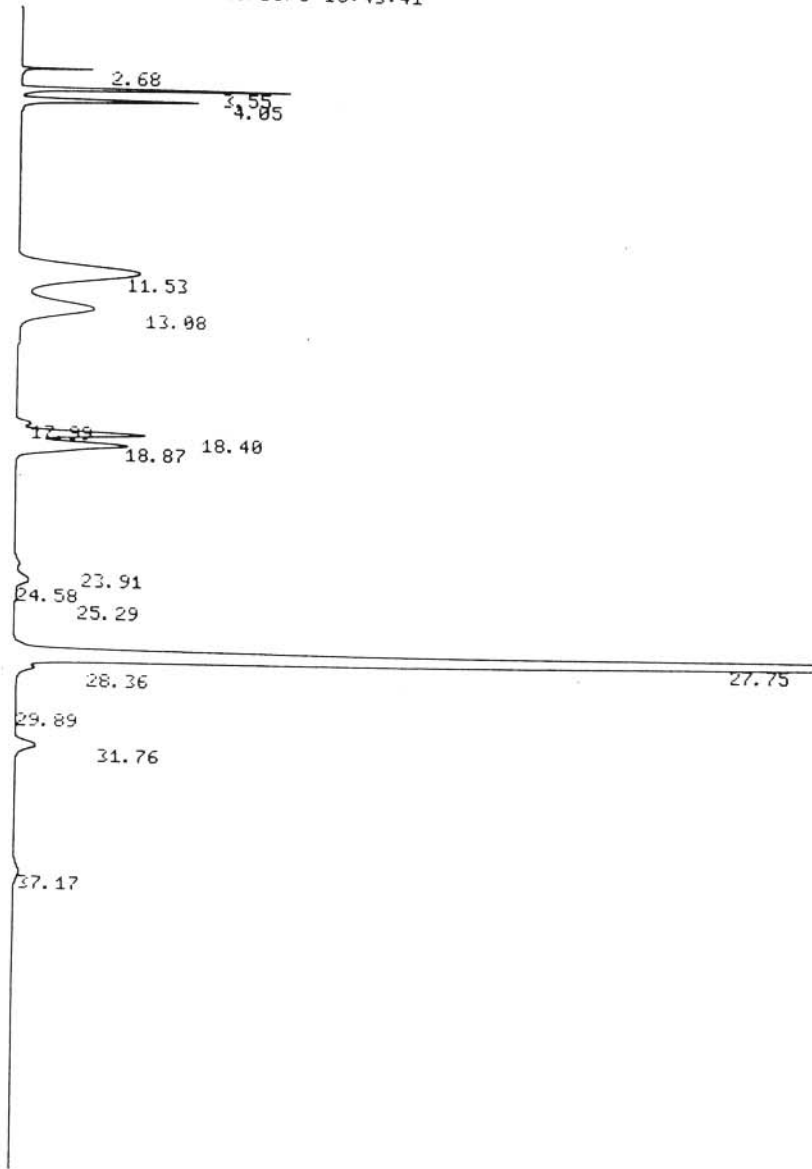
>10/30/0 16:43:41   CH= "A" PS= 1.

FILE 1.   METHOD 0.   RUN 11   INDEX 11

PEAK#	AREA%	RT	AREA	BC
1	0.31	2.68	4120	01
2	2.36	3.55	31317	02
3	2.111	4.05	28012	03
4	7.547	11.53	100163	02
5	4.462	13.08	59214	03
6	0.274	17.99	3638	02
7	2.602	18.4	34527	02
8	3.601	18.87	47793	03
9	0.265	23.91	3513	02
10	0.588	24.58	7802	02
11	0.08	25.29	1061	03
12	74.473	27.75	988392	02
13	0.4	28.36	5307	03
14	0.012	29.89	161	01
15	0.662	31.76	8790	01
16	0.254	37.17	3368	01

TOTAL   100.   1327178

160

Chromatogram D.3 *n*-Hexane cracking over the 39% XRD crystalline H-ZSM-5-based sample.

CHANNEL A   INJECT)10/50/0 17:41:27

1.1453
2.90
2.36
10.82
12.17
16.77 17.17 17.62
21.13
22.63
23.30
24.01
26.53
27.11
28.61
29.67
30.44
34.25
35.81
37.09
44.42
47.59
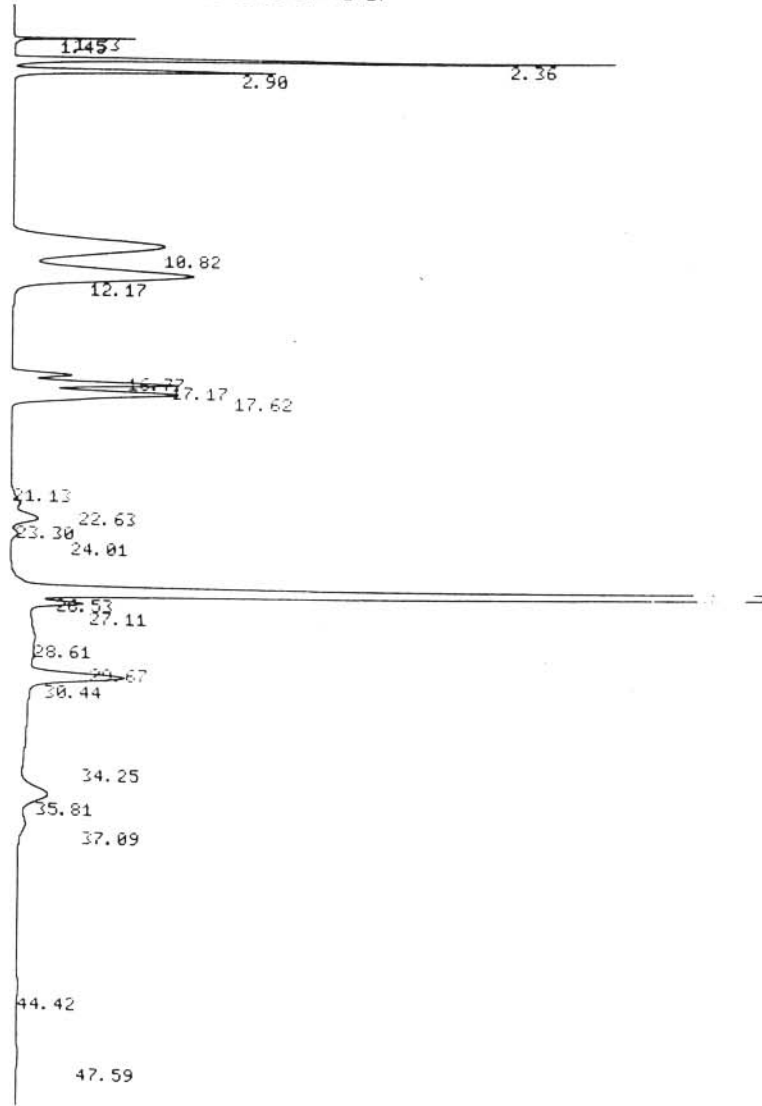
)10/50/0 17:41:27   CH= "A" PS= 1.

FILE 1.   METHOD 0.   RUN 23   INDEX 23

PEAK#	AREA%	RT	AREA	BC
1	0.003	1.33	36	02
2	0.594	1.45	7779	03
3	5.969	2.36	79116	08
4	3.511	2.9	45956	05
5	10.336	10.82	135277	02
6	10.097	12.17	132137	03
7	1.23	16.77	16101	02
8	3.697	17.17	48390	02
9	5.815	17.62	76107	03
10	0.05	21.13	659	02
11	0.48	22.63	6276	02
12	1.131	23.3	14805	02
13	0.194	24.01	2537	03
14	39.334	26.53	514773	02
15	1.845	27.11	24142	02
16	3.124	28.61	40879	02
17	0.818	29.67	10706	02
18	9.27	30.44	121314	08
19	0.001	34.25	7	05
20	1.784	35.81	350	06
21	0.431	37.09	.635	07
22	0.172	44.42	2247	01
23	0.115	47.59	1508	01
TOTAL	100.		1308737	

Chromatogram D.4 *n*-Hexane cracking over the 63% XRD crystalline H-ZSM-5-based sample.

```
CHANNEL A      INJECT  >10/50/0 13:25:05
```
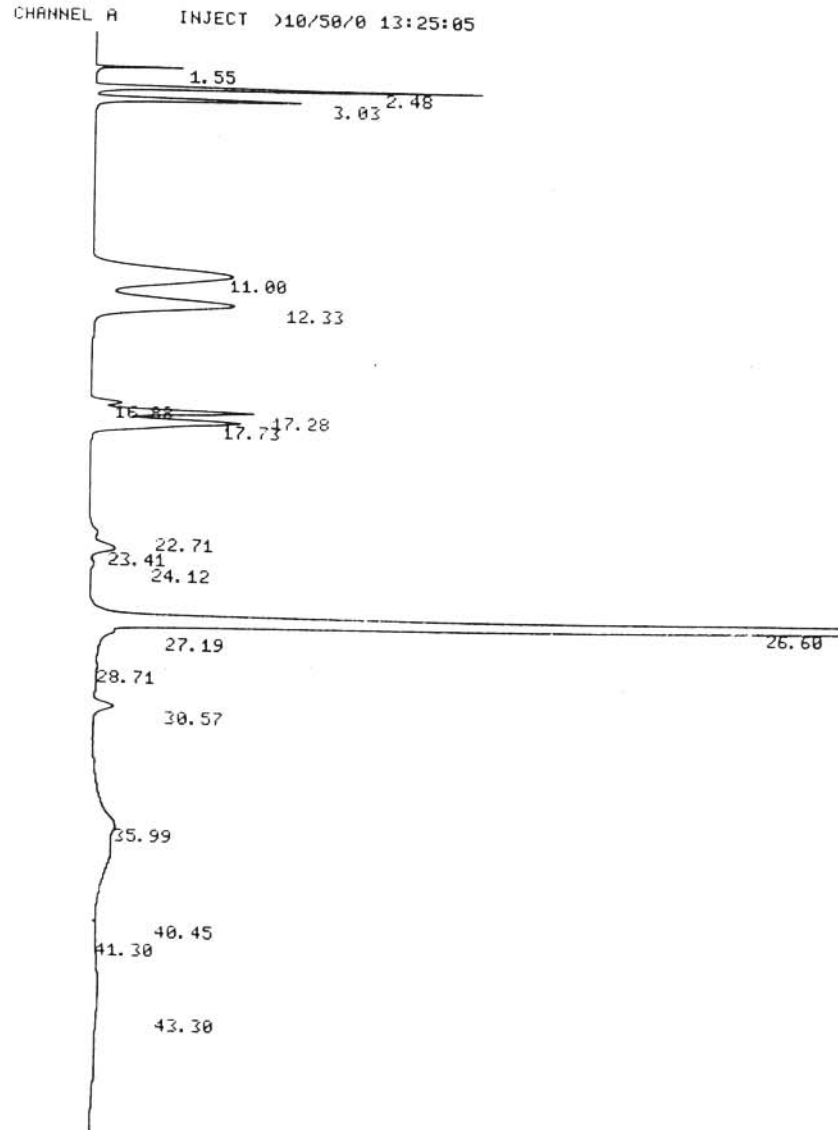


```
                              >10/50/0 13:25:05    CH= "A"  PS=  1.
FILE  1.      METHOD  0.    RUN  17      INDEX  17

PEAK#     AREA%       RT      AREA BC

   1      0.378      1.55      5444 01
   2      3.464      2.48     49857 02
   3      2.553      3.03     36748 03
   4      8.574     11.      123423 02
   5      6.758     12.33     97283 03
   6      0.573     16.88      8255 02
   7      3.219     17.28     46336 02
   8      4.701     17.73     67662 03
   9      0.33      22.71      4752 02
  10      0.965     23.41     13888 02
  11      0.134     24.12      1932 03
  12     64.814     26.6     932960 02
  13      0.953     27.19     13720 02
  14      0.451     28.71      6496 02
  15      0.717     30.57     10316 03
  16      0.673     35.99      9682 01
  17      0.09      40.45      1294 02
  18      0.004     41.3         64 03
  19      0.648     43.3       9329 01

TOTAL   100.                1439441
```

Chromatogram D.5 *n*-Hexane cracking over the 80% XRD crystalline H-ZSM-5-based sample.

Gas chromatograms of the products from *n*-hexane cracking over H-ZSM-5-based samples of different percentage XRD crystallinities synthesized with stirring in the in-house built autoclave


```
CHANNEL A      INJECT          08:30:27

              .56
           2.00
              2.77




           12.05
             12.71


           16.73
             17.21


        23.16

                                              25.66


        36.66
```
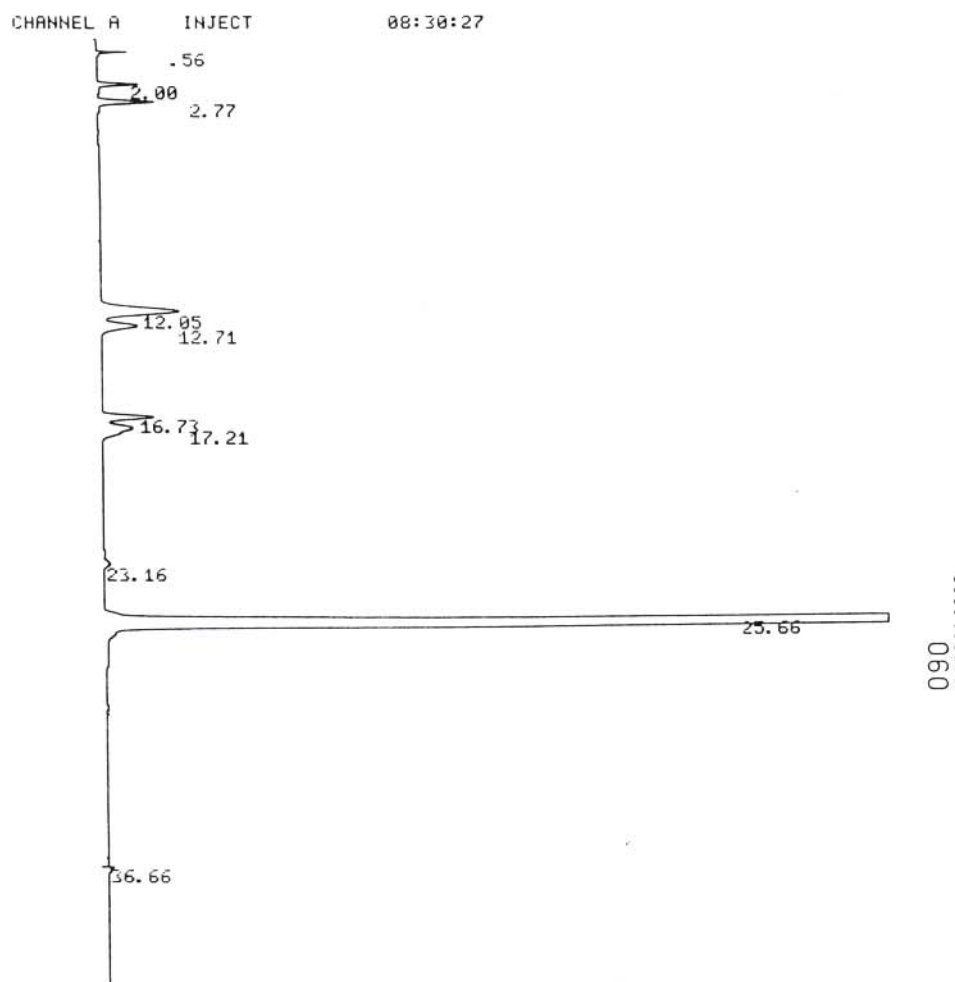
```
                            08:30:27    CH= "A"   PS=  1.
FILE  1.      METHOD  0.     RUN 105     INDEX 105

PEAK#      AREA%       RT        AREA BC

   1       0.105     0.56        1708 01
   2       0.321     2.          5242 01
   3       0.613     2.77       10002 01
   4       1.863    12.05       30397 02
   5       0.761    12.71       12410 03
   6       0.763    16.73       12442 02
   7       0.849    17.21       13843 03
   8       0.083    23.16        1360 01
   9      94.627    25.66     1543578 01
  10       0.015    36.66         249 01

TOTAL    100.                 1571221
```

Chromatogram E.1 *n*-Hexane cracking over the 5% XRD crystalline H-ZSM-5-based sample.

CHANNEL A   INJECT   01:39:35

.59

2.15
3.06

12.78
13.25

16.42 16.79
17.22

23.05 22.57

26.19   25.61

29.25
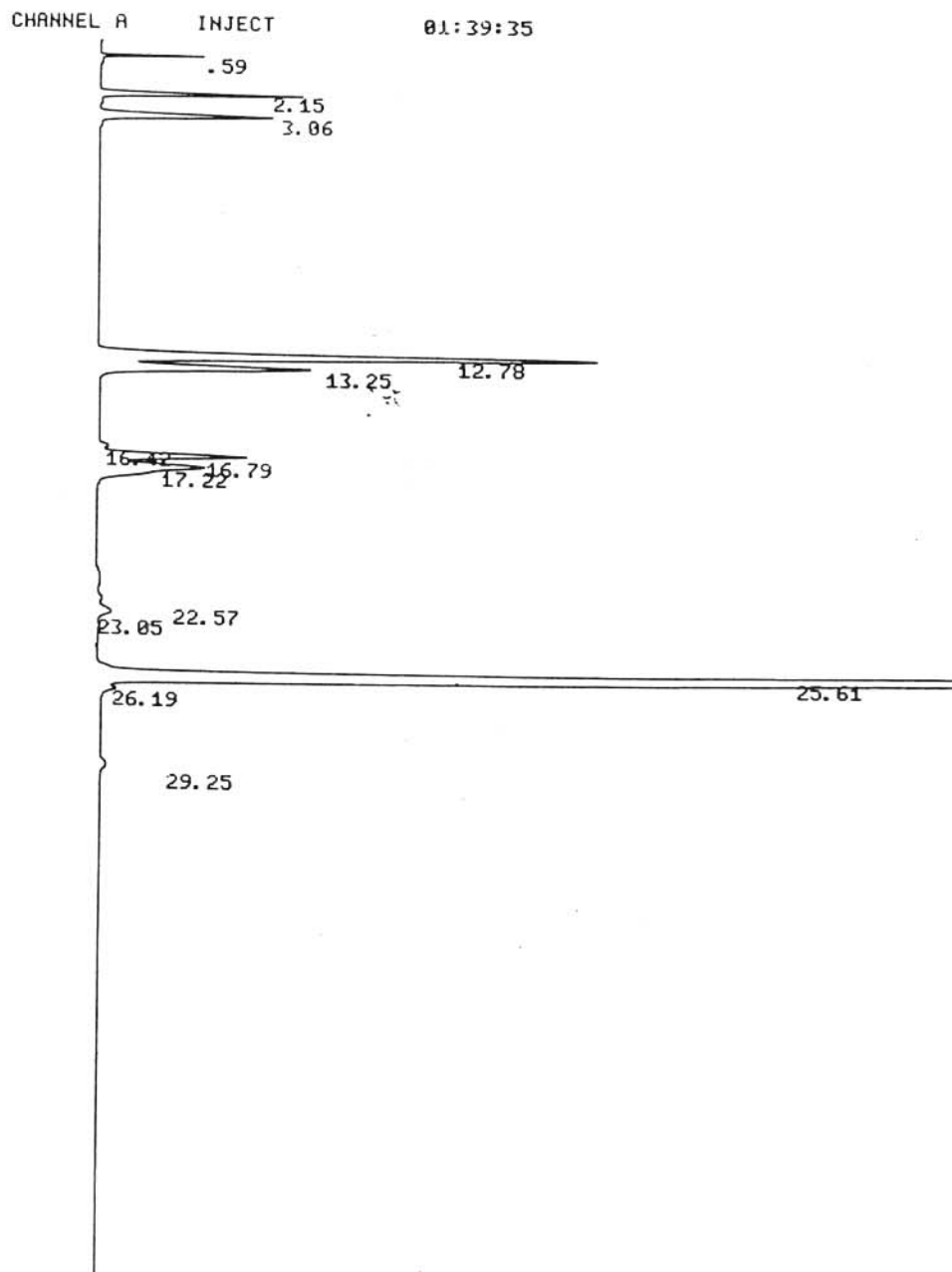
083

01:39:35   CH= "A"   PS= 1.

FILE 1.   METHOD 0.   RUN   92   INDEX   92

PEAK#	AREA%	RT	AREA	BC
1	0.381	0.59	5665	01
2	1.844	2.15	27402	01
3	2.281	3.06	33897	01
4	8.026	12.78	119265	02
5	3.667	13.25	54485	03
6	0.147	16.42	2188	02
7	2.255	16.79	33505	02
8	2.788	17.22	41437	03
9	0.084	22.57	1246	02
10	0.359	23.05	5330	03
11	77.738	25.61	1155190	02
12	0.234	26.19	3484	03
13	0.196	29.25	2909	01

TOTAL   100.   1486003

Chromatogram E.2 *n*-Hexane cracking over the 33% XRD crystalline H-ZSM-5-based sample.

```
CHANNEL A      INJECT              22:27:21
```

.55

2.01
2.86

12.59
13.08

16.34 16.73
17.16

23.01

25.62
26.16

29.19

```
                            22:27:21    CH= "A"   PS=  1.

FILE  1.      METHOD  0.      RUN  87      INDEX  87

PEAK#     AREA%       RT      AREA BC

   1      0.599      0.55     5151 01
   2      4.29       2.01    36921 01
   3      3.223      2.86    27736 01
   4     13.391     12.59   115243 02
   5      5.933     13.08    51062 03
   6      0.298     16.34     2564 02
   7      2.929     16.73    25206 02
   8      3.689     17.16    31743 03
   9      0.367     23.01     3156 01
  10     62.37      25.62   536744 02
  11      1.301     26.16    11195 03
  12      1.61      29.19    13855 01

TOTAL   100.                860576
```

Chromatogram E.3 *n*-Hexane cracking over the 54% XRD crystalline H-ZSM-5-based sample.

```
CHANNEL A      INJECT              04:40:23
                      .58
                                    2.14
                       3.05



                                              12.74
                                   13.21
      16.38
               17.18 16.76

          21.61
      22.53
      23.05
      23.62
                                                      25.61
      26.17

          29.25
```
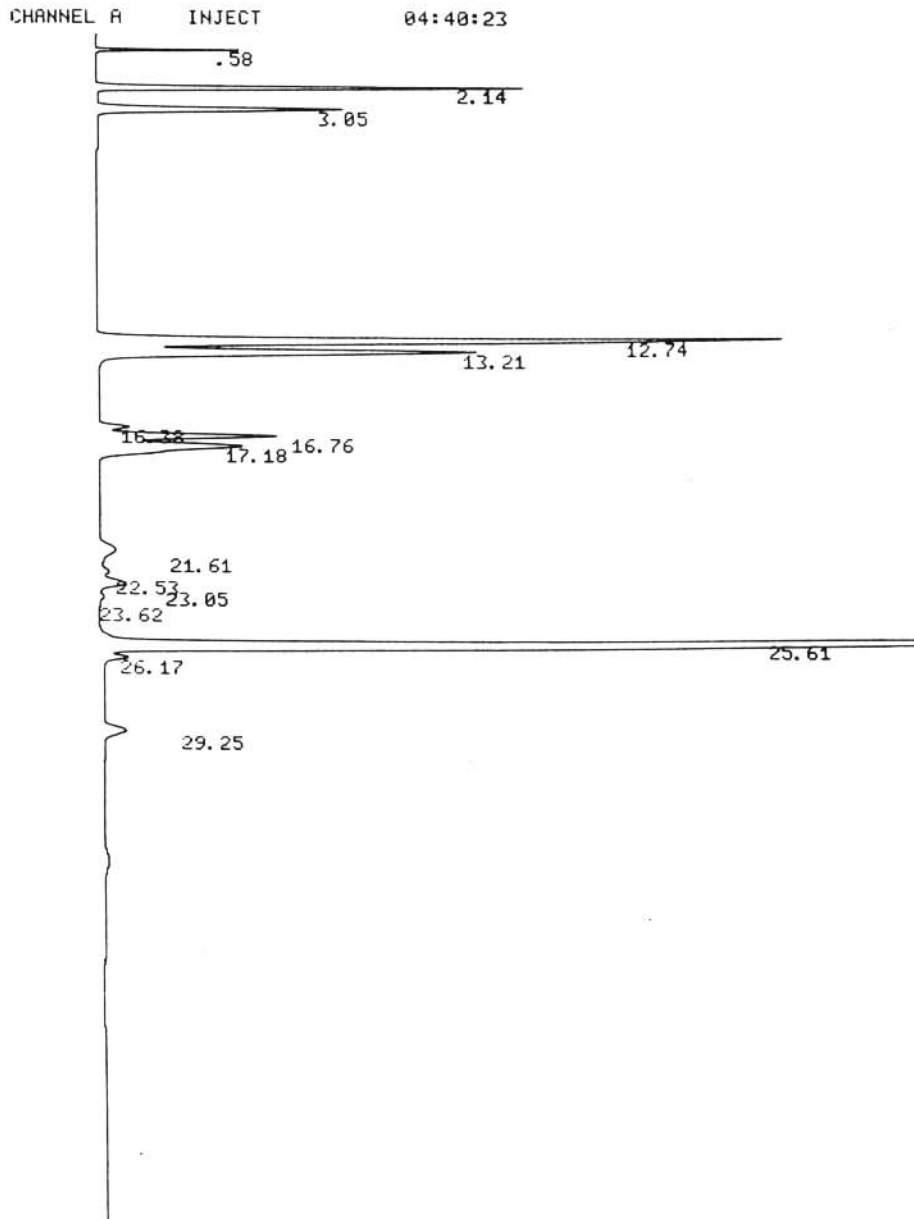
086

```
                              04:40:23    CH= "A"   PS=  1.

FILE  1.      METHOD  0.      RUN  97      INDEX  97

PEAK#     AREA%        RT        AREA BC

   1      0.616       0.58       8268 01
   2      4.477       2.14      60118 01
   3      3.784       3.05      50822 01
   4     12.923      12.74     173546 02
   5      7.633      13.21     102513 03
   6      0.474      16.38       6371 02
   7      3.182      16.76      42728 02
   8      4.352      17.18      58449 03
   9      0.798      21.61      10716 02
  10      0.281      22.53       3771 02
  11      0.754      23.05      10131 02
  12      0.106      23.62       1427 03
  13     59.543      25.61     799623 02
  14      0.407      26.17       5467 03
  15      0.669      29.25       8990 01

TOTAL   100.                  1342940
```
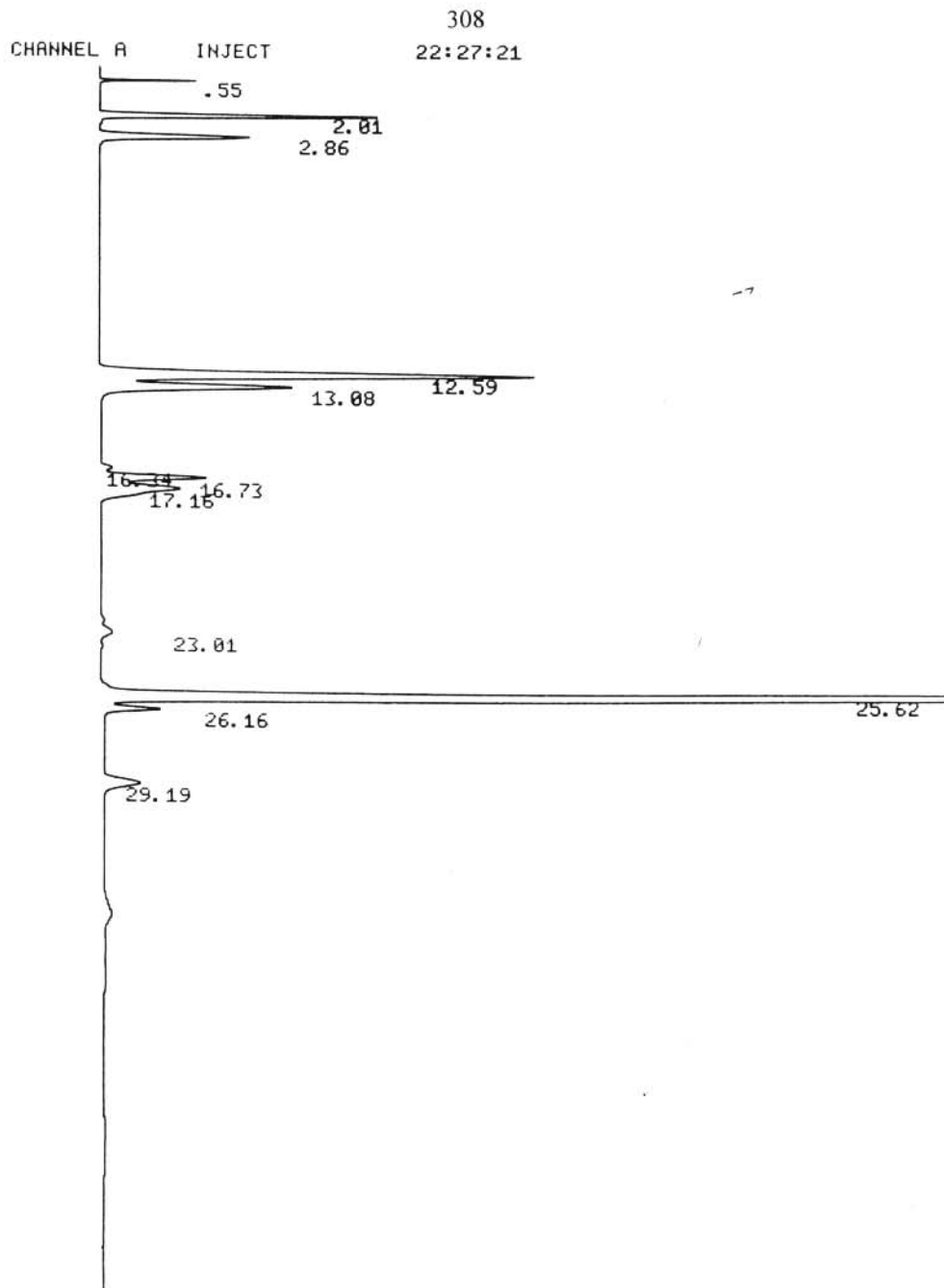
Chromatogram E.4 *n*-Hexane cracking over the 65% XRD crystalline H-ZSM-5-based sample.

REFERENCES

AHMED, S., EL-FAER, M.Z., ABILLAHI, M.M., SIDDIQUI, M.A.B. & BARRI, S.A.I. 1996. Investigation of the rapid crystallization method for the synthesis of MFI-type zeolites and study of the physicochemical properties of the products. *Zeolites*, 17:373-380.

ANDERSON, J.R., FOGER, K., MOLE, T., RAJADHYAKSHA, R.A. & SANDERS, J.V. 1979. Reactions on ZSM-5-type catalysts. *Journal of Catalysis*, 58:114-130.

ASENSI, M.A., CORMA, A., MARTINEZ, A., DEREWINSKI, M., KRYSCIAK, J. & TAMHANKAR, S.S. 1998. Isomorphous substitution in ZSM-22 zeolite. The role of zeolite acidity and crystal size during the skeletal isomerization of *n*-butene. *Applied Catalysis A: General*, 174:163-175.

BAERLOCHER, C. & McCUSKER, L.B. 1994. Practical aspects of powder diffraction data analysis. (*In* Jansen, J.C., Stöcker, M., Karge, H.G. & Weitkamp, J., *eds.* Advanced zeolite science and applications. Studies in surface science and catalysis, Volume 85. Amsterdam : Elsevier. p391-428).

BANDIERA, J. & TAARIT, Y.B. 1990. Catalytic investigation of the dehydrogenation properties of pentasil type zeolites as compared with their cracking properties. *Applied Catalysis*, 62:309-316.

BESCHMANN, K., RIEKERT, L. & MÜLLER, U. 1994. Shape-selectivity of large and small

crystals of zeolite ZSM-5. *Journal of Catalysis*, 145:243-245.

BISCARDI, J.A., MEITZNER, G.D. & IGLESIA, E. 1998. Structure and density of active Zn species in Zn/H-ZSM-5 propane aromatization catalysts. *Journal of Catalysis*, 179:192-202.

BORDIGA, S., BUZZONI, R., GEOBALDO, F., LAMBERTI, C., GIAMELLO, E., ZECCHINA, A., LEOFANTI, G., PENTRINI, G., TOZZOLA, G. & VLAIC, G. 1996. Structure and reactivity of framework and extraframework iron in Fe-silicate as investigated by spectroscopic and physicochemical methods. *Journal of Catalysis*, 158:486-501.

BOXHOORN, G., KORTBEEK, A.G.T.G., HAYS, G.R. & ALMA, N.C.M. 1984. A high-resolution solid-state ^{29}Si n.m.r. study of ZSM-5 type zeolites. *Zeolites*, 4:15-21.

BRONIĆ, J., SUBOTIĆ, B. & ŠKERBLIN, M. 1999. Investigation of the influence of seeding on the crystallisation of zeolite A in the membrane-type reactor. *Microporous and Mesoporous Materials*, 28:73-82.

BUTLER, A.C. & NICOLAIDES, C.P. 1993. Catalytic skeletal isomerization of linear butenes to isobutene. *Catalysis Today*, 18:443-471.

BYGGNINGSBACKA, R., KUMAR, N. & LINDFORS, L.-E. 1998. Comparative study of the catalytic properties of ZSM-22 and ZSM-35/ferrierite zeolites in the skeletal isomerization of 1-butene. *Journal of Catalysis*, 178:611-620.

CARTLIDGE, S., NISSEN, H.-U., SHATLOCK, M.P. & WESSICKEN, R. 1992. Solid-state

and catalytic characterization of intergrown zeolite structures based on six-membered rings. *Zeolites*, 12:889-897.

CASCI, J.L. & LOWE, B.M. 1983. Use of pH-measurements to monitor zeolite crystallization. *Zeolites*, 3:186-187.

CHEUNG, T.-K., LANGE, F.C. & GATES, B. C. 1996. Propane conversion catalyzed by sulfated zirconia, iron-and manganese-promoted sulfated zirconia, and USY zeolite. *Journal of Catalysis*, 159:99-106.

CHUNG, F.H. & SCOTT, R.W. 1973. A new approach to the determination of crystallinity of polymers by X-ray diffraction. *Journal of Applied Crystallography, 6:225-230.*

CONCEPCIÓN, N.P., LOPEZ NIETO, J.M., MIFSUD, A. & PÉREZ-PARIENTE, J. 1996. Preparation and characterisation of Mg-containing AFI and chabazite-type materials. *Zeolites*, 16:56-64.

COOMBS, D.S., ELLIS, A.J., FYFE, W.S. & TAYLOR, A.M. 1959. The zeolite facies, with comments on the interpretation of hydrothermal syntheses. *Geochimica et Cosmochimica Acta*, 17:53-107.

COPPERTHWAITE, R.G., HUTCHINGS, G.J. & VAN DER RIET, M. 1986. Preparation and evaluation of a synthetic zeolite catalyst. *Journal of Chemical Education*, 63:631-634.

CORMA, A. 2001. Verbal communication with the author.

CORMA, A., MIGUEL, P.J. & ORCHILLÉS, A.V. 1997. Can microscopic parameters, such as conversion and selectivity, distinguish between different cracking mechanisms on acid catalysts? *Journal of Catalysis*, 172:355-369.

CORMA, A. & ORCHILLÉS, A.V. 2000. Current reviews on the mechanism of catalytic cracking. *Microporous and Mesoporous Materials*, 35-36:21-30.

COSTA, C., DZIKH, I.P., LOPES, J.M., LEMOS, F. & RIBEIRO, F.R. 2000. Activity-acidity relationship in zeolite ZSM-5. Application of Brønsted-type equations. *Journal of Molecular Catalysis A: Chemical*, 154:193-201.

DAI, F.Y., SUZUKI, M., TAKAHASHI, H. & SAITO, Y. 1986. Mechanism of zeolite crystallization without using template reagents of organic bases. (*In* Murakami, Y.L.J., Iijima, A. & Ward, J.W., *eds.* New developments in zeolite science and technology. Studies in surface science and catalysis, Volume 28. Amsterdam : Elsevier. p223-230).

DAVIS, E. & HIGGINS, J.B. 1992. Zeolites and molecular sieves. (*In* Wachs, I. E. & Fitzpatrick, L.E., *eds.* Charactarization of catalytic materials. London : Butterworth-Heineman. p129-148).

DEBRAS, G., GOURGUE, A., NAGY, J.B. & DE CLIPPELEIR, G. 1986. Phisico-chemical characterization of pentasil type materials. III. High power solid state ^{27}Al, ^{23}Na and ^{29}Si n.m.r. of precursors and calcined samples. *Zeolites*, 6:161-168.

DEGNAN, T.F., CHITNIS, G.K. & SCHIPPER, P.H. 2000. History of ZSM-5 fluid catalytic

cracking additive development at Mobil. *Microporous and Mesoporous Materials,* 35-36:245-252.

DEROUANE, E.G., DETREMMERIE, S., GABELICA, Z. & BLOM, N. 1981. Synthesis and characterization of ZSM-5 type zeolites. I. Physico-chemical properties of precursors and intermediates. *Applied Catalysis,* 1:201-224.

DIJKSTRA, P.C., NICOLAIDES, C.P. & WEISS, K.I.J. 1991. Evidence for non-site-isolation in ZSM-5 from ion-exchange and catalytic studies. *Catalysis Letters,* 10:375-382.

DI RENZO, F. 1998. Zeolites as tailor-made catalysts: control of the crystal size. *Catalysis Today,* 41:37-40.

DUTTA, P.K. & BRONIĆ, J. 1994. Mechanism of zeolite formation: seed-gel interaction. *Zeolites,* 14:250-250.

DUTTA, P.K., RAO, K.M. & PARK, J.Y. 1992. Vibrational spectroscopic study of the evolution of the framework of the zeolite ferrierite. *Langmuir,* 8:722-726.

DWYER, J. 1984. Zeolite structure, composition and catalysis. *Society of Chemical Industry,* 2:258-369.

DYER, A. 1988. An introduction to zeolite molecular sieves. New York : Wiley. 149p.

EMEIS, C.A. 1993. Determination of integrated molar extinction coefficients for infrared ab-

sorption bands of pyridine adsorbed on solid acid catalysts. *Journal of Catalysis, 141*:347-354.

ENGELHARDT, G. 1991. Solid state NMR spectroscopy applied to zeolites. (*In* Van Bekkum, H., Flanigen, E.M. & Jansen, J.C., *eds*. Introduction to zeolite science and practice. Studies in surface science and catalysis, Volume 58. Amsterdam : Elsevier. p285-315).

ERNST, S., WEITKAMP, J., MARTENS, J.A. & JACOBS, A. 1989. Synthesis and shape-selective properties of ZSM-22. *Applied Catalysis*, 48:137-148.

FEGAN, S.G. & LOWE, B.M. 1986. Effect of alkalinity on the crystallization of silicalite-1 precursors. *Journal of Chemical Society, Faraday Transactions 1*, 82:785-799.

FEIJEN, E.J.P., MARTENS, J.A. & JACOBS, P.A. 1994. Zeolites and their mechanism of synthesis. (*In* Weitkamp, J., Karge, H.G., Pfeifer, H. & Hölderich, W., *eds*. Zeolites and related microporous materials: state of the art 1994. Studies in surface science and catalysis, Volume 84. Amsterdam : Elsevier. p3-21).

FLANIGEN, E.M. 1991. Zeolites and molecular sieves: an historical perspective (*In* Van Bekkum, H., Flanigen, E.M. & Jansen, J.C., *eds*. Introduction to zeolite science and practice. Studies in surface science and catalysis, Volume 58. Amsterdam : Elsevier. p13-33).

FRAISSARD, J. & ITO, T. 1988. ^{129}Xe n.m.r. study of absorbed xenon: a new method for studying zeolites and metal-zeolites. *Zeolites*, 8:350-361.

FYFE, C.A., THOMAS, J.M., KLINOWSKI, J. & GOBBI, G.C. 1983. MAS-NMR spectros-

copy and structure of zeolites. *Angewandte Chemie,* 95:257-273.

GATES, B.C. 1992. Catalytic chemistry. Singapore : Wiley. 458p.

GONTHIER, S. & THOMPSON, R.W. 1994. Effect of seeding on zeolite crystallisation, and the growth behavior of seeds. (*In* Jansen, J.C., Stöcker, M., Karge, H.G. & Weitkamp, J., *eds.* Advanced zeolite science and applications. Studies in surface science and catalysis, Volume 85. Amsterdam : Elsevier. p43-73).

GRAMLICH-MEIER, R., GRAMLICH, V. & MEIER, W.M. 1985. The crystal structure of the monoclinic variety of ferrierite. *American Mineralogist,* 70:619-623.

GRANDVALLET, P., DE JONG, K.P., MOOIWEER, H.H., KORTBEEK, A.G.T.G. & KRAUSHAAR-CZARNETZKI, B. 1992. Process for the conversion of a feedstock comprising linear olefins. European Patent 0501577 Al. Shell International Research Maatschappij. B.V. 21 February 1992. 7p.

GUNAWARDANE, R.P., GIES, H. & MARLER, B. 1988. Long-chain polyamines and amine-boric acid pairs as templates for the synthesis of porous tectosilicates. *Zeolites,* 8:127-134.

HAAG, W.O. 1994. Catalysis by zeolites - science and technology. (*In* Weitkamp, J., Karge, H.G., Pfeifer, H. & Hölderich, W., *eds.* Zeolites and related microporous materials: state of the art 1994. Studies in surface science and catalysis, Volume 84. Amsterdam : Elsevier. p1375-1394).

HAAG, W.O. & DESSAU, R.M. 1984. Duality of mechanism for acid-catalyzed paraffin cracking (*In* Proceedings 8th International Congress on Catalysis, Berlin, Volume 2. Frankfurt-am-Main : Dechema. p305-315).

HARDENBERG, A.T.J., MERTENS, L., MESMAN, P., MULLER H.C. & NICOLAIDES, C.P. 1992. A catalytic method for the quantitative evaluation of crystallinities of ZSM-5 zeolite preparations. *Zeolites,* 12:685-689.

HARRISON, I.D., LEACH, H.F. & WHAN, D.A. 1987. Comparison of the shape selective properties of ferrierite, ZSM-5 and ZSM-11. *Zeolites,* 7:21-27.

HUTCHINGS, G.J., NICOLAIDES, C.P. & SCURRELL, M.S. 1992. Developments in the production of methyl *tert*-butyl ether. *Catalysis Today,* 15:23-49.

ITO, T., BONARDET, J.L., FRAISSARD, J., NAGY, J.B., ANDRÉ, C., GABELICA, Z. & DEROUANE, E.G. 1988. About coke deposition on zeolite HY: a ^{129}Xe-NMR study. *Applied Catalysis,* 43:L5-L11.

IWAMOTO, M. 1994. Zeolites in environmental catalysis. (*In* Weitkamp, J., Karge, H.G., Pfeifer, H. & Hölderich, W., *eds.* Zeolites and related microporous materials: state of the art 1994. Studies in surface science and catalysis, Volume 84. Amsterdam : Elsevier. p1395-1410).

JACOBS, P.A., BEYER, H.K. & VALYON, J. 1981. Properties of the end members in the pentasil-family of zeolites: characterisation as adsorbents. *Zeolites,* 1:161-168.

JACOBS, P.A. & MARTENS, J.A. 1987. Synthesis of high-silica aluminosilicate zeolites. Studies in surface science and catalysis, Volume 33. Amsterdam : Elsevier. 390p.

JANSEN, J.C. & WILSON, S.T. 1991. The preparation of molecular sieves. (*In* Van Bekkum, H., Flanigen, E.M. & Jansen, J.C., *eds.* Introduction to zeolite science and practice. Studies in surface science and catalysis, Volume 58. Amsterdam : Elsevier. p77-136).

JIANQUAN, L., GUANGHUAN, L., JINGXIANG, D., TAO, D. & INUI, T 1994. Zeolite ZSM-5 synthesised in the extremely dense system. (*In* Weitkamp, J., Karge, H.G., Pfeifer, H. & Hölderich, W., *eds.* Zeolites and related microporous materials: state of the art 1994. Studies in surface science and catalysis, Volume 84. Amsterdam : Elsevier. p195-202).

KACIREK, H. & LECHERT, H. 1975. Investigations on the growth of the zeolite type NaY. *Journal of Physical Chemistry,* 79:1589-1593.

KARMAKAR, S. & GREENE, H.L. 1992. Oxidative destruction of chlorofluorocarbons (CFC11 and CFC12) by zeolite catalysts. *Journal of Catalysis,* 138:364-376.

KASAHARA, S., ITABASHI, K. & IGAWA, K. 1986. Clear aqueous nuclei solution for faujasite synthesis. (*In* Murakami, Y.L.J., Iijima, A. & Ward, J.W., *eds.* New Developments in zeolite science and technology. Studies in surface science and catalysis, Volume 28. Amsterdam : Elsevier. p185-192).

KERR, I.S. 1966. Crystallography: structure of ferrierite. *Nature,* 210:294-295.

KIBBY, C.L., PERROTTA, A.J. & MASSOTH, F.E. 1974. Composition and catalytic properties of synthetic ferrierite. *Journal of Catalysis,* 35:256-275.

KIM, W.J., LEE, M.C. & HAYHURST, D.T. 1998. Synthesis of ZSM-5 at low temperature and atmospheric pressure in a pilot-scale batch reactor. *Microporous and Mesoporous Materials,* 26:133-141.

KLINOWSKI, J. 1991. Solid-state NMR studies of molecular sieve catalysts. *Chemical Reviews,* 91:1459-1479.

KRANNILA, H., HAAG, W.O. & GATES, B.C. 1992. Monomolecular and bimoleculer mechanisms of paraffin cracking: *n*-butane cracking catalyzed by HZSM-5. *Journal of Catalysis,* 135:115-124.

KOIZUMI, M. & ROY, R. 1960. Zeolite studies. 1. Synthesis and stability of the calcium zeolites. *Journal of Geology,* 68:41-53.

KOKOTAILO, G.T., LAWTON, S.L. & OLSON, D.H. 1978. Structure of synthetic zeolite ZSM-5. *Nature,* 272:437-438.

KOTREL, S., KNÖZINGER, H. & GATES, B.C. 2000. The Haag-Dessau mechanism of protolytic cracking of alkanes. *Microporous and Mesoporous Materials,* 35-36:11-20.

KOTREL, S., ROSYNEK, M.P. & LUNSFORD, J.H. 1999. Intrinsic catalytic cracking activity of hexane over H-ZSM-5, H-β and H-Y zeolites. *Journal of Physical Chemistry B,* 103:818-824.

KUWABARA, H., OKUHARA, T. & MISONO, M. 1992. Catalytic removal of trimethylamine, an offensive-odor component, by selective oxidative decomposition to N_2, CO_2, and H_2O over copper-exchanged zeolites. *Chemistry Letters,* 6:947-450.

KWAK, B.S. & SACHTLER, W.M.H. 1994. Effect of Ga/proton balance in Ga/HZSM-5 catalysts on C_3 conversion to aromatics. *Journal of Catalysis,* 145:456-463.

KWAK, B.S., SACHTLER, W.M.H. & HAAG, W.O. 1994. Catalytic conversion of propane to aromatics: effect of adding Ga and/or Pt to HZSM-5. *Journal of Catalysis,* 149:465-473.

LE, T.S. & LE VAN MAO, R. 2000. Preparation of fluorinated-desilicated ZSM-5 zeolites with high surface acidity properties. *Microporous and Mesoporous Materials,* 34:93-97.

LI, Y. & ARMOR, J.N. 1993. Selective catalytic reduction of NO_x with methane over metal exchanged zeolites. *Applied Catalysis B: Environmental,* 2:239-256.

LIPPMAA, E., MÄGI, M., SAMOSON, A., ENGELHARDT, G. & GRIMMER, A.-R. 1980. Structural studies of silicates by solid-state high-resolution ^{29}Si NMR. *Journal of American Chemical Society,* 102:4889-4893.

LIPPMAA, E., MÄGI, M., SAMOSON, A., TARMAK, M. & ENGELHARDT, G. 1981. Investigation of the structure of zeolites by solid-state high-resolution ^{29}Si NMR spectroscopy. *Journal of American Chemical Society,* 103:4992-4996.

MAHADA, P.A., PRINSLOO, J.J., RAMATSETSE, P.B. & NICOLAIDES, C.P. 1999. Syn

thesis and characterization of ZSM-5 zeolite batches with different SiO_2/Al_2O_3 ratios. (*In* Abstracts of the Catalysis Conference 1999, CATSA, 31 October - 02 November 1999, Rustenburg. p51).

MARTINO, G. 2000. Catalysis for oil refining and petrochemistry, recent developments and future trends, (*In* Corma, A., Melo, F.V., Mendioroz, S. & Fierro, J.L.G., *eds.* 12th International Congress on Catalysis. Studies in surface science and catalysis, Volume 130A. Amsterdam : Elsevier. p83-103).

MAXWELL, I.E. 1997. Innovation in applied catalysis. *CATTECH*, March:5-14.

MEIER, W.M. & OLSON, D.H. 1987. Atlas of zeolite structure types. 2nd ed. London : Butterworths. 152p.

MÉRIAUDEAU, P. & NACCACHE, C. 1995. Comments on: evidence for reversible formation of a catalytic active site for propane aromatization for Ga_2O_3/H-ZSM-5. *Catalysis Letters*, 32:235-236.

MINTOVA, S. & VALTCHEV, V. 1996. Deposition of zeolite A on vegetal fibers. *Zeolites.* 16:31-34.

MOOIWEER, H.H., DE JONG, K.P., KRAUSHAAR-CZARNETZKI, B., STORK, W.H.J. & KRUTZEN, B.C.H. 1994. Skeletal isomerisation of olefins with the zeolite ferrierite as catalyst. (*In* Weitkamp, J., Karge, H.G., Pfeifer, H. & Hölderich, W., *eds.* Zeolites and related microporous materials: state of the art 1994. Studies in surface science and catalysis, Volume

84. Amsterdam : Elsevier. p2327-2334).

MOSCOU, L. 1991. The zeolite scene. (*In* Van Bekkum, H., Flanigen, E.M. & Jansen, J.C., *eds.* Introduction to zeolite science and practice. Studies in surface science and catalysis, Volume 58. Amsterdam : Elsevier. p1-12).

MURTHY, N.S. & REIDINGER, F. 1996. X-ray analysis. (*In* Sibilia, J.P., *ed.* A guide to materials characterization and chemical analysis. 2nd ed. New York : VCH. p143-165).

NABER, J.E., DE JONG, K.G., STORK, W.H. J., KUIPERS, H.P.C.E. & POST M.F.M. 1994. Industrial applications of zeolite catalysis. (*In* Weitkamp, J., Karge, H.G., Pfeifer, H. & Hölderich, W., *eds.* Zeolites and related microporous materials: state of the art 1994. Studies in surface science and catalysis, Volume 84. Amsterdam : Elsevier. p2197-2219).

NANNE, J.M., POST, M.F.M. & STORK, W.H.J. 1980. A process for the preparation of ferrierite, ferrierite thus obtained and its use as catalyst or catalyst carrier for converting hydrocarbons and for separating hydrocarbons. European Patent 0012473 A1. Shell International Research Maatschappij. B.V. 03 December 1979. 10p.

NICOLAIDES, C.P. 1996. Aluminosilicate catalyst, a process for the manufacture thereof and a process for the skeletal isomerization of linear olefins. U.S.A. Patent 5,503,818. CSIR. 02 April 1996. 14p.

NICOLAIDES, C.P. 1999. A novel family of solid acid catalysts: substantially amorphous or partially crystalline zeolitic materials. *Applied Catalysis A: General*, 4641:1-7.

NICOLAIDES, C.P., SCURRELL, M.S. & VINK, J. 1989. Quality control in the preparation of zeolite ZSM-5 using a catalytic test reaction. *Applied Catalysis*, 55:259-264.

NICOLAIDES, C.P., WAPIENNIK, M., WEISS, K.I.G., VAN DEN AKKER, H., VAN ZALK, B. & WIELAARD, P. 1991. Alkali metal cation exchange of HZSM-5 and the catalytic properties of alkalized zeolites. *Applied Catalysis*, 68:31-39.

NICOLAIDES, C.P., KUNG, H.H, MAKGOBA, N.P., SINCADU, N.P & SCURRELL, M.S. 2002a. Characterization by ammonia adsorption microcalorimetry of substantially amorphous or partially crystalline ZSM-5 materials and correlation with catalytic activity. *Applied Catalysis A: General*, 223:29-33.

NICOLAIDES, C.P., SINCADU, N.P. & SCURRELL, M.S. 2002b. NAS (novel alumino-silicates) as catalysts for the aromatisation of propane-studies of zinc and gallium modified zeolite-based systems having various extends of XRD crystallinity. *Catalysis Today*, 71:429-435.

OCELLI, M.L., BIZ, S. & AUROUX, A. 1999. Effects of isomorphous substitution of Si with Ti and Zr in mesoporous silicates with the MCM-41 structure. *Applied Catalysis A: General*, 183:231-239.

OLSON, D.H., HAAG, W.O. & LAGO, R.M. 1980. Chemical and physical properties of ZSM-5 substitutional series. *Journal of Catalysis*, 61:390-396.

OLSON, D.H., CALVERT, R.B. & VALYOCSIK, E.W. 1984. A process for isomerizing xyle-

nes. European Patent 0 102716. Mobil Oil Corporation. 14 March 1984. 23p.

ONO, Y. & KANAE, K. 1991. Transformation of butanes over ZSM-5 zeolites: Part 2 - Formation of aromatic hydrocarbons over Zn-ZSM-5 and Ga-ZSM-5. *Journal of Chemical Society, Faraday Transactions*, 87:669-675.

ONO, Y., OSAKO, K., KIM,.G.-J. & INOUE, Y. 1994. Ag-ZSM-5 as a catalyst for Aromatization of alkanes, alkenes, and methanol. (*In* Weitkamp, J., Karge, H.G., Pfeifer, H. & Hölderich, W., *eds.* Zeolites and related microporous materials: state of the art 1994. Studies in surface science and catalysis, Volume 84. Amsterdam : Elsevier. p1773-1780).

OTERO AREÁN, C., ESCALONA PLATERO, E., PEÑARROYA MENTRUIT, M., RODRÍQUEZ DELGADO, M., LLBRÉS I XAMENA, F.X., GARCÍA-RASO, A. & MORTERRA, C. 2000. The combined use of acetonitrile and adamantane-carbonitrile as IR spectroscopic probes to discriminate between external and internal surfaces of medium pore zeolites. *Microporous and Mesoporous Materials*, 34:55-60.

PADOVAN, M., LEOFANTI, G., SOLARI, M. & MORETTI, E. 1984. Studies on the ZSM-5 zeolite formation. *Zeolites*, 4:295-299.

PARK, M., CHOI, C.L., LIM, W.T., KIM, M.C., CHOI, J. & HEO, N.H. 2000. Molten-salt method for the synthesis of zeolitic materials. II. Characterization of zeolite materials. *Microporous and Mesoporous Materials*, 37:91-98.

PELLET, J., CASEY, D.G., HUANG, H.-M., KESSLER, R.V., KUHLMAN, E.J., O' YOUNG, C.-L., SAWICKI, R.A. & UGOLINI, J.R. 1995. Isomerization of n-butene to isobutene by ferrierite and modified ferrierite catalysts. *Journal of Catalysis*, 157:423-435.

RABO, J.A., BEZMAN, R.D. & POUTSMA, M.L. 1978. Zeolites in industrial catalysis. (a) Unifying principles in zeolite catalysis. *Acta Physica et Chemica*, 24:39-50.

RAMATSETSE, P.B. 1998. Synthesis and characterisation of zeoilites. Pietersburg : University of the North. (Dissertation-M.Sc.) 167p.

REIMSCHUESSEL, A.L., MACUR, J.E. & MARTI, J. 1988. Microscopy. (*In* Sibilia, J.P., *ed.* A guide to material characterization and chemical analysis. 2nd ed. New York : VCH. p137-166).

SANFILIPPO, D. 2000. Dehydrogenation of paraffins. Key technology for petrochemicals and fuels. *CATTECH*, 4(1):56-72.

SCHARPF, E.W., CRECELY, R.W., GATES, B.C. & DYBOWSKI, C. 1986. Characterization of NiNa-Y zeolite by Xe-129 NMR spectroscopy. *Journal of Physical Chemistry*, 90:9-11.

SIE, S.T. 1992. Acid catalyzed cracking of paraffin hydrocarbons. 1. Discussion of existing mechanisms and proposal of new mechanism. *Industrial and Engineering Chemistry Research*, 31:1881-1889.

SIE, S.T. 1994. Past, present and future role of microporous catalyst in the petroleum industry.

(*In* Jansen, J.C., Stöcker, M., Karge, H.G. & Weitkamp, J., *eds.* Advanced zeolite science and applications. Studies in surface science and catalysis, Volume 85. Amsterdam : Elsevier. p587-631).

SIMON, M.W., SUIB, S.L. & O'YOUNG, C.-L. 1994. Synthesis and characterization of ZSM-22 zeolites and their catalytic behavior in 1-butene isomerization reactions. *Journal of Catalysis*, 147:484-493.

SMART, L. & MOORE, E. 1995. Solid state chemistry: An introduction. 2nd ed. London : Chapman & Hall. 379p.

SMIRNIOTIS, P.G., DAVYDOV, L. & RUCKENSTEIN, E. 1999. Composite zeolite-based catalysts and sorbents. *Catalysis Reviews. Science and Engineering*, 41(1):43-113.

STAPLES, L.W. 1955. X-Ray investigation of ferrierite, a zeolite. *American Mineralogist*, 40:1095-1099.

STÖCKER, M. 1994. Review on recent NMR results. (*In* Jansen, J.C., Stöcker, M., Karge, H.G. & Weitkamp, J., *eds.* Advanced zeolite science and applications. Studies in surface science and catalysis, Volume 85. Amsterdam : Elsevier. p429-507).

STÖCKER, M 1999. Methanol-to-hydrocarbons: catalytic materials and their behavior. *Microporous and Mesoporous Materials*, 29:3-48.

SUZUKI, K., KIYOZUMI, Y., SHIN, S., FUJISAWA, K., WATANABE, H., SAITO, K. &

NOGUCHI, K. 1986. Zeolite synthesis in the system pyrrolidine-Na_2O-Al_2O_3-SiO_2-H_2O. *Zeolites,* 6:290-298.

SZOSTAK, R. 1989. Molecular sieves: principles of synthesis and identification. New York : Van Nostrand Reinhold. 524p.

THOMPSON, R.W. & DYER, A. 1985. Nucleation of zeolite Na-A crystals in hydrothermal systems. *Zeolites,* 5:302-308.

TURKEVICH, J. 1968. Zeolites as catalysts. (*In* Heinemann, H., *ed.* Catalysis review. New York : Marcell Dekker. p1-81).

VAN HOOFF, J.H.C. & ROELOFSEN, J.W. 1991. Techniques of zeolite characterization. (*In* Van Bekkum, H., Flanigen, E.M. & Jansen, J.C., *eds.* Introduction to zeolite science and practice. Studies in surface science and catalysis, Volume 85. Amsterdam : Elsevier. p241-283).

VAN GRIEKEN, R., SOTELO, J.L., MENÉNDEZ, J.M. & MELERO, J.A. 2000. Anomalous crystallization mechanism in the synthesis of nanocrystalline ZSM-5 *Microporous and Mesoporous Materials,* 39:135-147.

VAN SANTEN, R.A. & KRAMER, G.J. 1995. Reactivity theory of zeolitic Brønsted acidic sites. *Chemical Reviews,* 95:637-660.

VAUGHAN, P.A. 1966. The crystal structure of the zeolite ferrierite. *Acta Crystallographica,* 21:983-990.

VENUTO, P.B. 1994. Organic catalysis over zeolites: a perspective on reaction paths within micropores. *Microporous Materials,* 2:297-411.

VERDONCK, J.J., JACOBS, P.A. & UYTTERHOEVEN, J.B. 1979. Catalysis by a ruthenium complex heterogenized in faujasite-type zeolites: the water gas-shift reaction. *Journal of Chemical Society, Chemical Communication,* 4:181-182.

VON BALLMOOS, R. & HIGGINS, J.B. 1990. Zeolites. Collection of simulated XRD powder patterns for zeolites. 2nd ed. Stoneham : Butterworth-Heinemann. 514p.

WARZYWODA, J., ELDELMAN, R.D. & THOMSOM R.W. 1991. Crystallization of high-silica ZSM-5 in the presence of seeds. *Zeolites,* 11:318-324.

WARZYWODA, J. & THOMPSOM, R.W. 1991. Synthesis of zeolite A in the sodium/potassium system and the effect of seeding. *Zeolites,* 11:577-578.

WENYANG, X., JIANQUAN, L., WENYUAN, L., HUIMING, Z. & BINGCHANG, L. 1989. Nonaqueous synthesis of ZSM-35 and ZSM-5. *Zeolites,* 9:468-473.

WHAN, D.A. 1981. Structure and catalytic activity of zeolites. *Chemistry in Britain,* 17:532-535.

WHITTINGHAM, S. 1995. Synthesis and characterization of the zeolite ZSM-5. A size and shape selective catalyst for xylene isomerization. [webs:] http://imr.chem.binghamton.edu/labs/zeolite/zeolite.htm. [Date of access: 29 Aug. 1998].

WOOLERY, G.L., ALEMANY, L.B., DESSAU, R.M. & CHESTER, A.W. 1986. Spectroscopic evidence for the presence of internal silanols in highly siliceous ZSM-5. *Zeolites,* 6:14-16.

XU, W.-Q., YIN, Y.-G., SUIB, S.L. & O'YOUNG, C.-L. 1994. Selective conversion of *n*-butene to isobutylene at extremely high space velocities on ZSM-23 zeolites. *Journal of Catalysis,* 150:34-35.

XU, W.-Q., YIN, Y.-G., SUIB, S.L., EDWARDS, J.C. & O'YOUNG, C.-L. 1995a. *n*-Butene skeletal isomerization to isobutylene on shape selective catalysts: ferrierite/ZSM-35. *Journal of Physical Chemistry,* 99:9443-9451.

XU, W.-Q., YIN, Y.-G., SUIB, S.L. & O'YOUNG, C.-L. 1995b. Coke formation and its effects on shape selective and catalytic properties of ferrierite. *Journal of Physical Chemistry,* 99:758-765.

YI, K.-H. & IHM, S.-K. 1993. Crystallization mechanism for atmospheric synthesis of high-silica ZSM-5. *Microporous Materials,* 1:115-122.

ZHDANOV, S.P. 1971. Problems of zeolite crystallization. (*In* Gould R.F. *ed.* Molecular sieve zeolites-1. Advances in Chemistry Series, Volume 101. Washington : American Chemical So-

ciety. p20-43).